Aberrant prelimbic activity is associated with elevated fear in SAPAP3 knockout mice

by

Zoe Frohman LaPalombara

BS, Yale University, 2013

Submitted to the Graduate Faculty of the

School of Medicine in partial fulfillment

of the requirements for the degree of

Doctor of Philosophy

University of Pittsburgh

2020

UNIVERSITY OF PITTSBURGH

SCHOOL OF MEDICINE

This dissertation was presented

by

Zoe Frohman LaPalombara

It was defended on

July 15, 2020

and approved by

Rebecca Seal, Ph.D, Associate Professor, Department of Neurobiology, University of Pittsburgh

Aryn Gittis, Ph.D, Associate Professor, Department of Biological Sciences, Carnegie Mellon University

Anthony Grace, Ph.D, Professor, Department of Neuroscience, University of Pittsburgh

Mary Torregrossa, Ph.D, Associate Professor, Department of Psychiatry, University of Pittsburgh

Ekaterina Likhtik, Ph.D, Assistant Professor, Department of Biology, Hunter College & The Graduate Center, City University of New York

Dissertation Director: Susanne Ahmari, M.D., Ph.D, Associate Professor, Department of Psychiatry, University of Pittsburgh

Aberrant prelimbic activity is associated with elevated fear in SAPAP3 knockout mice

Zoe Frohman LaPalombara, PhD

University of Pittsburgh, 2020

Obsessive compulsive disorder (OCD), characterized by intrusive thoughts and repetitive actions, affects 1-3% of the population. One theory of OCD pathophysiology is that patients form maladaptive fear responses to neutral stimuli, leading to heightened fear and anxiety that drive repetitive behaviors. Thus, understanding abnormal fear processing in OCD may provide new treatment avenues.

To investigate the mechanisms of aberrant fear processing in OCD, I used SAPAP3 KO mice, an OCD-relevant model. In Chapter 2, I characterize fear conditioning in KOs and WTs and examine nociception and audition, which are relevant to fear learning. KO mice display elevated fear conditioning compared to WTs that cannot be explained by altered nociceptive or auditory signaling.

In Chapter 3, I assess conditioning-related neural activity in fear-associated regions using the proxy of cFos expression. cFos in the prelimbic cortex (PL) and basolateral amygdala (BLA) is significantly correlated in KOs, but not WTs. In contrast, PL cFos is correlated with freezing in WT mice only. This suggests that freezing behavior is linked to PL activity in WTs, while broad alterations in fear-related circuitry in KOs may be unrelated to behavioral output, and may impair normal fear learning.

Finally, in Chapter 4 I examine PL/BLA circuitry in KOs and WTs using fiber photometry. Interestingly, modulation in this circuit, particularly the PL, is associated with online learning of specific aversive associations in WTs. In KOs, modulation is absent, suggesting that their behavior

is driven by both specific and generalized fear. Next, I directly determined that KOs generalize more than WTs during discriminative fear conditioning. Finally, I demonstrate that PL activity underlies online fear processing via optogenetic inhibition during fear conditioning.

Together, these data suggest that modulation within the PL/BLA circuit, particularly the PL node, is critical for online fear processing in WTs. Conversely, a lack of PL modulation across conditioning trials could indicate that fear learning is driven by both specific and generalized fear learning in KOs. These data provide the first systematic characterization of PL/BLA functioning during online fear processing in WTs and a viable model for studying aberrant fear processing in the context of OCD.

Table of Contents

List of Tables

List of Figures

Preface

The work presented in this dissertation would not have been possible without the guidance and support of my mentor, peers, friends, and family. I owe each of these individuals a debt of gratitude for their role in getting me to this point. First and foremost, I would like to thank my mentor, Susanne Ahmari. I could not have asked for a better advisor throughout my time in graduate school. Susanne is that rare principal investigator who strikes the perfect balance between offering oversight and letting her trainees work independently. Over the past six years, she has given me the freedom to pursue the questions I find most compelling, while still providing me with critical guidance. My ability to design a research project, analyze data, and synthesize findings to create a coherent, comprehensive story is a testament to her tutelage. Scientific prowess and mentorship aside, Susanne is a truly inspiring leader. She is fair, considerate, funny, and eminently passionate about the work that we do. Her enthusiasm and fun-loving nature set the tone for the whole lab. In addition, she is a fierce advocate for her trainees, both professionally and personally. The health and well-being of her trainees is paramount – this has never been more apparent than during the last few months. The fact that she sets aside time to check on us and to discuss how we can learn and grow together as a lab during times of crisis (pandemic, civil unrest over systemic racism, and otherwise) speaks volumes of her character. I have experienced my fair share of scientific and personal strife over the course of graduate school, throughout which Susanne has been a constant source of support. I am particularly grateful for how she handled the events of 2017. Starting a completely new project at the beginning of my fourth year of graduate school was challenging, to say the least. However, with the help and support of Susanne, I was able to design

and execute a project of which I am proud, without significant delays to my timeline. For these reasons and many more, I am truly fortunate to have had Susanne as a mentor.

In addition to Susanne, I have benefited from the guidance of many other scientists. Among these individuals are my committee members – Becky Seal, my chair, and Aryn Gittis, both of whom have been on my committee since my first-year reprint exam; Tony Grace, who joined during my comprehensive exam; and Mary Torregrossa, who became a member prior to my thesis proposal. Each of these professors has contributed greatly to my dissertation and scientific education in general. Their feedback has challenged me to look at my data in new and interesting ways, and the final product is immeasurably better for it. I would also like to thank my outside examiner, Katya Likhtik. Her work has been influential in how I conceptualize my data, both on its own and as it fits into the literature at large. I am thankful that she agreed to serve in this capacity, despite the unusual challenges presented by an ongoing pandemic. I am only sorry that we were unable to host her in person so that the Pittsburgh neuroscience community could benefit from her expertise outside of the virtual realm.

Beyond my committee, I have received guidance from the talented investigators that make up the Translational Neuroscience Program (TNP). Chiefly, this pertains to the scientists whose lab space is contiguous with that of the Ahmari lab: Yanhua Huang, Ryan Logan, Colleen McClung, Rui Peixoto, Marianne Seney, and Mary Torregrossa. These individuals are generous with their time, always willing to troubleshoot or discuss experimental design and analysis. I cannot count the number of occasions I've wandered into one of their offices with a problem and walked out with a solution. Members of the second half of the TNP, such as Zachary Freyberg, Jill Glausier, Dave Lewis, Matt MacDonald, Rob Sweet, and Tobias Techert, have also contributed to this work via their insightful feedback during my periodic presentations to the group.

I would be remiss if I didn't mention my undergraduate mentor, Ralph DiLeone, and the postdoc with whom I most closely worked during that time, Rich Trinko. Ralph was influential in my decision to pursue a Ph.D in neuroscience. He gave me my first opportunity to design and execute an independent research project, employed me as a research assistant after I gained my undergraduate degree, and encouraged me to apply to graduate school. He continues to take an interest in my life and career to this day, for which I am grateful. Likewise, Rich was instrumental in shaping my passion for neuroscience. He is also responsible for teaching me many of the techniques, skills, and best practices that enabled me to hit the ground running upon entering graduate school. In addition, although she did not contribute to this project having left the University of Pittsburgh prior to its inception, Linda Rinaman was an excellent mentor during my first graduate school rotation.

The success of this project is due in no small part to the advice, feedback, and guidance of the members of the Ahmari lab. From an experimental standpoint, I would like to specifically thank Jamie Pierson, who in addition to keeping the lab afloat contains a wealth of information about fear conditioning, and JP Gamboa, who helped me collect preliminary data for my final set of experiments. From a personal standpoint, I would like to thank each and every one of the lab members for creating a fun, supportive environment. As residents of the same lab bay, Britny Hildebrandt, Jared Kopelman, and Jamie Pierson deserve a special mention. My daily interactions with them have immeasurably enriched my graduate experience. Though I know they'd prefer I use the pun-based term they created to reference our bay (which, as a hater of puns, I cannot bring myself to do), the fact that I'm acknowledging its existence should suffice. To the rest of the lab members – Britt Chamberlin, JP Gamboa, Matt Geramita, Grace Liu, Sara Springer, and newest

members Nick Bannon, Hayley Fisher, and Sean Sweat – thank you for everything you've done, big or small.

Although they have since moved on to new and exciting ventures, the past lab members have been equally influential. I owe a particular debt of gratitude to Sean Piantadosi, whose attention to detail saved me countless hours of unnecessary work. I would also like to thank Victoria Corbit, for helping me improve our photometry analysis techniques; James Hyde, for always being game to join me in creating a random contraption or system out of odds and ends; Xiaojun Li, for being a constant source of positivity and enthusiasm; Lizzie Manning, for her boundless insightful input; Ruth Snyder, for her technical assistance; and Jesse Wood, for teaching me how to code in Matlab. Prior undergraduate researchers Julia St. John and Joey Wise also provided assistance along the way.

There are several other individuals both within the University of Pittsburgh and at other institutions that have contributed to this work by providing input on experimental design and analysis and access to equipment, including Megan Bertholomey, Clare Choi, Bill Goins, Eyal Kimchi, Zach Paden, and Jenna Shold (née Parrish).

I would like to thank the leadership, faculty, and staff of the Center for Neuroscience at the University of Pittsburgh (CNUP), TNP, and Departments of Neurobiology and Neuroscience. I want to specifically highlight the past and present administrators of these programs, who work tirelessly on behalf of the students and faculty: Joan Blaney, Natalee Bright, Margaret Carter, Carol Moore, Michele Nace, Marlene Nieri, Lisa Summe (who is also a good friend), and, of course, Patti Argenzio. I only know a fraction of what Patti does, and even that seems like too much. I cannot thank her enough for all she has done.

These acknowledgements would not be complete without a tribute to my fellow graduate students. While there are many individuals that I wish to thank – including Matt Getz, Jane Huang, Becca Krall, Alison Kreisler, Jongwon Lee, Matt Rich, Laura Rupprecht, Nate Vogler, and Yang Yeh – I would like to focus on several members of my graduate cohort: Meghan Bucher, Kristine Ojala, Diana Olivos-Stewart, and Sarah Najjar. I could not have picked a better group with which to weather the ups and downs of graduate school. Each of these women is a brilliant scientist and even better friend. I cannot wait to see what the future holds for them.

There are many individuals that have enriched my life outside of the lab. These are the people with whom I have celebrated birthdays and weddings, enjoyed game nights and dinner parties, attended concerts and shows, played basketball and trivia, and countless other activities: Ashlee Adams, Michaël Aklin, Kyle Bahnsen, Sarah Castleman, Carla Chow, Scott Dempsey, Carmen Fisac, Jane Hartung, Kyle Johnson, Jared Kopelman, Raj Kumar, Sima Lofti, Meri Long, Randall McAuley, John Miller, Vidhya Nagarajan, Laura Paler, Celia Paris, Aishwarya Ramesh, Nathan Ruggles, Will Spaniel, Jim Stevenson, and Ray and Cassandra Van Cleve. This also includes several people who have already been mentioned: Megan Bertholomey, Meghan Bucher, Matt Getz, Britny Hildebrandt, Jared Kopelman, Lizzie Manning, Sarah Najjar, Kristine Ojala, Diana Olivos-Stewart, Sean Piantadosi, Jamie Pierson, and Lisa Summe. As my roommates for my first four years in Pittsburgh, Ashlee Adams and Sarah Najjar deserve a special mention. These women were a constant presence in my life. They were there for me during the highest and lowest points of graduate school, professionally and personally. They are some of the most genuine, thoughtful, and supportive people I know, and I am deeply grateful for their friendship.

Lastly, I would like to thank my family. My extended family – a stellar crew of scholars, educators, scientists, lawyers, and artists – has been there for me in innumerable ways. The

Ciccones (Nancy, Dennis, Josh, Matthew, and by extension, Erin Simmons) have made me feel at home in Pittsburgh even before I moved here. My future in-laws Howard and Sheree Poznansky, sister-in-law Amy Benton, her husband Rob, and their daughters Emilia and Stella, have welcomed me with open arms. In particular, my parents, Susan and Marc, sisters Hannah and Alicia, and brother-in-law Zach have provided me with unconditional love and support. None of this would have been possible without them. Finally, thank you to my fiancé, Mike. He has supported me in more ways than I can count – he has listened to me complain, championed me and my accomplishments, encouraged me to take breaks, provided distraction when necessary, motivated me to keep going, and much, much more. I could not have asked for a better partner and I am eternally grateful that he is a part of my life.

1.0 Introduction

The ability to form associations between a stimulus in the environment and a specific outcome is a critical behavior for all organisms. This is particularly true for aversive outcomes, wherein failing to form an association can result in harm or even death. On the other end of the spectrum, enhanced fear and anxiety are also maladaptive and are hallmarks of anxiety disorders such as post-traumatic stress disorder, panic disorder, and obsessive-compulsive disorder (OCD). Understanding how fear is processed in disorders like OCD could provide critical insight into the pathogenesis of anxiety disorders and provide new areas of exploration for potential treatment approaches. The broad goal of my dissertation was to examine fear in in the context of OCD in a preclinical model, in which more mechanistic examinations of the neural mechanisms underlying fear learning are attainable than in people. In the following sections, I will outline background pertaining to the relevance of fear to OCD pathogenesis, the known neural correlates of fear, the mouse model that I used to study OCD-relevant behaviors, and the specific goals of this dissertation.

1.1 Obsessive compulsive disorder

1.1.1 Burden of OCD

Obsessive compulsive disorder (OCD) is a debilitating psychiatric illness that is characterized by intrusive thoughts or ideas (obsessions) and repetitive behaviors (compulsions).

These compulsions are often performed to reduce the anxiety associated with obsessions. According to current theories, OCD consists of four symptom domains: 1) contamination obsessions paired with compulsive cleaning; 2) symmetry obsessions paired with compulsive repeating, counting, and ordering; 3) harm and doubt obsessions paired with compulsive checking; and 4) taboo obsessions paired with compulsive neutralizing behavior (Mataix-Cols et al., 2004; Pinto et al., 2007; Pauls et al., 2014; Wood and Ahmari, 2015). Across all symptom dimensions, OCD has a prevalence of 1-3% in the United States (Kessler et al., 2005, 2012) and an average age of onset in adolescence or early adulthood (Kessler et al., 2005). OCD is associated with a lower overall quality of life, poorer physical health, comorbid mental disorders, impaired social functioning, difficulties in workplace and personal settings (Bobes et al., 2001), and increased mortality (Eaton et al., 2008). In 1990, the World Health Organization ranked OCD as the tenth leading cause of disability worldwide (Murray and Lopez, 1996). First-line therapies for this disorder include selective serotonin reuptake inhibitors (SSRIs) and cognitive behavioral therapy (CBT). Unfortunately, neither intervention is wholly successful in alleviating OCD symptoms. SSRI treatment is ineffective in ~30% of patients (Pittenger and Bloch, 2014). In those that experience some effect of treatment, a mere 10-20% exhibit full remission (Soomro et al., 2008). With CBT, or more specifically exposure with response prevention (ERP), roughly two thirds of patients experience symptom relief, with one third experiencing substantial improvement (Hezel and Simpson, 2019). However, 25-30% discontinue treatment (Law and Boisseau, 2019), likely due to the challenging nature of the therapy. Owing to the early average age of onset, severe disruptions in everyday life, and varied effectiveness of first-line pharmacological and cognitive-behavioral therapies, OCD incurs substantial financial costs, totaling an estimated $10.6 billion per year in the United States alone (Eaton et al., 2008). Given the substantial personal and

institutional burden, it is necessary to gain further insight into the mechanisms of OCD symptomology to facilitate the development of improved treatments.

1.1.2 The role of fear in OCD

Fear and anxiety are critical features of OCD (VanElzakker et al., 2014; Pittig et al., 2018). In fact, it has been theorized that heightened fear and improper discrimination between potential and immediate threats drive obsessive-compulsive symptoms (Tracy et al., 1999; Fiddick, 2011). In support of this theory, fear measured by the Panic Disorder Severity Scale (PDSS) is associated with contamination, harm avoidance, unacceptable thoughts, and symmetry obsessions in a community population sample (Raines et al., 2015). In pediatric OCD subjects, fear of separation (e.g. separation anxiety) is predictive of aggressive, sexual, religious, and somatic obsessions and checking compulsions, while fear of physical harm predicts symmetry obsessions and order, counting, and repeating compulsions (Rozenman et al., 2017). Furthermore, compulsions that are driven by fear are correlated with worse long-term outcomes in adult OCD patients, as measured by the Yale-Brown Obsessive Compulsive Scale (YBOCS) (Ferreira et al., 2020). In addition, ERP, a first-line cognitive-behavioral therapy for OCD, is based on the principles of fear learning and extinction. Considering that 25-30% of patients discontinue treatment, it is possible that aberrant fear learning is disrupted to a greater extent in cases of refractory OCD. This presence of within-disease heterogeneity further underscores the relevance of fear processing to OCD pathophysiology and the need to study it further.

1.1.3 Fear conditioning studies in OCD patients

In the both the clinical and pre-clinical laboratory setting, fear learning is studied using fear conditioning, a paradigm in which subjects learn to associate an initially neutral stimulus (conditioned stimulus; CS) with an innately aversive stimulus (unconditioned stimulus; US) (Fendt and Fanselow, 1999; Maren, 2001). Subjects are typically presented with several CS-US pairings during conditioning. In a subsequent extinction session, the association between the CS and US is degraded by presenting the CS repeatedly in the absence of the US. In many cases, extinction is followed by an extinction recall test the next day: the CS is again presented without the US in order to assess how well extinction learning was retained. As a whole, fear conditioning paradigms allow mechanistic investigation of how subjects acquire, express, and extinguish fear. Such information has proven instrumental in elucidating the mechanisms of normal fear learning (Davis, 1992; Fendt and Fanselow, 1999; Maren, 2001). Moreover, studying fear conditioning in animal models of pathological fear and anxiety can provide critical insight into psychiatric disorders, such as OCD.

Surprisingly, there are very few fear conditioning studies in OCD patients. Within this small set of studies, results have been mixed – both deficits and normal functioning have been reported in acquisition, extinction, and extinction recall. In a non-clinical population, individuals with high obsessive-compulsive scores on the Maudsley Obsessive Compulsive Inventory (MOCI) displayed enhanced aversive eyeblink conditioning (Tracy et al., 1999). Enhanced fear conditioning acquisition has also been reported in pediatric OCD patients (Geller et al., 2017). In another study of pediatric OCD, CS-evoked skin conductance response (SCR; a measure of autonomic arousal) during conditioning was correlated with symptom severity; however, there were no differences in acquisition SCRs between OCD subjects and healthy controls (McGuire et

al., 2016). Likewise, several other studies have found no fear acquisition deficits in pediatric (Geller et al., 2019) or adult OCD (Nanbu et al., 2010; Milad et al., 2013; McLaughlin et al., 2015; Giménez et al., 2019). During extinction, abnormalities have been observed in both pediatric (Geller et al., 2017) and adult patients (Nanbu et al., 2010), but other studies have reported normal extinction compared to healthy controls (Milad et al., 2013; McLaughlin et al., 2015; Giménez et al., 2019). Two studies have reported impaired extinction retention in adults with OCD (Milad et al., 2013; McLaughlin et al., 2015). Interestingly one of these studies observed a correlation between extinction retention and symptom severity (Milad et al., 2013), while the other did not (McLaughlin et al., 2015). Conversely, a more recent experiment reported normal extinction recall in OCD patients, both behaviorally and physiologically (Giménez et al., 2019). Of note, however, activity in ventromedial PFC (vmPFC), a region associated with fear extinction, was negatively correlated with performance during recall specifically in OCD patients, suggesting that fear-relevant neural abnormalities are present in OCD.

Taken together, there is significant heterogeneity in fear conditioning studies in OCD patients, with findings of both abnormal and unaltered fear acquisition, extinction, and extinction recall. While there are commonalities in all of these studies – each included both medicated and unmedicated patients, used SCR as a measure of fear, and did not investigate specific OCD symptom dimensions – the differences may be illuminating. For instance, enhanced acquisition and impaired extinction recall were exclusively reported in pediatric (McGuire et al., 2016; Geller et al., 2017) and adult OCD (Milad et al., 2013; McLaughlin et al., 2015), respectively. Conversely, extinction deficits were reported across both youth and adult subjects (Nanbu et al., 2010; Geller et al., 2017). This may indicate that age plays a role in fear processing in OCD. Alternatively, these data could be explained by differences in the conditioning paradigm: in all of the pediatric OCD

studies, the CS consisted of fearful faces and the US was an aversive scream (McGuire et al., 2016; Geller et al., 2017, 2019). The adult studies, on the other hand, used either computer images of a room (Milad et al., 2013; McLaughlin et al., 2015; Giménez et al., 2019) or a light stimulus as the CS (Nanbu et al., 2010), with a mild shock as a US. It is possible that the distinct qualities of these stimuli (e.g. the additional emotional valence of faces and human screaming) can account for behavioral differences. In addition, heterogeneity within age groups could be explained by sample size. In a study of 64 pediatric patients, no acquisition abnormalities were observed (Geller et al., 2019), while acquisition SCR was enhanced in a sample of 39 patients (Geller et al., 2017). Similarly, extinction recall was unaltered in a sample of 37 patients vs. 18 controls (McLaughlin et al., 2015), but impaired in a sample of 21 patients vs. 21 controls (Milad et al., 2013). Considering that most of these studies had small to moderate groups sizes (n=18-64) (Nanbu et al., 2010; Milad et al., 2013; McLaughlin et al., 2015; McGuire et al., 2016; Geller et al., 2017, 2019; Giménez et al., 2019), it is not surprising that there are discrepancies in significant findings. However, despite these differences, all of these studies found that individuals with OCD exhibit elevated fear during one or more stages of conditioning. Therefore, it is evident that fear processing is broadly disrupted in OCD, indicating that this is an important area of exploration.

1.2 The neural correlates of fear conditioning

1.2.1 Rodent fear conditioning studies

While human fear conditioning studies are useful for exploring fear processing abnormalities in disorders such as OCD since preclinical models cannot fully capture the

complexities of human cognition, studies in rodents have nonetheless been instrumental in the discovery of the neural correlates of fear acquisition, expression, and extinction. Decades of research in this area have provided ample evidence for the role of several key structures in fear acquisition, expression, and extinction, including the basolateral amygdala (BLA) and medial prefrontal cortex (mPFC) (Maren, 2001; Fanselow and Poulos, 2005; Milad and Quirk, 2012; Duvarci and Pare, 2014; Giustino and Maren, 2015; Izquierdo et al., 2016). These two structures, which are bidirectionally connected, form key nodes in the canonical fear conditioning circuit. More specifically, the BLA and prelimbic (PL) subdivision of the mPFC have been implicated in fear acquisition and expression[1], while the BLA and infralimbic (IL) subregion of the mPFC are involved in fear extinction. Table 1-1 summarizes the findings in these regions during various

[1] **A brief note on terminology:** throughout this dissertation, I will use the terms fear acquisition and expression. As such, it is important to precisely define them. In the fear conditioning literature, fear acquisition refers to the formation of a fear association, while expression refers to the performance of a previously-learned fear association. In both cases, this is generally measured during a recall session on the next day – the dissociation of the two processes is achieved by intervening at different timepoints: pre-training for acquisition and post-training for expression. Critically, this means that whether or not an animal acquires an association is assessed via behavioral output (e.g. freezing, fear-potentiated startle) during CS presentations the following day (recall), **not** via behavior during the conditioning session itself. Pre-training interventions (e.g. lesions, muscimol) and manipulations during conditioning (e.g. optogenetic stimulation or inhibition) can be said to affect acquisition if they modulate fear responses during recall. Conversely, fear expression is assessed via post-training manipulations, typically immediately prior to or during recall. Although the aforementioned description is the predominant use of the term "acquisition" in the field, fear responses during the conditioning session are occasionally referred to as acquisition as well (e.g. an acquisition curve). However, for clarity I will instead exclusively refer to these responses as "online fear processing" throughout the dissertation.

stages of fear conditioning. The following sections will outline the specific role of each of these three regions in fear processing in turn.

Table 1-1. BLA, PL, and IL activity during the stages of fear conditioning

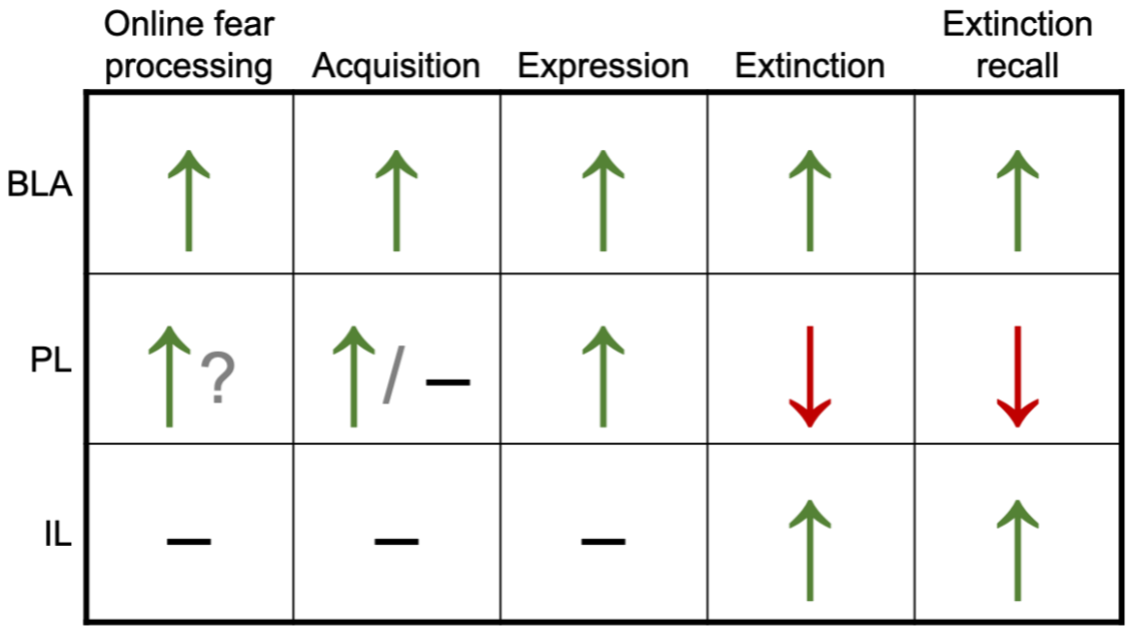

Activity in the BLA (top row), PL (middle row), and IL (bottom row) during the stages of fear conditioning: online fear processing, acquisition, expression, extinction, and extinction recall. **BLA:** The BLA is active during all stages of conditioning. However, different cell populations are active during the early (online fear processing, acquisition, expression) versus late (extinction, extinction recall) stages. **PL:** The role of the PL in online fear processing is unclear – only one study has reported that PL activity is necessary, while most see no effect or do not look at this stage. Acquisition results are mixed. Many studies have found that the PL is not required, but more recent studies have shown that manipulation of specific cell types or signaling processes can affect acquisition. PL activity decreases during extinction and extinction recall. **IL:** The IL is inactive during online fear processing, acquisition, and expression, but active during extinction and extinction recall.

1.2.1.1 Basolateral amygdala

The basolateral amygdala (BLA), a structure located in the temporal lobe, is considered a major locus of fear learning (Fanselow and Poulos, 2005; Duvarci and Pare, 2014; Gafford and Ressler, 2016). It can be subdivided into the lateral (LA) and basal (BA) nuclei, with the latter being further segmented into the basolateral (BL) and basomedial (BM) [i.e. accessory BA (AB)] nuclei (Sun et al., 2020). The BLA predominantly consists of glutamatergic principal cells and GABAergic interneurons, which are morphologically and functionally similar to cortical pyramidal cells and interneurons (Capogna, 2014; Duvarci and Pare, 2014). There is a considerable amount of phenotypic diversity within the interneuron population (Capogna, 2014; Duvarci and Pare, 2014; Gafford and Ressler, 2016). The two most-studied types of interneurons, those that express parvalbumin (PV) and somatostatin (SOM), are strong modulators of principal neuron output. PV+ interneurons preferentially synapse onto the proximal dendrites, soma, and axon initial segment of principal neurons, thereby exerting potent control over the firing patterns of these neurons (Capogna, 2014; Duvarci and Pare, 2014). Conversely, SOM+ interneurons target distal dendrites, thereby regulating principal neuron synaptic integration (Capogna, 2014; Duvarci and Pare, 2014). These distinct roles align with PV+ and SOM+ GABAergic interneuron functionality throughout the brain. The BLA receives input from the hippocampus and various cortical and thalamic nuclei, including sensory cortex and thalamus and both the PL and IL subdivisions of the mPFC (Duvarci and Pare, 2014; Hübner et al., 2014). The BLA sends efferent projections to the central amygdala (CeA) (which is the output nucleus of the amygdala), as well as the thalamus, cortex (including PL and IL), bed nucleus of the stria terminalis (BNST), hypothalamus, and neuromodulatory cell populations in the basal forebrain and brainstem (Duvarci and Pare, 2014). These projection patterns primely position the BLA as a hub for fear

processing: convergent sensory cortical and thalamic input results in fear-induced plasticity, which subsequently promotes expression of fear behavior via projections to the CeA (Sun et al., 2020).

Accordingly, numerous studies have found the BLA to be critical in the acquisition, expression, and extinction of fear. For example, both pre-training lesions and muscimol-mediated inactivation of the BLA – either the whole structure or specific subnuclei – impair fear acquisition, as measured by freezing during fear memory retrieval (LeDoux et al., 1990; Sananes and Davis, 1992; Campeau and Davis, 1995a; Muller et al., 1997; Maren, 1999; Wilensky et al., 1999; Goosens and Maren, 2001; Nader et al., 2001). Similarly, post-training BLA lesions and muscimol-mediated inactivation attenuate fear expression (Sananes and Davis, 1992; Campeau and Davis, 1995a; Muller et al., 1997; Maren, 1999; Anglada-Figueroa and Quirk, 2005; Amano et al., 2011; Sierra-Mercado et al., 2011). Moreover, markers of neuronal activity and plasticity including cFos, Zif268, and Arc, are elevated in the BLA after conditioning and fear memory retrieval (Herry and Mons, 2004; Senn et al., 2014; Zhu et al., 2018). In addition, neurons in both the lateral and basal nuclei of the BLA exhibit tone-related responses after conditioning (Quirk et al., 1995; Maren, 2000; Goosens et al., 2003; Herry et al., 2008; Amano et al., 2011; Wolff et al., 2014), and optogenetic manipulation of specific BLA interneurons during CS-US presentations can alter fear acquisition and expression (Wolff et al., 2014).

The BLA is equally important for extinction and extinction recall (Quirk and Mueller, 2008; Marek et al., 2013; Duvarci and Pare, 2014). Initial studies found that disruption of BLA via NMDA receptor or kinase antagonism prior to extinction training impaired extinction recall (Falls et al., 1992; Lu et al., 2001; Lin et al., 2003). Subsequent studies built upon this work by demonstrating that signaling perturbation prior to extinction training disrupts both online expression of extinction and consolidation of the extinction memory (Kim et al., 2007; Sotres-

Bayon et al., 2007). Several other studies found that BLA disruption during extinction training attenuates or completely blocks freezing within-session (Akirav et al., 2006; Herry et al., 2006). These results suggest that BLA activity supports both extinction expression and consolidation. Accordingly, neuronal activity markers are present in the BLA after extinction training (Zhu et al., 2018) and extinction recall (Herry and Mons, 2004; Hefner et al., 2008; Senn et al., 2014). Interestingly, one of these studies observed elevated cFos specifically in IL-projecting BLA neurons (Senn et al., 2014). Data obtained using *in vivo* techniques complements these findings. For instance, several studies have reported the existence of "extinction cells" in the BLA, which develop CS responses over the course of extinction training (Herry et al., 2008; Amano et al., 2011). These neurons were found to have reciprocal connections with the mPFC (Herry et al., 2008). Another study found that the electric field potential (EFP) amplitude of BLA-mPFC projections increases during extinction training (Vouimba and Maroun, 2011). Critically, the majority of the mPFC recording sites in this study were in the upper IL. Similarly, IL-projecting BA neurons are activated during presentations of the extinguished CS and exhibit elevated burst firing after extinction (Senn et al., 2014). Furthermore, specific inhibition of BA-IL projections during extinction retrieval impairs extinction recall (Senn et al., 2014), supporting a functional role of the BLA-IL circuit in extinction.

1.2.1.2 Prelimbic cortex

The mPFC, located in the frontal lobe, is a laminar cortical structure consisting of glutamatergic pyramidal neurons and GABAergic inhibitory interneurons (Giustino and Maren, 2015). This region receives input from a variety of areas related to fear processing, including the midline thalamus, hippocampus, contralateral mPFC, and BLA (Giustino and Maren, 2015), and projects to fear-associated regions such as the BLA and periaqueductal gray (PAG). Projection

patterns for the PL and IL mPFC subdivisions are generally similar. Both regions provide comparable input to BLA principal neurons and interneurons (Cho et al., 2013; Hübner et al., 2014), with the PL exhibiting higher connection rates to interneurons compared to principal neurons (Marek et al., 2018). However, there are some notable differences between PL and IL afferents and efferents. For example, the IL sends direct projections to the CeA, while the PL does not (Giustino and Maren, 2015). In addition, BLA input to the PL and IL is distinct: although amygdala- and PAG-projecting neurons in both mPFC subregions receive BLA input, the BLA preferentially targets PL over IL corticoamygdalar neurons and IL cortico-PAG over IL corticoamygdala neurons (Cheriyan et al., 2016). In addition, unidirectional projections have been found originating in the PL and terminating in the IL (Marek et al., 2018).

Like the BLA, the PL is critical for fear expression. Inactivation of the PL with tetrodotoxin (TTX) or muscimol prior to fear memory retrieval impairs fear expression (Corcoran and Quirk, 2007; Sierra-Mercado et al., 2011), and optogenetic inhibition of PL soma during recall tones decreases freezing (Do-Monte et al., 2015b). Similarly, reducing PL intrinsic excitability prior to fear recall attenuates freezing (Santini and Porter, 2010). Conversely, PL microstimulation during retrieval tones slows extinction and impairs extinction recall, suggesting that PL activity is necessary for fear expression (Vidal-Gonzalez et al., 2006). Moreover, after conditioning, PL principal neurons exhibit sustained tone-related responses (Baeg, 2001; Burgos-Robles et al., 2009) that are correlated with freezing (Burgos-Robles et al., 2009), while parvalbumin-positive (PV+) interneurons are inhibited to tones, presumably facilitating principal neuron activation (Courtin et al., 2014). These data suggest that the PL undergoes synaptic plasticity after fear conditioning which underlies proper expression of fear memories. Accordingly, markers of neuronal activity and plasticity (such as cFos, zif268, pMAPK, and neuroregulin-1) are elevated

in the PL after retrieval (Herry and Mons, 2004; Do-Monte et al., 2015b; Chen et al., 2017; Jacques et al., 2019). Furthermore, disruption or activation of plasticity-related signaling in the PL prior to retrieval impairs or enhances expression, respectively (Chen et al., 2017).

However, while it is evident that the PL is necessary for fear expression, the specific role of the PL in fear acquisition is less clear. Several studies have shown that the PL is necessary for acquisition in trace fear conditioning, a variant of standard delay fear conditioning that involves a time gap (trace period) between the end of the CS and onset of the US. For example, PL neurons exhibit sustained tone responses during both the CS and trace period throughout conditioning (Gilmartin and McEchron, 2005). In addition, mPFC inactivation via muscimol or NMDA receptor antagonism prior to conditioning impairs fear memory recall (Gilmartin and Helmstetter, 2010). Specific inactivation of the PL using muscimol or NR2A-containing NMDA receptor antagonism has the same effect (Gilmartin et al., 2013a). Similarly, optogenetic inhibition of the PL during the entire CS-trace-US period decreases freezing during memory retrieval (Gilmartin et al., 2013b) and antagonism of PL muscarinic acetylcholine receptors prior to training delays learning during conditioning and reduces freezing during recall (Kirry et al., 2019). Likewise, disruption of plasticity-related signaling decreases fear memory recall (Runyan et al., 2004). Together, these data indicate that pre-conditioning disruption of PL signaling can attenuate fear acquisition in trace conditioning. However, unlike delay conditioning, the time gap in trace conditioning requires working memory, which may engage the PL in additional ways compared to standard fear conditioning.

In classic delay fear conditioning, the predominant view has been that the PL is only necessary for expression, not acquisition (Giustino and Maren, 2015). In support of this theory, PL inactivation with TTX prior to conditioning attenuates freezing during the conditioning session

itself (online fear processing), but does not affect memory acquisition, as assessed by fear memory recall (Corcoran and Quirk, 2007). Similarly, pre-training lesions encompassing the PL do not affect acquisition (Morgan et al., 1993; Quirk et al., 2000). In contrast, several studies have shown that manipulation of specific neuronal subtypes or signaling pathways in the PL can disrupt acquisition. For example, increasing mPFC excitatory/inhibitory balance using stable step function opsins prior to conditioning (Yizhar et al., 2011) or inhibiting PL somatostatin-expressing interneurons during conditioning CS-US presentations (Cummings and Clem, 2020) impairs fear memory retrieval without affecting freezing during conditioning. Similarly, pre-conditioning constitutive BDNF knockout (Choi et al., 2010a), bilateral NR2A antagonism, (Gilmartin et al., 2013a), or disruption of Gadd45γ signaling (Li et al., 2019) in the PL attenuates fear memory recall. Furthermore, mPFC neurons increase responding to tones during olfactory fear conditioning (Laviolette et al., 2005), suggesting that the PL is involved in online processing of CS-US associations. In addition, several studies have more clearly revealed a role of PL plasticity during acquisition – specifically, suppression or knockdown of plasticity-related molecules prior to conditioning disrupts fear memory formation, but not conditioning itself (Morrow et al., 1999; Chen et al., 2017), while overexpression enhances fear retrieval (Xue et al., 2015; Chen et al., 2017). In sum, emerging data have challenged the traditional view that the PL is not involved in fear acquisition, further underscoring the important role of the PL in fear processing.

1.2.1.3 BLA and PL reciprocal circuits

Given the importance of the PL and BLA in fear expression and the fact that they are bidirectionally connected, many studies have explored the relationship between these two regions during fear conditioning. Broadly, mPFC-BLA evoked field potentials (EFPs) increase after fear conditioning and decrease after fear extinction, while BLA-mPFC EFPs increase during extinction

(Vouimba and Maroun, 2011). When looking more specifically at BLA projections to the PL, inhibition of all BLA cells or exclusively PL-projecting BLA neurons after conditioning decreases tone-evoked PL responses (Sotres-Bayon et al., 2012) and freezing during extinction recall, respectively (Senn et al., 2014). Similarly, BLA-responsive mPFC neurons increased their CS-related activity during olfactory fear conditioning, and inactivation of the BLA impairs this activity (Laviolette et al., 2005). In addition, PL-projecting basal amygdala (BA) neurons increase overall burst firing and tone-specific responses after fear conditioning and exhibit elevated cFos expression that is correlated with fear learning (Senn et al., 2014). Like BLA-to-PL projections, the PL-to-BLA arm of the circuit has been implicated in fear learning: inhibition of PL-BLA terminals during retrieval tones attenuates freezing (Do-Monte et al., 2015b) and PL-BLA synapses are potentiated 24 hours after fear conditioning (Arruda-Carvalho and Clem, 2014). Taken together, these data provide compelling evidence for the role of PL-BLA reciprocal circuits in fear acquisition and expression.

1.2.1.4 Infralimbic cortex

As described in the previous section, the IL is structurally quite similar to the PL. However, unlike the PL, the IL is involved *not* in fear acquisition and expression, but rather in extinction and extinction recall (Barad, 2005; Quirk and Mueller, 2008; Milad and Quirk, 2012; Marek et al., 2013; Duvarci and Pare, 2014; Giustino and Maren, 2015; Izquierdo et al., 2016). Pre-conditioning lesions of the IL have been found to delay extinction learning (Morgan et al., 1993; Morgan and LeDoux, 1995) and impair extinction recall (Quirk et al., 2000) without affecting fear acquisition. Similarly, pre-conditioning inhibition via muscimol or pre-extinction reduction of IL intrinsic excitability impairs both extinction acquisition and recall (Santini and Porter, 2010; Sierra-Mercado et al., 2011). Conversely, increasing intrinsic excitability prior to extinction training

enhances extinction and extinction recall (Santini and Porter, 2010). Using more temporally-restricted approaches, optogenetic activation or electrical microstimulation during extinction CS presentations facilitates extinction and extinction recall (Milad and Quirk, 2002; Vidal-Gonzalez et al., 2006; Kim et al., 2010; Do-Monte et al., 2015a), and optogenetic activation during recall enhances extinction expression (Kim et al., 2016). In turn, IL optogenetic inhibition during extinction or extinction recall tones impairs extinction retrieval (Do-Monte et al., 2015a; Kim et al., 2016). Moreover, specific NMDA receptor antagonism immediately after extinction training disrupts recall (Burgos-Robles et al., 2007). Given that this antagonism reduces burst firing, it was hypothesized that IL bursting is required for extinction consolidation. Indeed, several studies have reported increased bursting post-extinction that is correlated with the degree of extinction recall (Burgos-Robles et al., 2007; Santini et al., 2008). Another study found that IL neurons fire specifically during extinction recall tones and the increase in IL firing is negatively correlated with freezing (Milad and Quirk, 2002). In support of these findings regarding the importance of the IL in extinction acquisition and recall, numerous studies have observed increases in activity- and plasticity-related markers in the IL after both extinction training (Morrow et al., 1999; Zhu et al., 2018) and retrieval (Herry and Mons, 2004; Hefner et al., 2008; Knapska and Maren, 2009; Knapska et al., 2012).

Like with the PL, bidirectional connections between the IL and BLA have been implicated in fear processing. For example, increased cFos expression was observed post-extinction recall specifically in LA-projecting IL neurons (Knapska et al., 2012). Moreover, extinction increases the excitability of the IL-BLA pathway, and chemogenetic inhibition of these projections prior to extinction training impairs recall (Bloodgood et al., 2018). In the other direction of this circuit, cFos is expressed in IL-projecting BLA neurons after extinction (Senn et al., 2014). These neurons

are responsive to the extinguished CS and exhibit increased burst firing after extinction. In addition, optogenetic inhibition of BA-IL neurons during extinction retrieval increases freezing (Senn et al., 2014). Moreover, BLA-mPFC (mostly localized to the upper IL) EFP amplitude increases across extinction training (Vouimba and Maroun, 2011). Intriguingly, a recent study has also implicated PL-IL projections in fear extinction (Marek et al., 2018). IL-projecting PL neurons have increased cFos expression after extinction, and optogenetic stimulation and inhibition of these projections during extinction tones enhances and impairs extinction, respectively. These novel data reveal a previously overlooked role of the PL in extinction, via interaction with the IL. Taken together, these data underscore the importance the IL in extinction acquisition and retrieval.

1.2.2 Human homologs and their abnormalities in OCD

Although there have been both fewer and less direct studies of the neural correlates of fear processing in humans compared to rodents, the functional and anatomical human homologs of the BLA, PL, and IL – the amygdala (Rosen and Donley, 2006), dorsal anterior cingulate cortex (dACC), and ventromedial prefrontal cortex (vmPFC) (Milad and Quirk, 2012), respectively – have been implicated in similar processes. An initial study found that patients who had undergone unilateral temporal lobectomy, inclusive of the amygdala, had impairments in the acquisition of fear conditioning (LaBar et al., 1995). Subsequent imaging studies demonstrated that the amygdala is active during fear acquisition and recall (Büchel et al., 1998; LaBar et al., 1998; Cheng et al., 2003; Phelps et al., 2004; Knight et al., 2005; Kalisch et al., 2006), and that this activity is correlated with SCR (LaBar et al., 1998; Cheng et al., 2003; Phelps et al., 2004; Knight et al., 2005). Likewise, the dACC is active during fear conditioning (Büchel et al., 1998; Knight et al., 2004; Phelps et al., 2004; Milad et al., 2007a) and activity both during conditioning (Milad et al.,

2007a) and at rest (Linnman et al., 2012) is correlated with SCR. Moreover, dACC thickness is associated with SCR to the CS (Milad et al., 2007a). Notably, there is a specific increase in amygdala-dACC resting-state functional connectivity after fear acquisition, and this connectivity is predictive of subjective fear rating (Feng et al., 2014). Finally, like the IL, the vmPFC in humans is associated with extinction acquisition and recall (Quirk and Mueller, 2008). The majority of studies have focused on extinction consolidation, demonstrating that the vmPFC is active during recall (Phelps et al., 2004; Kalisch et al., 2006; Milad et al., 2007b) and that vmPFC cortical thickness is correlated with the degree of extinction retention (Milad et al., 2005; Hartley et al., 2011). However, a recent study provided evidence of an active role of the vmPFC during extinction learning (Raij et al., 2018). In this study, a prefrontal target that is functionally connected with the vmPFC was stimulated via transcranial magnetic stimulation (TMS) during extinction CS presentations. As a result, SCR magnitude was attenuated during subsequent extinction recall. These data suggest that active manipulation of the vmPFC can facilitate extinction, which has potential implications for the treatment of anxiety disorders such as OCD. Critically, structural and functional abnormalities have been reported in the amygdala, dACC, and vmPFC in individuals with OCD. The following sections will detail these abnormalities both as it pertains to fear processing and more generally.

1.2.2.1 Dorsal anterior cingulate cortex

The dACC is one of the most heavily studied regions in OCD. Abnormalities have been found at rest and in numerous contexts, including error processing (Fiddick, 2011; McGovern and Sheth, 2017; Norman et al., 2019), working memory (Koch et al., 2012; Diwadkar et al., 2015), and motor tasks (Friedman et al., 2017). Moreover, dorsal anterior cingulotomy is one of two lesion-based treatments for refractory OCD and is generally quite successful (Banks et al., 2015;

Brown et al., 2016). The other, anterior capsulotomy, is hypothesized to work in part by decreasing functional connectivity between the dACC and ventral striatum (Yin et al., 2018). Of note, chronic dACC stimulation significantly reduced OCD symptoms in a case study (De Ridder et al., 2017), which seems at odds with the cingulotomy literature given that it results in increased dACC activity; however, this is the only report of its kind. Alternatively, the cingulotomy and stimulation data together may indicate that any disruption in dACC signal – whether depressing or activating – may ameliorate OCD symptoms.

A variety of dACC structural and functional abnormalities have been observed in OCD. Structural abnormalities in adult OCD subjects include impaired white matter integrity (Wang et al., 2017), reduced grey matter volume (Matsumoto et al., 2010), and decreased cortical thickness (Kühn et al., 2013). Cortical thickness is negatively correlated with YBOCS score (Kühn et al., 2013), suggesting that dACC integrity is a predictor of disease severity. In addition, there is elevated neuroinflammation in the ACC, which could be related to structural changes (Attwells et al., 2017). Reduced dACC volume has also been reported in pediatric OCD subjects (Gilbert et al., 2018). Conversely, a separate study found that pediatric OCD patients have larger ACC volumes that are positively correlated with YBOCS obsessive subcategory scores (Rosenberg and Keshavan, 1998). However, a meta-analysis found most studies report reduced dACC structural integrity in OCD (McGovern and Sheth, 2017).

At rest, individuals with OCD display broad disruptions in glutamatergic signaling in the dACC that are correlated with symptom severity (Yücel et al., 2008). In addition, although hypoactivity was observed in a community sample with high Obsessive-Compulsive Inventory-Revised (OCI-R) scores (Cavanagh et al., 2010), most reports indicate that the dACC is hyperactive in OCD patients (McGovern and Sheth, 2017). Functional connectivity studies, on the

other hand, are mixed: one study found impaired connectivity between the dACC and the right operculum (Fitzgerald et al., 2010), while another found decreased and increased connectivity between the thalamus and right and left dACC, respectively (Chen et al., 2019). A third study found increased connectivity between the left dACC, middle temporal gyrus, and auditory cortex; increased right dACC and caudate connectivity; and decreased connectivity between the right dACC, premotor area, and supplementary motor area (Zhang et al., 2017b). In this study, right dACC and caudate connectivity was correlated with symptom severity. Together, these structural and functional connectivity studies suggest that dACC abnormalities play an important role in OCD symptomology.

The findings regarding dACC functioning in OCD during symptom provocation are much clearer. While one study did not observe any ACC changes during provocation (Chen et al., 2004), most have reported elevated dACC activity (Rauch et al., 1994; Breiter et al., 1996; Adler et al., 2000; Mataix-Cols et al., 2004; Simon et al., 2010, 2014), with specific hyperactivation during presentation of washing- and checking-related images (Mataix-Cols et al., 2004). Moreover, after treatment with either SSRIs or CBT, ACC activity during symptom provocation is reduced (Nakao et al., 2005). In addition, dACC activation when viewing fearful faces is correlated with aggression and checking symptom dimensions (Via et al., 2014). Interestingly, several studies found specific abnormalities in dACC-amygdala circuitry. For example, OCD patients displayed decreased functional and structural dACC-amygdala connectivity during threat assessment, both of which were inversely correlated with symptom severity (Admon et al., 2012). Conversely, prefrontal-amygdala connectivity is enhanced during symptom provocation (Paul et al., 2020) and presentation of fearful faces (Cardoner et al., 2011), underscoring potential differences at rest and during fear-relevant tasks. As previously mentioned, there are very few fear conditioning studies

in OCD, and of these, only one has looked at the dACC. In this study, dACC activity was negatively correlated with extinction retention in OCD patients (Milad et al., 2013). Combined with the findings of hyperactivity during symptom provocation and presentation of fearful faces, these data indicate that elevated dACC activity may be related to improper threat assessment (Fiddick, 2011; McGovern and Sheth, 2017).

While not directly related to fear processing, an important area of research regarding the dACC and OCD is error signaling. Investigators have repeatedly found that individuals with OCD display heightened error processing, and that this behavior is associated with hyperactivity in the dACC (Norman et al., 2019). Initially, one group observed larger and more prolonged electrophysiological error-related negativity (ERN) signals that correlated with symptom severity in OCD patients during an interference task (Gehring et al., 2000). ERNs are typically thought to arise from the dACC, and the recordings in this study were consistent with ACC localization. Subsequent studies verified that the ACC was hyperactive (Ursu et al., 2003) and found specific increases in functional connectivity between the dACC and prefrontal regions during error processing (Schlösser et al., 2010). Similar results were found in pediatric OCD: dACC activity was elevated during an interference task (Fitzgerald et al., 2010) and the development of OCD in a longitudinal sample was associated with enhanced performance monitoring and reduced dACC volume (Gilbert et al., 2018). Similarly, individuals with high OCI-R scores displayed impaired dACC inactivation during errors (i.e. dACC hyperactivity) (Cavanagh et al., 2010). In contrast to these studies, the ACC was more active during error processing after treatment with SSRIs or CBT compared to pre-treatment (Nakao et al., 2005). With the exception of this study, the overall findings are consistent: patients with OCD display elevated error monitoring that is associated with dACC hyperactivity. This, combined with accumulating evidence of impaired inhibitory control

in distinct circuits (Norman et al., 2019), has led some to postulate that aberrant error signaling drives some OCD symptom. If error processing is elevated and inhibitory control impaired, then individuals with OCD may be unable to adapt their behavior – the feeling that something is "off" will persist (obsessions), generating distress and anxiety. The lack of error correction will render attempts to correct those feelings via performance of compulsive behaviors ineffective, thus causing patients to become stuck in compulsive loops (Norman et al., 2019). An inability to resolve perceived errors could therefore promote threat overestimation and fear generalization (Fiddick, 2011; McGovern and Sheth, 2017).

1.2.2.2 Amygdala

As with the dACC, the amygdala is purported to play an important role in OCD symptomology (Wood and Ahmari, 2015). In addition to abnormalities in dACC-amygdala signaling (Cardoner et al., 2011; Admon et al., 2012; Paul et al., 2020), structural and functional changes have been reported in the amygdala itself, albeit with more mixed results than the dACC. For instance, in pediatric OCD patients, one study found no alterations in amygdala volume (Rosenberg and Keshavan, 1998), while another reported increased volume (Szeszko et al., 2004). In the latter study, the investigators further demonstrated that enlarged amygdala volume was reduced following pharmacological treatment with SSRIs. Other studies have found impaired structural connectivity between the amygdala and other regions (Reess et al., 2016; Rus et al., 2017) that is negatively correlated with symptom severity (Rus et al., 2017). Enhanced functional connectivity between the amygdala and other regions has been reported as well (Rus et al., 2017).

During symptom provocation, only one study observed no differences in amygdala activity (Adler et al., 2000). Rather, most studies have reported enhanced amygdala activation (Breiter et al., 1996; Mataix-Cols et al., 2004; van den Heuvel et al., 2004; Simon et al., 2010, 2014). In one

such study, amygdala hyperactivation was found to be specifically associated with washing-related symptoms (Mataix-Cols et al., 2004). In addition to symptom provocation, several studies have observed amygdala hyperactivation during presentation of fearful faces (Cardoner et al., 2011; Via et al., 2014). One of these studies found that task-dependent amygdala hyperactivation was correlated with the severity of aggression/checking and sexual/religious symptom dimensions (Via et al., 2014). Regarding fear processing, the only study in which amygdala activity was measured during fear conditioning in OCD patients found no abnormalities (Milad et al., 2013). However, given that this is the only study of its kind, more research is required. Finally, a recent study found that effective deep brain stimulation of the ventral anterior limb of the internal capsule – a treatment for refractory OCD that reduces anxiety, obsession, and compulsions – is associated with decreased functional connectivity between the amygdala and insula, and increased top-down control via the vmPFC (Fridgeirsson et al., 2020).

1.2.2.3 Ventromedial prefrontal cortex

Compared to the dACC and amygdala, there are significantly fewer studies of the vmPFC in OCD. Despite the relative dearth of research, there have been reports of structural abnormalities and dysfunction during reward, interference, and fear processing. Broadly, a meta-analysis revealed dysconnectivity focused around the vmPFC both between and within commonly-studied brain networks (Gürsel et al., 2018). When considering task-based abnormalities, one study reported vmPFC hyperactivity to errors incurring loss in an interference task, as well as enhanced functional connectivity between the vmPFC and anterior insula/frontal operculum and thalamus, in OCD patients compared to healthy controls (Stern et al., 2011). Several other studies reported vmPFC dysfunction in OCD patients during reward processing, including stronger connectivity with the orbitofrontal cortex (Alves-Pinto et al., 2019) and posterior cingulate cortex (Koch et al.,

2018). In addition, individuals with OCD displayed vmPFC hyperactivity to ambiguous feedback, such that there was no difference between the vmPFC signal to negative and ambiguous feedback (Becker et al., 2014). This was in stark contrast to healthy controls, whose vmPFC signal differentiated between these types of feedback.

In the context of fear conditioning, only two studies have investigated the role of the vmPFC in OCD. In the first study, the vmPFC was hypoactive during both extinction and extinction recall in individuals with OCD, in which deficits in extinction retrieval were observed (Milad et al., 2013). Conversely, the second study found that despite a lack of behavioral or physiological impairments in extinction recall in OCD compared to healthy controls, vmPFC activity during retrieval was negatively correlated with task performance in the OCD group alone (Giménez et al., 2019). This suggests individual differences in vmPFC functionality are relevant to fear extinction. In support of these observations, decreased cortical thickness in a vmPFC subregion was reported in OCD patients (Fullana et al., 2014). Furthermore, diminished resting-state functional connectivity between the BLA and vmPFC was predictive of better CBT outcomes (Fullana et al., 2017). Given that CBT is an extinction-based therapy, these data provide further support for the theory that fear extinction circuitry is altered in OCD.

As an interesting side note, many of the vmPFC, amygdala, and dACC studies in OCD individuals reported significant effects of laterality. Abnormalities were predominantly observed in the left hemisphere for both the dACC (Rauch et al., 1994; Mataix-Cols et al., 2004; Matsumoto et al., 2010; Simon et al., 2010; Zhang et al., 2017b; Yin et al., 2018) and amygdala (Mataix-Cols et al., 2004; Szeszko et al., 2004; van den Heuvel et al., 2004; Simon et al., 2010, 2014; Reess et al., 2016; Fridgeirsson et al., 2020). Several studies reported selective effects in the right dACC (Adler et al., 2000; Banks et al., 2015; Zhang et al., 2017b; Gilbert et al., 2018; Chen et al., 2019),

while only one amygdala study favored the right hemisphere (Via et al., 2014). In the vmPFC, three studies reported selective effects in the left hemisphere (Milad et al., 2013; Fullana et al., 2014; Koch et al., 2018). The remaining studies either did not specify or reported bilateral effects in both regions. However, the relative importance of the left hemisphere is still worth noting: given this lateralization, paired with emerging evidence of lateralization in model systems (Rodgers and Andrew, 2002; Halpern et al., 2005), specific investigation of the left hemisphere in both clinical and OCD-relevant preclinical models may advance our understanding of OCD and uncover potential treatments targets. In summary, individuals with OCD display elevated fear processing and threat-related abnormalities in dACC, amygdala, and vmPFC signaling. These data indicate that fear processing is an important component of OCD and underscore the need to investigate these deficits in a mechanistic manner.

1.3 SAPAP3 knockout mouse model for studying OCD-relevant behavior

In order to assess the neural underpinnings of aberrant fear processing in the context of compulsive behavior, it is useful to turn to mouse models. Working with mice enables mechanistic dissection of circuitry and direct assessment of causality. The SAPAP3 knockout (KO) mouse model, first developed by Welch et al. (2007), is the most commonly used genetic model of OCD-relevant behavior. The *Sapap3* protein, otherwise known as *Dlgap3*, is located at excitatory postsynaptic densities and either directly or indirectly interacts with a variety of signaling and structural molecular families, including post-synaptic density protein 95 (PSD95), metabotropic glutamate receptors (mGluRs), NMDA receptors, Shank, and Homer (Kindler et al., 2004; Welch et al., 2004; Ade et al., 2016). Critically, the human *Sapap3*/*Dlgap3* gene has been linked to OCD.

For example, multiple rare mutations were detected in the *Sapap3* gene in patients with comorbid OCD and trichotillomania (a compulsive hair-pulling disorder) (Züchner et al., 2009). Similarly, in OCD patients with comorbid grooming disorders (trichotillomania, skin-picking, nail-biting), several *Sapap3* single nucleotide polymorphisms were associated with pathological grooming (Bienvenu et al., 2009). Moreover, recent postmortem work from our lab has found that *Sapap3* mRNA expression is decreased in the orbitofrontal cortex (OFC), caudate, and nucleus accumbens of OCD patients (Piantadosi et al., 2019). In addition, other members of the *Sapap* gene family have been implicated in OCD. Although it failed to reach genome-wide significance, *Sapap1* has been consistently identified as a strong candidate gene in OCD genome-wide association studies (GWAS) (Stewart et al., 2013; Mattheisen et al., 2015; Den Braber et al., 2016; IOCDF-GC and OCGAS, 2018). Moreover, there was a trend towards association between several SNPs in the *Sapap2* gene and OFC volume in a sample of pediatric OCD patients (Wu et al., 2013).

In SAPAP3 KO mice, the global removal of the *Sapap3* gene results in compulsive grooming and elevated anxiety-like behavior (Welch et al., 2007). Treatment with SSRIs ameliorates both of these behaviors, indicating that this model has predictive validity for OCD. Moreover, numerous studies have observed deficits in cortico-striatal signaling in KO mice (Welch et al., 2007; Chen et al., 2011; Wan et al., 2011, 2014; Burguière et al., 2013; Ade et al., 2016; Corbit et al., 2019; Hadjas et al., 2020), which is broadly consistent with findings of aberrant cortico-striatal functioning in human OCD (Huey et al., 2008; Del Casale et al., 2011; Wu et al., 2012; Naaijen et al., 2015; Piras et al., 2015). Interestingly, striatum-specific reintroduction of *Sapap3* in KO mice rescues both grooming and anxiety-like behavior (Welch et al., 2007). Together, these data support the use of SAPAP3 KO mice in modeling OCD-relevant behavior and neural circuitry.

1.4 Goals of the current dissertation

The main goal of this work was to elucidate the mechanisms of aberrant fear processing in animals with OCD-like behavior. First, I characterized fear processing in SAPAP3 KO mice, an OCD-relevant model (Chapter 2). To achieve this, I assessed freezing during fear conditioning and baseline sensory processing important for interpretation of results from our paradigm. Next, I looked at broad neural activation patterns in fear-associated regions after fear conditioning in SAPAP3 KO and WT mice (Chapter 3). This was measured via histological examination of the protein form of the immediate early gene, cFos. Finally, I conducted *in vivo* analysis of the role of the prelimbic cortex (PL) and basolateral amygdala (BLA) in aberrant fear processing (Chapter 4). In the first part of this chapter, I describe the activity of these regions in SAPAP3 KO and WT mice during fear conditioning as observed via *in vivo* fiber photometry. Lastly, I examined the functional role of the PL in fear acquisition via optogenetic inhibition. Taken together, these data shed light on the mechanisms of aberrant fear processing in SAPAP3 KO mice, which may have implications for both the neural basis of and potential therapies for OCD.

2.0 SAPAP3 knockout mice display enhanced fear conditioning

2.1 Introduction

Obsessive-compulsive disorder (OCD), which is characterized by intrusive thoughts (obsessions) and repetitive behaviors (compulsions) that are often performed to alleviate the anxiety that accompanies those obsessions, is a devastating psychiatric illness that affects 1-3% of the Unites States population (Kessler et al., 2005, 2012). This disorder is associated with an overall lower quality of life, poorer physical health, comorbid mental disorders, impairments in professional and personal settings (Bobes et al., 2001), and increased mortality (Eaton et al., 2008). From a financial perspective, the estimated burden is $10.6 billion per year in the United States alone (Eaton et al., 2008). Unfortunately, despite the significant societal and economic costs, both current pharmacological (Soomro et al., 2008; Farris et al., 2013; Pittenger and Bloch, 2014) and cognitive-behavioral therapies (Hezel and Simpson, 2019; Law and Boisseau, 2019) have limited efficaciousness.

Fear is a key component of OCD – it is associated with many OCD symptom domains (Raines et al., 2015; Rozenman et al., 2017), and compulsions that are related to fear are predictive of worse long-term outcomes (Ferreira et al., 2020). One theory of OCD pathogenesis is that patients form maladaptive fear associations with neutral stimuli, leading to maintenance of fear and avoidance. This was initially supported by findings of accelerated eyeblink conditioning to a neutral stimulus in individuals with obsessive-compulsive traits (Tracy et al., 1999). Subsequent work bolstered this theory by reporting enhanced acquisition (Geller et al., 2017), impaired fear extinction (Nanbu et al., 2010; Geller et al., 2017), blunted extinction recall (Milad et al., 2013;

McLaughlin et al., 2015), and elevated skin conductance responses during fear conditioning (McGuire et al., 2016) in OCD patients compared to healthy controls. Moreover, structural and functional imaging studies have identified abnormalities in the amygdala in OCD patients (Szeszko et al., 2004; Diniz et al., 2012; Reess et al., 2016; Rus et al., 2017), indicating that fear circuitry may be altered. Despite this evidence, there is a scarcity of investigations into the neural mechanisms of aberrant fear processing in OCD. Understanding how fear is processed in OCD seems particularly important when considering current treatment options: exposure with response prevention (ERP), a first-line OCD treatment, is an extinction-based therapy. Thus, elucidating the neural mechanisms of how individuals with OCD extinguish fear could help improve existing treatments. Moreover, examining how OCD patients initially acquire maladaptive fear associations could facilitate the development of both pharmacological and behavioral non-extinction-based therapies.

In order to examine the neural underpinnings of fear learning in the context of OCD, we turned to the SAPAP3 knockout (KO) mouse model. These mice, in which the post-synaptic density gene *Sapap3* has been globally removed, demonstrate several OCD-relevant behaviors. Chief amongst these is perseverative self-grooming behavior, which KO mice will perform despite substantial self-harm (Welch et al., 2007). In addition to grooming, SAPAP3 KO mice display elevated anxiety behavior. These behaviors are correlated with alterations in cortico-striatal signaling (Welch et al., 2007; Chen et al., 2011; Wan et al., 2011, 2014; Burguière et al., 2013; Ade et al., 2016; Corbit et al., 2019), which aligns with the large body of work describing cortico-striatal abnormalities in human OCD (Saxena et al., 1998; Pittenger et al., 2011; Ting and Feng, 2011). Moreover, selective viral reintroduction of the SAPAP3 protein into the striatum reduces both anxiety- and compulsive-like behavior in these mice (Welch et al., 2007). Critically, treatment

with SSRIs, the only first-line pharmacotherapy for OCD, is also effective in reducing compulsive grooming and anxiety-like behavior in KOs (Welch et al., 2007), further bolstering the translational potential of this model. While fear conditioning has yet to be explicitly examined in these mice, unpublished data from our lab suggest that abnormalities are present. Specifically, during a platform-mediated avoidance task (Bravo-Rivera et al., 2014), KO mice spent more time freezing to the CS than WT mice (data not shown). Based on these data, we hypothesized that KO mice would display broad abnormalities in fear learning and therefore be a useful model in which to study fear in the context of OCD-relevant behavior.

The aim of the following experiments was to characterize fear processing in SAPAP3 KO mice. To that end, we first conducted auditory fear conditioning in SAPAP3 KO and WT mice. After demonstrating that KO mice display elevated fear conditioning, we examined the potential contribution of sensory processes relevant to our paradigm to these findings. We found that there are no differences in nociception between KO and WT mice. Interestingly, we did observe slightly elevated reactivity to sequential tone presentations in KO mice; however, these differences cannot fully account for the enhanced fear conditioning seen in KO mice. Taken together, SAPAP3 KOs display elevated fear conditioning that cannot be attributed to abnormalities in nociception or auditory signaling.

2.2 Methods

2.2.1 Animals

Male *Sapap3*-KOs and WT littermates were used for these experiments. Mice were group-housed in reverse light cycle conditions and had *ad libitum* access to food and water. The fear conditioning cohort consisted of 12 WT and 13 KO mice, all 4-6 months old at the time of testing. Nociceptive testing was conducted in these same mice 8 weeks after fear conditioning. The tone-only conditioning cohort consisted of 10 WT and 9 KO 4-6-month-old mice. These mice were exposed to the acoustic startle paradigm two days later. All experiments were approved by the Institutional Animal Use and Care Committee at the University of Pittsburgh in compliance with National Institutes of Health guidelines for the care and use of laboratory animals.

2.2.2 Fear conditioning

Fear conditioning consisted of three sessions on consecutive days: habituation, conditioning, and recall (Figure 2-1). Mice were handled daily for a week prior to testing. Each day began with a 1-hour acclimatization period in the room immediately outside of the fear conditioning room (holding room). During the habituation session, mice were exposed to the fear conditioning chamber (Coulbourn Instruments Mouse Test Cage) without any tone presentations. The habituation session duration was equal to the duration of the conditioning session on the following day (Figure 2-1a). On day two, mice underwent fear conditioning. The session began with a 3-minute pre-tone period, followed by three CS-US pairings separated by pseudorandom (90-120s) ITIs (Figure 2-1b). The CS was a 20-second, 75 dB, 5 kHz tone that co-terminated with

a 2-second, 1 mA shock (US). Recall was assessed 24 hours later. This session began with a 3-minute pre-tone period, followed by 5 CS presentations separated by a pseudorandom ITI of 30-60 seconds (Figure 2-1c).

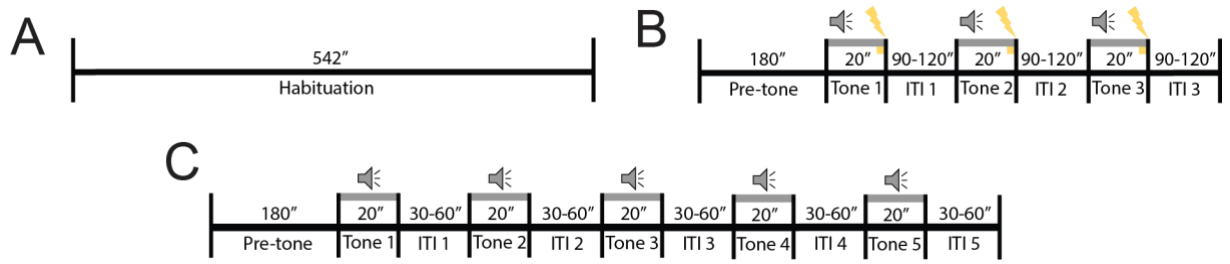

Figure 2-1. Fear conditioning protocol

A) Habituation session. Mice were exposed to the conditioning chamber without any stimuli for 542 seconds. **B)** Conditioning session. After a 3-minute pre-tone period, mice were exposed to 3 CS-US pairings (20-second tone co-terminating with a 2-second shock). CS-US pairings were separated by a pseudorandom ITI of 90-120 seconds. **C)** Recall session. After a 3-minute pre-tone period, mice were exposed to 5 CS presentations (20-second tone). Tones were separated by a pseudorandom ITI of 30-60 seconds.

Habituation and conditioning sessions were run in Context A, which consisted of the standard fear conditioning chamber with shock bar floor, housed within a sound-attenuating chamber; lemon scent; and red overhead room (not chamber) light. Recall was conducted in Context B, which consisted of a smooth, solid floor; experimenter-fabricated triangular chamber insert; anise scent; and white overhead room light. Chambers were cleaned between animals using an odorless 5mM NaOH solution. After each session, mice were left undisturbed in the holding room for 1 hour. For the tone-only control group, habituation and conditioning sessions were conducted as described above, except with the omission of the US during conditioning. All freezing was hand-scored by well-trained, blinded observers using The Observer XT (Noldus), with the exception of recall freezing for the initial cohort, which was scored automatically using FreezeFrame (Actimetrics).

2.2.3 Nociceptive sensitivity

2.2.3.1 von Frey test

Mechanical nociception was tested using von Frey filaments. The testing apparatus consisted of bottomless clear acrylic chambers placed on top of a wire mesh grid. On the first day, mice were allowed to habituate to the chambers for 20 minutes. On the testing day, mice were given another 20-minute habituation period. Then, when the subject was still and all four paws were on the mesh grid, the 3.84 size filament (0.6 grams of force) was pressed against the plantar surface of the left hind paw until the filament buckled. This was done three times to comprise one trial. If the mouse sharply withdrew or began licking its paw during or immediately after any of the three presentations, that trial was marked as a response. If there were no discernable responses to any of the three presentations, it was marked as a non-response. The same process was repeated for the right hind paw. Testing then proceeded according to the simplified up-down method (SUDO) (Bonin et al., 2014): if the previous trial was marked as a non-response, the next largest von Frey filament was used on the subsequent trial, while the next smallest was used following response trials. This continued until 5 trials had been completed on each hind paw, with trials alternating between the left and right hind paws. There was a minimum of 10 minutes between each trial on the same hind paw. Paw withdrawal threshold (PWT) was then calculated using the SUDO method. All testing was conducted under red light.

2.2.3.2 Hargreaves test

Thermal nociception was assessed using the Hargreaves test. The testing apparatus consisted of clear acrylic chambers placed on top of a clear glass surface. Mice were given 20 minutes to habituate to the chambers on a separate day. On the subsequent day, mice were again

given 20 minutes of habituation, after which testing began. When the subject was still and all four paws were on the glass floor, an infrared light beam (Plantar Analgesia Meter, IITC Life Science) was focused onto the plantar surface of the left hind paw. Upon removal of the paw, the light beam was turned off and paw withdrawal latency was recorded. This process was repeated for the right hind paw and then twice more for each paw, for a total of three times per hind paw. There was a minimum of 5 minutes between each trial on the same hind paw. Paw withdrawal latency was calculated by taking an average of the three trials. All testing was conducted under red light.

2.2.4 Acoustic startle

Acoustic startle threshold was assessed using the SR-LAB Startle Response System (San Diego Instruments). Mice were handled daily beginning 4 days prior to the experiment. At the start of each day, mice were given a 20-minute acclimatization period outside of the testing room. On the first day, mice were habituated to the startle chambers with just white noise (65 dB). On day 2, mice were habituated to the chambers for 5 minutes, after which 4 baseline startle stimuli of 120 dB were presented. Next, there were 10 presentations (40 ms) each of 70, 80, 90, 100, 110, and 120 dB stimuli. These stimuli were given a pseudorandom order such that there was equal distribution across both halves of the session and no single stimulus type had more than two sequential presentations. The session ended with another 4 presentations of 120 dB stimuli. ITIs range from 5-30 seconds, with an average of 15 seconds. 65 dB white noise was present throughout the session, except during 40ms stimuli presentations. Testing was conducted in reverse light cycle conditions, so startle chambers lights were not illuminated. Startle amplitude was normalized to body weight.

2.2.5 Statistics and data analysis

Data were analyzed using Microsoft Excel and Graphpad Prism. Repeated measures ANOVAs were used for fear conditioning and acoustic startle data. T-tests were used for analysis of von Frey and Hargreaves tests, as well as post-hoc analysis of ANOVAs. Geisser-Greenhouse corrections were used for all ANOVAs.

2.3 Results

2.3.1 SAPAP3 KO mice display enhanced fear conditioning

To characterize fear processing in SAPAP3 KO mice, we conducted auditory fear conditioning in WTs and KOs (WT n=12, KO n=13). After a 3-minute pre-tone period, mice were exposed to three CS-US pairings (Figure 2-2a). As expected, both groups increased freezing to the tones across the conditioning session [Figure 2-2b; main effect of time: $F(2.506,57.65)=123.5$, $p<0.0001$]. However, KO mice exhibited a steeper learning curve, indicating enhanced fear learning [main effect of genotype: $F(1,23)=14.25$, $p=0.001$; time x genotype interaction: $F(3,69)=9.234$, $p<0.0001$. Post-hoc tests: WT vs. KO tones 2 ($p<0.0001$) and 3 ($p=0.0003$); pre-tone vs. tones 2 and 3, tones 1 vs. 2, 1 vs. 3, and 2 vs. 3 for both WTs and KOs (all p-values <0.001)]. This increase in freezing to conditioned tones was still apparent when tested 24 hours later [Figure 2-2c, d; main effect of time: $F(3.794,87.26)=18.48$, $p<0.0001$; main effect of genotype: $F(1,23)=18.97$, $p=0.0002$. Post-hoc tests: WT vs. KO tones 1 ($p=0.02$), 3 ($p=0.0009$), 4

(p=0.0432), and 5 (p=0.0373); pre-tone vs. all tones for WTs and KOs (all p<0.05), except WT pre-tone vs. tone 3].

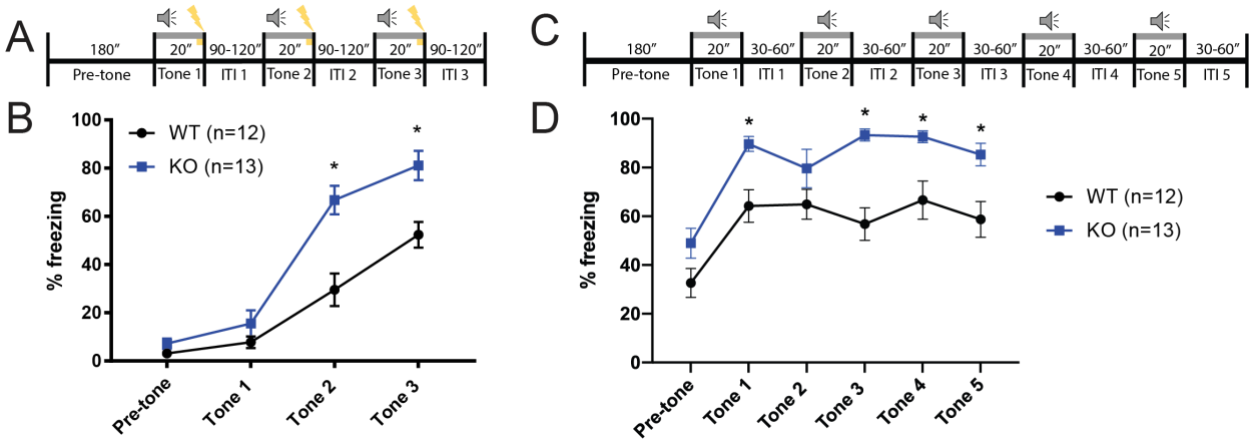

Figure 2-2. SAPAP3 KO mice display enhanced fear conditioning

A) Timeline of fear conditioning protocol. Sessions began with a three-minute pre-tone period, followed by three CS/US pairings. The CS was a 20-second tone that co-terminated in a 2-second foot-shock. CS/US pairings were separated by a pseudorandom ITI of 90-120 seconds. **B)** % freezing for SAPAP3 WTs and KOs during the pre-tone period and tones. KOs (blue squares; n=13) have a greater increase in % freezing to the tone over time compared to WTs (black circles; n=12). Main effect of time [F(2.506,57.65)=123.5, p<0.0001] and genotype [F(1,23)=14.25, p=0.001]; time x genotype interaction [F(3,69)=9.234, p<0.0001]. Post-hoc tests: WT vs. KO, tones 2 (p<0.0001) and 3 (p=0.0003); tones 1 vs. 2, 1 vs. 3, and 2 vs. 3 for both WTs and KOs (all p-values <0.0001). **C)** Timeline of fear recall. Sessions began with a three-minute pre-tone period, followed by 5 CS presentations (20s). ITIs were pseudorandom and ranged from 30-60 seconds. **D)** % freezing for WTs and KOs during recall. KO mice have elevated freezing compared to WT mice. Main effect of time [F(3.794,87.26)=18.48, p<0.0001] and genotype [F(1,23)=18.97, p=0.0002]. Post-hoc tests: WT vs. KO tones 1 (p=0.02), 3 (p=0.0009), 4 (p=0.0432), and 5 (p=0.0373); pre-tone vs. all tones for both WTs and KOs (all p<0.05), except WT pre-tone vs. tone 3.

2.3.2 There are no differences in nociception between SAPAP3 WT and KO mice

A potential explanation for the enhanced fear conditioning seen in KOs is that they perceive the shock as a more painful stimulus than WT mice. In order to assess this possibility, we measured mechanical and thermal nociception in WT and KO mice. 8 weeks after fear conditioning, the same cohort of mice (WT: n=12, KO: n=13) was exposed to the von Frey test (Figure 2-3a). In this paradigm, which measures mechanical nociception, weighted filaments that apply different levels of force are pressed against the mouse's hind paw. The weight is increased until a withdrawal or pain response is observed. Filaments surrounding the target filament are then used to narrow in on the pain withdrawal threshold (PWT) force. As shown in Figure 2-3b, there were no differences in PWT force between WT and KO mice for either the left ($p=0.878$, $t=0.155$, $df=23$) or right hind paw ($p=0.245$, $t=1.193$, $df=23$). One day after the von Frey test, thermal nociception was assessed using the Hargreaves test. In this paradigm, an infrared beam is aimed at the hind paw and paw withdrawal latency is recorded (Figure 2-3c). As with mechanical pain, there were no differences in thermal nociception between WT and KO mice for either the left ($p=0.992$, $t=0.0104$, $df=23$) or right hind paw ($p=0.0889$, $t=1.776$, $df=23$) (Figure 2-3d).

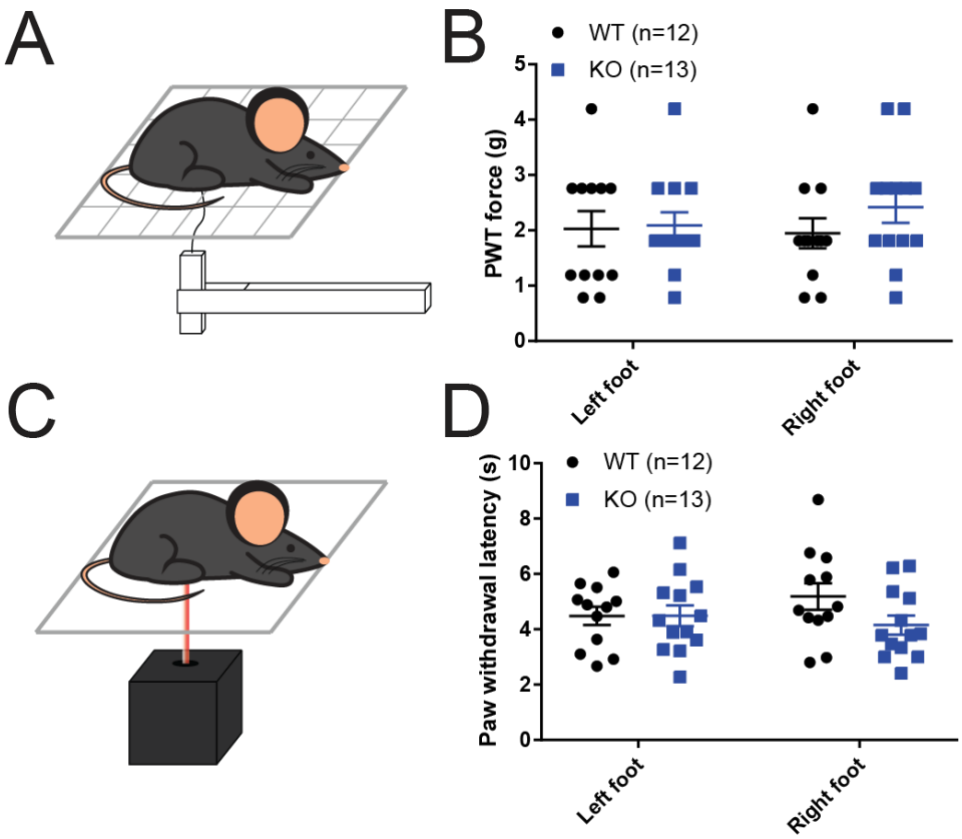

Figure 2-3. Nociception does not differ between SAPAP3 KO and WT mice

Mechanical and thermal nociception as measured by the von Frey (**A**) and Hargreaves (**C**) tasks. **B)** The force measured at the paw withdrawal threshold (PWT) in the von Frey test is not different for WT (n=12) and KO (n=13) mice for either the left (p=0.878, t=0.155, df=23) or right hind paw (p=0.245, t=1.193, df=23). **D)** Paw withdrawal latency in the Hargreaves test is not different for WT (n=12) and KO (n=13) mice for either the left (p=0.992, t=0.0104, df=23) or right hind paw (p=0.0889, t=1.776, df=23).

2.3.3 Acoustic sensitivity in SAPAP3 KO mice is largely unaltered

Another possible explanation for the enhanced fear conditioning seen in KO mice is altered acoustic sensitivity. Accordingly, we tested auditory processing using two measures. First, we exposed mice to the same fear conditioning protocol as before, except without any shocks (Figure 2-4a). Surprisingly, in this "tone-only" conditioning, KO mice displayed a slight increase in

freezing over time compared to WTs (Figure 2-4b): there was both a main effect of time [F(1.401,23.82)=5.365, p=0.02] and a time x genotype interaction [F(3,51)=4.211, p=0.0098], as well as a nearly significant main effect of genotype [F(1,17)=4.334, p=0.0528]. Post-hoc tests revealed that KO mice froze more to tone 3 than WT mice (p=0.0037). Moreover, freezing during the pre-tone period was lower than freezing to both tones 2 (p=0.008) and 3 (p=0.0001) and tone 1 freezing was lower than tone 3 freezing (p=0.0063) for KO mice, while there were no within-genotype differences for WTs.

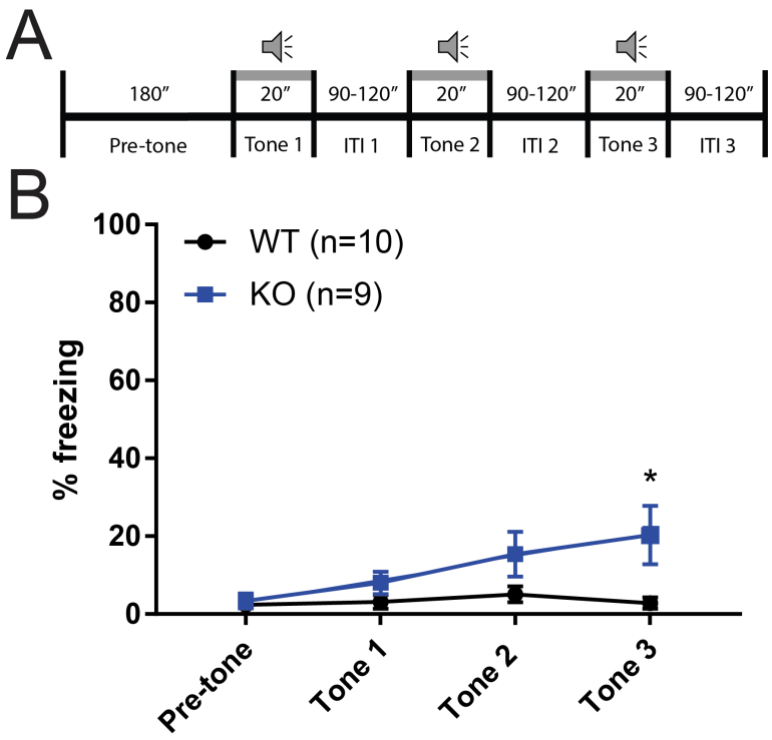

Figure 2-4. SAPAP3 KO mice display a small increase in freezing during tone-only conditioning

A) Timeline of tone-only conditioning experiment. Following a 3-minute pre-tone period, mice were exposed to 3 CS presentations. Each CS lasted 20s and was separated from the subsequent trial by a pseudorandom ITI of 90-120". **B)** % freezing for tone-only exposure: main effect of time [F(1.401,23.82)=5.365, p=0.02]; time x genotype interaction [F(3,51)=4.211, p=0.0098]; trend effect of genotype [F(1,17)=4.334, p=0.0528]. Post-hoc tests: WT vs. KO, tone 3 (p=0.0037).

As a second measure of audition, we assessed acoustic startle threshold by exposing mice (WT n=10, KO n=9) to auditory stimuli of varying intensities and measuring the amplitude of their startle response (Figure 2-5a). There was a main effect of decibel, indicating that both WT and KO startled more to louder stimuli [Figure 2-5b; $F(1.289,21.92)=35.01$, $p<0.0001$]. Interestingly, there was a trend decibel x genotype interaction [$F(5,85)=2.174$, $p=0.0645$], wherein KO mice displayed a slightly blunted startle amplitude to higher decibel stimuli compared to WT mice. However, because the output of the startle chambers is dependent on force, the weight of each animal is a strong determinant of startle amplitude. Since SAPAP3 KO mice weigh significantly less than their WT littermates [acoustic startle cohort (Figure 2-5c; $p=0.0046$, $t=3.261$, $df=17$)], we corrected for this factor by dividing each animal's startle amplitude by its weight. While there was a still a main effect of decibel [Figure 2-5d; $F(1.337,22.72)=41.76$, $p<0.0001$], there was not a main effect of genotype or a decibel by genotype interaction, indicating that the normalized startle amplitudes for WT and KO mice did not differ.

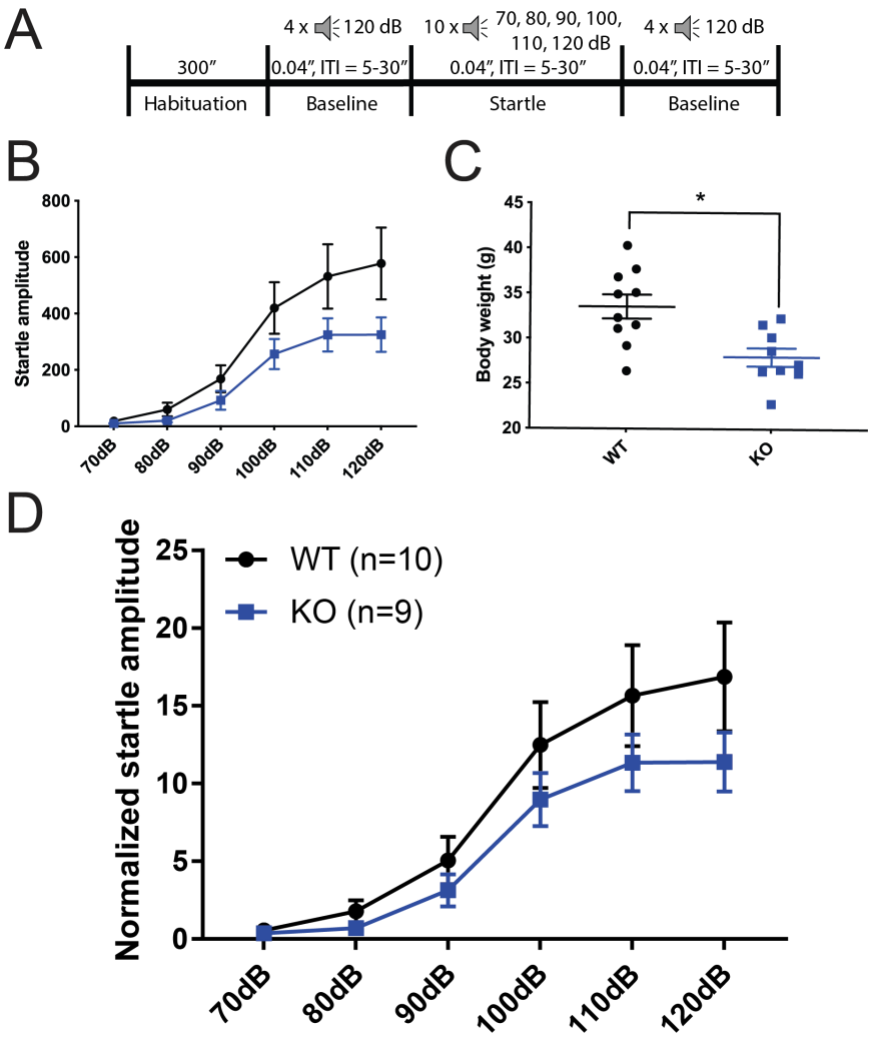

Figure 2-5. Acoustic startle threshold does not differ between SAPAP3 KO and WT mice

A) Timeline of acoustic startle threshold paradigm. A 5-minute habituation period was followed by 4 baseline presentations of a 120dB stimulus. During the startle section of the session, there were 10 presentations each of 70, 80, 90, 100, 110, and 120dB stimuli. The session ended with 4 more baseline presentations of a 120dB stimulus. **B)** Startle amplitude to each stimulus for WT (n=10) and KO (n=9) mice. Main effect of decibel [$F(1.289,21.92)=35.01$, $p<0.0001$]; trend decibel x genotype interaction [$F(5,85)=2.174$, $p=0.0645$]. **C)** Body weight for WT (n=10) and KO (n=9) mice. KO mice weigh less than WT mice ($p=0.0046$, $t=3.261$, $df=17$). **D)** Startle amplitude normalized to body weight for WT and KO mice. No main effect of genotype on acoustic startle amplitude [$F(1,17)=1.588$, $p=0.2247$]; main effect of decibel [$F(1.337,22.72)=41.76$, $p<0.0001$].

2.4 Discussion

In these studies, we first demonstrated that SAPAP3 KO mice display enhanced fear conditioning, as measured by the percentage of time spent freezing to the CS. These data were in line with our predictions. Preliminary platform-mediated avoidance data in this same strain showed that KOs spent more time freezing during the CS than WTs, suggesting that this would also be the case in standard fear conditioning. Furthermore, given that SAPAP3 KO mice are used to model OCD-relevant behaviors, such as compulsions and anxiety, it is not surprising that they exhibited heightened fear. As mentioned in the introduction, fear as measured by self-reports is associated with OCD symptoms (Raines et al., 2015; Rozenman et al., 2017) and worse long-term outcomes in individuals with OCD (Ferreira et al., 2020). Moreover, patients with OCD exhibit deficits in fear conditioning, including elevated acquisition (Geller et al., 2017), impaired extinction (Nanbu et al., 2010; Geller et al., 2017), and diminished extinction retention (Milad et al., 2013; McLaughlin et al., 2015).

Next, we examined the contribution of sensory processing to the enhanced fear conditioning we saw in KO mice. We found that there were no differences in either mechanical or thermal nociception. A potential confound in these data is that the mice had been exposed to fear conditioning prior to nociceptive testing. Thus, it is possible that exposure to foot shocks could have differentially altered pain signaling in KO vs. WT mice. However, given both the long period of time in between fear conditioning and nociceptive analysis (8 weeks) and the fact that we did not see any genotype differences, we think this concern is minimal. Moreover, our data complement findings from the original characterization of SAPAP3 KO mice, wherein no differences were found in sensory innervation of facial tissue (Welch et al., 2007). This does not rule out the possibility of altered sensory innervation of paw tissue, which is directly relevant to

our experiment. Taken together, however, these data strongly suggest that nociception abnormalities are not contributing to the observed fear-learning abnormalities in SAPAP3 KO mice.

Finally, we assessed acoustic sensitivity in SAPAP3 KO and WT mice using two measures: acoustic startle threshold and tone-only conditioning. Prior to body weight correction, KO mice exhibited a trend toward lower startle amplitudes to high intensity acoustic stimuli than WT mice. This trend is in the opposite direction from what we might have predicted. If acoustic sensitivity contributes to enhanced fear conditioning in KO mice, we might expect the KO startle amplitude to be higher than the WT amplitude at a given decibel. The fact that we observed the opposite suggests that this is not the case. However, since startle amplitude is measured by movement force and KO mice weigh less than WTs, it was necessary to consider body weight as a potential confound. After correcting for body weight, there were no genotype differences in acoustic startle threshold. Conversely, we did find genotype differences during tone-only conditioning, a paradigm which was identical to original fear conditioning test, except with the exclusion of a US. We observed a small, but significant, increase in freezing across trials in KO mice, with significantly more freezing to the final tone in KOs than WTs after post-hoc analysis. This suggests that KO mice have more fearful reactions to unpredicted stimuli in their environment, even absent any valence, which could be explained by their general anxiety phenotype. However, given the low level of freezing (~20%), elevation in freezing to unpaired tone exposures cannot completely account for their enhanced fear response to CS-US presentations.

These data from the tone-only conditioning test suggest that there are small baseline abnormalities in auditory signaling in KO mice. While the type and duration of the startle and tone-only acoustic stimuli are distinct, it is still useful to see where the tone-only CS might fall on the

acoustic startle curve. At 75 dB, the tone should elicit a similarly negligible startle response in both KO and WT mice. This, combined with the lack of differences in acoustic startle in general, suggests that the tone-only conditioning genotype differences are not due to alterations in startle response. Instead, a more intriguing explanation for the tone-only conditioning results is altered sensorimotor gating. This refers to the process by which incoming sensory information is used to modulate motor output. The most common test of sensorimotor gating is prepulse inhibition (PPI) of startle responses. In this paradigm, the presentation of a weak auditory stimulus prior to an intense, startle-inducing stimulus inhibits or reduces the startle response. Intriguingly, both sensorimotor deficits (Hoenig et al., 2005; Rossi et al., 2005; De Leeuw et al., 2010; Ahmari et al., 2012; Russo et al., 2014) and general sensitivity to sensory stimuli (Hazen et al., 2008) have been reported in OCD. Individuals with OCD display decreased PPI (Hashimoto et al., 2008; Nanbu et al., 2010), indicating that their ability to use sensory information to modulate startle responses is diminished. Deficits in P50 auditory suppression, an electrophysiological marker of sensorimotor gating, have also been reported in OCD, with one study showing disruptions during fear conditioning specifically (Nanbu et al., 2010). Of note, unpublished data from our lab show that SAPAP3 KO mice display decreased PPI compared to WTs (Manning et al., 2019b). Therefore, while the tone-only condition paradigm used here is not a direct measure of sensorimotor gating, these results may be partially related to abnormalities in these processes.

Alternatively, the elevated freezing to non-US-paired tones could simply reflect an enhanced orienting response. By this logic, KO mice may be reactive to disruptive stimuli in their environment, regardless of the valence. KOs could express this elevation in orienting by ceasing movement and attending to the CS, which could be difficult to dissociate from freezing at such low levels. Interestingly, enhanced orienting has been reported in pediatric OCD: patients

exhibited both greater reactivity to novel stimuli and an early attention bias to threat during fear conditioning (Geller et al., 2017). However, while this is a plausible explanation for the tone-only genotype differences, it is important to note that the observed increase in freezing to a neutral tone is still quite low compared to freezing to a CS (~20% vs. ~80% by the third stimulus). Therefore, it is highly unlikely that this can completely account for the increased fear conditioning seen in KO mice. A potential confound in these data is that tone-only conditioning and acoustic startle were conducted in the same mice. As such, prior exposure to tones could have affected the acoustic startle threshold. However, we think this is unlikely, due to the stark contrast between the auditory stimuli used in these experiments. For tone-only conditioning, the stimulus was a 20-second, 75 dB, 5 kHz tone, while the acoustic startle stimulus was 40 milliseconds of white noise. Furthermore, acoustic startle data from a smaller cohort that did not undergo tone-only conditioning showed the same patterns as the data presented here (data not shown). These data were excluded from analysis simply because we did not obtain body weight for those animals, and thus could not calculate normalized startle amplitudes.

In summary, we found that SAPAP3 KO mice exhibited elevated fear conditioning that cannot be explained by alterations in nociceptive or auditory sensitivity. Our characterization of fear processing in SAPAP3 KOs suggests that this is a useful model for studying fear acquisition and expression in the context of OCD-related behaviors.

3.0 Enhanced fear conditioning in SAPAP3 KO mice is associated with alterations in immediate early gene expression in fear-related brain regions

3.1 Introduction

In Chapter 2, we characterized fear processing in SAPAP3 KO mice, a model of OCD-relevant behavior. We found that KOs display enhanced fear conditioning compared to WT mice, as evidenced by increased freezing both during the conditioning session itself (online fear processing) and a subsequent recall session. Moreover, this behavior could not be attributed to aberrant baseline nociception or audition. These data suggested that alterations in the neural regions underlying fear acquisition and expression are present in SAPAP3 KO mice. There are many regions that have been implicated in these processes, as well as freezing behavior in general, such as the basolateral amygdala (BLA), prelimbic (PL) subdivision of the medial prefrontal cortex (mPFC), central amygdala (CeA), oval and anteromedial bed nucleus of the stria terminalis (ovBNST, amBNST), and dorsolateral and ventrolateral periaqueductal gray (dlPAG, vlPAG). In addition, given that we observed a small, but significant, increase in freezing to sequential presentation of tones in KOs vs WTs, it is possible that there are abnormalities in cortical or thalamic auditory nuclei in SAPAP3 KO mice – the primary auditory cortex (Au1), secondary auditory cortex (dorsal and ventral aspects, AuD and AuV), and medial geniculate nucleus of the thalamus (MGN). Considering that there are numerous regions related to fear acquisition and expression, we examined immediate early gene expression to get a broad sense of potential abnormalities that could contribute to the enhanced fear conditioning observed in SAPAP3 KO mice. The following sections will expound upon the rationale for each of these regions.

The BLA and PL, which are bidirectionally-connected, have been repeatedly implicated in fear acquisition and expression (Maren, 2001; Fanselow and Poulos, 2005; Milad and Quirk, 2012; Duvarci and Pare, 2014; Giustino and Maren, 2015; Izquierdo et al., 2016). The BLA, which receives convergent sensory input related to the CS and US, is widely regarded as the locus of fear learning. Lesions and muscimol-mediated inactivation of this region either pre- or post-training critically impair fear acquisition and expression (LeDoux et al., 1990; Sananes and Davis, 1992; Campeau and Davis, 1995a; Muller et al., 1997; Maren, 1999; Wilensky et al., 1999; Goosens and Maren, 2001; Nader et al., 2001; Anglada-Figueroa and Quirk, 2005; Amano et al., 2011; Sierra-Mercado et al., 2011). Moreover, BLA neurons display CS-related responses (Quirk et al., 1995; Maren, 2000; Goosens et al., 2003; Herry et al., 2008; Amano et al., 2011; Wolff et al., 2014) and activity and plasticity markers are elevated after conditioning and fear recall (Herry and Mons, 2004; Senn et al., 2014; Zhu et al., 2018)

Similarly, the PL is necessary for fear expression. PL post-training inactivation, optogenetic inhibition during recall tones, and reduction of intrinsic excitability impair fear expression (Corcoran and Quirk, 2007; Santini and Porter, 2010; Sierra-Mercado et al., 2011; Do-Monte et al., 2015b), while microstimulation during retrieval tones impairs extinction and extinction recall (Vidal-Gonzalez et al., 2006). Furthermore, CS-related activity (Baeg, 2001; Burgos-Robles et al., 2009; Courtin et al., 2014) and activity- and plasticity-related molecules (Herry and Mons, 2004; Do-Monte et al., 2015b; Chen et al., 2017; Jacques et al., 2019) have been detected in the PL following fear conditioning. The role of the PL in fear acquisition, on the other hand, is less clear. Several studies have shown that pre-training lesions of the PL do not affect fear acquisition (Morgan et al., 1993; Quirk et al., 2000). Likewise, PL pre-training inactivation disrupts online expression of fear without impairing fear memory formation (Corcoran and Quirk,

2007). However, several studies have shown that more specific manipulations within the PL can attenuate fear acquisition (Morrow et al., 1999; Choi et al., 2010a; Yizhar et al., 2011; Gilmartin et al., 2013a; Xue et al., 2015; Chen et al., 2017; Li et al., 2019; Cummings and Clem, 2020). Considering that SAPAP3 KO mice displayed elevated freezing both during and after fear conditioning, further investigation of the PL is warranted.

Like the BLA and PL, the CeA is a critical nucleus in fear conditioning. With direct input from the BLA (Savander et al., 1996) and projections to brainstem and hypothalamic regions that control behavioral and autonomic fear responses (Duvarci and Pare, 2014; Gafford and Ressler, 2016), the CeA is considered the output nucleus of the amygdala. Pre- and post-training lesions of this nucleus disrupt fear acquisition (Hitchcock et al., 1989; Goosens and Maren, 2001; Nader et al., 2001; Zimmerman et al., 2007) and expression (Zimmerman et al., 2007), respectively. Similarly, disrupting signaling pathways or temporarily deactivating the CeA prior to conditioning impairs acquisition (Goosens and Maren, 2003; Wilensky et al., 2006; Zimmerman et al., 2007; Ciocchi et al., 2010), while comparable interventions prior to recall attenuate fear expression (Hitchcock and Davis, 1986; Kim and Davis, 1993; Campeau and Davis, 1995a; Wilensky et al., 2006; Zimmerman et al., 2007; Ciocchi et al., 2010; Zimmerman and Maren, 2010). Moreover, a recent study by Yu et al. (2017) found that the CeA plays an active role during fear conditioning by conveying US-related information to the BLA. These data suggest that the CeA may be involved in both online processing and acquisition of fear associations in SAPAP3 KOs.

The bed nucleus of the stria terminalis (BNST) is akin to the CeA in many ways – in fact, the BNST is often grouped into the “extended amygdala”. These two structures share similar input, such as the BLA and mPFC, and output, such as the hypothalamus and PAG (McDonald et al., 1999; Marek et al., 2013; Lebow and Chen, 2016). In addition, the BNST and CeA are

bidirectionally connected. Unlike the CeA, the BNST is generally associated with stress and anxiety, as opposed to discrete instances of fear (Lebow and Chen, 2016). However, two specific subregions of the BNST have been implicated in fear conditioning: the oval and anteromedial nuclei. The oval nucleus, located in the anterior division of the BNST, receives input from the BLA, projects to the ventral tegmental area and lateral hypothalamus, and is reciprocally connected with the CeA (Lebow and Chen, 2016). Interestingly, ovBNST neurons appear to mediate the fear conditioning-enhancing effects of SSRIs (Pelrine et al., 2016), suggesting that they can facilitate fear acquisition[2]. Like the ovBNST, the amBNST is part of the anterior division of the BNST. This subregion receives input from the hypothalamus, medial amygdala, and posterior BNST, and sends projections to the CeA, vlPAG, and neuroendocrine nuclei (Dong and Swanson, 2006; Lebow and Chen, 2016). Notably, amBNST neurons develop excitatory tone responses after auditory fear conditioning (Haufler et al., 2013). Based on these data, it is worth investigating the amBNST and ovBNST in SAPAP3 KO mice.

Another region of interest is the periaqueductal gray (PAG). Broadly, this midbrain nucleus is involved in regulating behavioral and autonomic fear responses (Behbehani, 1995). More specifically, stimulation of the vlPAG has been shown to generate freezing, while dlPAG stimulation elicits freezing and escape-like responses in an intensity-dependent manner (Vianna et

[2] Previous studies have shown that treatment with SSRIs enhances fear conditioning (Burghardt et al., 2004; Ravinder et al., 2013). Notably, SSRI treatment prior to conditioning induces immediate early gene expression in ovBNST neurons, most of which express the 5-HT2C serotonin receptor (Pelrine et al., 2016). Accordingly, pre-training local administration of a 5-HT2C receptor (5HT2CR) antagonist into the ovBNST blocks the enhancing effects of SSRIs on fear conditioning. Thus, treatment with SSRIs may cause elevated fear acquistion by driving activity in 5-HT2CR+ ovBNST neurons.

al., 2001a). The PAG receives nociceptive input from the spinal cord (Behbehani, 1995) and direct projections from both the PL and IL (Floyd et al., 2000), among other regions. In addition, the CeA and PAG are reciprocally connected (Rizvi et al., 1991). A particularly interesting study found that a subset of GABAergic neurons in the BLA and CeA send bifurcating projections to the mPFC and vlPAG (Sun et al., 2019), which could have interesting implications for fear processing. As it pertains to fear, many studies have implicated the PAG in contextual fear conditioning. For example, ventral PAG (vPAG) pre-training lesions (Kim et al., 1993; De Oca et al., 1998) or specific inhibition of GABAergic interneurons during conditioning (Lowery-Gionta et al., 2018) impair acquisition of contextual fear. Similarly, post-training vPAG lesions disrupt fear expression (De Oca et al., 1998; Vianna et al., 2001b). Conversely, pre-training lesions of the dlPAG enhance contextual fear acquisition (De Oca et al., 1998). In line with these findings, contextual fear conditioning induces strong and moderate cFos expression in the vlPAG and dlPAG, respectively (Carrive et al., 1997). Interestingly, vlPAG-projecting mPFC neurons are active during and promote contextual fear discrimination (Rozeske et al., 2018), underscoring the potential importance of this input.

While there are fewer reports in cued fear conditioning, several studies have found that the PAG plays a critical role in fear acquisition. Pre-training lesions or inactivation of the PAG block auditory fear acquisition (LeDoux et al., 1988; Johansen et al., 2010), while post-training lesions disrupt expression (Amorapanth et al., 1999). Moreover, naturally-occurring US responses in the PAG are attenuated across conditioning trials (Johansen et al., 2010) and fear conditioning potentiates synapses onto PAG-projecting CeA neurons (Penzo et al., 2014), suggesting that modulation of PAG activity contributes to fear acquisition. In accordance with these findings, local infusion of NMDA into the dlPAG during olfactory fear conditioning is sufficient to form a fear

association, indicating that dlPAG activation functionally replicates a US (Kincheski et al., 2012). Similarly, electrical stimulation of the dlPAG during auditory fear conditioning promotes fear acquisition (Di Scala et al., 1987; Kim et al., 2013). Together, these data indicate that the dlPAG and vlPAG are involved in fear acquisition, fear expression, and general regulation of freezing behavior.

In addition to these regions, auditory cortex and thalamus play crucial roles in auditory fear conditioning. For example, it has been argued that the MGN, not the BLA, is the locus of fear conditioning (Weinberger, 2011). The MGN receives convergent auditory and somatosensory input (Weinberger, 2011) and is responsive to both types of stimuli (Bordi and LeDoux, 1994). It sends projections to a variety of regions, including the BLA and auditory cortices (LeDoux et al., 1985, 1991; Herry and Johansen, 2014; Lucas et al., 2016). Pre- and post-training lesions of the MGN disrupt fear acquisition and expression, respectively (Campeau and Davis, 1995b), while MGN microstimulation paired with a CS is sufficient to drive fear acquisition (Cruikshank et al., 1992). Similarly, combined pre-training lesions of the MGN and auditory cortex (inclusive of Au1, AuV, and AuD) (Romanski and LeDoux, 1992) impair acquisition. Moreover, optogenetic co-stimulation of AuV and MGN terminals in the BLA paired with a US effectively replicates fear conditioning (Kwon et al., 2014). In addition, MGN neurons develop CS responses during and after conditioning (Disterhoff and Stuart, 1976; Supple and Kapp, 1989; Edeline and Weinberger, 1992; McEchron et al., 1995; Maren, 2001) and plasticity within the MGN is necessary for fear acquisition and recall (McEchron et al., 1996; McKernan and Shinnick-Gallagher, 1997; Apergis-Schoute et al., 2005; Parsons et al., 2006; Han et al., 2008).

Like the MGN, the auditory cortex sends projections to the BLA. Initial investigations suggested that the primary auditory cortex (Au1) was indirectly connected with the amygdala via

projections to secondary auditory cortices (LeDoux et al., 1991; Romanski and Ledoux, 1993). However, while recent reports have verified that there are strong reciprocal connections between AuD/AuV and the BLA, they have also demonstrated that Au1 and the BLA are bidirectionally connected (da Costa et al., 2017; Tsukano et al., 2019). In addition, both primary and secondary auditory cortices receive projections from motor and sensory cortices, MGN, mPFC, and contralateral auditory cortices (LeDoux et al., 1985; Herry and Johansen, 2014; da Costa et al., 2017). Many studies have found that the auditory cortex, particularly the secondary auditory cortex, is associated with remote memory retrieval. For example, immediate early gene expression is elevated in secondary auditory cortex after remote fear memory retrieval (Kwon et al., 2012; Grosso et al., 2017) and post-training inactivation (Cambiaghi et al., 2016b, 2017) or disconnection of this region with the retrosplenial cortex (Todd et al., 2018) inhibits remote memory recall. This may be due in part to alterations in communication with the BLA – remote recall is associated with enhanced secondary auditory cortex-BLA synchrony (Cambiaghi et al., 2016a) and secondary auditory cortex inactivation disrupts this synchrony (Cambiaghi et al., 2017). While manipulations of the primary auditory cortex did not replicate these effects on remote fear recall, co-inactivation of the primary and secondary auditory cortices did attenuate recent memory expression (Cambiaghi et al., 2016b).

More germane to our data, however, are the studies concerning the role of the auditory cortex in fear acquisition and expression. As mentioned previously, combined lesion of the MGN and auditory cortices – both primary and secondary – prior to conditioning impairs fear acquisition (Romanski and LeDoux, 1992) and optogenetic stimulation of AuV- and MGN-BLA terminals with US presentations can generate fear associations (Kwon et al., 2014). Similarly, broad pre- and post-training inactivation of the auditory cortex attenuates fear acquisition and expression,

respectively (Letzkus et al., 2011; Yang et al., 2016). Interestingly, specific pre-training Au1 lesions fail to disrupt fear acquisition, while post-training lesions of the secondary, but not primary, auditory cortex block fear expression (Campeau and Davis, 1995b). Although these data suggest that the secondary auditory cortex is primarily involved in fear acquisition, findings of enhanced Au1-PL coherence during fear discrimination indicate that primary auditory cortex may play a role as well (Concina et al., 2018). In support of this hypothesis, numerous studies have shown that neurons in both the primary and secondary auditory cortex develop long-latency CS responses during conditioning that may represent a US-anticipatory signal (Disterhoff and Stuart, 1976; Maho et al., 1995; Quirk et al., 1997; Armony et al., 1998; Leon et al., 2017). Furthermore, US responses have also been observed after fear conditioning (Ide et al., 2013). Several other studies have demonstrated that auditory cortex receptive fields rapidly tune to the CS during training (Edeline et al., 1993; Weinberger et al., 1993; Weinberger, 1998). In line with these findings, fear conditioning potentiates auditory cortico-amygdalar synapses (Tsvetkov et al., 2002) and induces spine formation within the auditory cortex (Moczulska et al., 2013; Yang et al., 2016; Lai et al., 2018).

In summary, there are many regions that have been implicated in fear acquisition and expression. Thus, we used a broad metric to assess neural potential abnormalities in KO mice: expression of the protein form of the immediate early gene cFos, a marker of neuronal activity, in fear-related regions after fear conditioning. In addition to the regions listed above (BLA, PL, CeA, ovBNST, amBNST, dlPAG, vlPAG, Au1, AuV, AuD, and MGN), we measured cFos in the IL due to its importance for fear extinction (Barad, 2005; Quirk and Mueller, 2008; Milad and Quirk, 2012; Marek et al., 2013; Duvarci and Pare, 2014; Giustino and Maren, 2015; Izquierdo et al., 2016). Using these methods, we observed an overall increase in correlated activity between fear-

related regions in KO compared to WT mice. In particular, cFos expression was correlated between the PL and BLA in KOs, but not WTs. Counterintuitively, we also observed a positive correlation between PL cFos expression in WT, but not KO, mice. These findings suggest that while KOs exhibit broad synchrony across fear-related regions, this may be unrelated to fear learning. Instead, PL activity is associated with freezing in WT mice, which may reflect a more specific understanding of the CS-US relationship.

3.2 Methods

3.2.1 Animals

Male *Sapap3*-KOs and WT littermates were used for these experiments. Mice were group-housed in reverse light cycle conditions and had *ad libitum* access to food and water. The fear conditioning cohort consisted of 7 WT and 10 KO mice, all 4-6 months old at the time of testing. All experiments were approved by the Institutional Animal Use and Care Committee at the University of Pittsburgh in compliance with National Institutes of Health guidelines for the care and use of laboratory animals.

3.2.2 Fear conditioning

Fear conditioning was conducted as described in section 2.2.2. Briefly, mice were habituated to the conditioning chamber on day 1 (Figure 3-1a). On the following day, mice were exposed to 3 CS-US pairings separated by pseudorandom (90-120s) ITIs (Figure 3-1b). The CS

was a 20-second, 75 dB, 5 kHz tone that co-terminated with a 2-second, 1 mA shock (US). All freezing was hand-scored by well-trained, blinded observers using The Observer XT (Noldus).

Figure 3-1. Fear conditioning with perfusion for cFos analysis protocol

A) Habituation session. Mice were exposed to the conditioning chamber without any stimuli for 542 seconds. **B)** Conditioning session. After a 3-minute pre-tone period, mice were exposed to 3 CS-US pairings (20-second tone co-terminating with a 2-second shock). CS-US pairings were separated by a pseudorandom ITI of 90-120 seconds. Mice were perfused 60 minutes after the third and final tone for cFos analysis.

3.2.3 Immunohistochemistry

Mice were sacrificed via transcardial perfusion with 4% paraformaldehyde (PFA) one hour after the third and final conditioning tone. Brains were harvested and left in 4% PFA for 24 hours, followed by 30% sucrose until the brains sunk to the bottom of the tubes. The samples were then rapidly frozen on dry ice and sectioned into 35-micron free-floating slices using a cryostat.

3.2.3.1 Antigen retrieval

Prior to DAB staining, antigen retrieval was performed using a method specifically designed for free-floating sections (Jiao et al., 1999). All steps were conducted at room temperature unless otherwise specified. First, sections were rinsed in a 0.1M PB (pH 7.4) solution 3 times for 5 minutes each. Next, the samples were incubated in 10mM sodium citrate buffer (pH 8.5) in an 80ºC preheated water bath for 30 minutes. Sections were then cooled at room temperature while

remaining in the 10mM sodium citrate solution, after which they were rinsed 3 times in 0.1M PB (pH 7.4) for 5 minutes each.

3.2.3.2 cFos 3,3'-Diaminobenzidine (DAB) staining

cFos protein DAB staining was performed immediately after antigen retrieval. All steps were conducted at room temperature unless otherwise specified. First, sections were washed in 1% H_2O_2 (Sigma-Aldrich, 95321) in TBS (Sigma-Aldrich, T5912) for 10 minutes, followed by two 10-minute rinses in TBS. Samples were then incubated in blocking buffer – 3% NGS (Vector Laboratories, S-1000) in TBS – for 30 minutes. Next, samples were incubated in the primary antibody solution for 48 hours at 4ºC. The primary antibody concentration was 1:5000 (cFos rabbit anti-cFos, SYSY 226 003, lot #4-66) in blocking buffer (3% NGS in 1xTBS). After 48 hours, the sections were rinsed 3 times in TBS with 0.3% Triton X-100 (Fisher Scientific, BP151) for 10 minutes each. The samples were then incubated in a 1:500 secondary solution (biotinylated goat anti-rabbit, Vector Laboratories, BA-1000, in blocking buffer), followed by a 1-hour incubation in ABC tertiary solution (Vector Laboratories, Vectastain ABC-HRP Kit, PK-4000). Next, slices were washed 3 times for 10 minutes each in TBS prior to DAB exposure. DAB was prepared using a DAB Peroxidase (HRP) Substrate Kit (Vector Laboratories, SK-4100) at a ratio of 1:2:1 of buffer, DAB, and H_2O_2 solutions. Samples were exposed to the DAB solution for 5 minutes, after which they were immediately transferred to TBS to stop the peroxidase reaction. Slices were then washed a final 3 times in TBS for 10 minutes each before being mounted onto activated slides (Fisher Scientific, FisherBrand Superfrost Plus, 12-550-15). After the slices had dried completely, slides were dipped into TBS and then rinsed for 3 minutes each in 70%, 80%, and 95% ethanol. Next, the slides were rinsed in two separate washes of 100% ethanol for 3 minutes each, ending in

a 3-minute wash in xylene substitute (Sigma-Aldrich, A5597). Finally, slides were cover-slipped using DPX mounting medium (Sigma-Aldrich, 06522).

3.2.3.3 Microscopy and cell counting

Slides were scanned at 20x magnification under bright field conditions using an Olympus inverted slide scanning microscope. cFos positive cells in regions of interest (ROIs) were automatically detected using CellSens (Olympus). ROIs included the prelimbic cortex (PL), infralimbic cortex (IL), oval and anteromedial nuclei of the bed nucleus of the stria terminalis (ovBNST, amBNST), basolateral amygdala (BLA), central amygdala (CeA), primary auditory cortex (Au1), dorsal and ventral secondary auditory cortex (AuD, AuV), medial geniculate nucleus (MGN), and dorsolateral and ventrolateral periaqueductal grey (dlPAG, vlPAG) (Appendix Figure 1). Each ROI consisted of an average of 6 samples (3 bilateral sections along the anterior-posterior extent of the region), which were manually checked for artifacts by experimenters blind to condition and behavior.

3.2.4 Statistics and data analysis

Data were analyzed using Microsoft Excel and Graphpad Prism. A repeated measures ANOVA was used to analyze the fear conditioning data and t-tests were used for post-hoc analysis. Geisser-Greenhouse corrections were used for all ANOVAs. Pearson correlations were used for analysis of cFos data. Sidak and Benjamini, Krieger, and Yekutieli methods were used to correct for multiple comparisons.

3.3 Results

3.3.1 cFos expression in fear-related regions is similar between SAPAP3 KO and WT mice

In order to assess broad circuit alterations in SAPAP3 KO and WT mice after fear conditioning, we examined expression of the protein product of the immediate early gene cFos in a number of fear-associated regions. A new cohort of 10 SAPAP3 KO and 7 WT mice were exposed to 3 CS-US pairings, as in Chapter 2. 60 minutes after the third and final tone, mice were sacrificed via transcardial perfusion and cFos protein was detected using immunohistochemistry (Figure 3-2a). In line with the initial cohort, WT and KO mice both showed increased freezing to the tones, but KO mice exhibited a faster learning curve [Figure 3-2b; main effect of time: $F(1.673,25.09)=25.92$, $p<0.0001$; main effect of genotype: $F(1,15)=7.89$, $p=0.0132$; time x genotype interaction: $F(3,45)=4.683$, $p=0.0063$. Post-hoc tests: WT vs. KO tone 3 ($p=0.0002$); pre-tone vs. tone 2 ($p=0.0443$), trend pre-tone vs. tone 3 ($p=0.0658$), and trend tone 1 vs. 2 ($p=0.0898$) for WT; pre-tone vs. tones 2 and 3 and tones 1 vs. 2 and 1 vs. 3 (all p values <0.0001), and trend tones 2 vs. 3 ($p=0.0561$) for KOs]. Paralleling previous work (Morrow et al., 1999; Senn et al., 2014), fear conditioning induced robust cFos expression in a variety of regions, including the PL and BLA (Figure 3-2c). Surprisingly, when comparing cFos+ cell densities between genotypes, there were no differences across any of the regions of interest after correction for multiple comparisons (Figure 3-2d).

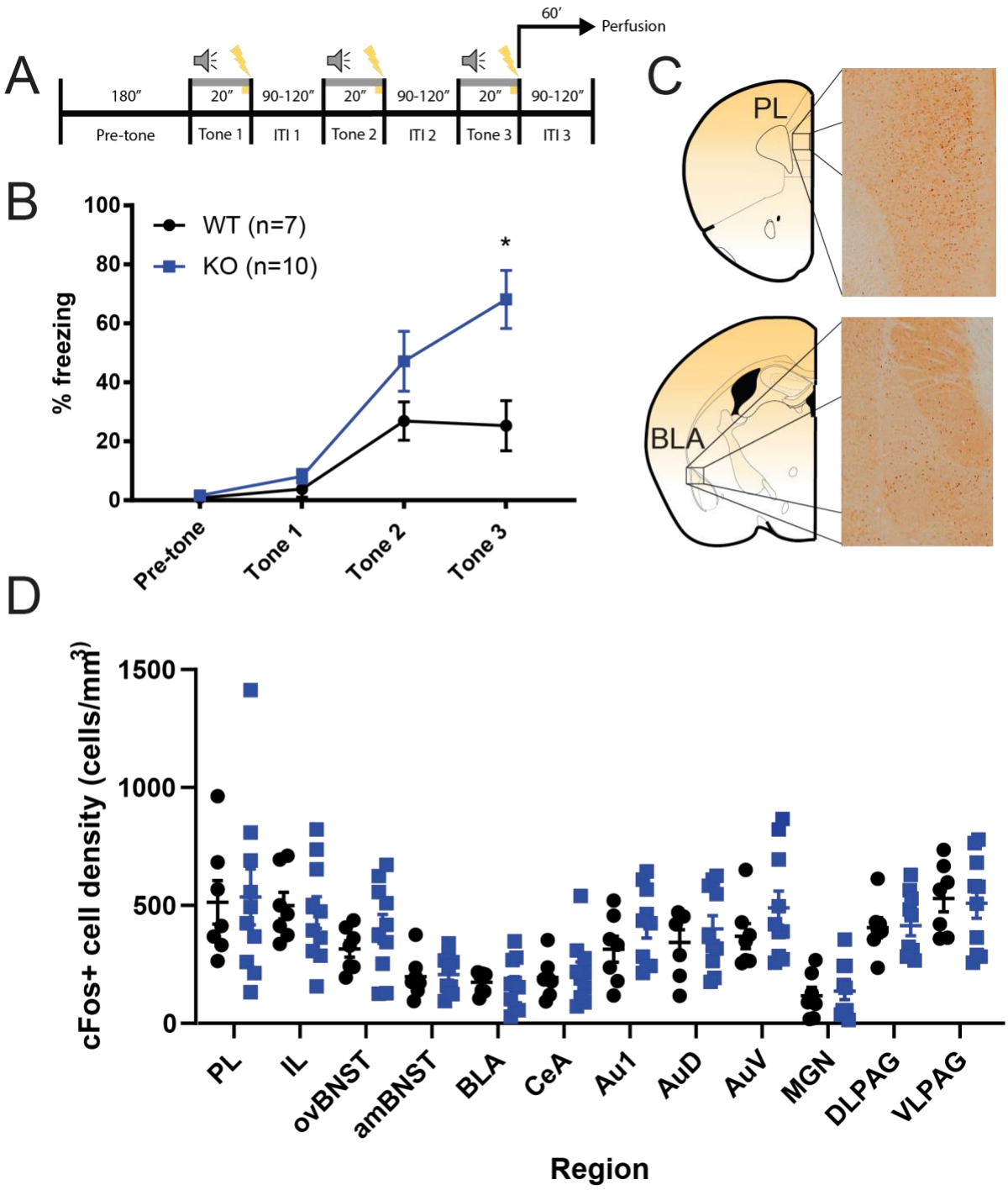

Figure 3-2. cFos+ cell density does not differ between SAPAP3 KO and WT mice

A) Timeline of fear conditioning protocol with perfusions. **B)** % freezing to the pre-tone period and tones 1-3 for WT and KO mice. Main effect of time [$F(1.673,25.09)=25.92$, $p<0.0001$] and genotype [$F(1,15)=7.89$, $p=0.0132$]; time x genotype interaction [$F(3,45)=4.683$, $p=0.0063$]. Post-hoc: WT vs. KO, tone 3 ($p=0.0002$). **C)**

Example cFos histology in the prelimbic cortex (PL) and basolateral amygdala (BLA). **D)** No WT vs. KO differences in cFos+ cell density.

3.3.2 cFos expression is correlated between fear-associated regions in all animals

Next, we looked at cFos+ cell density correlations between fear-related regions. When looking at both genotypes combined, there were many positive inter-regional correlations, and no negative correlations (Figure 3-3). Nearly all of these correlations were significant or trended towards significance (Table 3-1). However, after correction for multiple comparisons, only a few of these correlations remained significant (Table 3-2). In this combined dataset of KOs and WTs, significant correlations included PL vs. IL, BLA, and AuD ($r=0.88$, $p<0.0001$; $r=0.77$, $p=0.0003$; $r=0.69$, $p=0.00213$); IL vs. BLA, CeA, and AuD ($r=0.84$, $p<0.0001$; $r=0.65$, $p=0.00508$; $r=0.74$, $p=0.00067$); amBNST vs. AuD ($r=0.69$, $p=0.002$); BLA vs. CeA, AuD, MGN, dlPAG, and vlPAG ($r=0.70$, $p=0.0019$; $r=0.68$, $p=0.00249$; $r=0.76$, $p=0.00045$; $r=0.67$, $p=0.00307$; $r=0.68$, $p=0.00283$); CeA vs. AuD ($r=0.64$, $p=0.00548$); Au1 vs. AuD, AuV, MGN, and dlPAG ($r=0.84$, $p<0.0001$; $r=0.93$, $p<0.0001$; $r=0.75$, $p=0.00047$; $r=0.74$, $p=0.00071$); AuD vs. AuV, dlPAG, and vlPAG ($r=0.79$, $p=0.00016$; $r=0.76$, $p=0.00035$; $r=0.65$, $p=0.00475$); AuV vs. MGN and dlPAG ($r=0.73$, $p=0.0009$; $r=0.73$, $p=0.00095$); MGN vs. dlPAG and vlPAG ($r=0.78$, $p=0.00019$; $r=0.71$, $p=0.00147$); and dlPAG vs. vlPAG ($r=0.79$, $p=0.00017$). These data indicate that in general, fear conditioning causes concurrent activation in many fear-associated regions.

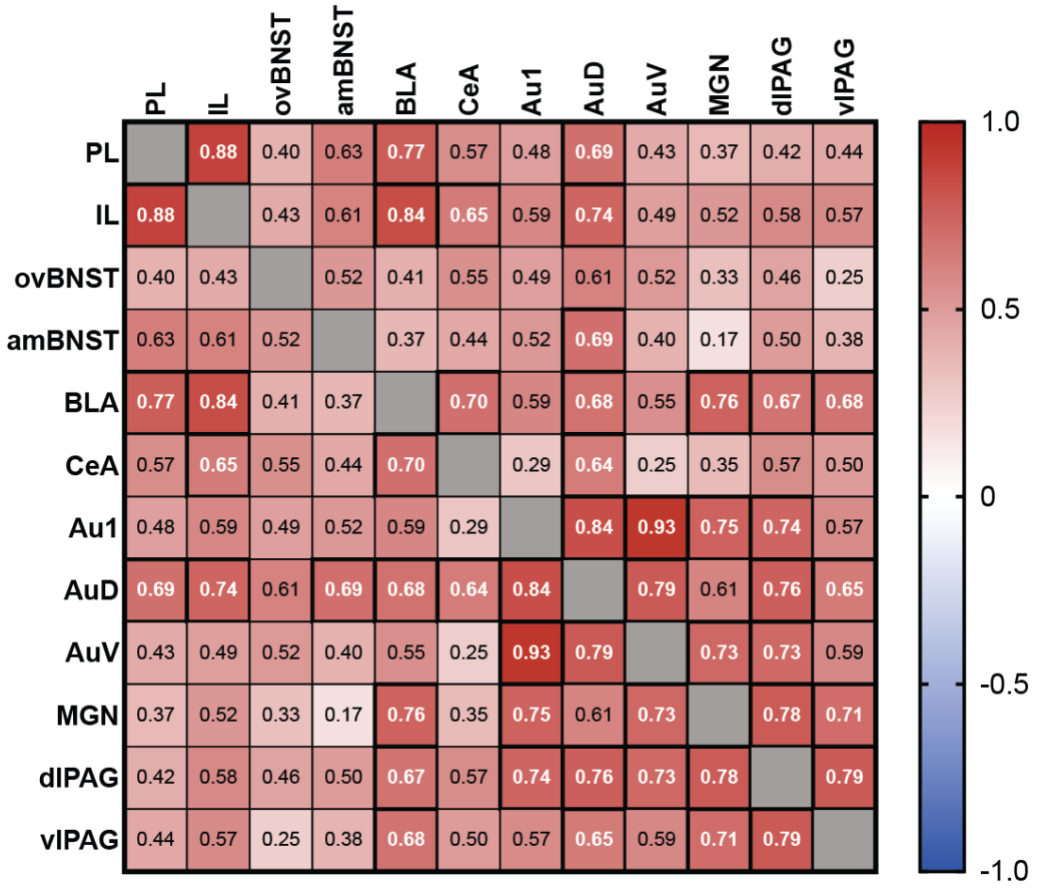

Figure 3-3. cFos expression is correlated between fear-associated regions in all animals

cFos+ cell density correlations between fear ROIs in both WT and KO mice. R-values range from -1 (blue) to 1 (red). Black and white numbers indicate non-significant and significant correlatins, respectively, after correcting for multiple comparisons. Significant correlations include PL vs. IL, BLA, and AuD; IL vs. BLA, CeA, and AuD; amBNST vs. AuD; BLA vs. CeA, AuD, MGN, dlPAG, and vlPAG; CeA vs. AuD; Au1 vs. AuD, AuV, MGN, and vlPAG; AuD vs. AuV, dlPAG, and vlPAG; AuV vs. MGN and dlPAG; MGN vs. dlPAG and vlPAG; and dlPAG vs. vlPAG. Abbreviations: PL (prelimbic cortex), IL (infralimbic cortex), ovBNST (oval nucleus of the bed nucleus of the stria terminalis), amBNST (anteromedial nucleus of the bed nucleus of the stria terminalis), BLA (basolateral amygdala), CeA (central amygdala), Au1 (primary auditory cortex), AuD (dorsal portion of secondary auditory cortex), AuV (ventral portion of secondary auditory cortex), MGN (medial geniculate nucleus), dlPAG (dorsolateral periaqueductal grey), vlPAG (ventrolateral periaqueductal grey).

Table 3-1. Uncorrected p-values for cFos correlations between ROIs in all mice

	PL	IL	ovBNST	amBNST	BLA	CeA	Au1	AuD	AuV	MGN	dlPAG	vlPAG
PL		4.1E-06	0.11265	0.00708	0.00031	0.01767	0.04924	0.00213	0.08388	0.1494	0.09552	0.0747
IL	4.1E-06		0.08314	0.00896	2.4E-05	0.00508	0.01349	0.00067	0.04645	0.03056	0.01401	0.01599
ovBNST	0.11265	0.08314		0.03058	0.10266	0.02101	0.04732	0.00862	0.03391	0.20181	0.06059	0.33652
amBNST	0.00708	0.00896	0.03058		0.14283	0.07559	0.03331	0.002	0.11538	0.52253	0.03967	0.1316
BLA	0.00031	2.4E-05	0.10266	0.14283		0.0019	0.01192	0.00249	0.02171	0.00045	0.00307	0.00283
CeA	0.01767	0.00508	0.02101	0.07559	0.0019		0.25086	0.00548	0.32677	0.16326	0.01758	0.03908
Au1	0.04924	0.01349	0.04732	0.03331	0.01192	0.25086		3E-05	5.5E-08	0.00047	0.00071	0.0168
AuD	0.00213	0.00067	0.00862	0.002	0.00249	0.00548	3E-05		0.00016	0.01003	0.00035	0.00475
AuV	0.08388	0.04645	0.03391	0.11538	0.02171	0.32677	5.5E-08	0.00016		0.0009	0.00095	0.01309
MGN	0.1494	0.03056	0.20181	0.52253	0.00045	0.16326	0.00047	0.01003	0.0009		0.00019	0.00147
dlPAG	0.09552	0.01401	0.06059	0.03967	0.00307	0.01758	0.00071	0.00035	0.00095	0.00019		0.00017
vlPAG	0.0747	0.01599	0.33652	0.1316	0.00283	0.03908	0.0168	0.00475	0.01309	0.00147	0.00017	

cFos+ cell density p-values between ROIs in all mice, prior to multiple comparison correction. Values marked in red are significant, values in yellow are trends.

Table 3-2. Corrected p-values for cFos correlations between ROIs in all mice

	PL	IL	ovBNST	amBNST	BLA	CeA	Au1	AuD	AuV	MGN	dlPAG	vlPAG
PL		4.1E-06	0.11265	0.00708	0.00031	0.01767	0.04924	0.00213	0.08388	0.1494	0.09552	0.0747
IL	4.1E-06		0.08314	0.00896	2.4E-05	0.00508	0.01349	0.00067	0.04645	0.03056	0.01401	0.01599
ovBNST	0.11265	0.08314		0.03058	0.10266	0.02101	0.04732	0.00862	0.03391	0.20181	0.06059	0.33652
amBNST	0.00708	0.00896	0.03058		0.14283	0.07559	0.03331	0.002	0.11538	0.52253	0.03967	0.1316
BLA	0.00031	2.4E-05	0.10266	0.14283		0.0019	0.01192	0.00249	0.02171	0.00045	0.00307	0.00283
CeA	0.01767	0.00508	0.02101	0.07559	0.0019		0.25086	0.00548	0.32677	0.16326	0.01758	0.03908
Au1	0.04924	0.01349	0.04732	0.03331	0.01192	0.25086		3E-05	5.5E-08	0.00047	0.00071	0.0168
AuD	0.00213	0.00067	0.00862	0.002	0.00249	0.00548	3E-05		0.00016	0.01003	0.00035	0.00475
AuV	0.08388	0.04645	0.03391	0.11538	0.02171	0.32677	5.5E-08	0.00016		0.0009	0.00095	0.01309
MGN	0.1494	0.03056	0.20181	0.52253	0.00045	0.16326	0.00047	0.01003	0.0009		0.00019	0.00147
dlPAG	0.09552	0.01401	0.06059	0.03967	0.00307	0.01758	0.00071	0.00035	0.00095	0.00019		0.00017
vlPAG	0.0747	0.01599	0.33652	0.1316	0.00283	0.03908	0.0168	0.00475	0.01309	0.00147	0.00017	

Threshold: p-values less than 0.00562556255626 are discoveries

cFos+ cell density p-values between ROIs in all mice after Benjamini, Krieger, and Yekutieli false discovery rate correction. P-values less than 0.00562556255626 were considered discoveries, and are marked in red.

3.3.3 cFos expression between fear-related regions is correlated in KO, but not WT, mice

When we looked at inter-regional cFos+ cell density correlations within genotype, we observed an interesting pattern that was occluded in the combined correlations. Correlations between regions in WT mice varied in their directionality (Figure 3-4a), while KO correlations were all positive (Figure 3-4b). Prior to multiple comparison correction, only a few correlations were significant in WT mice (Table 3-3), including PL vs. IL, amBNST, and AuD (r=0.80, p=0.0294; r=0.97, p=0.00042; r=0.76, p=0.0463); IL vs. AuD (r=0.77, p=0.0422); ovBNST vs. BLA and MGN (r=-0.78, p=0.0372; r=-0.89, p=0.00651); BLA vs. MGN (r=0.78, p=0.0369); Au1 vs. AuV and dlPAG (r=0.90, p=0.00539; r=0.76, p=0.483); AuV vs. MGN and dlPAG (r=0.81, p=0.0259; r=0.89, p=0.0075); and MGN vs. dlPAG and vlPAG (r=0.77, p=0.0438; r=0.78, p=0.397). Conversely, nearly all of the cFos+ cell density correlations between regions in KO mice were significant (Table 3-4). Interestingly, after correcting for multiple comparisons, none of the WT correlations were statistically significant (Table 3-5). This was not the case in KO mice (Table 3-6): cFos+ cell density was positively correlated between PL vs. IL and BLA (r=0.91, p<0.0001; r=0.91, p=<0.0001); IL vs BLA (r=0.91, p=<0.0001); Au1 vs AuD and AuV (r=0.91, p<0.0001; r=0.95, p<0.0001); AuD vs. AuV (r=0.89, p<0.0001); and dlPAG vs. vlPAG (r=0.88, p=0.0001). Considering the importance of the PL/BLA reciprocal circuit in fear conditioning, this correlation was particularly intriguing. This specific correlation is plotted in Figure 3-4 [WTs (Figure 3-4c; R_2=0.006, p=0.869); KOs (Figure 3-4d; R_2=0.837, p=0.0002)].

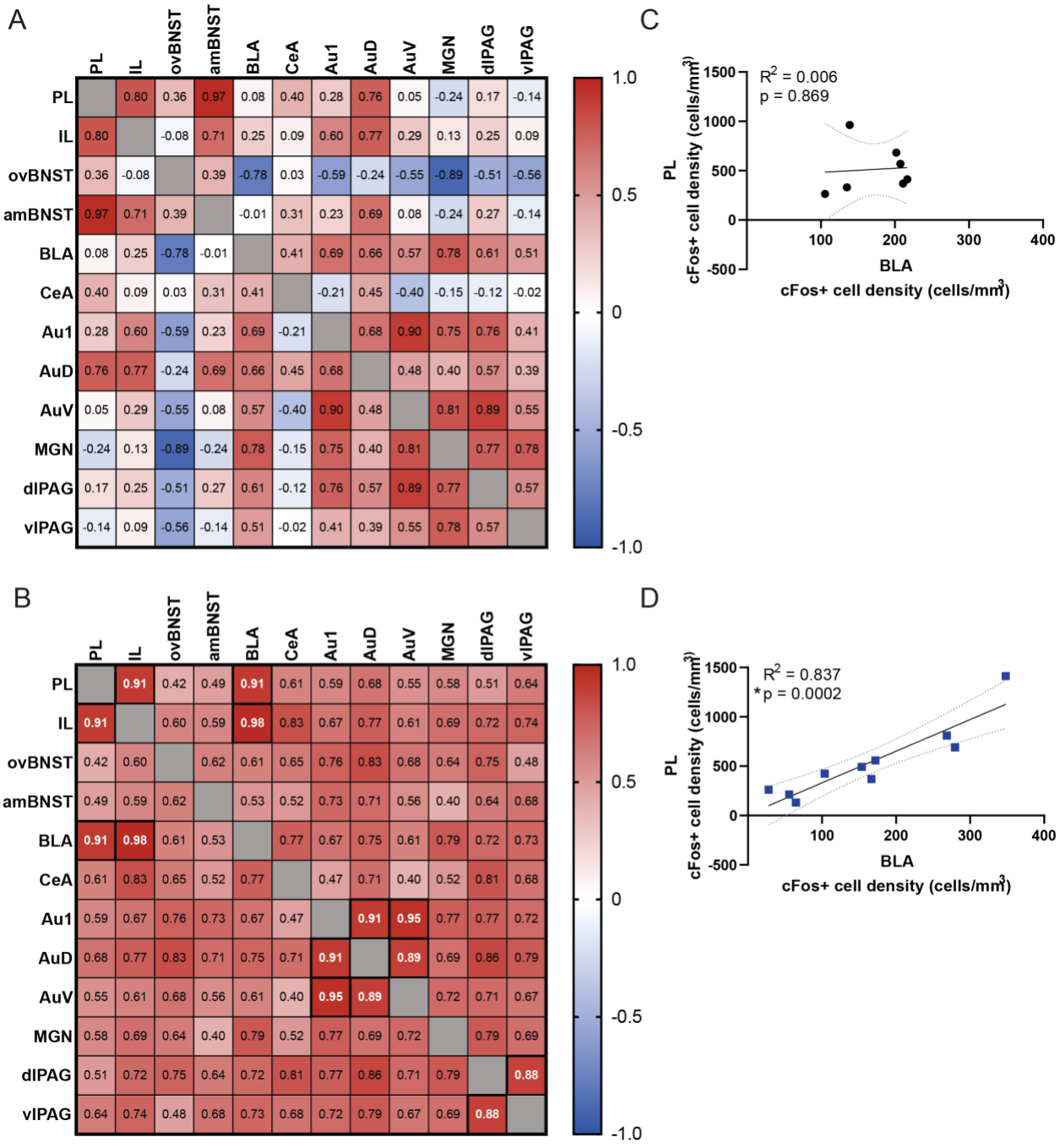

Figure 3-4. cFos expression between fear-related regions is correlated in KO, but not WT, mice

A,B) Correlation matrices for WT (E) and KO (F) mice. Box color represents the r-value, ranging from -1 (blue) to +1 (red). Black and white numbers represent nonsignificant and significant p-values, respectively, after correcting for multiple comparisons. **A)** No significant cFos+ cell density correlations between regions for WT animals. **B)** Several significant cFos+ cell density correlations between regions for KO animals, including PL/IL (r=0.91), PL/BLA (r=0.91), and IL/BLA (r=0.98). **C)** PL and BLA cFos+ cell densities are not correlated in WT mice

(R_2=0.006, p=0.869) **D)** PL and BLA cFos+ cell densities are correlated in KO mice (R_2=0.837, p=0.0002). Abbreviations: PL (prelimbic cortex), IL (infralimbic cortex), ovBNST (oval nucleus of the bed nucleus of the stria terminalis), amBNST (anteromedial nucleus of the bed nucleus of the stria terminalis), BLA (basolateral amygdala), CeA (central amygdala), Au1 (primary auditory cortex), AuD (dorsal portion of secondary auditory cortex), AuV (ventral portion of secondary auditory cortex), MGN (medial geniculate nucleus), dlPAG (dorsolateral periaqueductal grey), vlPAG (ventrolateral periaqueductal grey).

Table 3-3. Uncorrected p-values for cFos correlations between ROIs in WT mice

	PL	IL	ovBNST	amBNST	BLA	CeA	Au1	AuD	AuV	MGN	dlPAG	vlPAG
PL		0.02943	0.43154	0.00042	0.86879	0.38	0.54471	0.04634	0.91907	0.60763	0.71032	0.76234
IL	0.02943		0.86491	0.07155	0.58378	0.8467	0.15575	0.04222	0.52587	0.77828	0.59456	0.85614
ovBNST	0.43154	0.86491		0.38173	0.0372	0.94285	0.16124	0.59879	0.2047	0.00651	0.23917	0.19338
amBNST	0.00042	0.07155	0.38173		0.97827	0.49573	0.6239	0.08788	0.86923	0.59692	0.55247	0.76273
BLA	0.86879	0.58378	0.0372	0.97827		0.3621	0.0885	0.10538	0.18262	0.03691	0.14954	0.24751
CeA	0.38	0.8467	0.94285	0.49573	0.3621		0.64863	0.30878	0.38026	0.74274	0.79236	0.967
Au1	0.54471	0.15575	0.16124	0.6239	0.0885	0.64863		0.09584	0.00539	0.05116	0.04833	0.36358
AuD	0.04634	0.04222	0.59879	0.08788	0.10538	0.30878	0.09584		0.27732	0.36975	0.17767	0.38187
AuV	0.91907	0.52587	0.2047	0.86923	0.18262	0.38026	0.00539	0.27732		0.0259	0.0075	0.20423
MGN	0.60763	0.77828	0.00651	0.59692	0.03691	0.74274	0.05116	0.36975	0.0259		0.04383	0.03972
dlPAG	0.71032	0.59456	0.23917	0.55247	0.14954	0.79236	0.04833	0.17767	0.0075	0.04383		0.17719
vlPAG	0.76234	0.85614	0.19338	0.76273	0.24751	0.967	0.36358	0.38187	0.20423	0.03972	0.17719	

cFos+ cell density p-values between ROIs in WT mice, prior to multiple comparison correction. Values marked in red are significant, values in yellow are trends.

Table 3-4. Uncorrected p-values for cFos correlations between ROIs in KO mice

	PL	IL	ovBNST	amBNST	BLA	CeA	Au1	AuD	AuV	MGN	dlPAG	vlPAG
PL		0.00030	0.23007	0.14907	0.00021	0.05961	0.07162	0.03148	0.10157	0.07753	0.13286	0.04591
IL	0.0003		0.06522	0.07279	0.00000	0.00326	0.03344	0.00882	0.05950	0.02595	0.0177	0.01363
ovBNST	0.23007	0.06522		0.05386	0.06137	0.03983	0.01066	0.00283	0.03161	0.04655	0.01225	0.16075
amBNST	0.14907	0.07279	0.05386		0.11384	0.12574	0.01676	0.02036	0.09060	0.24631	0.04431	0.03201
BLA	0.00021	0.00000	0.06137	0.11384		0.00969	0.03271	0.01337	0.06149	0.00615	0.01809	0.01617
CeA	0.05961	0.00326	0.03983	0.12574	0.00969		0.17273	0.0227	0.25854	0.12259	0.00436	0.03027
Au1	0.07162	0.03344	0.01066	0.01676	0.03271	0.17273		0.00023	0.00002	0.00847	0.00879	0.01838
AuD	0.03148	0.00882	0.00283	0.02036	0.01337	0.0227	0.00023		0.00052	0.02774	0.00138	0.00689
AuV	0.10157	0.05950	0.03161	0.0906	0.06149	0.25854	0.00002	0.00052		0.01873	0.02024	0.03488
MGN	0.07753	0.02595	0.04655	0.24631	0.00615	0.12259	0.00847	0.02774	0.01873		0.0062	0.0258
dlPAG	0.13286	0.01770	0.01225	0.04431	0.01809	0.00436	0.00879	0.00138	0.02024	0.0062		0.00067
vlPAG	0.04591	0.01363	0.16075	0.03201	0.01617	0.03027	0.01838	0.00689	0.03488	0.0258	0.00067	

cFos+ cell density p-values between ROIs in KO mice, prior to multiple comparison correction. Values marked in red are significant, values in yellow are trends.

Table 3-5. Corrected p-values for cFos correlations between ROIs in WT mice

	PL	IL	ovBNST	amBNST	BLA	CeA	Au1	AuD	AuV	MGN	dlPAG	vlPAG
PL		0.02943	0.43154	0.00042	0.86879	0.38	0.54471	0.04634	0.91907	0.60763	0.71032	0.76234
IL	0.02943		0.86491	0.07155	0.58378	0.8467	0.15575	0.04222	0.52587	0.77828	0.59456	0.85614
ovBNST	0.43154	0.86491		0.38173	0.0372	0.94285	0.16124	0.59879	0.2047	0.00651	0.23917	0.19338
amBNST	0.00042	0.07155	0.38173		0.97827	0.49573	0.6239	0.08788	0.86923	0.59692	0.55247	0.76273
BLA	0.86879	0.58378	0.0372	0.97827		0.3621	0.0885	0.10538	0.18262	0.03691	0.14954	0.24751
CeA	0.38	0.8467	0.94285	0.49573	0.3621		0.64863	0.30878	0.38026	0.74274	0.79236	0.967
Au1	0.54471	0.15575	0.16124	0.6239	0.0885	0.64863		0.09584	0.00539	0.05116	0.04833	0.36358
AuD	0.04634	0.04222	0.59879	0.08788	0.10538	0.30878	0.09584		0.27732	0.36975	0.17767	0.38187
AuV	0.91907	0.52587	0.2047	0.86923	0.18262	0.38026	0.00539	0.27732		0.0259	0.0075	0.20423
MGN	0.60763	0.77828	0.00651	0.59692	0.03691	0.74274	0.05116	0.36975	0.0259		0.04383	0.03972
dlPAG	0.71032	0.59456	0.23917	0.55247	0.14954	0.79236	0.04833	0.17767	0.0075	0.04383		0.17719
vlPAG	0.76234	0.85614	0.19338	0.76273	0.24751	0.967	0.36358	0.38187	0.20423	0.03972	0.17719	

Threshold: no p-values marked as discoveries

cFos+ cell density p-values between ROIs in WT mice after Benjamini, Krieger, and Yekutieli false discovery rate correction. No values were marked as discoveries.

Table 3-6. Corrected p-values for cFos correlations between ROIs in KO mice

	PL	IL	ovBNST	amBNST	BLA	CeA	Au1	AuD	AuV	MGN	dlPAG	vlPAG
PL		**0.00030**	0.23007	0.14907	**0.00021**	0.05961	0.07162	0.03148	0.10157	0.07753	0.13286	0.04591
IL	**0.0003**		0.06522	0.07279	**0.00000**	0.00326	0.03344	0.00882	0.05950	0.02595	0.0177	0.01363
ovBNST	0.23007	0.06522		0.05386	0.06137	0.03983	0.01066	0.00283	0.03161	0.04655	0.01225	0.16075
amBNST	0.14907	0.07279	0.05386		0.11384	0.12574	0.01676	0.02036	0.09060	0.24631	0.04431	0.03201
BLA	**0.00021**	**0.00000**	0.06137	0.11384		0.00969	0.03271	0.01337	0.06149	0.00615	0.01809	0.01617
CeA	0.05961	0.00326	0.03983	0.12574	0.00969		0.17273	0.02270	0.25854	0.12259	0.00436	0.03027
Au1	0.07162	0.03344	0.01066	0.01676	0.03271	0.17273		**0.00023**	**0.00002**	0.00847	0.00879	0.01838
AuD	0.03148	0.00882	0.00283	0.02036	0.01337	0.02270	**0.00023**		**0.00052**	0.02774	0.00138	0.00689
AuV	0.10157	0.05950	0.03161	0.09060	0.06149	0.25854	**0.00002**	**0.00052**		0.01873	0.02024	0.03488
MGN	0.07753	0.02595	0.04655	0.24631	0.00615	0.12259	0.00847	0.02774	0.01873		0.0062	0.0258
dlPAG	0.13286	0.01770	0.01225	0.04431	0.01809	0.00436	0.00879	0.00138	0.02024	0.00620		**0.00067**
vlPAG	0.04591	0.01363	0.16075	0.03201	0.01617	0.03027	0.01838	0.00689	0.03488	0.02580	**0.00067**	

Threshold: p-values less than 0.001 are discoveries

cFos+ cell density p-values between ROIs in KO mice after Benjamini, Krieger, and Yekutieli false discovery rate correction. P-values less than 0.001 were considered discoveries, and are marked in red.

3.3.4 PL cFos expression is correlated with freezing in WT, but not KO, mice

Finally, we assessed the relationship between cFos+ cell density and freezing. After collapsing across both genotypes (Table 3-7), there was a significant correlation between percent freezing to tone 3 and cFos expression in the PL ($r=0.512$, $p=0.0355$), as well as trend correlations with expression in the IL ($r=0.43$, $p=0.0852$), ovBNST ($r=0.458$, $p=0.647$), and CeA ($r=0.463$, $p=0.0614$). For both the ovBNST and CeA correlations, the trend significance can be attributed to the combined power of analyzing all the mice: the WT and KO correlations were quite similar, but neither were significant on their own. The combined PL and IL correlations, on the other hand, were primarily driven by WT and KO mice, respectively: PL cFos and freezing were nearly significantly correlated in WT (Figure 3-5a; $r=0.742$, $p=0.056$), but not KO (Figure 3-5b; $r=0.47$, $p=0.171$), mice, while there was a trend correlation between IL cFos and freezing in KO ($r=0.566$, $p=0.0879$), but not WT ($r=0.347$, $p=0.445$), mice. In addition, there was a significant positive correlation between amBNST cFos+ cell density and freezing in WT mice ($r=0.76$, $p=0.0475$), which was not apparent in KOs.

Table 3-7. Correlations between cFos and freezing

	Combined	WT	KO
PL	**r=0.512**	**r=0.742**	r=0.470
	***p=0.0355**	***#p=0.056***	*p=0.171*
IL	**r=0.430**	r=0.347	**r=0.566**
	#p=0.0852	*p=0.445*	***#p=0.0879***
ovBNST	**r=0.458**	r=0.492	r=0.389
	#p=0.0647	*p=0.262*	*p=0.267*
amBNST	r=0.364	**r=0.760**	r=0.141
	p=0.151	***p=0.0475**	*p=0.697*
BLA	r=0.365	r=0.0493	r=0.534
	p=0.149	*p=0.916*	*p=0.112*
CeA	**r=0.463**	r=0.328	r=0.517
	#p=0.0614	*p=0.472*	*p=0.126*
Au1	r=0.244	r=0.173	r=0.123
	p=0.346	*p=0.711*	*p=0.735*
AuD	r=0.362	r=0.621	r=0.182
	p=0.153	*p=0.137*	*p=0.614*
AuV	r=0.157	r=0.204	r=-0.0101
	p=0.548	*p=0.661*	*p=0.978*
MGN	r=0.132	r=-0.155	r=0.226
	p=0.613	*p=0.740*	*p=0.530*
dlPAG	r=0.187	r=0.337	r=0.118
	p=0.472	*p=0.460*	*p=0.746*
vlPAG	r=-0.00775	r=0.109	r=-0.0231
	p=0.976	*p=0.816*	*p=0.950*

Correlations between cFos+ cell density in each ROI and % freezing to the final conditioning tone for both genotypes combined, or WT and KO mice separately. R- and p-values are displayed for each region. Significant and trend correlations are bolded and marked with asterisks and hashtags, respectively.

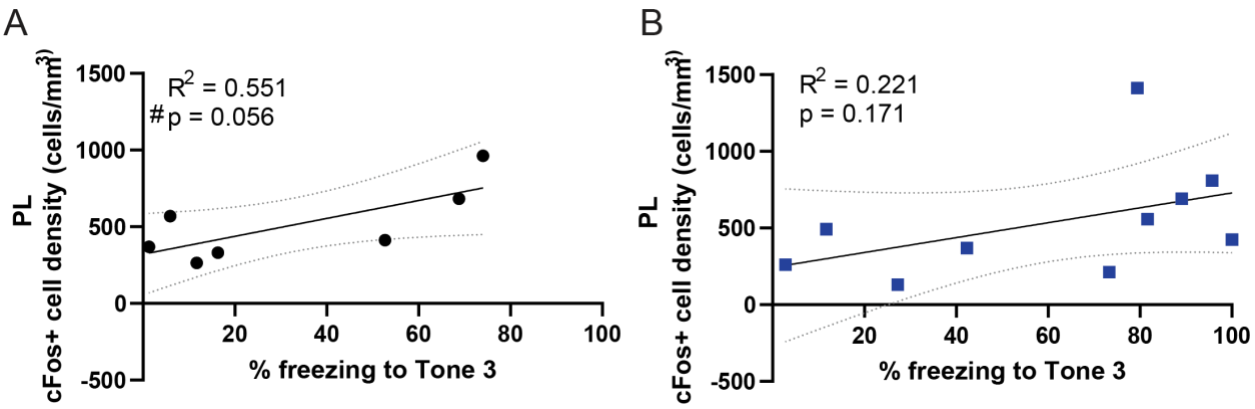

Figure 3-5. PL cFos expression is correlated with freezing in WT, but not KO, mice

A) Trend correlation between PL cFos+ cell density and % freezing to tone 3 in WT mice (R_2=0.551, p=0.056). **B)** PL cFos+ cell density is not correlated with % freezing to tone 3 for KOs (R_2=0.221, p=0.171). Solid black lines represent linear fit, dotted grey lines represent 95% confidence intervals.

3.4 Discussion

The goal of these experiments was to assess broad alterations in fear-related networks in SAPAP3 KO and WT mice. To that end, we analyzed expression of the protein product of the immediate early gene cFos after fear conditioning. We found that there were no differences in cFos+ cell density between WT and KO mice for any of regions of interest. However, we did observe significant correlations between regions, both when combining all animals and within genotype. Considering that the genotype-specific correlations were often quite similar, it appears that the vast majority of significant correlations in the combined dataset arose from increased power. This was true of all significant correlations involving Au1, AuD, AuV, MGN, dlPAG, and vlPAG (Au1 vs. AuD, AuV, MGN and dlPAG; AuD vs. PL, IL, amBNST, BLA, CeA, AuV, dlPAG, and vlPAG; AuV vs. MGN; MGN vs. BLA and vlPAG; dlPAG vs. BLA and vlPAG; and vlPAG vs. BLA). Unsurprisingly, these data suggest that activity in the auditory cortices and

thalamus is associated with activity in areas required for fear learning (PL, BLA) and freezing behavior (CeA, dlPAG, vlPAG) during auditory fear conditioning. Moreover, the correlation between AuD and amBNST cFos complements data showing that amBNST neurons have elevated firing rates to the CS after fear conditioning (Haufler et al., 2013). In addition to these correlations, SAPAP3 KO and WT mice displayed similar patterns that contribute to the significant combined correlations between cFos expression in the PL and IL, and BLA and CeA. The combined correlation between cFos+ cell density in the BLA and CeA is intuitive: the BLA is the locus of fear learning and projects to the CeA, which regulates freezing behavior via its output to various regions. At first pass, the correlation between PL and IL cFos, is more puzzling, considering that these regions are differentially involved in fear acquisition and extinction, respectively. However, several studies have shown that cFos expression increases in the IL after fear conditioning (Morrow et al., 1999; Herry and Mons, 2004), suggesting that the correlation between PL and IL is simply due to concurrent conditioning-associated activation. Taken together, these data indicate that co-activation of several regions involved in fear conditioning is consistent across both SAPAP3 KO and WT mice.

Despite the commonalities between fear-related activity in SAPAP3 KO and WT mice, there were several notable differences in inter-regional correlations when comparing the combined and separated matrices. Specifically, the IL vs. CeA correlation was significant when both groups were collapsed, but failed to reach significance when considering each genotype on its own. However, examination of the genotype-specific correlations suggests that this effect is predominantly driven by KOs (KO: r=0.83; WT: r=0.09). A similar pattern was seen in the IL vs. BLA and PL vs. BLA comparisons, which were significant in the combined dataset. These correlations were strong and significant in KO mice (IL vs. BLA: r=0.98; PL vs. BLA: r=0.91),

but were weak or close to zero in WTs (IL vs. BLA: r=0.25; PL vs. BLA: r=0.08). As briefly discussed in the results section, the correlation between PL and BLA cFos+ cell density is particularly noteworthy, given the importance of these bidirectionally connected regions in fear acquisition and expression. Moreover, the KO correlation structure is characterized by strong, positive correlations, several of which are statistically significant. The WT structure, on the other hand, consists of more varied correlations, both in strength and directionality, of which none are significant. Combined, these data suggest that heightened co-activation of fear-related regions, and perhaps more specifically the relationship between the PL and BLA, underlies the enhanced fear conditioning seen in KOs.

In contrast to these data, correlations between freezing and cFos expression tell a somewhat different story. Several of these correlations are intuitive, such as the trend correlation between freezing and CeA cFos+ cell density in the combined dataset. CeA, the output nucleus of the amygdala, directly modulates freezing behavior via its downstream projections, so it is logical that CeA activity and freezing would be positively correlated. In addition, combining all animals revealed a trend correlation between ovBNST cFos and freezing. This supplements data demonstrating that ovBNST activity can enhance fear acquisition (Pelrine et al., 2016). However, other data points, such as the correlations between freezing and cFos expression in the PL and amBNST, are seemingly at odds with the behavioral and intra-regional correlation data. Considering that amBNST neurons develop CS responses after conditioning (Haufler et al., 2013) and KO mice display greater freezing that WTs, it seems counterintuitive that freezing and amBNST cFos are correlated in the latter and not the former. A similar pattern is true of the correlation between freezing and PL cFos, which is significant when combining all animals. Surprisingly, although there was a significant correlation between PL and BLA cFos and elevated

freezing in KO mice, this is effect is driven by WT mice, which exhibit a nearly significant correlation where KOs do not. This raises the possibility that PL activity is related to freezing, and therefore the CS-US association, in WT mice alone. In KOs, PL/BLA correlated activity could simply reflect an overall increase in concurrent activity in distributed fear networks, as evidenced the presence of multiple between-region correlations (Figure 3-3b). Moreover, the lack of correlation between PL cFos and freezing in KOs suggests that activity in this network may be unrelated to CS-US associations.

There are several limitations to this study. First, we did not include a non-conditioned control (e.g. pseudoconditioning, shock only, tone only). Thus, it is possible that the cFos expression we report is not significantly different from baseline or is related to tone or shock exposure alone, not the association between the two. However, increased cFos relative to controls has been consistently reported after fear conditioning in wildtype rats and mice (Morrow et al., 1999; Herry and Mons, 2004). Moreover, we observed similar levels of cFos expression in regions such as the PL, IL, and BLA in our WT mice compared to previous studies (Herry and Mons, 2004), suggesting that this experiment achieved comparable neural activation. While fear conditioning-associated cFos has not been studied in SAPAP3 KO mice, the fact that we see no genotype differences in cFos expression across all measured regions indicates that robust activation was attained in KO mice as well. Therefore, we believe these concerns are minimal. A second limitation is the small sample size of WT mice relative to KOs. With only 7 animals, it is possible that we lacked the power to detect patterns in inter-regional correlations. If we had a larger group, some of the correlations could have potentially survived correction for multiple comparisons. However, it is important to note that for the most critical comparison in our study – namely the correlation between PL and BLA cFos expression – the r-value in WT mice was

virtually zero. In this case, increasing the sample size by 3 animals to match the KO group would almost certainly have had no effect. Therefore, while a larger group might reveal significant correlations between some regions, the primary findings appear to be quite robust.

In summary, we demonstrated that SAPAP3 KO and WT mice have distinct activity patterns in fear-associated regions after fear conditioning. KO mice are characterized by broadly distributed co-activation in numerous regions, with a particularly strong correlation between PL and BLA cFos expression. However, since there is no correlation between PL cFos expression and freezing, this activity is dissociable from behavioral output. Conversely, there is a nearly significant correlation between PL cFos and freezing in WT mice, despite their lower freezing level relative to KOs. Counterintuitively, these data suggest that PL activity is related to behavioral output, and therefore CS-US associations, in WT, but not KO, mice.

4.0 Prelimbic activity is modulated during and required for online processing of fearful associations in WT, but not KO, mice

4.1 Introduction

In the previous two chapters, we demonstrated that SAPAP3 KO mice display enhanced fear conditioning and altered activity patterns in fear-related regions. Specifically, conditioning-related cFos expression is correlated between many fear-associated regions in KO, but not WT, mice. The most notable of these correlations is between the prelimbic cortex (PL) and basolateral amygdala (BLA). With a WT correlation of nearly zero and a strong, significant correlation in KOs, this comparison constituted the largest difference in r-value between genotypes. Moreover, previous literature has provided strong evidence for the role of the PL and BLA in fear conditioning, indicating that these are excellent candidates for the neural correlates of enhanced fear in KO mice. More specifically, these two regions are critical nodes in the fear expression circuit (Maren, 2001; Fanselow and Poulos, 2005; Duvarci and Pare, 2014; Izquierdo et al., 2016) and bidirectional connections between the PL and BLA have been implicated in fear conditioning (Laviolette et al., 2005; Vouimba and Maroun, 2011; Sotres-Bayon et al., 2012; Arruda-Carvalho and Clem, 2014; Senn et al., 2014; Do-Monte et al., 2015b). In addition, the BLA is necessary for fear acquisition (Maren, 2001; Fanselow and Poulos, 2005; Duvarci and Pare, 2014; Izquierdo et al., 2016). The role of the PL in fear acquisition, however, is less clear. Several studies have shown that pre-training lesions or inactivation of the PL do not affect memory consolidation (Morgan et al., 1993; Quirk et al., 2000; Corcoran and Quirk, 2007). Notably, however, pre-training inactivation with TTX did attenuate freezing during the conditioning session itself (Corcoran and

Quirk, 2007). Conversely, more targeted interventions during or prior to conditioning – such as somatostatin-positive interneuron inhibition (Cummings and Clem, 2020), BDNF knockdown (Choi et al., 2010a), NR2A antagonism (Gilmartin et al., 2013a), Gadd45γ signaling disruption (Li et al., 2019), or alteration of the excitatory/inhibitory balance (Yizhar et al., 2011) – impair acquisition without affecting online fear processing.

Taken together, these data paint a complicated picture of the role of the PL in fear acquisition – specifically, broad, temporally diffuse inhibition of this region does not appear to affect fear memory formation, while specific manipulations of distinct cell-types, receptors, or molecules prior to or during conditioning can alter acquisition. Furthermore, PL inactivation can disrupt online fear processing without affecting acquisition (Corcoran and Quirk, 2007). Perhaps due to these conflicting results, few studies have investigated or manipulated PL activity during fear conditioning, as opposed to during fear memory recall or fear extinction, leaving open the question of the role of the PL in online processing of CS-US associations. This is particularly intriguing considering that we consistently observe elevated freezing in SAPAP3 KO mice during the conditioning session itself.

In summary, our immediate early gene data suggest that heightened correlated activity in PL and BLA regions drives elevated fear conditioning in KOs and that impairment in online processing of fearful associations may be a critical factor in this behavior. However, cFos analysis merely provides a snapshot of neural activity at a given timepoint. In order to directly assess PL and BLA activity during fear conditioning, we collected neural data in the PL/BLA circuit via *in vivo* multi-site, dual-color fiber photometry. Using this technique, we acquired calcium signals during both initial CS-US pairings and recall tones. We found that activity within the PL/BLA circuit – most notably the PL – was positively modulated across conditioning trials in WT, but not

KO, mice. Counterintuitively, these data suggest that PL activity during fear conditioning underlies specific learning of the CS-US relationship: i.e., PL modulation in WT mice enables the formation of proper fear associations, while static PL activity across trials in KOs suggests that both specific learning and generalized fear and anxiety may be driving elevated freezing. In support of this theory, we found that KO mice generalize more during discriminative fear learning. Finally, we examined the role of PL activity specifically during conditioning tones using optogenetic inhibition. We found that PL inhibition decreases freezing for both WT and KO mice during conditioning, but not retrieval. However, inhibition in KOs does not decrease freezing to the level of uninhibited WTs, bolstering our theory that KOs engage additional fear generalization circuitry. Taken together, these data suggest that tone-associated PL modulation across trials in WT animals is critical for online CS-US processing, but not the acquisition of a long-term CS-US association, while a lack of PL modulation in KOs could indicate that fear learning is driven by both specific CS-US associations in PL circuits and generalized fear in distinct circuits.

4.2 Methods

4.2.1 Animals

Male *Sapap3*-KOs and WT littermates were used for these experiments. Mice were group-housed in reverse light cycle conditions and had *ad libitum* access to food and water. For all behavioral experiments, mice were 4-6 months old. For fiber photometry and optogenetic experiments, mice underwent stereotaxic surgery 5 weeks earlier such that they were 4-6 months old at the time of behavioral testing. The fiber photometry cohort consisted of 11 WT and 13 KO

mice. The optogenetic inhibition cohort consisted of 32 WT and 31 KO mice, half of which were injected with AAV5-CaMKII-eYFP (WT=16, KO=16) and the other half with AAV5-CaMKII-ArchT-GFP (WT=16, KO=15). Discriminative fear conditioning was conducted using 11 WTs and 13 KOs. All experiments were approved by the Institutional Animal Use and Care Committee at the University of Pittsburgh in compliance with National Institutes of Health guidelines for the care and use of laboratory animals.

4.2.2 Fear conditioning

Fear conditioning with concurrent fiber photometry recording or optogenetic inhibition was conducted as described in Chapter 2.2.2, with a few key differences (Figure 4-1). First, handling prior to experimentation included scruffing and plugging the mice into fiberoptic cables. Second, there were two days of habituation prior to conditioning (Figure 4-1a, b). Finally, the number of CS-US pairings was increased to five (Figure 4-1c). All freezing was hand-scored by well-trained, blinded observers using The Observer XT (Noldus). For freezing probability analysis, freezing was first binarized and grouped into 1-second bins. Freezing during each tone was then averaged within genotype. For baseline freezing, 5 30-second bins were averaged for each animal and the averaged within genotype. Locomotion was first scored using EthoVision XT (Noldus) and then manually corrected to account for inadvertent tracking of the photometry cable instead of the subject. As with freezing, velocity traces were binned into 1-second bins. Velocity during each tone was averaged within genotype. Baseline velocity was an average of 5 separate 30-second bins per animal during the pre-tone period, which was then averaged within genotype.

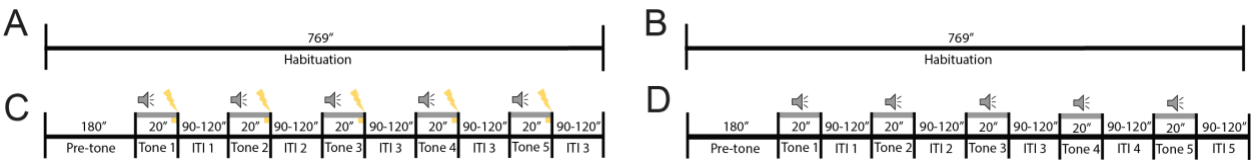

Figure 4-1. Fear conditioning with concurrent fiber photometry or optogenetics

A) Day 1 habituation session. Mice were exposed to the conditioning chamber without any stimuli for 769 seconds. **B)** Day 2 habituation session. **C)** Conditioning session. After a 3-minute pre-tone period, mice were exposed to 5 CS-US pairings (20-second tone co-terminating with a 2-second shock). CS-US pairings were separated by a pseudorandom ITI of 90-120 seconds. For optogenetic experiments, illumination occurred during each 20s CS-US presentation. **D)** Recall session. After a 3-minute pre-tone period, mice were exposed to 5 CS presentations (20-second tone). Tones were separated by a pseudorandom ITI of 90-120 seconds.

4.2.3 Discriminative fear conditioning

Discriminative fear conditioning consisted of three sessions across consecutive days: habituation, conditioning, and recall. As with fear conditioning, handling was conducted for a week prior the experiment, each session was preceded by a 1-hour acclimatization period in the holding room, and sessions ended with a second undisturbed hour in the holding room. The habituation session consisted of a 3-minute pre-tone period, followed by 5 presentations each of the CS+ and CS- in a pseudorandom order. The conditioned stimuli were a 4 kHz and a 12 kHz tone, both 20s and 75 dB. CS+/CS- assignment was counterbalanced across animals. CS presentations were separated by pseudorandom (90-120s) ITIs. The conditioning session consisted of a 3-minute pre-tone period, followed by 10 presentations each of the CS+ and CS- (20s, 75 dB, 4 or 12 kHz). CS+ presentations co-terminated with a 0.5s, 0.5mA shock (US). CS order and ITI duration (90-120s) were pseudorandom. During recall, sessions began with a 3-minute pre-tone period, followed by 5 presentations each of the CS+ and CS- (20s, 75 dB, 4 or 12 kHz). As with

previous session, CS order and ITI length (90-120s) were pseudorandom. Habituation and conditioning sessions were run in Context A while recall was run in Context B, as described in the fear conditioning methods. Freezing and darting were hand-scored by well-trained, blinded observers using The Observer XT (Noldus).

4.2.3.1 Discriminator and generalizer classification

To separate mice into discriminators and generalizers, freezing and darting were combined into a single variable. First, all percent freezing values during every tone across both CS types (CS+, CS-) and genotypes (WT, KO) were collapsed into one data set. Values below 1% were excluded from the analysis, as they were exclusively due to spillover from freezing initiated in the prior ITI[3]. Freezing scores above the median were assigned a value of 1, while scores below were given a 0. The same was done for darting percentages. Next, for each animal, a difference score for freezing vs. darting was obtained for every CS+ or CS- presentation [(% freezing - % darting)/(% freezing + % darting)]. This yielded a bounded score between -1 and 1 that indicated the predominant behavioral strategy each animal used during a given tone. The values for all of the CS+ or CS- presentations were then divided by 10 (the total number of presentations of each CS type) to create a single value for each animal. If the value was between -1 and -0.5, the animal's strategy for that CS type was marked as darting, while 0.5 to 1 was marked as freezing and -0.5 to

[3] If an animal initiated freezing during an ITI but stopped freezing during a tone, it could create a bout that amounts to less than 1% of time spent freezing. For example, a 20-second bout that begins towards the end of an ITI and ends 0.05 seconds into a tone would yield a 19.95-second bout during the ITI and 0.05-second bout during the tone. If the animal did not freeze during the remainder of that tone, the resulting percentage of time spent freezing during the tone would be <1% (0.25%). These instances of spillover were excluded from analysis.

0.5 was considered a mixed strategy. This resulted in two values per animal that indicated behavioral strategy, one each for the CS+ and CS-. CS+ and CS- strategy sets were then compared for each animal. If the strategy changed between the CS+ and CS-, the animal was considered a discriminator; if the strategies were the same, the animal was considered a generalizer.

4.2.4 Stereotaxic surgeries

Stereotaxic surgeries were performed under 2% isoflurane anesthesia. Holes were drilled at target coordinates and viruses were injected using syringes (Hamilton) affixed to a pump (Harvard Scientific). PE10 tubing with a 30-gauge cannula at one end was attached to the Hamilton syringe and the cannula was lowered into the brain for injections. Fiber optic implants were implanted using black dental cement (Lang; Contemporary Ortho-Jet Liquid, 1504BLK; Contemporary Ortho-Jet Powder, 1530BLK). Body temperature and breathing was monitored throughout surgery, and mice were given analgesic treatment (topical lidocaine, intraperitoneal carprofen) immediately afterwards. In addition, post-operative analgesic treatment was administered for 3 days after surgery.

For fiber photometry experiments, AAV9-syn-GCaMP6m-WPRE-SV40 and AAV1-syn-NES-jRGECO1a-WPRE-SV40 were unilaterally injected into the left prelimbic cortex (PL; AP +1.98, ML +/-0.4, DV -1.3) and basolateral amygdala (BLA; AP -1.2, ML +/-2.8, DV -3.5), respectively. An additional control group received injections of AAV9-syn-eGFP and AAV2-syn-tdTomato into the PL and BLA. 200 μM metal fiber optic implants that are optimized for low autofluorescence (Neurophotometrics) were then chronically implanted at the same coordinates. For optogenetic experiments, AAV5-CaMKII-ArchT-GFP or AAV5-CaMKII-eYFP was

bilaterally injected into the PL. 200 µM ceramic fiber optic implants, manufactured in house, were then chronically implanted at a 15º mediolateral angle (AP +1.98, ML +/-0.8, DV -1.4).

4.2.5 Fiber photometry

Fiber photometry experiments were conducted using a Neurophotometrics Fiber Photometry System. 470, 560, and 415nm LEDs were used to image GCaMP6M, jREGECO1a, and isosbestic signals, respectively. A Doric 4x branching patch cord (Doric Lenses, BFP(4)_200/220/900-0.37_2.44m_SMA*-4xMF1.25) was used in order to record from two regions in two animals each simultaneously. Point Grey Blackfly S cameras were used to record behavior. Photometry signals and videos were simultaneously acquired using Bonsai (Open Ephys). As with other fear conditioning experiments, mice were handled daily starting one week prior to the experiment. However, for these experiments, mice were additionally scruffed and plugged into fiberoptic cables for several minutes each day starting on the fourth day of handling. At the beginning of each recording day, the photometry system was turned on with all 3 LEDs (415, 470, and 560 nm) at full power for at least 30 minutes to pre-bleach the cable. LED output was then set to 30-90 µW for all three wavelengths: during habituation, the power was 30-50 µW, and it was increased slightly on subsequent days to account for potential bleaching. At the beginning of each session, mice were plugged in and allowed to sit for 3 minutes prior to the session start (distinct from the pre-tone period). This was meant to allow time for the signal to stabilize, as there is often a prominent decay at the beginning of each recording session. Photometry signals were recorded during day two of habituation, conditioning, and recall. Mice were hooked up to the system on day one of habituation as well, but no data was collected.

4.2.5.1 Signal processing and analysis

Fiber photometry signals were processed using custom Matlab scripts. Briefly, motion artifacts were manually removed using the isosbestic (415nm) trace as a reference. Next, calcium traces were corrected for exponential decay using a binomial fit. Traces were then low-pass filtered (order 6, frequency 3) and a moving minimum correction was used to normalize large fluctuations across the session. Finally, calcium data was z-scored using the pre-tone period, excluding all freezing-related activity, as a baseline. In addition, photometry and behavioral data were aligned and synchronized. For comparison with freezing probability and velocity, calcium data was binned into 1-second bins. Signal during each tone was then averaged within genotype. For baseline activity, 5 30-second bins were averaged for each animal and the averaged within genotype.

4.2.6 Optogenetics

For optogenetic experiments, the PL was bilaterally inhibited during fear conditioning using 532nm lasers (300mW, Shanghai Laser and Optics Century Co., Ltd., 532nm Green DPSS Laser T3). Fiber optic patch cables and ferrules were manufactured in house and bilateral commutators (Doric Lenses, FRJ_1x2i_FC-2FC_0.22) were used to minimize stress on cables. Handling procedures were the same as in the photometry experiments. For every experimental day, mice were plugged into fiber optic cables to ensure constant exposure to scruffing and cable dynamics across the experiment. However, inhibition was limited to the conditioning day and occurred specifically during CS-US presentations (10mW, constant light, 20s).

4.2.7 Histology

After fiber photometry and optogenetics experiments, mice were sacrificed via transcardial perfusion with 4% paraformaldehyde (PFA). Brains were then harvested and kept in PFA at 4º C. After 24 hours, the brains were transferred into a 30% sucrose solution and remained there until they sunk, at which point they were rapidly frozen on dry ice. Next, brains were sectioned into 35-micron free-floating slices using a cryostat. Slices were mounted onto activated slides and fluorescent images were obtained using an Olympus inverted slide scanning microscope. Fiber optic implant placement and viral spread were then recorded.

4.2.8 Statistics and data analysis

Data were analyzed using Microsoft Excel, Matlab, and Graphpad Prism. Repeated measures ANOVAs were used to analyze freezing, darting, and spinning behavior during fear conditioning and discriminative fear conditioning, as well as tone and co-shock/tone AUC within genotype. Geisser-Greenhouse corrections were used for all ANOVAs. Pearson correlations were used to compare freezing probability and velocity to calcium signal. T-tests were used for post-hoc analysis and between-genotype AUC comparisons.

4.3 Results

4.3.1 PL tone-associated activity is modulated across conditioning trials in WT, but not KO, mice

To assess potential abnormalities in PL/BLA circuitry during fear conditioning in SAPAP3 KO mice, we conducted multisite, dual-color *in vivo* fiber photometry. In order to increase the amount of neural data, we altered the fear conditioning paradigm to include five CS-US pairings instead of three (Figure 4-2a). Five weeks prior to conditioning, we injected AAV9-syn-GCaMP6m-WPRE-SV40 (GCaMP6m) and AAV1-syn-NES-jRGECO1a-WPRE-SV40 (jRGECO1a) unilaterally into the PL and BLA, respectively, of WT (n=11) and KO (n=13) mice and chronically implanted fibers in both sites (Figure 4-2b). This design theoretically enables us to image the complete PL/BLA circuit: PL soma in green and BLA-PL terminals in red from the PL fiber, and BLA soma in red and PL-BLA terminals in green from the BLA fiber. However, we were unable to record reliable signals from BLA-PL terminals (see Chapter 4.4: Discussion). Histological confirmation of injections revealed clear staining of GFP-tagged PL soma (Figure 4-2d) and RFP-tagged BLA soma (Figure 4-2e). PL terminals formed a dense GFP projection field in the BLA (Figure 4-2e), while BLA terminals in the PL were sparse, but reliably detectable via immunofluorescence (Figure 4-2d). As in previous cohorts, WT and KO mice increased freezing to tones across conditioning, with KO mice exhibiting enhanced conditioning [Figure 4-2c; main effect of time: $F(3.791,83.41)=18.41$, $p<0.0001$; main effect of genotype: $F(1,22)=19.1$, $p=0.0002$; time x genotype interaction: $F(5,110)=3.597$, $p=0.0047$. Post-hoc tests: WT vs. KO, tones 1 ($p=0.0002$), 2 ($p<0.0001$), and 4 ($p=0.0004$)]. However, in contrast to previous cohorts, KO mice froze more than WTs to the first tone, prior to experiencing any shocks [post-hoc tests, WT: pre-

tone vs. tones 3 ($p=0.0091$), 4 ($p=0.0389$), and 5 ($p<0.0001$); tones 1 vs. 5 ($p<0.0001$) and 2 vs. 5 ($p=0.0005$); trend tone 1 vs. 3 ($p=0.051$). KO: pre-tone vs. tones 1 ($p=0.0445$) and 2-5 ($p<0.0001$); tone 1 vs. tones 2 ($p=0.0136$), 4 ($p=0.0021$), and 5 ($p=0.0346$)]. A potential explanation for this is due to the nature of the particular experiment. Fiber photometry recordings require that the mice be scruffed, plugged into fiberoptic cables, and tethered for the entire session. Furthermore, our fiber photometry system is not compatible with optical rotary joints, meaning that excessive movement can put tension on the cable, likely generating additional stress. Although mice were habituated to these conditions, KOs may still be more susceptible to fear in this environment given their overall increased anxiety phenotype. Therefore, presence of a disruptive stimulus could generate a fear response in and of itself, similar to the results of the "tone-only" conditioning group (Chapter 2, Figure 2-4).

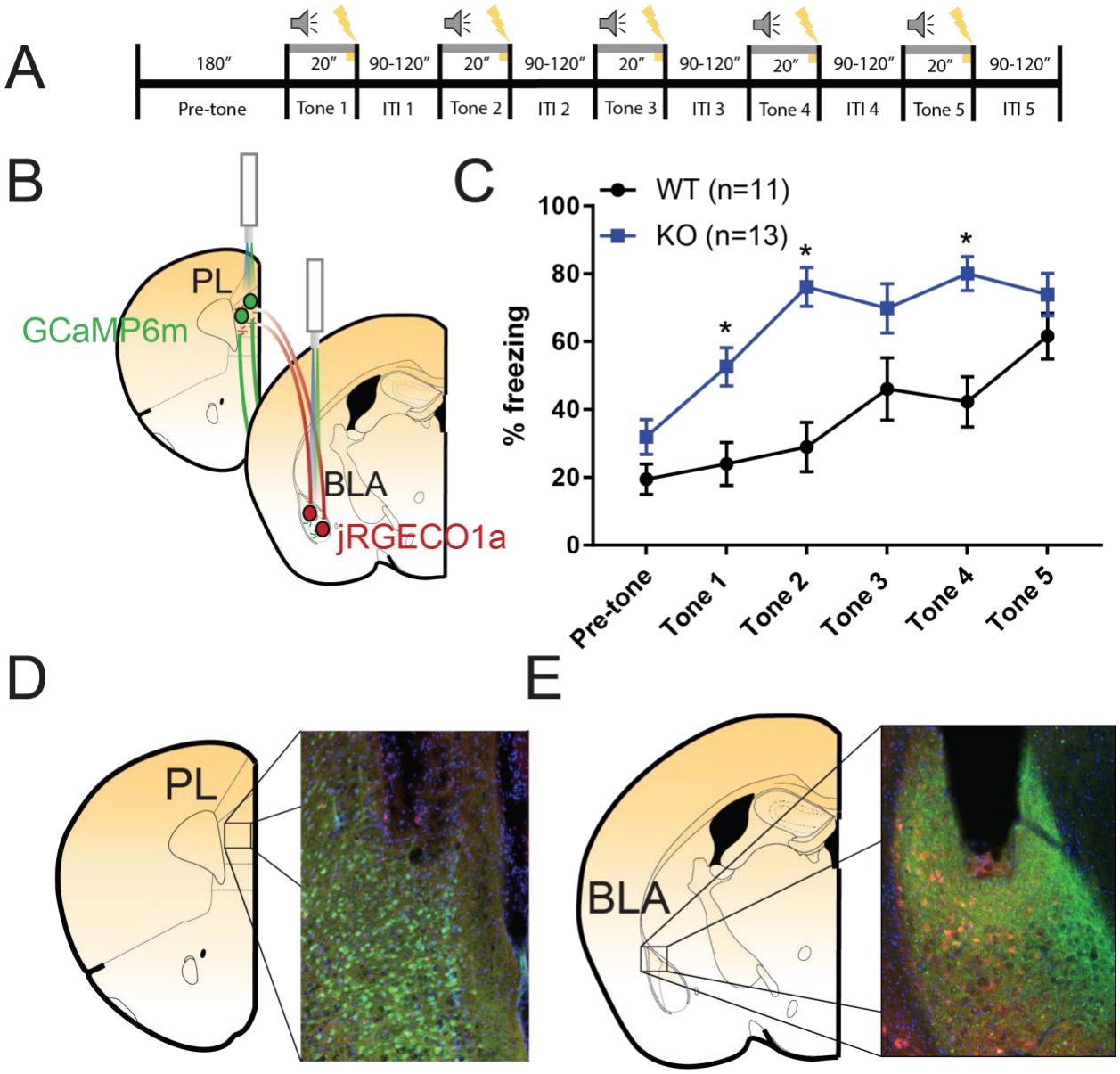

Figure 4-2. Fear conditioning with multi-site, dual color fiber photometry

A) Timeline of fear conditioning with fiber photometry. **B)** Schematic of dual-site, dual-color fiber photometry in the PL and BLA. **C)** % freezing to the pre-tone period and tones 1-5 for WT and KO mice. Main effect of time [$F(3.791,83.41)=18.41$, $p<0.0001$] and genotype [$F(1,22)=19.1$, $p=0.0002$]; time x genotype interaction [$F(5,110)=3.597$, $p=0.0047$]. Post-hoc: WT vs. KO, tones 1 ($p=0.0002$), 2 ($p<0.0001$), and 4 ($p=0.0004$). **D,E)** Example soma and terminal expression of GCaMP6m and jRGECO1a in the PL (D) and BLA (E).

On average, calcium signals in the PL were large and easily detectable. For WT mice, only 3 of 11 animals were excluded due to placements (2) or poor signal (1), and no animals were excluded from the KO group (Appendix Figure 2). Both groups demonstrated an increase in normalized fluorescence to tone (0 sec) and shock (18 sec) onset (Figure 4-3a, b). The signal had a similar shape for both WTs and KOs – a moderately sharp increase and subsequent steady drop-off throughout the tone, followed by a large, short-latency increase to the shock and a steady decay afterwards. These signals had distinct patterns when compared to control animals injected with AAV9-syn-eGFP (GFP) and AAV2-syn-tdTomato (tdTomato) (Appendix Figure 3d; Appendix Figure 4, left). Interestingly, tone-associated PL activity showed a different pattern for the fourth tone compared to other trials in WT mice. PL activity was larger and more sustained up until the shock, such that activity to tone 4 was significantly greater than tone 1 [Figure 4-3a, top; main effect of time: $F(5.098,178.4)=83.10$, $p<0.0001$; time x trial interaction: $F(208,1820)=1.440$, $p<0.0001$; post-hoc: tones 1 vs. 4, 8-8.75s ($p<0.05$), and 1 vs. 5, 26.75-29.75s ($p<0.05$)]. In addition, there was a nearly significant decrease in shock-associated activity across trials [post-hoc: trial 1 vs. 5, 19.25-20s ($p=0.0511$)]. The effect on tone-evoked activity is more pronounced when looking at the area under the curve (AUC) for the tone-only period (0-18 sec): tone 4 AUC was significantly greater than tone 1 AUC [Figure 4-3a, bottom left; $F(3.447,24.13)=3.772$, $p=0.0198$. Post-hoc: tone 1 vs. 4, $p=0.0335$]. This difference was not present in KO PL signals when considering either the full trace [Figure 4-3b, top; main effect of time: $F(5.514,330.8)=85.86$, $p<0.0001$] or tone-only AUC (Figure 4-3b, bottom left). In addition, co-shock/tone AUC (18-20 sec) decreased across trials for both WT and KO mice [**WTs:** Figure 4-3a, bottom right; $F(2.036,14.25)=4.851$, $p=0.0243$. Post-hoc: shocks 1 and 3 vs. 5 ($p=0.0063$, $p=0.0473$); trend shocks 2 and 4 vs. 5 ($p=0.0691$, $p=0.0816$). **KOs:** Figure 4-3b, bottom right; $F(2.711,32.53=6.134$,

p=0.0026. Post-hoc: shock 1 vs. 4 (p=0.0188); trend shock 1 vs. 3 and 5 (p=0.0975, p=0.0686) and 2 vs. 4 (0.0939)].

Comparing trial-by-trial WT and KO PL activity, there are no genotype differences for trials 1, 3, and 5 [**Trial 1:** Figure 4-3c, left; main effect of time: $F(3.335,63.37)=34.19$, $p<0.0001$. **Trial 3:** Figure 4-3e, left; main effect of time: $F(4.563,86.7)=27.43$, $p<0.0001$. **Trial 5:** Figure 4-3g, left; $F(6.3,119.7)=27.18$, $p<0.0001$]. For trial 2, there is a time x genotype interaction [Figure 4-3d, left; main effect of time: $F(5.106,97.02)=47.99$, $p<0.0001$; time x genotype interaction: $F(52,988)=1.889$, $p=0.0002$], likely driven by low level sustained tone activity in WTs. During trial 4, however, there is a clear difference in tone-associated activity [Figure 4-3f, left; main effect of time: $F(5.132,97.5)=32.96$, $p<0.0001$; time x genotype interaction: $F(52,988)=2.80$, $p<0.0001$; trend effect of genotype: $F(1,19)=3.519$, $p=0.0761$]. This is apparent in tone-only AUC as well (Figure 4-3f, middle; $p=0.0061$, $t=3.083$, $df=19$). Tone-only (Figure 4-3c-e, g, middle) and co-shock/tone AUC (Figure 4-3c-g, right) do not differ between WTs and KOs for any other trial.

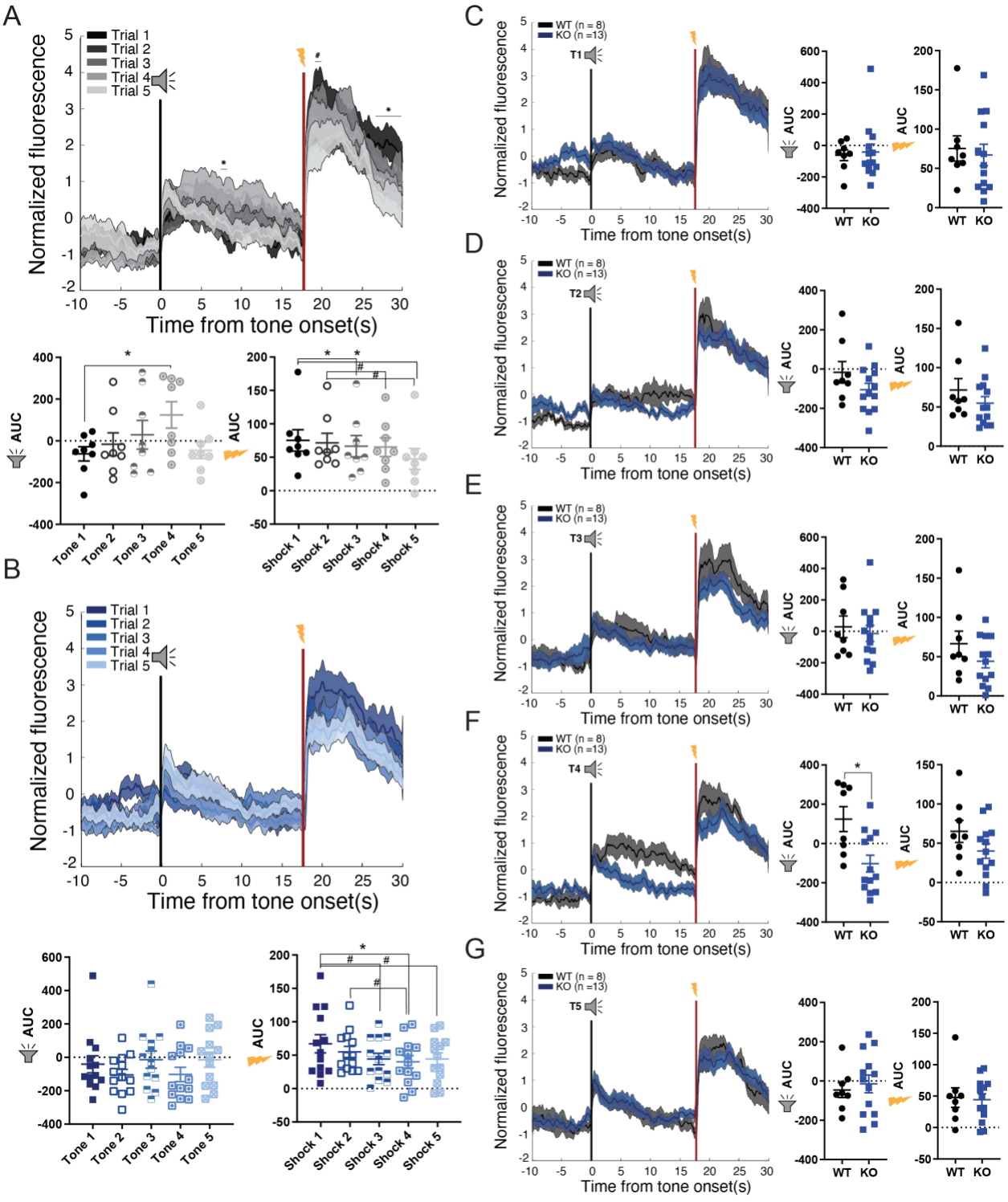

Figure 4-3. PL calcium activity is not modulated across conditioning tones in KO mice

A,B) Trial 1-5 calcium activity (top), tone AUC (bottom left), and shock AUC (bottom right) for WT (E) and KO (F) mice. **A)** Top: main effect of time [$F(5.098,178.4)=83.10$, $p<0.0001$]; time x trial interaction

[F(208,1820)=1.440, p<0.0001]. Post-hoc: tones 1 vs. 4, 8-8.75s (p<0.05) and 1 vs. 5, 26.75-29.75s (p<0.05); trend 1 vs. 5, 19.25-20s (p=0.0511). Bottom left: F(3.447,24.13)=3.772, p=0.0198. Post-hoc: tone 1 vs. 4, p=0.0335. Bottom right: F(2.036,14.25)=4.851, p=0.0243. Post-hoc: shocks 1 and 3 vs. 5 (p=0.0063, p=0.0473); trend shocks 2 and 4 vs. 5 (p=0.0691, p=0.0816). **B)** Left: main effect of time [F(5.514,330.8)=85.86, p<0.0001]. Bottom right: F(2.711,32.53=6.134, p=0.0026. Post-hoc: shock 1 vs. 4 (p=0.0188); trend shock 1 vs. 3 and 5 (p=0.0975, p=0.0686) and 2 vs. 4 (0.0939). **C-G)** WT and KO PL calcium activity (left), tone area under the curve (AUC; middle), and shock AUC (right) for trials 1-5 (G-K, top to bottom). **C)** Left: main effect of time [F(3.335,63.37)=34.19, p<0.0001]. **D)** Left: main effect of time [F(5.106,97.02)=47.99, p<0.0001]; time x genotype interaction [F(52,988)=1.889, p=0.0002]. **E)** Left: main effect of time [F(4.563,86.7)=27.43, p<0.0001]. **F)** Left: main effect of time [F(5.132,97.5)=32.96, p<0.0001]; time x genotype interaction [F(52,988)=2.80, p<0.0001]; trend effect of genotype [F(1,19)=3.519, p=0.0761]. Middle: WT vs. KO tone AUC (p=0.0061, t=3.083, df=19). **G)** Left: main effect of time [F(6.3,119.7)=27.18, p<0.0001].

In addition to during conditioning, we also collected photometry data during fear recall 24 hours later (Appendix Figure 5c; Appendix Figure 6, left). Recall tone-evoked responses were similar to trial 5 conditioning activity, with a short-latency peak and steady drop-off throughout the tone. In some cases, a smaller peak was seen immediately after tone offset (20 sec). However, unlike during conditioning, there were no within- or between-genotype effects, with the exception of a time x trial interaction for KO mice and subtle genotype differences between WTs and KOs during trials 1 and 2 [**KOs:** Appendix Figure 5c, right; main effect of time: F(6.369,382.1)=19.28, p<0.0001; time x trial interaction: F(208,3120)=1.233, p=0.0153. Post-hoc tests: trend trial 1 vs. 3, -0.25-0.5s (p=0.0524). **Trial 1:** Appendix Figure 6a, left; main effect of time: F(3.811,72.42)=10.19, p<0.0001; time x genotype interaction: F(52,988)=1.395, p=0.0359. **Trial 2:** Appendix Figure 6b, left; main effect of time: F(5.919,112.5)=10.70, p<0.0001; time x genotype interaction: F(52,988)=1.668, p=0.0025]. As with the conditioning photometry data, recall PL

activity was distinct from fluorophore control traces (Appendix Figure 7c; Appendix Figure 8, left).

Given that fear conditioning trials are typically marked by two distinct stages of behavior – freezing during the CS and an activity burst during the US – it is possible that the signals we observed were simply related to movement. Interestingly, PL activity is predominantly negatively correlated with freezing probability and positively correlated with velocity during tone presentations for both genotypes (Appendix Table 1). This is particularly true of KOs. However, there is no correlation between calcium signal and velocity for either genotype or calcium signal and freezing probability for WTs during the 3-minute pre-tone (baseline) period. Interestingly, there is still a negative correlation between freezing probability and fluorescence during the baseline period in KOs. Given that velocity and PL signal are uncorrelated in KO mice, this correlation may simply be related to an overall anxiety state. Together, these data suggest that the calcium signals we observed during conditioning were specifically related to CS-US presentations and do not represent a movement confound.

Finally, we looked at calcium signals during freezing onset and offset for both the conditioning and recall sessions. For these analyses, we exclusively analyzed freezing during the inter-trial intervals (ITIs) to avoid the potential confound of overlapping tone-associated and freezing activity. During conditioning, freezing onset was associated with a slow (~2s) decrease in activity (Appendix Figure 9b, left), while freezing offset was immediately followed by a short-latency increase in activity (Appendix Figure 9b, right) for both WT and KO mice. Interestingly, KO mice displayed significantly larger pre-onset and a trend towards larger post-offset PL activity than WT mice [**Onset:** Appendix Figure 9b, left; main effect of time: $F(3.631,69)=49.88$, $p<0.0001$; time x genotype interaction: $F(25,475)=1.973$, $p=0.0037$. **Offset:** Appendix Figure 9b,

right; main effect of time: $F(3.907,74.23)=22.58$, $p<0.0001$; trend time x genotype interaction: $F(25,475)=1.51$, $p=0.0554$]. Freezing offset during recall ITIs was characterized by similar calcium activity, but with a significant post-offset increase in KO activity compared to WT [Appendix Figure 10b, right; main effect of time: $F(3.473,62.51)=16.73$, $p<0.0001$; time x genotype interaction: $F(25,450)=2.685$, $p<0.0001$; post-hoc tests: trend 0.5-1.25s ($p=0.0563$)]. However, recall-associated freezing onset was marked by a unique pattern in KO compared to WT mice: calcium activity ramped up just prior to freezing onset, reaching a sharp peak that coincided with onset, after which it began to parallel WT signals [Appendix Figure 10b, left; main effect of time: $F(3.214,57.84)=12.53$, $p<0.0001$; time x genotype interaction: $F(25,450)=3.187$, $p<0.0001$; post-hoc tests: trend -0.25-0.5s ($p=0.0528$)]. As with tone- and shock-associated photometry signals, freezing-related activity was distinct from that of fluorophore controls (Appendix Figure 11a and d).

4.3.2 PL-BLA terminal activity is elevated to later tones in WT vs. KO mice, while KO activity decreases across trials

Unsurprisingly, PL-BLA terminal signals were smaller and harder to detect than PL soma signals. Accordingly, a total of 10 animals across the WT and KO groups (5 per genotype) were excluded from calcium data analysis (2 due to placements, 3 due to lack of signal for each group; Appendix Figure 2). Similar to the PL, PL-BLA signals in the remaining WT animals (n=6) increased slightly to tone onset and moderately to shock onset [Figure 4-4a, top; main effect of time: $F(8.708,217.7)=9.429$, $p<0.0001$)]. Moreover, there was a trend increase in tone AUC in trial 4 vs. 1 [Figure 4-4a, bottom left; $F(2.377,11.88)=4.148$, $p=0.0379$. Post-hoc: trend tone 1 vs. 4 ($p=0.0614$)], corresponding to the increase seen at tone 4 in the PL. KO PL-BLA terminal signal

(n=8) also broadly increased to tone and shock onset [Figure 4-4b, top; main effect of time: $F(8.637,302.3)=12.39$, $p<0.0001$]. However, KO tone and co-shock/tone AUC decreased across trials. Tone 3 AUC was smaller than tone 1 AUC [Figure 4-4b, bottom left; $F(2.32,16.24)=4.321$, $p=0.0269$. Post-hoc: tone 1 vs. 3 ($p=0.0743$)], and there were trend decreases between trial 1 and trials 4 and 5 co-shock/tone AUC [Figure 4-4b, bottom right; $F(2.52,17.64)=5.212$, $p=0.0121$. Post-hoc: shock 1 vs. 4 and 5 ($p=0.0914$, $p=0.0872$)]. In the case of co-shock/tone AUC, this appears to be driven by an interesting pattern. While early shock responses are characterized by a sharp uptick in PL-BLA signal that remains elevated for the duration of the shock and gradually drops off, later responses (i.e. tones 4 and 5) are marked by a short-latency increase in signal, followed by an immediate decay during the shock (18-20 sec). There is an additional post-shock increase in signal that restores PL-BLA activity to the shock level, after which it decays in a similar manner to early trials.

These effects are more apparent when comparing WT and KO signals across individual trials (Figure 4-4c-g). While there are no tone or co-shock/tone AUC differences for trials 1 and 2 (Figure 4-4c and d, middle and right), there are trend and significant time x genotype interactions for each respectively [**Trial 1**: Figure 4-4c, left; main effect of time: $F(6.668,80.01)=4.50$, $p=0.0004$; trend time x genotype interaction: $F(52,624)=1.303$, $p=0.0803$. **Trial 2**: Figure 4-4d, left; main effect of time: $F(5.857,70.29)=4.577$, $p=0.0006$; time x genotype interaction: $F(52,624)=1.445$, $p=0.0252$]. For the remaining trials, there are significant, in the case of trials 3 and 4, or trend, in the case of trial 5, main effects of genotype [**Trial 3:** Figure 4-4e, left; main effect of time: $F(5.229,62.75)=2.781$, $p=0.0231$; main effect of genotype: $F(1,12)=6.489$, $p=0.0256$; time x genotype interaction: $F(52,624)=1.381$, $p=0.0435$; post-hoc: 4.25-5.75s ($p<0.05$). **Trial 4:** Figure 4-4f, left; main effect of time: $F(6.435,77.22)=5.667$, $p<0.0001$; main

effect of genotype: F(1,12)=6.134, p=0.0291. **Trial 5:** Figure 4-4g, left; main effect of time: F(4.73,56.76)=6.788, p<0.0001; trend effect of genotype: F(1,12)=3.826, p=0.0741]. In each of these instances, WT mice display elevated tone-associated AUC compared to KOs [**Trial 3:** Figure 4-4e, middle: p=0.0052, t=3.405, df=12. **Trial 4:** Figure 4-4f, middle: p=0.0236, t=2.591, df=12. **Trial 5:** Figure 4-4g, middle: p=0.0436, t=2.255, df=12]. In addition, WT co-shock/tone AUC is greater than KO AUC during trial 4 and trending during trials 3 and 5 (**Trial 4:** Figure 4-4f, right; p=0.035, t=2.376, df=12. **Trial 3:** Figure 4-4e, right; p=0.0881, t=1.856, df=12. **Trial 5:** Figure 4-4g, right; p=0.0958, t=1.822, df=11). These differences are likely driven by the altered dynamics of KO shock-associated signals described above (Figure 4-4b, bottom right).

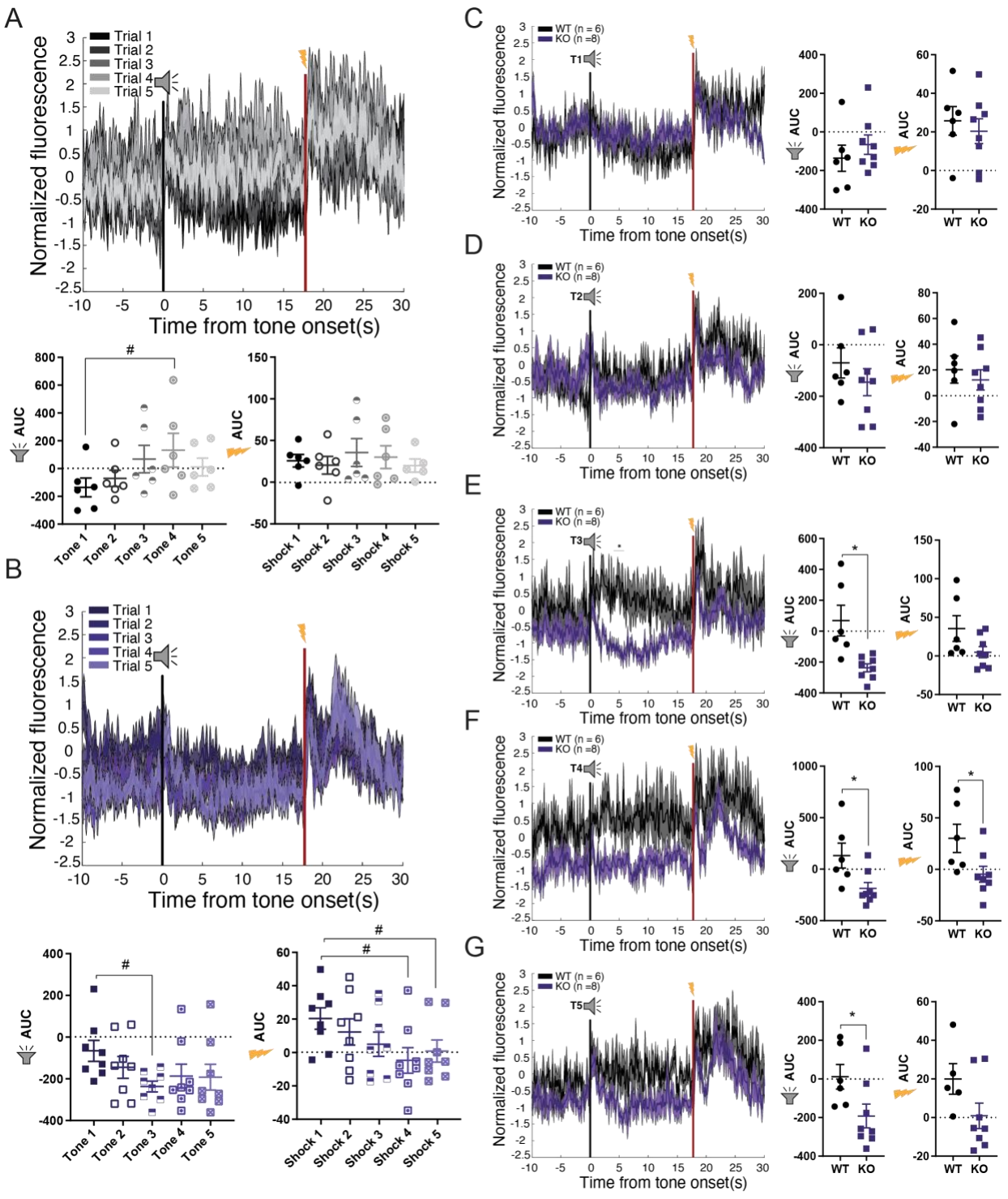

Figure 4-4. KO mice display diminished PL-BLA terminal calcium activity during late conditioning trials

A,B) Trial 1-5 calcium activity (top), tone AUC (bottom left), and shock AUC (bottom right) for WT (A) and KO (B) mice. **A)** Top: main effect of time [F(8.708,217.7)=9.429, p<0.0001]. Bottom left: F(2.377,11.88)=4.148, p=0.0379. Post-hoc: trend tone 1 vs. 4 (p=0.0614). **B)** Top: main effect of time [F(8.637,302.3)=12.39, p<0.0001].

Bottom left: F(2.32,16.24)=4.321, p=0.0269. Post-hoc: tone 1 vs. 3 (p=0.0743). Bottom right: F(2.52,17.64)=5.212, p=0.0121. Post-hoc: shock 1 vs. 4 and 5 (p=0.0914, p=0.0872). **C-G)** WT and KO PL-BLA calcium activity (left), tone AUC (middle), and shock AUC (right) for trials 1-5. **C)** Left: main effect of time [F(6.668,80.01)=4.50, p=0.0004]; trend time x genotype interaction [F(52,624)=1.303, p=0.0803]. **D)** Left: main effect of time [F(5.857,70.29)=4.577, p=0.0006]; time x genotype interaction [F(52,624)=1.445, p=0.0252]. **E)** Left: main effect of time [F(5.229,62.75)=2.781, p=0.0231] and genotype [F(1,12)=6.489, p=0.0256]; time x genotype interaction [F(52,624)=1.381, p=0.0435]. Post-hoc: WT vs. KO, 4.25-5.75s (p<0.05). Middle: WT vs. KO tone AUC (p=0.0052, t=3.405, df=12). **F)** Left: main effect of time [F(6.435,77.22)=5.667, p<0.0001] and genotype [F(1,12)=6.134, p=0.0291]. Middle: WT vs. KO tone AUC (p=0.0236, t=2.591, df=12). Right: WT vs. KO shock AUC (p=0.035, t=2.376, df=12). **G)** Left: main effect of time [F(4.73,56.76)=6.788, p<0.0001]; trend effect of genotype [F(1,12)=3.826, p=0.0741]. Middle: WT vs. KO tone AUC (p=0.0436, t=2.255, df=12).

As with the PL data, PL-BLA terminal tone-evoked responses have a similar shape during conditioning and recall, and within- and between-genotype effects during recall are minimal (Appendix Figure 5d; Appendix Figure 6, middle). There is a trend time x trial interaction for KO mice, a main effect of genotype during trial 3, and a trend effect of genotype during trial 5 [**KOs:** Appendix Figure 5d, right; main effect of time: F(6.669,233.4)=4.292, p=0.0002; trend time x trial interaction: F(208,1820)=1.15, p=0.08. **Trial 3:** Appendix Figure 6c, middle; trend effect of time: F(3.106,34.16)=2.584, p=0.0674; time x genotype interaction: F(52,572)=1.49, p=0.0173. Post-hoc tests: trend 23.25-24.5s (p=0.0672). **Trial 5:** Appendix Figure 6e, middle; trend effect of genotype: F(1,11)=4.61, p=0.0549]. In addition, PL-BLA terminal activity during conditioning and recall ITI freezing exhibited largely similar patterns to PL soma activity; however, there were no differences between KOs and WTs (Appendix Figure 9c, Appendix Figure 10c). Critically, like the PL data, PL-BLA signals have distinct patterns that are not apparent in fluorophore controls

during CS-US presentations and ITI freezing for both conditioning and recall (Appendix Figure 7d; Appendix Figure 8, middle; Appendix Figure 11b and e).

4.3.3 BLA early-conditioning shock and mid-conditioning tone activity is elevated in WT compared to KO mice

BLA signal was strong and detectable in most animals: only 2 WT and 2 KO mice were excluded (all missed placements; Appendix Figure 2), resulting in group sizes of 9 and 11, respectively. BLA activity in WT mice increased slightly to the tone, with a much larger shock-associated increase [Figure 4-5a, top; main effect of time: $F(6.518,260.7=17.02)=$, $p<0.0001$]. In addition, tone-associated activity was sustained throughout several trials, including trials 2 and 4 (Figure 4-5a, d, f). However, there were no differences across trials for either tone or co-shock/tone AUC (Figure 4-5a, bottom). KO mice, while consistently demonstrating shock-associated responses, displayed virtually no tone-associated modulation, with a slight increase in short-latency responses to tone 5 [Figure 4-5b, top; main effect of time: $F(6.312,315.6)=17.41$, $p<0.0001$]. As with WT mice, neither tone nor co-shock/tone AUC was modulated across trials (Figure 4-5b, bottom).

Comparisons of WT and KO BLA activity across trials reveal an interesting pattern. For trials 1, 2, and 3, WT mice display larger shock and post-shock activity than KOs [**Trial 1:** Figure 4-5c, left; main effect of time: $F(5.968,101.5)=6.915$, $p<0.0001$; main effect of genotype: $F(1,17)=7.548$, $p=0.0137$; time x genotype interaction: $F(52,884)=2.762$, $p<0.0001$; post-hoc tests: 18.5-19.25s ($p=0.0352$), 22.25-24.5s ($p<0.05$), 26.75-28.25s ($p<0.05$), and 29-29.75s ($p=0.0472$). **Trial 2:** Figure 4-5d, left; main effect of time: $F(5.019,90.34)=8.872$, $p<0.0001$; main effect of genotype: $F(1,18)=5.606$, $p=0.0293$; time x genotype interaction: $F(52,936)=2.114$, $p<0.0001$;

post-hoc tests: 18.5-19.25s (p=0.0311), and trends for 19.25-20s (p=0.0655) and 26.75-27.5s (p=0.088). **Trial 3:** Figure 4-5e, left; main effect of time: F(6.205,111.7)=7.284, p<0.0001; main effect of genotype: F(1,18)=5.302, p=0.0334; time x genotype interaction: F(52,936)=2.082, p<0.0001; post-hoc tests; 2-2.75s (p=0.0406), 18.5-19.25s (p=0.0108), and trends for 2.75-5.75s (p<0.09) and 19.25-20s (p=0.0656)]. This is reflected in co-shock/tone AUC as well (**Trial 1:** Figure 4-5c, right: p=0.0139, t=2.743, df=17. **Trial 2:** Figure 4-5d, right: p=0.0325, t=2.316, df=18. **Trial 3:** Figure 4-5e, right: p=0.0169, t=2.633, df=18). This pattern is attenuated in later trials, as evidenced by trend effects of genotype in trials 4 and 5 and a trend difference in co-shock/tone AUC during trial 4 [**Trial 4:** Figure 4-5f, left; main effect of time: F(3.726,67.08)=4.466, p=0.0036; trend effect of genotype; F(1,18)=4.183, p=0.0557. AUC: Figure 4-4f, right: p=0.0819, t=1.843, df=18. **Trial 5:** Figure 4-5g, left; main effect of time: F(4.205,75.69)=8.48, p<0.0001; trend effect of genotype: F(1,18)=3.794, p=0.0672]. However, there is an overall trend increase in tone AUC in WT mice compared to KOs during mid- and late-conditioning. While tone AUC is not different for trial 1, there is a trend difference for trial 2 and a significant difference for trial 3 (**Trial 1:** Figure 4-5c, middle. **Trial 2:** Figure 4-5d, middle; p=0.0841, t=1.829, df=18. **Trial 3:** Figure 4-5e, middle; p=0.0325, t=2.317, df=18). Moreover, there is a trend difference for both trials 4 and 5, indicating that this separation in genotype signaling is maintained as conditioning progresses (**Trial 4:** Figure 4-5f, middle; p=0.0739, t=1.898, df=18. **Trial 5:** Figure 4-5g, middle; p=0.0778, t=1.87, df=18).

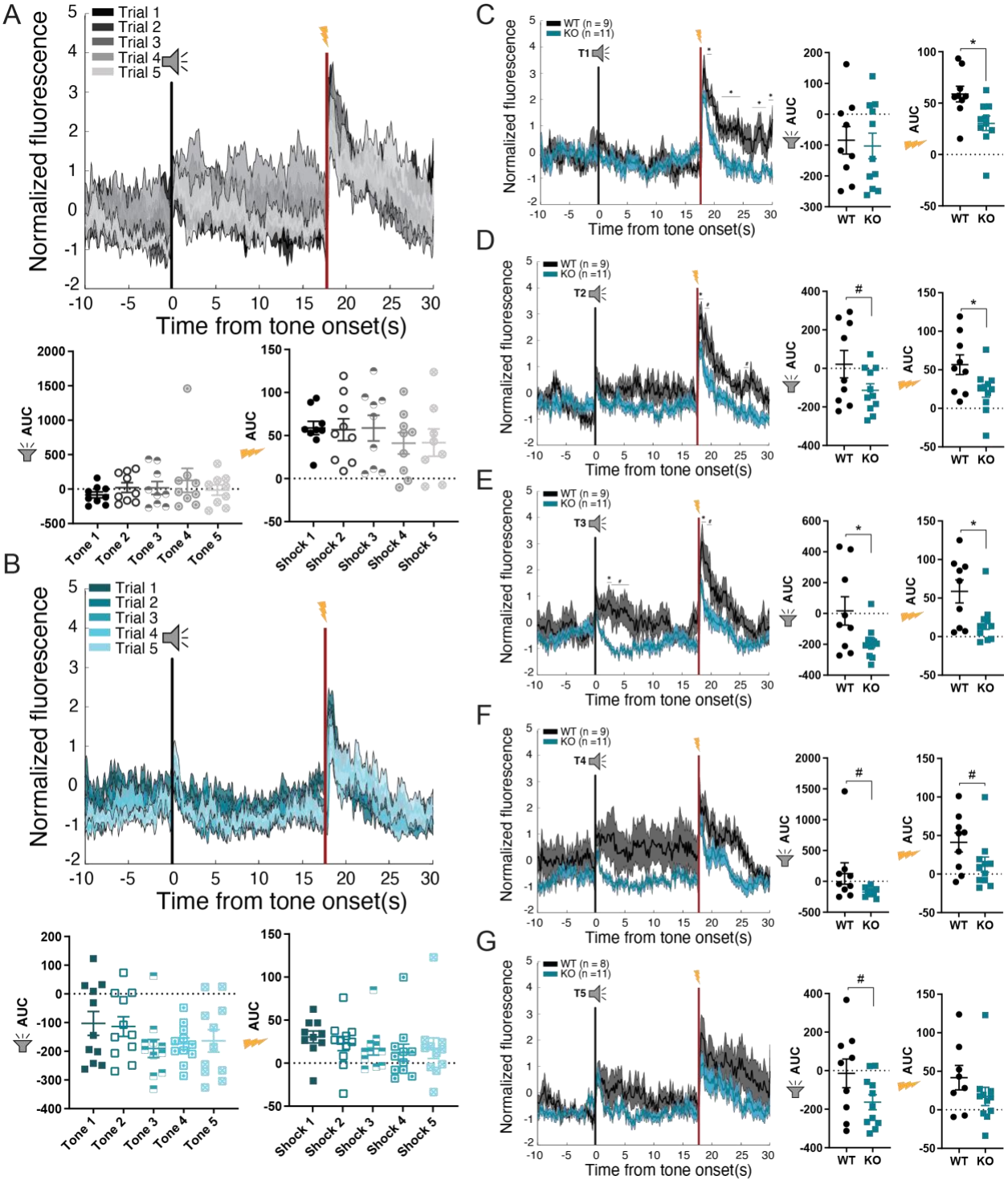

Figure 4-5. KO mice display blunted BLA calcium activity to early conditioning shocks

A,B) Trial 1-5 calcium activity (top), tone AUC (bottom left), and shock AUC (bottom right) for WT (A) and KO (B) mice. **A)** Top: main effect of time [F(6.518,260.7=17.02)=, p<0.0001]. **B)** Top: main effect of time [F(6.312,315.6)=17.41, p<0.0001]. **C-G)** WT and KO BLA calcium activity (left), tone AUC (middle), and shock

AUC (right) for trials 1-5. **C)** Left: main effect of time [$F(5.968,101.5)=6.915$, $p<0.0001$] and genotype [$F(1,17)=7.548$. $p=0.0137$]; time x genotype interaction [$F(52,884)=2.762$, $p<0.0001$]. Post-hoc: WT vs. KO, 18.5-19.25s ($p=0.0352$), 22.25-24.5s ($p<0.05$), 26.75-28.25s ($p<0.05$), and 29-29.75s ($p=0.0472$). Right: WT vs. KO shock AUC ($p=0.0139$, $t=2.743$, $df=17$). **D)** Left: main effect of time [$F(5.019,90.34)=8.872$, $p<0.0001$] and genotype [$F(1,18)=5.606$, $p=0.0293$]; time x genotype interaction [$F(52,936)=2.114$, $p<0.0001$]. Post-hoc: WT vs. KO, 18.5-19.25s ($p=0.0311$); trend 19.25-20s ($p=0.0655$) and 26.75-27.5 ($p=0.088$). Middle: WT vs. KO tone AUC trend ($p=0.0841$, $t=1.829$, $df=18$). Right: WT vs. KO shock AUC ($p=0.0325$, $t=2.316$, $df=18$). **E)** Left: main effect of time [$F(6.205,111.7)=7.284$, $p<0.0001$] and genotype [$F(1,18)=5.302$, $p=0.0334$]; time x genotype interaction [$F(52,936)=2.082$, $p<0.0001$]. Post-hoc: WT vs. KO, 2-2.75s ($p=0.0406$), 18.5-19.25s ($p=0.0108$); trend 2.75-5.75s ($p<0.09$) and 19.25-20s ($p=0.0656$). Middle: WT vs. KO tone AUC ($p=0.0325$, $t=2.317$, $df=18$). Right: WT vs. KO shock AUC ($p=0.0169$, $t=2.633$, $df=18$). **F)** Left: main effect of time [$F(3.726,67.08)=4.466$, $p=0.0036$]; trend effect of genotype [$F(1,18)=4.183$, $p=0.0557$]. Middle: WT vs. KO tone AUC trend ($p=0.0739$, $t=1.898$, $df=18$). Right: WT vs. KO shock AUC trend ($p=0.0819$, $t=1.843$, $df=18$). **G)** Left: main effect of time [$F(4.205,75.69)=8.48$, $p<0.0001$]; trend effect of genotype [$F(1,18)=3.794$, $p=0.0672$]. Middle: WT vs. KO tone AUC trend ($p=0.0778$, $t=1.87$, $df=18$).

As with both the PL and PL-BLA, BLA tone-evoked signals during recall were similar to those seen during the late stages of conditioning (Appendix Figure 5d; Appendix Figure 6, right). In addition, within- and between-genotype effects were minimal: the only observed genotype difference occurred during trial 3 [Appendix Figure 6c, right; main effect of time: $F(6.103,109.9)=4.102$, $p=0.0009$; time x genotype interaction: $F(52,572)=1.49$, $p=0.0173$]. BLA conditioning and recall calcium activity during ITI freezing onset and offset was comparable to PL activity (Appendix Figure 9d, Appendix Figure 10d). This is particularly true of freezing during recall, wherein KO mice displayed larger pre-onset and post-offset activity compared to WTs [**Onset:** Appendix Figure 10d, left; main effect of time: $F(2.726,49.06)=5.982$, $p=0.002$; time x genotype interaction: $F(25,450)=2.538$, $p<0.0001$. **Offset:** Appendix Figure 10d, right; main effect of time: $F(2.915,52.46)=18.02$, $p<0.0001$; time x genotype interaction: $F(25,450)=2.274$,

p=0.0005]. Consistent with the rest of the photometry data, BLA soma displayed different patterns during conditioning and recall trials and ITI freezing than control fluorophore data (Appendix Figure 7d; Appendix Figure 8, right; Appendix Figure 11c and f).

4.3.4 KO mice display elevated fear generalization compared to WTs

At first pass, our photometry data is counterintuitive. In line with previous behavioral cohorts, we see enhanced fear conditioning in KO mice compared to WTs. However, we observed little to no modulation in PL soma, PL-BLA terminals, and BLA soma activity in KO mice across conditioning. Moreover, KO mice tended to have to smaller calcium signals than WT mice at multiple stages of conditioning. Conversely, WT signals – PL soma and PL-BLA terminals in particular – significantly increased over the course of conditioning. Considering that KO mice display elevated freezing and the PL/BLA circuit is critical for fear acquisition and expression, we might have predicted the opposite pattern. In light of these findings, we theorized that differential signaling in this circuit represents specific learning of CS-US associations. The PL soma and PL-BLA terminal modulation seen in WT mice coincides with increased freezing to the tones, suggesting that this activity may drive online processing of the CS-US relationship. KO mice, on the other hand, already display elevated freezing to the first tone, prior to experiencing any shock. While they certainly still exhibit a learning curve after additional CS-US pairings, this initial increase in freezing indicates that generalized fear may be relevant to KO behavior. Thus, normal PL/BLA circuit activity may be necessary to form a more specific understanding of the CS-US relationship, as seen in WT, while freezing behavior in KO mice may be driven by a combination of specific and generalized fear.

To begin exploring this theory, we more concretely assessed fear generalization in KO mice by conducting discriminative fear conditioning (WT n=11, KO n=13). Mice were exposed to 10 presentations each of two distinct tones, of which one was paired with a US (CS+) and the other was not (CS-) (Figure 4-6a). As anticipated, KO mice froze more than WTs overall and generalized to the CS-, as evidenced by similar levels of freezing to both CS types [Figure 4-6b; main effect of time: $F(10,220)=17.46$, $p<0.0001$; main effect of genotype: $F(1,22)=23.98$, $p<0.0001$; time x genotype interaction: $F(10,220)=4.653$, $p<0.0001$]. Unexpectedly, WT mice also appeared to generalize to the CS-. However, we noticed during initial scoring of freezing behavior, both in this experiment and pilot experiments, that mice appeared to engage in darting. Darting, first described by Gruene et al. (2015), is a defensive behavior seen in fear conditioning and is characterized by brief, high velocity movements that are distinct from locomotion. Indeed, when we quantified this behavior, we saw that WT mice darted more than KOs, with a specific increase in darting during CS+ presentations relative to WT CS- trials and both KO CS+ and CS- trials [Figure 4-6c; main effect of time: $F(10,220)=4.783$, $p<0.0001$; main effect of genotype: $F(1,22)=39.07$, $p<0.0001$; time x genotype interaction: $F(10,220)=2.154$, $p=0.0217$; time x CS type interaction: $F(10,220)=2.15$, $p=0.0219$; time x genotype x CS type interaction: $F(10,220)=2.103$, $p=0.0253$]. [Of note, darting was not observed to a great extent in the fiber photometry cohort (Appendix Figure 12b, e)]. These data suggest that WT mice do discriminate between the CS+ and CS-, but that this is expressed using a different defensive response than freezing.

In order to assess the number of discriminators and generalizers in each group, we combined freezing and darting into one measure of discrimination (see Chapter 4.2: Methods for details; Appendix Figure 13). Each mouse's behavior was collapsed across all CS+ or CS- trials such that there was a single value for each. The values ranged from -1 to 1 and indicated what type

of behavior the animal predominantly used during either the CS+ or CS-: values from -1 to -0.5 were marked as darting, 0.5 to 1 were freezing, and -0.5 to 0.5 were considered a mixed strategy (Appendix Figure 13a, b). Mice were then classified as discriminators if they engaged in different defensive behaviors during CS+ and CS- presentations, or generalizers if their behavior was the same. Using this method, we found that a larger percentage of WT mice were discriminators than KO mice [Figure 4-6d; left, WT: 8 discriminators (72.73%), 3 generalizers (27.27%); right, KO: 5 discriminators (38.46%), 8 generalizers (61.54%)]. Most of the WT discriminators engaged in darting during the CS+ and a mixed strategy during the CS-, while most KO generalizers froze to both the CS+ and CS- (Appendix Figure 13c, e). In summary, these data demonstrate that WT mice are able to discriminate between aversive and neutral stimuli during fear conditioning via distinct defensive responses (darting vs. freezing), while KO mice exhibit the same fear response (freezing) to both stimuli.

In addition to online discrimination during conditioning, we also assessed discrimination acquisition via fear recall 24 hours later (Figure 4-6e). Surprisingly, KO mice discriminated between the CS+ and CS- in their freezing behavior [Figure 4-6f; main effect of time: $F(5,110)=15.38$, $p<0.0001$; main effect of genotype: $F(1,22)=11.99$, $p=0.0022$; time x genotype interaction: $F(5,110)=2.99$, $p=0.0144$; time x CS type interaction: $F(5,110)=2.929$, $p=0.016$]. Similar to conditioning, WT mice discriminated as well, but only when assessing darting [Figure 4-6g; main effect of time: $F(5,110)=6.365$, $p<0.0001$; main effect of genotype: $F(1,22)=8.552$, $p=0.0079$; main effect of CS type: $F(1,22)=4.545$, $p=0.0444$; time x CS type interaction: $F(5,110)=2.603$, $p=0.0289$; trend time x genotype interaction: $F(5,110)=2.171$, $p=0.0625$]. This pattern was also apparent when animals were classified on the recall day: WT and KO groups had roughly equal numbers of discriminators and generalizers (Figure 4-6h), with WT discriminators

predominantly engaging in darting (Appendix Figure 13d, left) and KO discriminators engaging in freezing (Appendix Figure 13d, right) during the CS+. These data suggest that unlike during conditioning, both WT and KO mice are able to discriminate during memory retrieval.

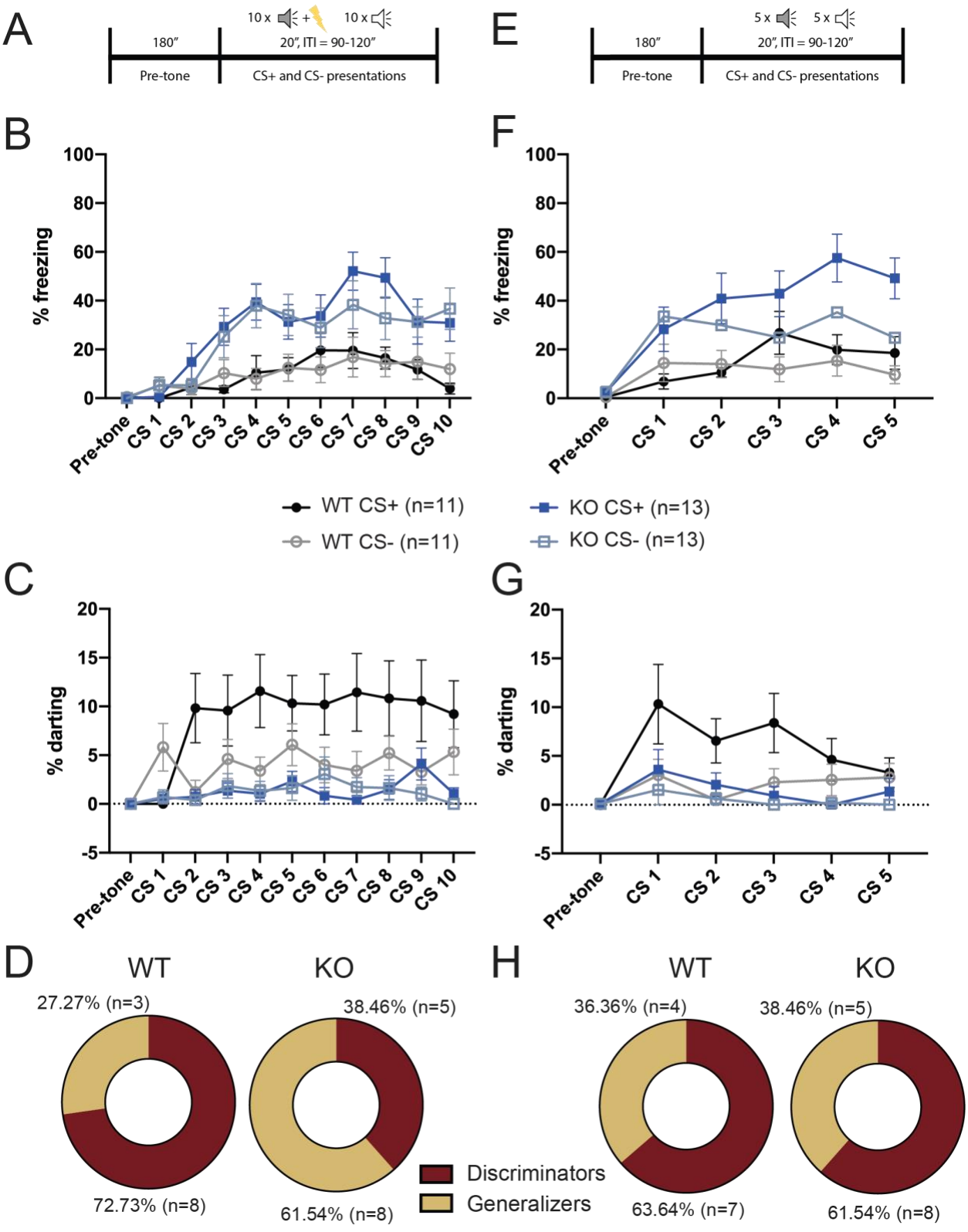

Figure 4-6. KO mice generalize between paired and unpaired tones, while WT mice discriminate using distinct defensive behaviors

A) Timeline for discriminative fear conditioning. After a 3-minute pre-tone period, there were 10 presentations each of a CS+/US and CS-. **B)** Conditioning % freezing for WT (n=11) and KO (n=13) mice during CS+ (black circles for WT, dark blue squares for KO) and CS- (grey open circles for WT, light blue open squares for KO) presentations. Main effect of time: $F(10,220)=17.46$, $p<0.0001$; main effect of genotype: $F(1,22)=23.98$, $p<0.0001$; time x genotype interaction: $F(10,220)=4.653$, $p<0.0001$. **C)** Conditioning % darting for WT and KO mice during CS+ and CS- presentations. Main effect of time: $F(10,220)=4.783$, $p<0.0001$; main effect of genotype: $F(1,22)=39.07$, $p<0.0001$; time x genotype interaction: $F(10,220)=2.154$, $p=0.0217$; time x CS type interaction: $F(10,220)=2.15$, $p=0.0219$; time x genotype x CS type interaction: $F(10,220)=2.103$, $p=0.0253$. **D)** Conditioning discriminator and generalizer breakdown for WTs (left) and KOs (right). **E)** Timeline for discriminative fear recall. After a 3-minute pre-tone period, there were 5 presentations each of a CS+ and CS-. **F)** Recall % freezing for WT and KO mice during CS+ and CS- presentations. Main effect of time: $F(5,110)=15.38$, $p<0.0001$; main effect of genotype: $F(1,22)=11.99$, $p=0.0022$; time x genotype interaction: $F(5,110)=2.99$, $p=0.0144$; time x CS type interaction: $F(5,110)=2.929$, $p=0.016$. **G)** Recall % darting for WT and KO mice during CS+ and CS- presentations. Main effect of time: $F(5,110)=6.365$, $p<0.0001$; main effect of genotype: $F(1,22)=8.552$, $p=0.0079$; main effect of CS type: $F(1,22)=4.545$, $p=0.0444$; time x CS type interaction: $F(5,110)=2.603$, $p=0.0289$; trend time x genotype interaction: $F(5,110)=2.171$, $p=0.0625$. **H)** Recall discriminator and generalizer breakdown for WTs (left) and KOs (right).

4.3.5 Temporally specific PL inhibition disrupts online CS-US association formation, but not fear acquisition

Our photometry data suggest that PL activity during later conditioning tones may underlie a specific understanding of the CS-US relationships in WTs, while KO behavior may be driven by a combination of specific and generalized fear learning. Thus, the lack of PL modulation seen in KOs may reflect a poorer understanding of CS-US association, while altered activity in distinct circuits could still result in increased freezing relative to WTs. In support of this theory, KO mice generalize more to the CS- during discriminative fear conditioning than WTs. To test this further,

we conducted temporally specific inhibition of PL excitatory neurons during fear conditioning. We reasoned that if PL activity during tones was necessary for online CS-US association formation in WTs, inhibition would decrease freezing. Conversely, if behavior in KO mice is attributable to both specific and generalized fear, inhibition would have either a limited effect or no effect at all on behavioral output. For these experiments, AAV5-CaMKII-ArchT-GFP (ArchT) or AAV5-CaMKII-eYFP (eYFP) was bilaterally injected and optogenetic fibers were chronically implanted into the PL of WT (n=16 for eYFP; n=16 for ArchT) and KO (n=16 for eYFP; n=15 for ArchT) mice five weeks prior to fear conditioning (Figure 4-7a,b). 3 WTs and 5 KOs in the ArchT condition were excluded due to placements and/or virus expression (Appendix Figure 14). During conditioning, the PL was inhibited throughout the duration of each of the 5 CS-US presentations (Figure 4-7c; 532nm laser, 10mW, constant light). 24 hours later, mice were exposed to 5 retrieval tones in the absence of illumination (Figure 4-7e).

As with previous cohorts, WT and KO mice increased freezing to the tones across conditioning [Figure 4-7d; main effect of time: $F(6.712,342.3)=56.79$, $p<0.0001$; main effect of genotype: $F(1,51)=27.46$, $p<0.0001$; time x genotype interaction: $F(10,510)=2.42$, $p=0.0081$]. However, ArchT-mediated inhibition of PL excitatory neurons decreased freezing in both WT and KO mice compared to eYFP controls [Figure 4-7d; main effect of virus: $F(1,51)=5.096$, $p=0.0283$; time x virus interaction: $F(10,510)=3.58$, $p=0.0001$]. Interestingly, PL inhibition affected freezing both during joint CS-US presentation and illumination and during subsequent unilluminated ITIs. Moreover, the effects appeared to be cumulative: inhibition did not differentially affect ArchT and eYFP groups during early tones and ITIs, but instead had a delayed effect on behavior later in conditioning. This was most evident in the KO ArchT group, which showed a similar level of freezing to the KO eYFP group up through tone 3. Beginning at ITI 3, however, freezing was

attenuated to the level of the WT eYFP group. Similarly, WT ArchT freezing was comparable to that of WT eYFP mice until ITI 3, after which there was a slight decrease in freezing.

As with the photometry cohort, we did not observe a significant amount of darting in this experiment (Appendix Figure 12c, f). While there were several instances of darting across both conditioning and recall sessions, there were no main effects or interactions and the overall level of darting was near zero. Notably, we did observe spinning behavior in several mice, wherein a mouse would move quickly and repeatedly in tight, small circles (Appendix Figure 15). The directionality (i.e. clockwise or counter-clockwise) was consistent within an animal. Accordingly, in many, but not all, of the mice that presented with this phenotype, there was slightly more viral expression directly under the fiber contralateral to the spinning direction (e.g. more virus on the left side was associated with clockwise spins and vice versa). Spinning predominantly occurred outside of illumination periods and did not immediately follow inhibition. This behavior was observed primarily in ArchT-expressing animals of both genotypes, but was also observed in one WT and KO eYFP animal each [Appendix Figure 15a; main effect of virus: $F(1,51)=7.177$, $p=0.0099$; trend effect of time: $F(2.936,149.7)=2.379$, $p=0.0734$; trend time x genotype interaction: $F(10,510)=1.705$, $p=0.0766$]. Importantly, spinning did not account for the observed changes in freezing during conditioning: when all spinners were excluded, the freezing data look quite similar (Appendix Figure 15b). As with the complete dataset, there were main effects of time, genotype, and virus, as well as a time x virus interaction [main effect of time: $F(5.555,216.6)=36.98$, $p<0.0001$; main effect of genotype: $F(1,39)=12.45$, $p=0.0011$; main effect of virus: $F(1,39)=6.786$, $p=0.0129$; time x virus interaction: $F(10,390)=3.776$, $p<0.0001$]. The only difference was a lack of a time x genotype interaction [$F(10,390)=1.455$, $p=0.1542$]; however, given that the overall

patterns are the same as the original data, this discrepancy is most likely due to decreased power associated with excluding animals.

Unlike during conditioning, inhibition-related differences in freezing were weak during fear memory recall, in the complete absence of illumination (Figure 4-7f). WT and KO mice both demonstrated freezing to recall tones, with greater fear expression in KOs [Figure 4-7f; main effect of time: $F(4.222,215.3)=14.9$, $p<0.0001$; main effect of genotype: $F(1,51)=38.31$, $p<0.0001$]; however, there was only a trend effect of virus [$F(1,51)=3.455$, $p=0.0688$], indicating that the carryover effect of inhibition during conditioning is limited. Considering that WT eYFP freezing decreases after tone 3, it is possible that PL inhibition during conditioning could enhance fear extinction in WT, and perhaps KO, animals. However, this would need to be tested in follow-up experiments.

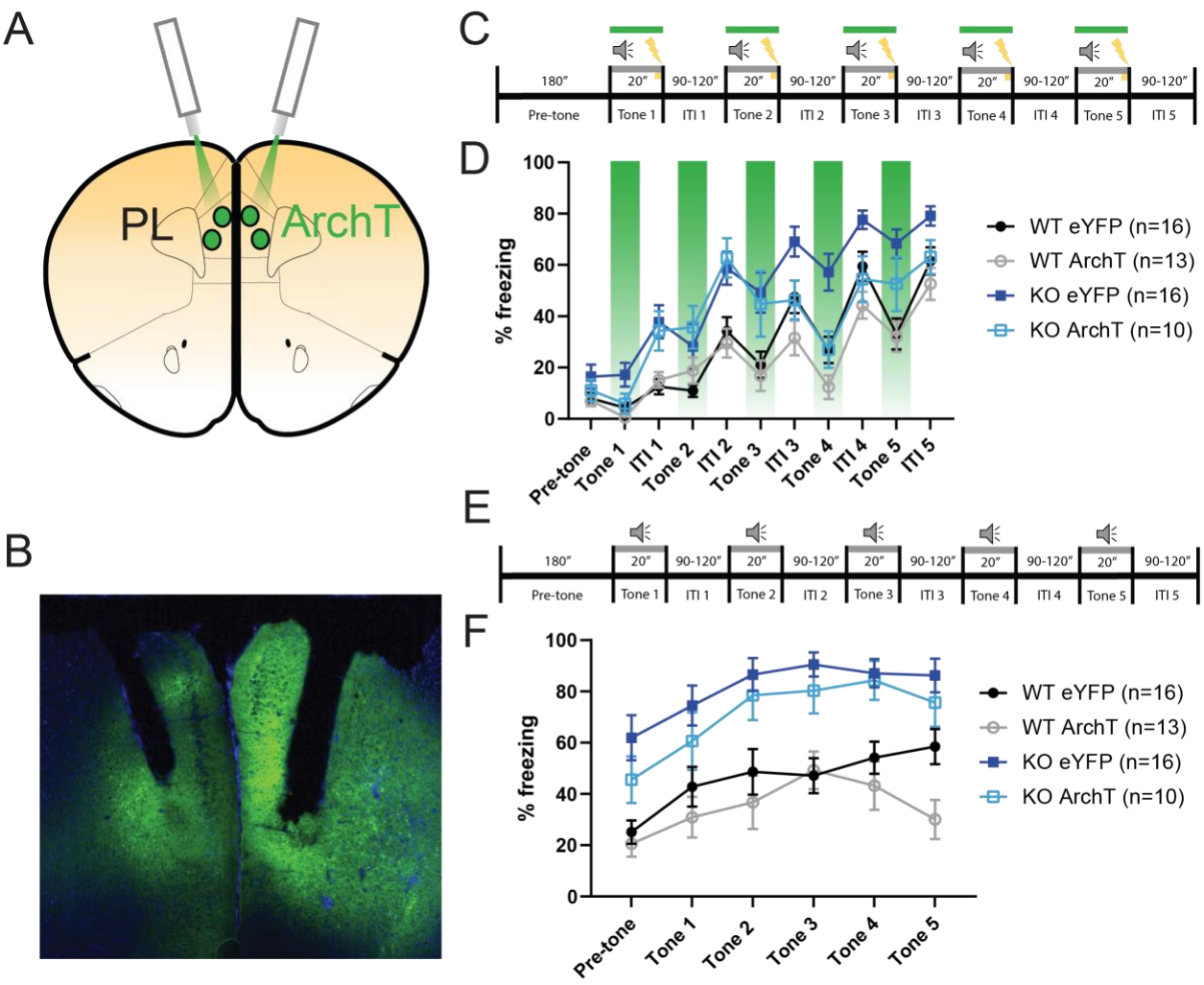

Figure 4-7. Optogenetic inhibition of PL excitatory neurons during conditioning tones attenuates freezing during conditioning, but not recall

A,B) Schematic of bilateral PL optogenetic inhibition (A) and example histology (B). **C)** Timeline of fear conditioning with optogenetic inhibition (top). Green bars represent periods of optogenetic inhibition. **D)** % freezing during the conditioning pre-tone period, tones 1-5, and ITIs 1-5 for WT eYFP (n=16; black filled circles), WT ArchT (n=13; grey open circles), KO eYFP (n=16; dark blue filled squares), and KO ArchT groups (n=10; light blue open squares). Green columns represent periods of illumination. Main effects of time [$F(6.712,342.3)=56.79$, $p<0.0001$], genotype [$F(1,51)=27.46$, $p<0.0001$], and virus [$F(1,51)=5.096$, $p=0.0283$]; time x genotype interaction [$F(10,510)=2.42$, $p=0.0081$]; time x virus interaction [$F(10,510)=3.58$, $p=0.0001$]. **E)** Timeline of recall session. **F)** % freezing during the recall pre-tone period and tones 1-5 for WT eYFP, WT ArchT, KO eYFP, and KO ArchT

groups. Main effect of time [$F(4.222,215.3)=14.9$, $p<0.0001$] and genotype [$F(1,51)=38.31$, $p<0.0001$]; trend effect of virus [$F(1,51)=3.455$, $p=0.0688$].

4.4 Discussion

In the present set of experiments, we examined the role of the PL/BLA circuit in fear conditioning in SAPAP3 KO and WT mice. Using multi-site, dual color fiber photometry, we collected neural activity in PL soma, PL-BLA terminals, and BLA soma during online processing of fearful associations. Interestingly, we saw modulation in these signals, particularly the PL, throughout conditioning in WT, but not KO, mice, despite observing enhanced freezing behavior in the latter. This led us to theorize that PL activity may represent specific learning of the CS-US relationship. Since WT mice freeze more later in the session and enhanced tone-associated PL activity only occurs at later tones, this suggests that PL tone activity is specifically related to fear learning during conditioning. Thus, in WT mice, the increased calcium activity in these regions during training could indicate a specific response to the CS-US, which is reflected in a more gradual increase in freezing. Conversely, KO mice display a steep learning curve, as well as increased freezing to the first tone. Since there is increased freezing across the session, this suggests that KOs are also learning the specific CS-US association. However, given the elevated freezing response to the first tone, which occurs prior to a CS-US pairing, KO mice are likely engaging generalized fear circuitry as well, which could explain the lack of tone-associated modulation in PL activity. In support of this theory, we found that KO mice generalize more than WTs during discriminative fear conditioning. Finally, we examined the role of PL activity by inhibiting glutamatergic neurons during CS-US presentations. In both genotypes, PL inhibition

decreased freezing to tone presentations and ITIs during conditioning itself, but not during recall. Of note, PL inhibition in KOs did not completely restore freezing to the level of uninhibited WTs, further supporting our hypothesis that additional generalized fear circuitry is relevant to KO behavior. Taken together, these data indicate that tone-associated PL modulation across trials drives online CS-US processing in WT mice. In KOs, therefore, the lack of PL modulation suggests that fear behavior is produced via a combination of increased specific and generalized fear compared to WTs.

Our PL/BLA imaging data complement and expand upon the existing literature in several key ways. These data provide the first extensive, simultaneous analysis of PL, PL-BLA terminal, and BLA signals during online processing of fearful associations. This is especially interesting in the case of the PL, given that studies have primarily focused on activity during recall and extinction. Similar to olfactory fear conditioning in rats (Laviolette et al., 2005), we found that PL signal increases during conditioning in WT mice. This supplements the numerous studies that have observed tone-associated PL signals after conditioning (Baeg, 2001; Burgos-Robles et al., 2009; Sotres-Bayon et al., 2012; Fitzgerald et al., 2014; Halladay and Blair, 2015; Dejean et al., 2016; Giustino et al., 2016). One study in particular found that the PL exhibits sustained tone responses post-conditioning that are correlated with freezing on a second-by-second timescale (Burgos-Robles et al., 2009). Interestingly, we found the opposite relationship in our dataset: PL activity was generally negatively correlated with freezing and positively correlated with velocity during tone presentations for both genotypes. However, such correlations were absent during the pre-tone period. Paired with the finding that only a small percentage of PL neurons are movement selective (Halladay and Blair, 2015), this suggests that the relationship between velocity and PL activity during tones is coincidental. With respect to freezing, additional studies have found a positive

relationship between freezing and mPFC tone-associated signals (Dejean et al., 2016), while other studies have reported either no correlation (Baeg, 2001) or a negative correlation when looking specifically at PL parvalbumin-positive (PV+) interneurons (Courtin et al., 2014). As Baeg (2001) aptly wrote, "there exists no simple relationship" between mPFC signal and freezing. Moreover, the study in which a correlation was detected specifically analyzed excitatory signals from tone-responsive single units (Burgos-Robles et al., 2009), which only constitute 20% of PL neurons (Burgos-Robles et al., 2009; Sotres-Bayon et al., 2012). In fact, there is significant heterogeneity in PL tone response profiles in the literature both within (Baeg, 2001; Dejean et al., 2016) and between (Sotres-Bayon et al., 2012; Courtin et al., 2014; Fitzgerald et al., 2014; Giustino et al., 2016) studies. For example, one study found that presumptive interneurons predominantly increased their firing to the CS and presumptive principal neurons decreased their firing (Baeg, 2001), while another study found that PV+ interneurons were inhibited to the CS (Courtin et al., 2014). Therefore, given that the present data was acquired from all tone-responsive PL cells, regardless of cell type, signal directionality, or signal dynamics, heterogeneity across and within cell types could account for the differences between our data and previous reports.

Like the PL data, our BLA data primarily complements the existing literature. In WT mice, we observed tone- and shock-related responses across conditioning. This is consistent with numerous studies showing that neurons in the BLA develop CS responses during and after training (Quirk et al., 1995; Maren, 2000; Goosens et al., 2003; Herry et al., 2008; Amano et al., 2011; Wolff et al., 2014). As with the PL data, however, there are differences in the neural response depending on the cell type and specific location. For example, PV+ interneurons are excited during CS presentations, which leads to disinhibition of principle neurons via inhibition of somatostatin-positive (SOM+) interneurons (Wolff et al., 2014). Moreover, only a subset of basal amygdala

neurons are classified as “fear neurons” – those that acquire CS responses during and after fear conditioning. When considering different subnuclei, neurons in the lateral amygdala exhibit short latency CS responses (Quirk et al., 1995; Maren, 2000), while basal amygdala neurons develop sustained responses throughout the duration of the CS (Amano et al., 2011; Pendyam et al., 2013). In our data, we see moderate CS responses in WT mice that appear to be sustained during later conditioning tones; however, the responses during recall tones are not sustained. This could be explained by the nature of our calcium signal, which includes both principal neurons and interneurons, as well as fiberoptic placement: a majority of placements were in more lateral aspects of the BLA as opposed to basal.

A benefit of our *in vivo* fiber photometry design is that we were able to collect neural data from nearly the complete PL/BLA circuit in the same animals. This enables us to more concretely assess a model of PL/BLA signaling during fear conditioning that was developed by Pendyam et al. (2013). In this model, lateral amygdala neurons develop short-latency CS responses which are then converted to sustained responses in the basal amygdala. Next, basal amygdala neurons facilitate conversion of short latency PL CS signals into sustained signals via direct projections. Finally, PL-to-basal amygdala signaling is necessary to maintain sustained CS responses. This model is empirically supported by the findings that basal amygdala “fear neurons” project to the mPFC (Herry et al., 2008); BLA-responsive mPFC neurons increase CS activity during olfactory fear conditioning and BLA inactivation impairs this response (Laviolette et al., 2005); BLA post-training inactivation decreases PL tone responses (Sotres-Bayon et al., 2012); PL-projecting basal amygdala neurons exhibit increases in CS responsiveness after training and inhibition of these cells attenuates fear expression (Senn et al., 2014); PL-BLA terminal inhibition decreases freezing

during recall (Do-Monte et al., 2015b); and PL-BLA synapses are potentiated following fear conditioning (Arruda-Carvalho and Clem, 2014).

In our data, we appear to see sustained BLA tone responses in WT mice develop across conditioning, albeit moderately. Late in conditioning, we also see a sustained PL response to the fourth tone that is reflected in PL-BLA terminals, highlighting the relevance of this specific projection. In KOs, we observed diminished tone and shock responses in the BLA compared to WTs. Perhaps due to a blunted BLA response, there is a marked lack of trial-related modulation in the PL and abnormal decreases in PL-BLA terminal tone- and shock-associated activity. Notably, we were unable to acquire BLA-PL terminal data in our study. There are several possible explanations for the lack of signal in our experiments. First, the terminal field, while readily detectable via immunofluorescence, is sparse compared to the PL-BLA terminals. Given the size of the fiberoptic implant (200μM), the number of terminals in the imaging field may have been insufficient for detection. Second, red calcium probes are notoriously dimmer than green, and while jRGECO1a is an improvement compared to previous indicators (Dana et al., 2016), this may still be a factor. Combined with the fact that terminal signals are weaker than soma signals, our power to detect BLA-PL terminal activity was diminished. Absent BLA-PL signals, we can only speculate about the relationship between BLA signals and the PL soma and PL-BLA terminal signals we observed in both the healthy and abnormal states. For example, we might predict that WT BLA-PL CS responses become sustained during conditioning, either prior to or in conjunction with changes in PL and PL-BLA signals. In addition, we hypothesize that there will be either no or diminished CS modulation in KO BLA-PL terminal signal. Future studies will endeavor to addresses these questions. Taken together, our data bolster existing models of PL/BLA signaling by providing evidence during initial CS-US pairings.

In addition to conditioning CS-US presentations, we also collected calcium data during recall CS presentations and inter-trial interval (ITI) freezing during both the conditioning and recall sessions. There were virtually no genotype differences in PL/BLA signaling during recall, suggesting that either 1) freezing during fear memory retrieval is driven by distinct circuits compared to online fear processing, 2) plasticity that occurs during or after conditioning is sufficient to drive elevated freezing during recall, or 3) differential signaling in generalized fear circuitry drives enhanced fear expression in KO mice. One or more of these mechanisms may be at play. During ITI freezing, we observed an interesting pattern: KO mice displayed elevated PL activity immediately pre-onset and post-offset compared to WTs. This was true for both conditioning and recall freezing, although the latter was characterized by sharper KO signals and a larger difference between KO and WT calcium activity. Moreover, the BLA exhibited similar activity to the PL during recall, with greater activation in KOs compared to WTs. These data are slightly at odds with tone- and shock-associated signals – during ITIs, elevated freezing is paired with enhanced PL/BLA activity, while similarly elevated freezing during CS-US presentations is marked by diminished PL/BLA activity in KOs relative to WTs. However, this pattern may be reflective of the overall anxiety phenotype in KO mice. In support of this theory, the mPFC has repeatedly been implicated in anxiety-like behavior (Adhikari et al., 2010, 2011; Likhtik et al., 2014; Stujenske et al., 2014; Likhtik and Paz, 2015; Padilla-Coreano et al., 2016; Marcus et al., 2019). Thus, elevated freezing without the presence of a discrete cue, such as during ITIs, might be driven by enhanced PL signaling that is associated with greater anxiety, while PL signaling during specific cued freezing could still remain unmodulated.

A particularly intriguing finding in our data was that WT mice exhibited significantly more darting to the CS+ than the CS- during discriminative fear conditioning. To our knowledge, this is

the first extensive report of darting in mice or in male rodents of any kind – thus far, conditioned darting has primarily been observed in female rats (Gruene et al., 2015; Colom-Lapetina et al., 2019; Greiner et al., 2019; Odynocki and Poulos, 2019). Anecdotal accounts of CS-induced activity bursts that could be described as darting have been reported in male rats (Baeg, 2001), but they have never been quantified or rigorously investigated. In line with our data, a recent study found that CS+, and not CS-, presentations "sometimes induced small startle responses" in male mice; however, unlike in our experiments, freezing was still the primary defensive strategy employed by these mice (Takemoto and Song, 2019).

Interestingly, we only observed significant darting during discriminative fear conditioning, not during fiber photometry or optogenetic fear conditioning experiments (Appendix Figure 12). A potential explanation for these differences is tethering – slight restrictions in the ease of movement may have caused mice to favor freezing over darting. However, while there was not a significant amount of darting with concurrent fiber photometry or optogenetics, there were several instances, indicating that mice can still perform this behavior. Moreover, shock-related behavior, which consists of rapid running and jumping, was qualitatively similar in untethered and tethered animals, and several tethered animals displayed sporadic jumping outside of shock periods. Taken together, these data suggest that tethering did not substantially restrict performance of more active behaviors. Another explanation for the darting differences across our experiments is the shock parameters. In the fear conditioning experiments, the US is a 2s, 1mA shock, while the discriminative fear conditioning shock is 0.5s and 0.5mA. Mice might treat a milder shock differently than a stronger shock: the former, which is both shorter and less intense, may be viewed as potentially escapable, resulting in active darting behavior, while the latter may be perceived as unavoidable. In the case where a shock is inescapable, darting would not achieve a different

outcome than freezing, so it may be preferable to conserve energy. A third possibility is that the presence of a CS- requires additional cognitive processing. With multiple stimuli predicting distinct outcomes, it is important to encode those stimuli differently. Thus, the response to a CS+, which predicts a certain, imminent threat, will be different than the response to a CS-, which does not. In the case of SAPAP3 KOs, differential encoding of the CS-US relationship may be impaired, leading to similar behavioral responses.

Another consideration pertaining to our discriminative fear conditioning data is the discriminator/generalizer classification. While this is a useful measure to get a broad sense of trends within the data, it should be taken with a grain of salt for several reasons. First, this combination of darting and freezing behavior is complex. The most logical analysis would be to summate the percentage of time spent freezing and darting for each animal to yield a metric of all defensive behaviors. However, the drastically different scales of these two behaviors make this impractical. The difference in scale is due to the way in which darting was scored – each dart, which is a relatively quick movement by nature (~1-2 seconds) was scored individually. However, animals typically dart more than once during the tone, with periods of quiescence in between darts. This behavior as a whole may be critical, meaning that the percent of time spent darting does not fully encompass the relevant behavioral state. Thus, as described in the methods, we devised a method of putting freezing and darting on the same scale. A second shortcoming of our classification analysis is that it is, in essence, an attempt to make continuous data categorical. Freezing and darting are on a spectrum of defensive behaviors. Therefore, the cutoffs we set (0.5 and -0.5) are arbitrary in some sense. Our rationale for choosing 0.5 and -0.5 was to ensure that the freezing and darting behavioral selection categories only included the most prominent freezers and darters. However, other cutoff points may be valid and would slightly alter the classification

of generalizers and discriminators. Moreover, there is significant heterogeneity within the mixed strategy group, underscoring the non-discrete nature of these behaviors. Taking these limitations into consideration, we do not use the classification analysis as the primary evidence of generalization in KO mice. However, though imperfect, it is nevertheless a good supplement to the discriminative fear conditioning findings in its ability to provide broad information about trends within the data.

In our final set of experiments, we directly assessed the relationship between PL activity and enhanced fear conditioning in SAPAP3 KOs via optogenetic inhibition. As far as we could ascertain, this was the first study in which PL glutamatergic neurons were selectively manipulated, positively or negatively, during conditioning CS-US presentations. Several previous studies have broadly inactivated or lesioned the PL prior to fear conditioning (Morgan et al., 1993; Quirk et al., 2000), while others have manipulated PL signaling during recall CS presentations (Vidal-Gonzalez et al., 2006; Do-Monte et al., 2015b). Additional studies have disrupted more specific aspects of PL signaling immediately prior to conditioning (Choi et al., 2010a; Yizhar et al., 2011; Gilmartin et al., 2013a; Li et al., 2019), but only one other study has modulated PL activity during conditioning trials (Cummings and Clem, 2020). Given the similarities in approach between this study and our own, a more thorough discussion of their data is warranted. Using fiber photometry, these authors found that SOM+ interneurons develop CS responses over the course of conditioning. Moreover, fear conditioning increases glutamatergic drive onto SOM+ interneurons and potentiates SOM+ synapses onto parvalbumin-positive (PV+) interneurons, resulting in disinhibition of principal neurons. Accordingly, optogenetic inhibition of PL SOM+ interneurons during CS-US presentations impairs fear acquisition and diminishes SOM+ plasticity. Intriguingly, this may be due to BLA input – after conditioning, the BLA more strongly recruits SOM+ over

PV+ interneurons and BLA optogenetic inhibition during CS-US presentations replicates the behavioral and SOM+ synaptic effects of SOM+ inhibition.

Comparing these data to own our, it is striking that in both cases tone responses in the PL develop late during conditioning. Given that our photometry data was collected using a calcium indicator driven by a generic neuronal promoter, the signals that we observed likely included SOM+ interneurons. Thus, our data replicates that of Cummings and Clem (2020) in some respect. However, there is a key difference between our findings. Although both studies selectively inhibited PL neurons during conditioning CS-US presentations, Cummings and Clem (2020) found that fear acquisition, but not online fear processing, was disrupted as a result of SOM+ interneuron inhibition. This is in contrast to our data, in which we reported the opposite effects when inhibiting glutamatergic neurons. Taken together, these data suggest that PL projection neurons are necessary for online learning while SOM+ interneurons are necessary for acquisition. In our experiments, it is possible that SOM+ plasticity still occurred, meaning that PL principal neuron inhibition during conditioning simply occluded the effects of SOM+-mediated disinhibition. In the absence of principal neuron inhibition on the following day, the WT mice in our experiments demonstrated that they had successfully acquired the CS-US association, further supporting this theory. Considering that SAPAP3 KO mice display elevated online fear processing and acquisition, it is also worth thinking about these data in context of aberrant fear. For example, it is possible that alterations in PL SOM+ signaling or plasticity, either in BLA-SOM+ or SOM-PV projections, drive the enhanced fear conditioning seen in KOs. This is an intriguing area of future exploration.

In summary, we found that enhanced fear conditioning in SAPAP3 KO mice is associated with a lack of modulation in the PL/BLA circuit. Considering increases in PL activity and freezing coincide in WTs, these data suggest that PL modulation reflects a specific understanding of the

CS-US relationship. Freezing behavior in KOs, conversely, may be driven by a combination of specific and generalized fear. In support of this theory, KO mice exhibit greater generalization than WTs during discriminative fear conditioning. Moreover, specific temporal inhibition of PL glutamatergic neurons during CS-US presentations attenuated online fear processing in both genotypes; however, KO freezing was not reduced to the level of uninhibited WTs, further indicating that distinct generalized fear circuits contribute to their behavior.

5.0 General discussion

5.1 Summary of findings

The aim of this dissertation was to investigate aberrant fear processing in an OCD-relevant model. Affecting 1-3% of the population worldwide, OCD is a debilitating psychiatric disorder characterized by intrusive thoughts and repetitive behaviors (Kessler et al., 2005, 2012). The limited effectiveness of current treatments, both pharmacological and cognitive-behavioral (Soomro et al., 2008; Pittenger and Bloch, 2014; Hezel and Simpson, 2019; Law and Boisseau, 2019), necessitates further investigation into the underlying mechanisms of this disease. A potentially fruitful area of exploration is fear processing – many studies have shown that fear is an essential component of OCD and that fear conditioning is impaired in these individuals (Tracy et al., 1999; Nanbu et al., 2010; Milad et al., 2013; McLaughlin et al., 2015; McGuire et al., 2016; Geller et al., 2017, 2019; Giménez et al., 2019). In fact, it has been proposed that aberrant fear processing underlies OCD pathophysiology. To test this, we turned to SAPAP3 KO mice, which display perseverative grooming and anxiety-like behavior. Using this model enables us to more directly probe the underlying neural mechanisms of aberrant fear processing in the context of OCD-relevant behavior.

In Chapter 2, we characterized fear processing in SAPAP3 KO and WT mice. First, we tested these mice in an auditory fear conditioning paradigm. We found that KOs displayed elevated freezing, both during online fear processing and fear memory recall. Next, we investigated the potential contribution of aberrant sensory signaling to the enhanced fear conditioning seen in KOs. There were no differences in thermal and mechanical nociception between KO and WT mice.

Similarly, there were no differences in acoustic startle threshold. However, we did see a small but significant increase in freezing to sequential tone presentation in KO mice. These data suggest that KOs may be prone to treating neutral stimuli in their environment as aversive. This improper assignment of valence could reflect a maladaptive orienting response to disruptive stimuli, perhaps attributable to an overall anxiety-like phenotype. Critically, the magnitude of this effect is small, suggesting that it cannot fully explain the differences in fear conditioning between genotypes.

The focus of Chapter 3 was examination of activity in fear-associated regions in KOs and WTs after fear conditioning. To that end, we conducted cFos immunohistochemistry. Because it is the protein encoded by an immediate early gene, cFos is a good marker of recently activated cells. Analysis of the cFos protein in fear-associated regions of interest (ROIs) can thereby give us a broad sense of neural activation pertaining to fear conditioning. Using this method, we did not observe genotype differences in cFos+ cell density in any ROIs. Instead, there were several interesting within-genotype findings. After correcting for multiple comparisons, there were no significant cFos+ cell density correlations between ROIs in WT mice. Conversely, there were many instances of correlated activity in KOs (including between the PL and BLA, primary and secondary auditory cortex, and dlPAG and vlPAG), indicating broad neural abnormalities during fear processing. When comparing genotypes, the most striking of these was the correlation between cFos expression in the PL and BLA: there was a strong positive correlation in KO mice, while the r-value in WTs was nearly zero. Since KO mice exhibit elevated freezing compared to WTs, these data suggest that enhanced co-activation of the PL and BLA may be a contributing factor. Interestingly, however, cFos expression in the PL was nearly positively correlated with freezing in WT, but not KO, mice. These data indicate that PL activity is only associated with behavioral output during conditioning in WTs, and not KOs. The correlation between PL and BLA

cFos expression in KOs, therefore, may instead be indicative of broadly enhanced signaling in fear-associated regions.

The experiments in Chapter 4 directly examine the role of the PL/BLA circuit in fear processing in SAPAP3 KO and WT mice by implementing *in vivo* techniques. First, we used multi-site, dual-color fiber photometry to measure calcium signals during fear conditioning. We observed differential activity within the PL/BLA circuit between WTs and KOs throughout conditioning. In particular, neurons in the PL exhibited sustained tone responses late in conditioning in WT, but not KO, mice. Given that this modulation coincided with increased freezing in WTs, these data suggest that PL activity may be related to the formation of specific CS-US associations. In KOs, the absence of PL modulation, paired with elevated freezing to the first CS presentation, suggest that their behavior is driven by a combination of specific and generalized fear circuits. To probe this more directly, we exposed KO and WT mice to discriminative fear conditioning. In line with our hypothesis, KO mice exhibited greater generalization to the unpaired CS than WTs during conditioning. As a final test of our theory, we optogenetically inhibited PL glutamatergic neurons during CS-US presentations specifically. We reasoned that if PL activity was associated with specific learning of CS-US associations, inhibition in WTs would decrease freezing. Moreover, if KO behavior is attributable to a combination of specific and generalized fear, inhibition in these mice would only partially attenuate freezing. Indeed, this is what we saw – inhibited WTs and KOs both exhibited decreased freezing, but the freezing in KOs was not attenuated to the level of uninhibited WTs. Interestingly, the effects of inhibition did not persist during tone presentations on the following day, highlighting the importance of the PL in online fear processing, as opposed to fear acquisition.

Together, these data reveal significant aberrations in fear processing in SAPAP3 KO mice. This is evident on both a behavioral and neural level. In addition, we report novel findings regarding the normal role of the PL in online fear processing. The following sections will more broadly discuss the implications of these findings in the context of fear processing, defensive behavioral selection, and OCD.

5.1.1 PL/BLA circuitry dynamics during online processing of fear associations

To our knowledge, this is the first systematic, simultaneous investigation of multiple nodes within the PL/BLA circuit during online fear learning, as opposed to fear expression or extinction. Combining all our photometry data, we can begin to form a model of how this circuit functions during online processing of CS-US relationships in both the healthy and abnormal state (Figure 5-1). During the early stages of fear conditioning, WT and KO mice display similar CS-associated activity throughout the PL/BLA circuit (Figure 5-1a, top). In response to early US exposure, WT mice displayed elevated BLA activity compared to KOs (Figure 5-1a, bottom). However, this does not yet result in increased freezing in WTs. Conversely, KO mice display elevated freezing at the outset without any changes in CS- and US-associated activity, suggesting that distinct generalized fear circuits contribute to this behavior.

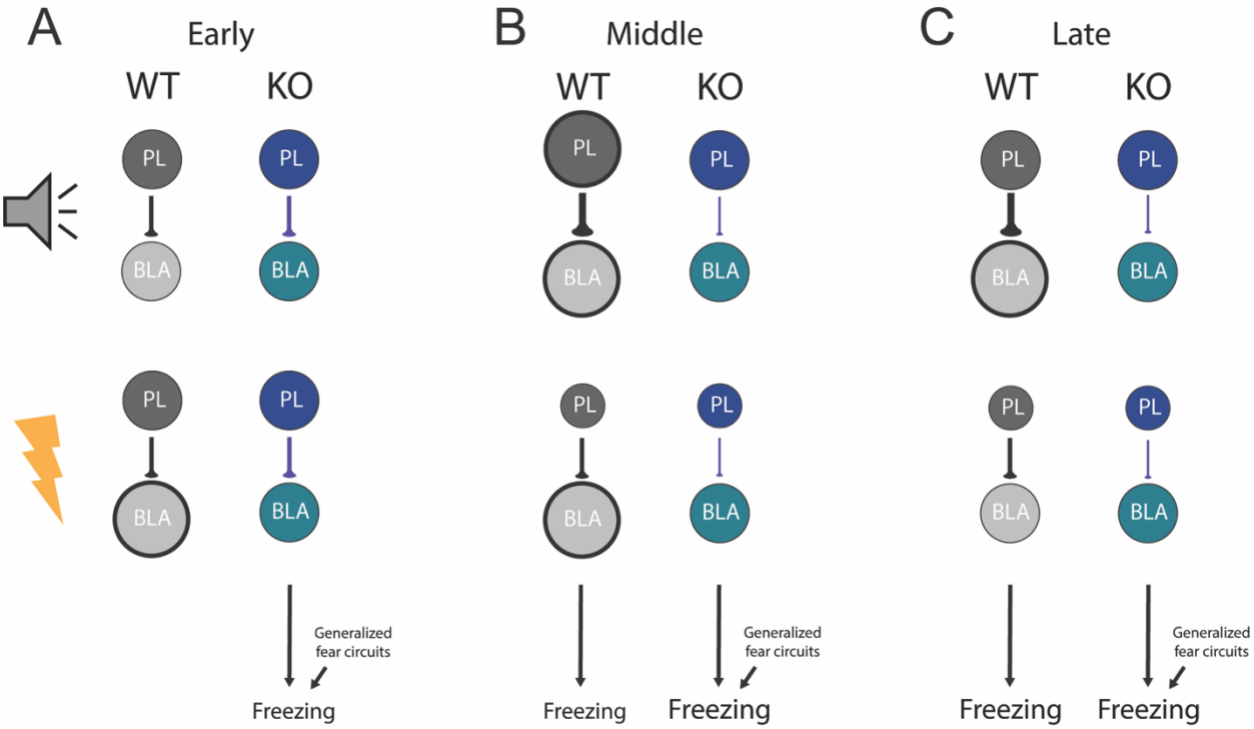

Figure 5-1. Model of PL/BLA circuit dynamics during online processing of fear associations

Model of PL/BLA activity to the tone (top) and shock (bottom) during the early (A), middle (B), and late (C) stages of fear conditioning. **A)** Top: PL/BLA during early tone presentations does not differ between WT and KO mice. Bottom: WT BLA activity is larger relative to KO mice during early shock presentations. KO mice already display elevated freezing, perhaps due to additional input from distinct generalized fear circuits. **B)** Top: During the middle stage of conditioning, WT tone-associated activity increases in the PL, PL-BLA projections, and BLA. Conversely, PL and BLA activity are not modulated in KOs while PL-BLA terminal activity decreases. Bottom: PL soma activity decreases to middle-session shocks in both WT and KO mice, likely reflecting desensitization. BLA soma activity remains high in WTs and these mice begin to display elevated freezing. In KOs, PL-BLA terminal activity decreases while BLA activity remains unaltered. In addition, freezing continues to increase. **C)** Top: In WT mice, PL activity to late tones returns to early-stage levels while PL-BLA terminal and BLA soma activity stays elevated. KO mice continue to display diminished PL-BLA terminal activity. Bottom: PL soma shock-associated activity is attenuated in both WT and KO mice and activity in the BLA is similar across both genotypes. Blunted PL-BLA terminal activity persists in KO mice. By the late conditioning stage, WT and KO mice display roughly equivalent levels of freezing.

At the middle stage of conditioning, WT mice begin to display CS-related changes in the PL/BLA circuit: activity is increased in the PL soma, PL-BLA terminals, and BLA soma (Figure 5-1b, top). KO mice, on the other hand, are characterized by decreased CS-associated PL-BLA terminal activity, with no changes in either PL or BLA soma signaling (Figure 5-1b, top). This decrease in terminal activity persists throughout mid-session US presentations, during which KO freezing continues to increase (Figure 5-1b, bottom). Similar to early trials, middle US trials are marked by relatively larger BLA signals in WT vs. KO mice (Figure 5-1b, bottom). It is around this time that WT mice begin to display freezing that is elevated above baseline. In addition, US-associated PL soma activity is diminished during mid-session trials in both genotypes. Late in conditioning, WT mice continue to exhibit elevated PL-BLA terminal and BLA soma activity to the CS (Figure 5-1c, top). PL activity, on the other hand, appears to return to baseline. In KO mice, CS-related PL-BLA terminal activity remains diminished while PL and BLA soma are unaltered (Figure 5-1c, top). As with the middle stage, PL-BLA terminal activity is reduced in KO mice during late US presentations (Figure 5-1c, bottom). In WT mice, BLA US-associated activity is no longer elevated compared to KOs. In addition, PL soma is less active to the US and freezing is roughly equivalent in both genotypes.

To summarize the model, normal online fear processing is characterized by reverberating activity within the PL/BLA circuit. BLA activity is elevated during initial US presentations, which occurs prior to behavioral adaptation. This activity is followed by enhanced CS-associated signaling throughout the PL/BLA circuit, concurrent with increases in freezing. By the end of conditioning, activity to the CS remains elevated while US-associated activity returns to baseline, suggesting that signals during the CS drive behavioral output at this stage. In KO mice, however, there is a notable lack of positive modulation. In fact, KO PL-BLA terminal activity actually

decreases to both the CS and US across conditioning, indicating that there are broad disruptions in PL/BLA signaling during online fear processing. These activity alterations, combined with input from additional generalized fear circuits, may contribute to aberrant fear conditioning seen in these mice. While the WT and KO models are quite different, there are two commonalities. First, both genotypes display similar signaling to initial CS presentations. This suggests that this circuit is not altered at baseline in KO vs. WT mice. Second, US-associated PL soma activity decreases across trials in both WT and KO mice. This likely reflects desensitization to the shock. Considering the behavioral differences between genotypes, this activity may be unrelated to online processing of CS-US associations, instead reflecting a common adaptive process to sensory stimuli. Alternatively, attenuated PL activity could be a critical feature of normal CS-US processing, but the lack of commensurate changes throughout the PL/BLA circuit in KOs could limit the effects of this modulation.

5.1.2 The mPFC and fear generalization

Based on our data, we developed a theory that hinges on excessive fear generalization in SAPAP3 KO mice. At first pass, it seems that there are discrepancies between our cFos and *in vivo* fiber photometry data. In Chapter 3, we presented evidence of heightened correlated activity across multiple fear-associated regions in KO, but not WT, mice. In particular, we found that PL and BLA cFos expression was positively correlated in KO mice and decidedly uncorrelated in WTs. Looking at these data, we might anticipate stronger *in vivo* signaling relationships between distinct nodes of the PL/BLA circuit in KOs vs. WTs, thereby resulting in enhanced conditioning in the former. In fact, we see the exact opposite. PL/BLA activity in WT mice is modulated throughout conditioning, with signals in one node (e.g. BLA) potentially generating modulation in others (e.g.

PL, PL-BLA terminals). KO activity, on the other hand, remains relatively static throughout training.

Together, these data appear contradictory. However, closer examination of data across all of our experiments reveals that they are actually quite complementary. First, PL cFos expression is nearly significantly correlated with freezing in WT, but not KO, mice. This suggests that PL activity is related to fear behavior in the former, but not the latter. In line with these data, WT mice are distinguished by PL modulation later during conditioning, coincident with an increase in freezing. Conversely, KO mice already display elevated freezing to the first tone, prior to pairing with a shock, and exhibit no modulation in the PL across training. Second, the correlation between cFos expression in the PL and BLA in KOs may simply be reflective of a general increase in associated activity in fear-related regions as opposed to specific CS-US-related signaling, perhaps driven by KOs' anxiety-like phenotype. Our photometry data collected during inter-trial interval (ITI) freezing suggest that this may be the case. During these instances of freezing, absent a discrete stimulus, KO PL and BLA signals display similar patterns and are elevated compared to WT mice. This is evident both during conditioning and recall, but is particularly true during recall. Importantly, the genotype differences only appear in the form of a time x genotype interaction. This indicates that there may not be overall differences in PL and BLA activity in WT and KO mice, but only differences when considering the data in a more nuanced fashion. This broadly aligns with our cFos data in which we see cFos expression correlations between the PL and BLA in KOs alone without any genotype differences for individual regions (e.g. PL, BLA). Third, several pieces of our data indicate that SAPAP3 KOs are prone to misassigning negative valence to neutral stimuli, which is a key aspect of fear generalization. In our initial characterization, we found that KOs increased their freezing to sequential tone presentations alone. This increase was

small, but significant. Similarly, KOs froze more to the first tone during our fiber photometry experiment, prior to experiencing any shocks. Given the heightened stressful nature of this experiment (e.g. scruffing, tethering), KO mice could be more disposed to reacting fearfully to a disruptive stimulus. Critically, additional findings indicate that behavior in both of these cases is not driven by aberrant auditory processing. In Chapter 2, we did not observe genotype differences in baseline acoustic startle threshold. Furthermore, we found similar within-genotype cFos correlations between the auditory cortices, auditory thalamus, and other fear-associated regions for both WTs and KOs, suggesting that auditory processing during fear conditioning itself is not altered in KOs. As a final piece of evidence supporting our generalization theory, we found that SAPAP3 KO mice generalize more than WTs during discriminative fear conditioning. Together, our findings across each set of experiments support the theory that fear conditioning alterations in SAPAP3 KO mice are at least partially driven by maladaptive fear generalization.

The fact that we observed fear generalization in SAPAP3 KO mice is not surprising given that they are a model of OCD-relevant behavior (Welch et al., 2007) and fear generalization is a hallmark of OCD (Pittig et al., 2018). Interestingly, although we did not record calcium signals during the fear generalization experiment, there is much evidence to suggest that the aberrant PL activity we observed during fear conditioning may be related to discrimination as well. For example, discrimination over time is associated with increased plasticity markers in the PL (Pollack et al., 2018). When looking at specific cell types, PL PV+ interneurons and principal neurons are selectively inhibited and disinhibited, respectively, to the CS+ and not the CS- (Courtin et al., 2014). Furthermore, PL principal neurons preferentially phase lock with dorsal mPFC (dmPFC) theta activity during CS+ presentations (Courtin et al., 2014; Dejean et al., 2016) and enhanced coherence between the PL and primary auditory cortex is associated with

discrimination between conditioned and novel stimuli (Concina et al., 2018). Moreover, specific disruption of mPFC CREB (Vieira et al., 2014) or NMDA signaling (Vieira et al., 2015) and general mPFC inhibition via muscimol prior to recall (Lee and Choi, 2012) result in fear generalization. Interestingly, all of these manipulations blocked discrimination by specifically increasing freezing to the CS- without altering CS+ freezing, suggesting that mPFC normally inhibits fear responses to non-specific stimuli. Similar findings have been reported in contextual, as opposed to auditory, fear conditioning. Distinct ensembles of PL neurons are activated to the conditioned and unconditioned contexts, and reactivation of the conditioned ensemble is correlated with the degree of discrimination (Corches et al., 2019). In addition, dmPFC projections to the vlPAG are activated during discrimination, and inhibition or activation of these projections promote generalization and discrimination, respectively (Rozeske et al., 2018). Likewise, disruption of mPFC synchrony (Xu et al., 2012), NMDA signaling (Lovelace et al., 2014), or CREB signaling (Vieira et al., 2014) results in contextual fear generalization.

The mPFC is also associated with fear and anxiety more broadly. BLA-PL projections, for instance, are active during stressful situations and can facilitate transition into an anxiety-like state (Marcus et al., 2019). Moreover, the mPFC, and more specifically communication between the ventral hippocampus (vHPC) and mPFC, has been repeatedly implicated in anxiety. mPFC theta power and vHPC-mPFC coherence is elevated in the safe compartments of the open field (OF) and elevated plus maze (EPM), decreases prior to exiting safe compartments, and increases prior to return, suggesting that the mPFC inhibits the exploration of anxiogenic spaces (Adhikari et al., 2010). In line with these data, inhibition of vHPC inputs to the mPFC disrupts both the representation of the aversiveness of a given space and anxiety-related behavior (Padilla-Coreano et al., 2016). In addition, mPFC single units represent the aversive structure of the EPM and change

their firing prior to movement between safe and aversive areas, further supporting the theory that the mPFC guides exploration of anxiogenic spaces (Adhikari et al., 2011). Intriguingly, mPFC neurons do not differentiate between open and closed EPM arms in mouse models of anxiety and avoidant WT mice, but do exhibit an overall increase in firing rate in the EPM compared to a safe, familiar context (Adhikari et al., 2011). This suggests that in anxious animals, such as SAPAP3 KOs, an increase in overall mPFC activity in anxiogenic environments may occlude differential single-unit signaling in open vs. closed arms. In other words, alterations in mPFC signal-to-noise ratio may disrupt differentiation between safe and dangerous spaces.

Interestingly, several studies have specifically implicated the mPFC-BLA circuit in fear discrimination and safety signaling (Likhtik et al., 2014; Stujenske et al., 2014; Likhtik and Paz, 2015). For instance, mice that discriminated during differential fear conditioning demonstrated increased theta synchrony between the mPFC and BLA to the CS+ compared to the CS-, while mice that generalized has similar neural responses to both CS types (Likhtik et al., 2014). Of note, BLA firing became entrained to mPFC theta during CS-, not CS+, presentations, suggesting that mPFC input regulates safety signaling via modulation of the BLA. Similar changes in mPFC-BLA theta synchrony and BLA entrainment were observed in the center and periphery of the OF, underscoring a broad role of the mPFC-BLA in learned and innate safety (Likhtik et al., 2014). A follow-up study found that BLA fast gamma power was specifically coupled to mPFC theta during safety, as represented by both CS- presentations in discriminative fear conditioning and the periphery of the OF (Stujenske et al., 2014), providing further evidence that the mPFC signals safety by regulating BLA activity.

While the PL is undoubtedly a strong candidate for the driver of increased fear generalization we observed in SAPAP3 KO mice, there are several other possible regions and

circuits (Asok et al., 2019). The BLA is one such region – in addition to the aforementioned abnormalities in the mPFC-BLA circuit, it has been implicated in discrimination in its own right. Neurons in both the lateral and basal amygdala preferentially respond to CS+ vs. CS- presentations (Goosens et al., 2003; Herry et al., 2008) and generalization is associated with similar CS+ and CS- responses in the lateral amygdala (Ghosh and Chattarji, 2015). In addition, enhanced contextual fear generalization is associated with increased cFos expression in the BLA (Rajbhandari et al., 2016). Beyond the BLA, aberrant signaling in the CeA (Ciocchi et al., 2010; Botta et al., 2015; De Bundel et al., 2016), BNST (De Bundel et al., 2016), auditory cortex (Aizenberg et al., 2015), MGN (Han et al., 2008), anterior cingulate cortex (Ortiz et al., 2019), nucleus reuniens (Xu and Südhof, 2013; Venkataraman et al., 2019), and zona incerta (Venkataraman et al., 2019) have all been implicated in auditory fear generalization. As an important note, several of these regions directly interact with the mPFC, including the auditory cortex, nucleus reuniens, zona incerta, and BNST. In addition, disrupting dopaminergic (Jones et al., 2015; De Bundel et al., 2016; Jo et al., 2018) and GABAergic signaling (Shaban et al., 2006; Lange et al., 2014; Zhang et al., 2017a) results in fear generalization. It is possible that dysfunction in these regions or systems may be present in SAPAP3 KO mice, either in isolation or conjunction with PL abnormalities.

5.1.3 Defensive behavioral selection

As discussed in the previous chapter, we observed a significant amount of darting in WT mice during discriminative fear conditioning. Given that darting had only previously been reported in female rats (Gruene et al., 2015; Colom-Lapetina et al., 2019; Greiner et al., 2019; Odynocki and Poulos, 2019), this was a noteworthy finding. Several potential explanations for this behavior

are outlined in Chapter 4.4. More broadly, however, the distinction between darting and freezing in the context of fear conditioning raises several interesting issues that warrant further exploration: namely, the conditions in which an animal would select one defensive behavior over the other, and the role of anxiety in this choice. Darting has been described as a more active defensive behavior and freezing more passive (Gruene et al., 2015). This is not to say that darting is the same as flight behavior during active avoidance paradigms; the availability of escape is a critical factor in such paradigms, as blocking the escape route causes rats to switch from flight to freezing (Blanchard and Blanchard, 2008). However, there are certainly similarities between darting and flight that might inform our data. Broadly speaking, flight and freezing are considered optimal in different situations. Conditions in which flight is thought to be adaptive include environments with a clear escape route and/or a spatiotemporally proximal threat, while conditions that promote freezing include spatiotemporally distal threats (e.g. a predator that may not have noticed the subject yet) and/or uncertainty surrounding the threat (Fanselow and Lester, 1988; Blanchard and Blanchard, 1989, 2008; Mobbs et al., 2020). If freezing is employed when flight is most beneficial, this could facilitate capture by a predator; likewise, if flight is used inappropriately, an animal could alert an otherwise unwitting threat to its presence.

A recent study elegantly examined the interplay between flight and freezing using a compound auditory stimulus, in which a pure tone was followed white noise and subsequent co-termination with a shock (Fadok et al., 2017). The authors found that mice exhibited freezing during the tone and flight during the white noise, likely reflecting both the proximity and certainty of the shock imminence. Moreover, conditioned flight extinguished faster than and was initially replaced by freezing, suggesting that the mice viewed the white noise as a more uncertain predictor of the shock during early extinction. Thus, using this flight/freezing framework, darting during

fear conditioning could be driven by a more accurate assessment of the certainty and/or proximity of the shock, and therefore be considered adaptive. In support of such an interpretation, darting in female rats was associated with better extinction recall (Gruene et al., 2015), raising the possibility that engaging in active coping strategies during threat presentation may be predictive of better fear outcomes (Jones and Monfils, 2016). Therefore, in the abnormal state, such as SAPAP3 KO mice, the lack of darting may be maladaptive. Freezing to both the CS+ and CS- may reflect an equal level of uncertainty of the relationship between the CS and US, an equal threat imminence assessment, or some combination of these factors.

Although darting is distinct from the defensive behaviors exhibited during active avoidance, it may still be useful to discuss the potential relevance of this literature – freezing is often considered an alternative defensive strategy that interferes with successful avoidance, a theory that is supported by consistent findings that poor avoiders exhibit high levels of freezing (Choi et al., 2010b; Lázaro-Muñoz et al., 2010; Bravo-Rivera et al., 2014). It is also worth noting that several recent studies have implicated the PL in avoidance (Martinez et al., 2013; Bravo-Rivera et al., 2014, 2015; Diehl et al., 2018; Martínez-Rivera et al., 2019; Capuzzo and Floresco, 2020). In a two-way active avoidance task, PL cFos expression is higher in good vs. poor avoiders and is positively correlated with shuttling (Martinez et al., 2013). Similarly, PL cFos expression is positively correlated with both avoidance expression during recall and persistent avoidance after training in a platform-mediated avoidance task (Bravo-Rivera et al., 2015). Further investigation revealed that cFos is exclusively expressed in BLA-projecting PL neurons following avoidance retrieval, while ventral striatum (VS)-projecting PL neurons are activated following extinction training (Martínez-Rivera et al., 2019). In line with these findings, optogenetic stimulation of PL-BLA and PL-VS terminals increases and reduces avoidance behavior, respectively (Diehl et al.,

2020). Moreover, broad post-training inactivation of the PL with muscimol impairs avoidance expression (Bravo-Rivera et al., 2014), primarily due to disruption of inhibitory signaling: optogenetic inhibition of excitatory PL neurons actually enhances, while excitation impairs, active avoidance (Diehl et al., 2018). Interestingly, the latter effects were only observed when manipulating the rostral PL (rPL), which aligns with our implant locations. In addition, distinct PL neurons are activated during freezing and escape-like behaviors, indicating that there are strategy-specific populations for different defensive behaviors (Halladay and Blair, 2015). Taken together, these data suggest that the PL may be broadly involved in defensive behavioral selection, which could explain the differences we report between SAPAP3 WT and KO mice during discriminative fear conditioning.

In addition to the PL, several other regions have been implicated in avoidance and defensive behaviors. cFos expression in the amygdala (including the BLA, CeA, and medial nuclei) is elevated in good vs. poor avoiders in two-way active avoidance and is negatively and positively correlated with freezing and shuttling, respectively (Martinez et al., 2013). Similarly, basal amygdala cFos is positively correlated with platform-mediated avoidance expression (Bravo-Rivera et al., 2015). Furthermore, pre-training lateral and basal amygdala lesions disrupt avoidance acquisition (Choi et al., 2010b; Lázaro-Muñoz et al., 2010). Given that we see blunted BLA activity in SAPAP3 KOs during fear conditioning, it is possible that defensive behavioral selection is impaired in these mice. Relevant regions beyond the BLA include the CeA, inferior colliculus (IC), ventromedial hypothalamus (VMH), and PAG. The CeA contains mutually-antagonistic cell populations that control freezing and flight (Fadok et al., 2017), and lesions of this nucleus decrease freezing and rescue avoidance performance in poor avoiders (Choi et al., 2010b; Lázaro-Muñoz et al., 2010). The ventral aspect of the IC (ICv) has been implicated in both freezing and

coordinated escape behavior, while the dorsal aspect (ICd) is involved in aimless, undirected running and jumping (Ferreira-Netto et al., 2007). Like the ICv, the dorsomedial VMH (VMHdm) is associated with well-directed escape behavior (Ferreira-Netto et al., 2007). Finally, the dlPAG and vlPAG are critical nuclei in the expression of flight and freezing behaviors, respectively (Vianna et al., 2001a, 2003; Ferreira-Netto et al., 2007; Halladay and Blair, 2015). Interestingly, the dlPAG and vlPAG are innervated specifically by the caudal PL (cPL) and rPL, respectively (Floyd et al., 2000), further underscoring the relevance of examination of specific subregions within the PL.

5.1.4 Molecular and signaling deficits in SAPAP3 mice

In the current study, we found that SAPAP3 KO mice exhibit fear generalization, enhanced fear conditioning, and PL/BLA circuit abnormalities. How these deficits relate specifically to the deletion of the *Sapap3* gene is still unknown. The *Sapap3* protein is located at excitatory postsynaptic densities and either directly or indirectly interacts with a variety of signaling and structural molecule families, including post-synaptic density protein 95 (PSD95), metabotropic glutamate receptors (mGluRs), NMDA receptors, Shank, and Homer (Kindler et al., 2004; Welch et al., 2004; Ade et al., 2016). Signaling deficits in SAPAP3 KOs after deletion of this gene have consistently been reported in cortico-striatal synapses (Welch et al., 2007; Chen et al., 2011; Wan et al., 2011, 2014; Burguière et al., 2013; Ade et al., 2016; Corbit et al., 2019). Such deficits include reduced extracellular field potentials, enhanced NMDAR-dependent signaling, and an overabundance of the NR2B NMDAR subunit compared to NR2A (Welch et al., 2007); elevated mGluR5-regulated AMPA receptor endocytosis, leading to an increase in silent synapses (Wan et al., 2011); heightened group I mGluR signaling, with a specific increase in striatal dendritic

mGluR5 expression (Chen et al., 2011); constitutive mGluR5 hyperactivation due to uncoupling with Homer proteins (Ade et al., 2016); elevated baseline striatal firing *in vivo* (Burguière et al., 2013); and specific abnormalities in projections from the lateral orbital frontal cortex (lOFC) and primary and secondary motor areas (M1, M2) (Corbit et al., 2019; Hadjas et al., 2020). Together, these data paint a clear picture of abnormal cortico-striatal signaling. However, no other circuits have been rigorously investigated to date, with the exception of thalamo-striatal projections, in which no deficits were observed (Wan et al., 2014).

Interestingly, a recent study reported broad disruptions in mGluR5 availability in the cortex and amygdala in SAPAP3 KO mice using positron emission tomography (Glorie et al., 2020). This suggests that some of the signaling abnormalities seen in previous studies, particularly those related to mGluR5 activity (Chen et al., 2011; Wan et al., 2011; Ade et al., 2016), may be present in the PL and BLA. However, although *Sapap3* is detectable in the amygdala, it is not enriched, particular in comparison to *Sapap1* and *Sapap4* (Welch et al., 2007). Thus, while deficits at cortico-amygdala synapses may exist, it seems unlikely given the expression levels of *Sapap3*. Conversely, *Sapap3* is highly expressed in both mouse and rat neocortex (Kindler et al., 2004; Welch et al., 2004), raising the possibility there are deficits in amygdalo-cortical signaling. Moreover, work from our lab has reported both baseline and task-dependent mPFC abnormalities in SAPAP3 KO mice. Specifically, there is increased serotonin turnover in the mPFC at baseline (Wood et al., 2018) and PL hyperactivity during reversal learning as measured by cFos (Manning et al., 2019a). Taken together, these data reveal broad disruptions in PL activity. Whether such abnormalities arise in part from alterations at amygdalo-cortical synapses is an avenue for future exploration.

5.1.5 Implications for OCD

Considering that SAPAP3 KO mice are used to model OCD-like behavior, it is important to discuss the relevance of our data to human OCD. Much of these data are outlined in the introduction. However, a brief review of the pertinent information is warranted. Generally speaking, abnormally elevated fear is associated with OCD (VanElzakker et al., 2014; Raines et al., 2015; Rozenman et al., 2017; Pittig et al., 2018; Ferreira et al., 2020) and aberrant fear processing has been identified as a possible driver of OCD pathophysiology (Tracy et al., 1999; Fiddick, 2011). While there are only a handful of studies that directly assess fear conditioning in individuals with OCD, the literature generally indicates that OCD is associated with enhanced fear acquisition and impaired extinction and extinction recall (Tracy et al., 1999; Nanbu et al., 2010; Milad et al., 2013; McLaughlin et al., 2015; McGuire et al., 2016; Geller et al., 2017, 2019; Giménez et al., 2019)

As with fear conditioning, there is broad evidence of increased fear generalization in patients with OCD. In a non-clinical sample, high threat assessment scores on the Obsessive Beliefs Questionnaire (OBQ-44) were associated with greater generalization during discriminative fear conditioning, as measured by fear-potentiated startle (Kaczkurkin and Lissek, 2013). In pediatric OCD, patients exhibit impaired discrimination during extinction and worse differential SCR scores (combined CS+ and CS- responses) are associated with poorer symptomology (McGuire et al., 2016). Furthermore, pediatric patients that respond to cognitive behavioral therapy (CBT) are better able to discriminate during extinction, while non-responders tend to generalize (Geller et al., 2019). Another study, however, found that pediatric patients discriminated as well as healthy controls (Geller et al., 2017). In an adult sample, one group reported that patients generalized during extinction recall (McLaughlin et al., 2015). OCD patients were also found to

discriminate during fear conditioning and extinction, but more weakly than healthy controls (Apergis-Schoute et al., 2017). After fear reversal in these same subjects, individuals with OCD generalized to both the CS+ and CS-. In addition, differential vmPFC signaling during the CS+ and CS- favored the CS- in healthy controls and the CS+ in OCD patients. This hyperactivation to the CS+ and/or hypoactivation to the CS- suggest that individuals with OCD have impaired safety signaling (Apergis-Schoute et al., 2017). Abnormal vmPFC activity was also observed in adult OCD patients during presentation of an extinguished and non-extinguished CS+: while healthy controls showed differential activation to the two stimuli, individuals with OCD did not (Milad et al., 2013). Synthesizing these data, individuals with OCD display physiological and behavioral markers of elevated fear and impaired discrimination.

Several of the aforementioned studies have found disruptions in vmPFC signaling during fear extinction and extinction recall. Since the vmPFC is the human homolog of the IL in rodents and the IL is critically involved in fear extinction (Giustino and Maren, 2015), this is not surprising. However, given the aberrant PL signaling we observed in SAPAP3 KO mice, it is also important to consider the importance of its functional and anatomical human equivalent, the dorsal anterior cingulate cortex (dACC) (Milad et al., 2007a). Although only one study has reported dACC dysfunction during fear conditioning specifically (Milad et al., 2013), dACC abnormalities have been widely observed in OCD and dorsal anterior cingulotomy is one of the most effective treatments for refractory OCD (Banks et al., 2015; Brown et al., 2016). dACC deficits include structural abnormalities (Rosenberg and Keshavan, 1998; Matsumoto et al., 2010; Kühn et al., 2013; Attwells et al., 2017; McGovern and Sheth, 2017; Wang et al., 2017; Gilbert et al., 2018), alterations in baseline activity (Yücel et al., 2008; Cavanagh et al., 2010; McGovern and Sheth, 2017), aberrant functional connectivity (Fitzgerald et al., 2010; Zhang et al., 2017b; Chen et al.,

2019), and abnormal signaling during symptom provocation (Rauch et al., 1994; Breiter et al., 1996; Adler et al., 2000; Mataix-Cols et al., 2004; Nakao et al., 2005; Simon et al., 2010, 2014; Via et al., 2014), working memory (Koch et al., 2012; Diwadkar et al., 2015), motor performance (Friedman et al., 2017), and error processing (Gehring et al., 2000; Ursu et al., 2003; Nakao et al., 2005; Cavanagh et al., 2010; Fitzgerald et al., 2010; Schlösser et al., 2010; Fiddick, 2011; McGovern and Sheth, 2017; Gilbert et al., 2018; Norman et al., 2019). On multiple occasions, these alterations have been found to be associated with symptom severity and/or treatment effectiveness (Rosenberg and Keshavan, 1998; Kühn et al., 2013; Zhang et al., 2017b; Gilbert et al., 2018). While not directly related to fear processing, the findings regarding error processing have nonetheless been hypothesized to contribute to this behavior: if individuals with OCD are unable to resolve perceived errors, this could lead to maladaptive threat assessment and fear generalization (Fiddick, 2011; McGovern and Sheth, 2017). In addition, complementing our data, several studies have reported specific alterations in prefrontal-amygdala circuitry (Cardoner et al., 2011; Admon et al., 2012; Paul et al., 2020).

Like the dACC, the amygdala has been repeatedly implicated in OCD symptomology (Wood and Ahmari, 2015). Several studies have observed alterations in amygdala structure (Szeszko et al., 2004) and functional connectivity (Reess et al., 2016; Rus et al., 2017). In addition, task-dependent abnormalities have been reported during symptom provocation (Breiter et al., 1996; Mataix-Cols et al., 2004; van den Heuvel et al., 2004; Simon et al., 2010, 2014) and exposure to fearful faces (Cardoner et al., 2011; Via et al., 2014). Moreover, deep brain stimulation of the ventral anterior limb of the internal capsule, which is an effective treatment for refractory OCD, is associated with alterations in amygdala functional connectivity (Fridgeirsson et al., 2020). Together, these data broadly indicate that amygdala structure and function are disrupted in OCD.

In summary, individuals with OCD display elevated fear processing, fear generalization, and threat-related abnormalities in dACC and amygdala signaling. These trends are broadly consistent with our findings that SAPAP3 KO mice display elevated fear conditioning, enhanced fear generalization, and altered PL/BLA circuit dynamics. In addition, recent work from our lab found aberrant PL activity during reversal learning in KOs (Manning et al., 2019a). This could indicate the presence of PL-driven maladaptive error processing, which has been consistently observed in the dACC of OCD patients. Taken together, these data further support the use of SAPAP3 KO mice as a model of OCD-like behavior and provide potential avenues of future research into the treatment of OCD.

5.2 Limitations and future directions

These studies have several limitations, a few of which are mentioned in the discussion sections for Chapters 2-4. I will not reiterate these points here, but instead consider a few broader limitations for this work as a whole. First, we did not directly measure baseline signaling in the PL/BLA circuit in SAPAP3 KO and WT mice. This is true for our cFos data, in which we did not include unconditioned and/or pseudo-conditioned controls, and our photometry data, in which our normalization methods preclude accurate assessment of baseline calcium signaling. Even though our cFos data represent conditioning-dependent activity, the fact that we do not see any genotype differences in cFos expression in any ROI could indicate that there are no baseline differences. However, *in vivo* examination of the PL/BLA circuit is necessary for that determination. This can be measured using *in vivo* electrophysiology. This technique would also allow us to establish if there are alterations in gain in the mPFC that align with the signal-to-noise disruptions seen in

other models of anxiety (Adhikari et al., 2011). Critically, the presence or absence of baseline genotype differences would not substantially affect our interpretation of the results: the lack of PL/BLA modulation in KO mice would still suggest an impairment in specific online fear processing.

A second limitation of our studies is that we were unable to determine the directionality of the effects within the PL/BLA circuit. Given the order of events (e.g. BLA shock-related activity precedes the development of sustained PL tone activity over the course of conditioning in WTs), we can make certain assumptions. However, these were not directly tested. We attempted to gain a general understanding of directionality by cross-correlating the PL soma, PL-BLA terminal, and BLA soma signals with one another. Unfortunately, these analyses were inconclusive, likely due to the moderately slow timescale of calcium indicators paired with the short latency responses to the events of interest (e.g. tone and shock onset). *In vivo* electrophysiology would benefit us in this regard as well. With millisecond accuracy, we would be able to more accurately assess directionality via cross-correlations and more powerful methods, such as Granger causality tests. Of note, fiber photometry was chosen over electrophysiology for our experiments because of the ability to acquire simultaneous recordings from the PL soma, PL-BLA terminals, BLA soma, and (theoretically) BLA-PL terminals. Moreover, using fiber photometry enabled us to record accurate shock-associated activity, which likely would have been contaminated by electrical artifact with electrophysiology. Thus, we consider the fiber photometry data a critical first step that will inform future electrophysiological experiments.

The final broad limitation of these experiments is the lack of projection- and cell-type specificity. Both calcium indicators that we used were driven by pan-neuronal promoters. Therefore, the activity we observed in the PL and BLA soma is undoubtedly driven by a

combination of principal glutamatergic neurons and GABAergic interneurons. This is particularly relevant given the role of certain interneuron subtypes during fear conditioning, both in the PL (Cummings and Clem, 2020) and BLA (Wolff et al., 2014). Cell-type specific calcium imaging during fear conditioning would greatly advance our understanding of the PL/BLA circuit in online fear processing and is an excellent area of future exploration. Moreover, it will be critical to further examine the role of PL-BLA and BLA-PL projections in online fear processing. Although we did exclusively inhibit glutamatergic projection neurons in the PL during fear conditioning, more specific inhibition of the PL-BLA pathway is warranted. With respect to BLA-PL projections, the initial goal will be to collect reliable calcium imaging data during fear conditioning. Subsequent projection-specific optogenetic manipulation is a likely follow-up.

In addition to the experiments listed above, there are several key areas of future exploration. The first is dissection of the specific role of the *Sapap3* gene in abnormal fear processing. Work surrounding cortico-striatal synapses in SAPAP3 KO mice can give us insight into the types of mechanisms worth investigating (Welch et al., 2007; Chen et al., 2011; Wan et al., 2011, 2014; Burguière et al., 2013; Ade et al., 2016; Corbit et al., 2019). For example, there may be alterations in the composition of NMDA receptors at amygdalo-cortical synapses, dissociation of mGluR5 and Homer proteins, and/or altered synaptic properties. Future molecular and *ex vivo* electrophysiological studies will examine these possibilities, focusing on BLA-PL synapses in particular. A second logical follow-up is a direct examination of the PL in fear generalization in SAPAP3 KO and WT mice. To that end, we will conduct multi-site, dual color fiber photometry in this mice during discriminative fear conditioning. Finally, our data suggest that defensive behavioral selection is disrupted in KO mice. Future studies will more concretely examine this, beginning with a thorough comparison of fear conditioning and active avoidance. We have already

collected preliminary data in a two-way shuttle avoidance paradigm with concurrent fiber photometry recordings in the PL/BLA circuit. Unsurprisingly, KO mice perform worse than WTs in this task, as measured by avoidance and escape frequency, latency, and learning over multiple days of training (Appendix Figures 16 and 17). Moreover, the photometry data indicate that there are tone-and shock-associated abnormalities in PL/BLA signaling in KO mice during avoidances, escapes, and failures. This is particularly true of the PL signal during escape trials (Appendix Figures 18 and 19). However, these data were collected in a cohort that had previously been exposed to fear conditioning. Thus, separate cohorts are needed to examine these effects. In addition, future experiments will inhibit the PL during CS-US presentations in two-way shuttle avoidance to provide a direct comparison to the present fear conditioning data.

5.3 Conclusions

The experiments in this dissertation detail a systematic investigation of fear processing and PL/BLA signaling during initial acquisition of aversive associations in SAPAP3 KO and WT mice. Our data indicate that PL modulation in particular is necessary for proper online processing of fear associations in WT mice. Conversely, in KOs, which display abnormally elevated fear, there is a lack of PL modulation throughout conditioning. This static activity pattern may be related to an overall fear generalization phenotype, which further supports the theory that PL is critical for learning specific fear associations. Our findings contribute to the existing literature in two chief ways. First, these data constitute the first comprehensive analysis of PL/BLA functioning during online fear processing and provide new evidence for the specific role of the PL in fear learning. Second, we provide strong evidence that SAPAP3 KO mice are an appropriate model of aberrant

fear processing in the context of OCD-relevant behavior. Taken together, these data not only enhance our understanding of how aversive associations are acquired in general, but also shed light on potential signaling abnormalities in anxiety disorders such as OCD.

Appendix A Supplemental data

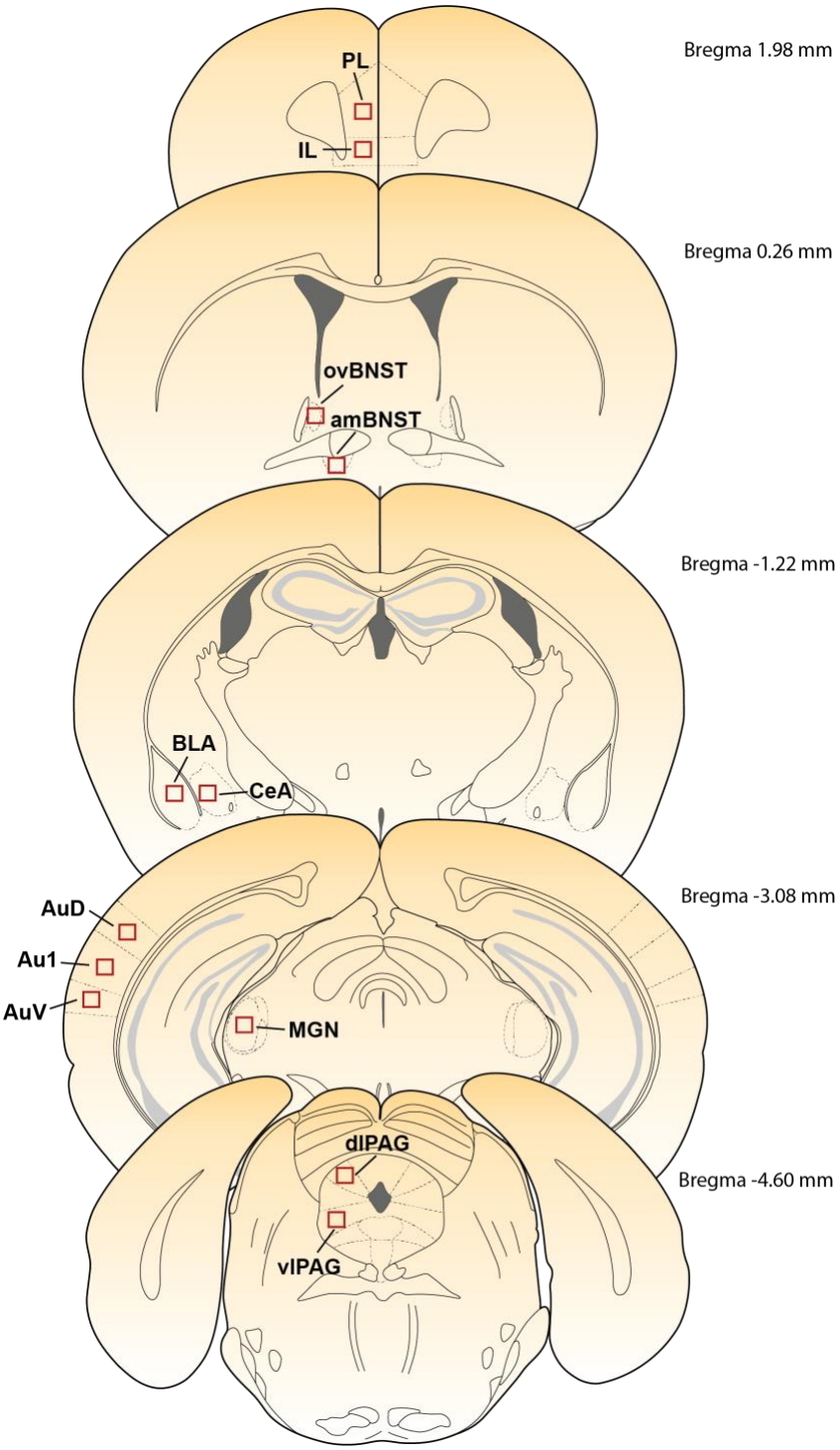

Appendix Figure 1. cFos analysis regions of interest

Regions of interest (ROIs) for cFos immunohistochemistry analysis. Red boxes mark ROI locations. From top to bottom: PL (prelimbic cortex), IL (infralimbic cortex), ovBNST (oval nucleus of the bed nucleus of the stria terminalis), amBNST (anteromedial nucleus of the bed nucleus of the stria terminalis), BLA (basolateral amygdala), CeA (central amygdala), AuD (dorsal secondary auditory cortex), Au1 (primary auditory cortex), AuV (ventral secondary auditory cortex), MGN (medial geniculate nucleus of the thalamus), dlPAG (dorsolateral periaqueductal gray), and vlPAG (ventrolateral periaqueductal gray).

A

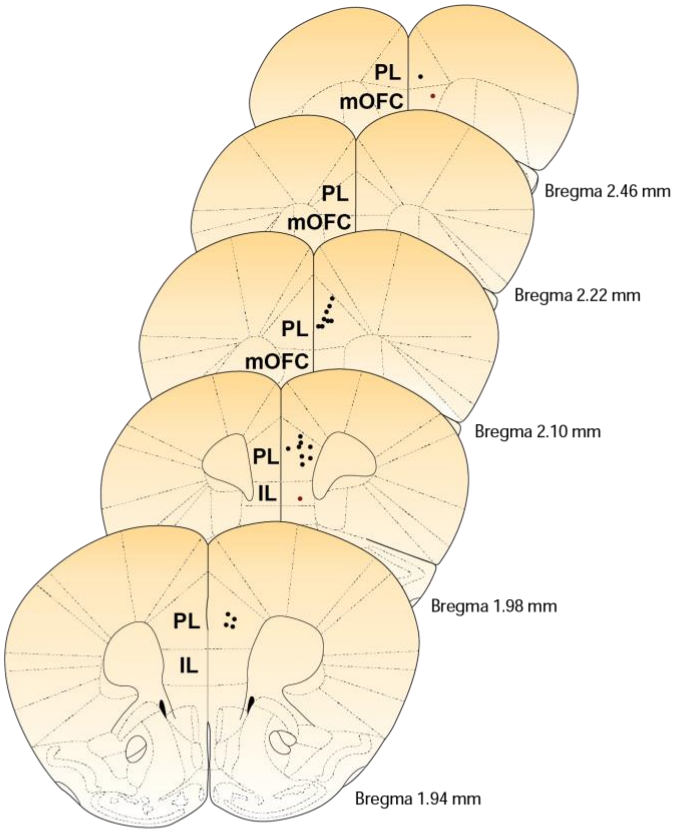
PL
mOFC
Bregma 2.46 mm
PL
mOFC
Bregma 2.22 mm
PL
mOFC
Bregma 2.10 mm
PL
IL
Bregma 1.98 mm
PL
IL
Bregma 1.94 mm

B

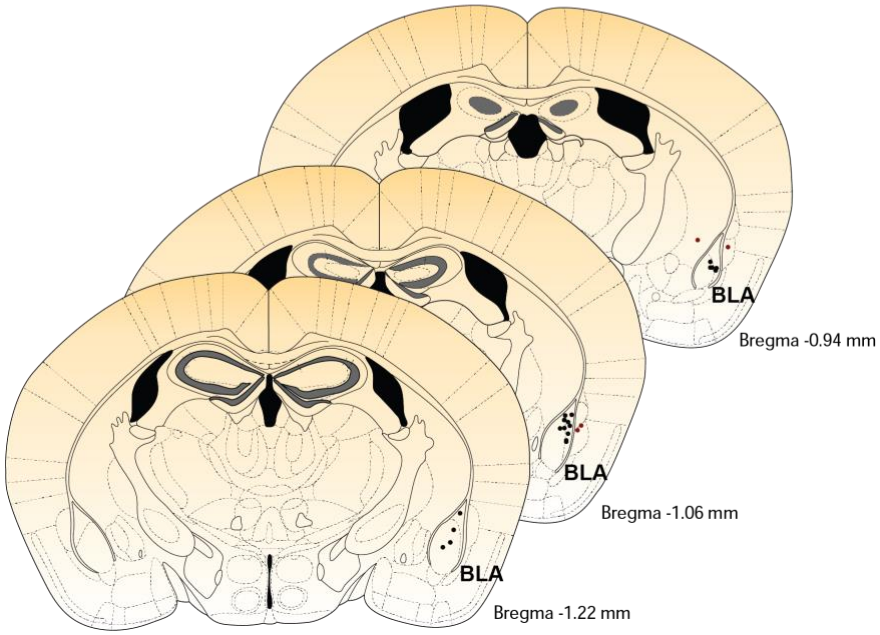
BLA
Bregma -0.94 mm
BLA
Bregma -1.06 mm
BLA
Bregma -1.22 mm

Appendix Figure 2. PL and BLA targeting of fiberoptic implants for fiber photometry

Location of fiberoptic implants in the PL (**A**) and BLA (**B**) for fiber photometry experiments. Dots represent the lowest point of the fiber tract. Black dots are hits, red dots are misses.

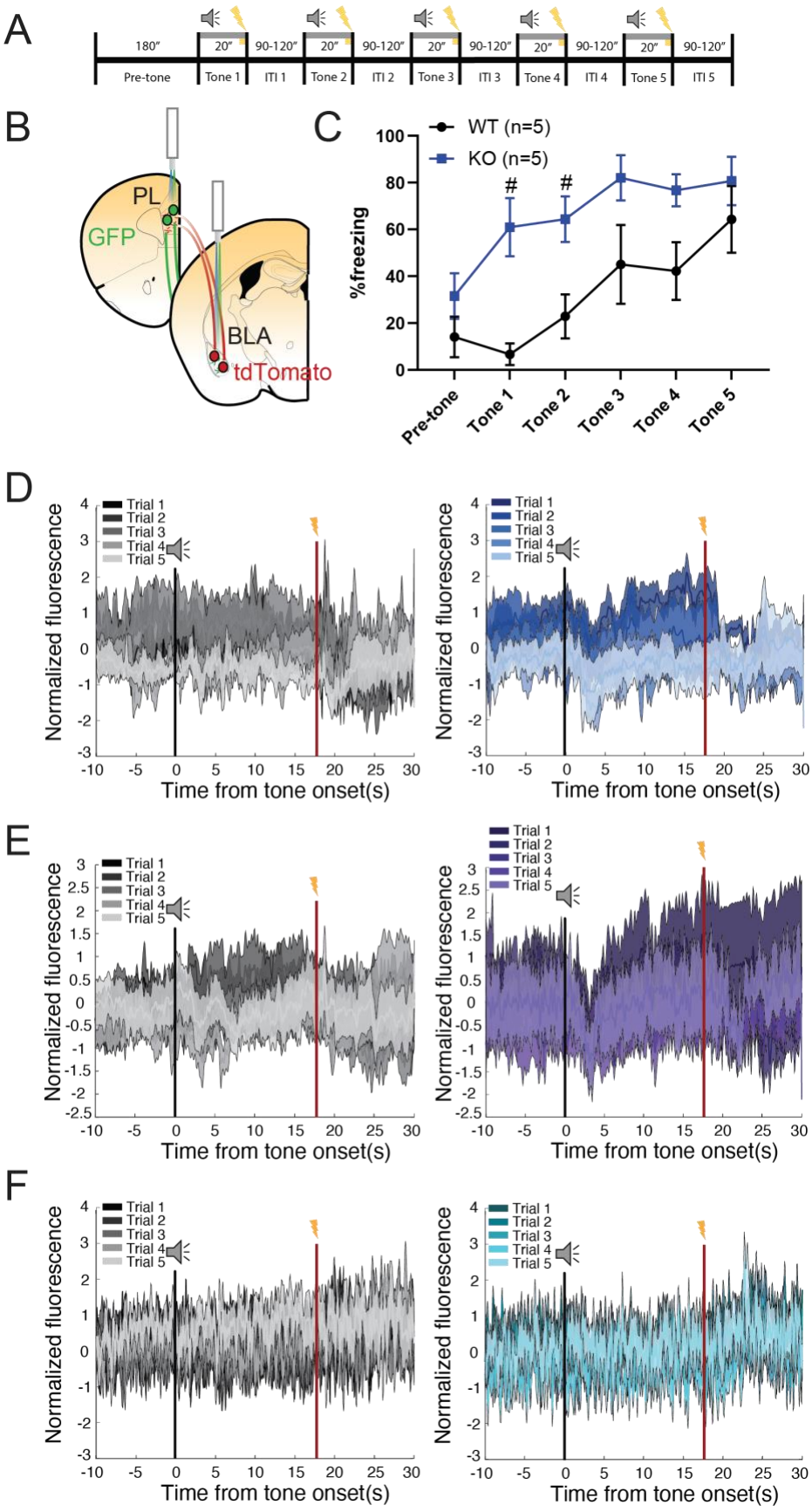
A
180″
20″
90-120″
Pre-tone
Tone 1
ITI 1
Tone 2
ITI 2
Tone 3
ITI 3
Tone 4
ITI 4
Tone 5
ITI 5
B
PL
GFP
BLA
tdTomato
C
WT (n=5)
KO (n=5)
%freezing
Pre-tone
Tone 1
Tone 2
Tone 3
Tone 4
Tone 5
D
E
F
Trial 1
Trial 2
Trial 3
Trial 4
Trial 5
Normalized fluorescence
Time from tone onset(s)

Appendix Figure 3. Within-genotype fluorescent fiber photometry control traces do not mirror calcium imaging conditioning patterns

A) Timeline of fluorescent fiber photometry control experiment. **B)** Schematic of dual-site, dual-color fiber photometry with GFP and tdTomato in the PL and BLA, respectively. **C)** % freezing to the pre-tone period and tones 1-5 for WT and KO mice. Main effect of time [$F(3.154,25.23)=7.493$, $p=0.0008$] and genotype [$F(1,8)=15.21$, $p=0.0045$]. Post-hoc: trend WT vs. KO tones 1 ($p=0.0525$) and 2 ($p=0.0888$); WT tone 2 vs. 5 ($p=0.045$) and trend tone 1 vs. 5 ($p=0.0821$) **D-F)** Trial 1-5 control traces for WT (left) and KO (right) mice for PL soma (D), PL-BLA terminals (E), and BLA soma (F). **D)** Left: main effect of time [$F(4.92,97.05)=2.792$, $p=0.0218$]; time x trial interaction [$F(204,1006)=1.377$, $p=0.0011$]. **E)** Right: main effect of time [$F(50, 971)=1.731$, $p=0.0015$]. **F)** Right: main effect of time [$F(5.372,107.4)=4.02$, $p=0.0017$].

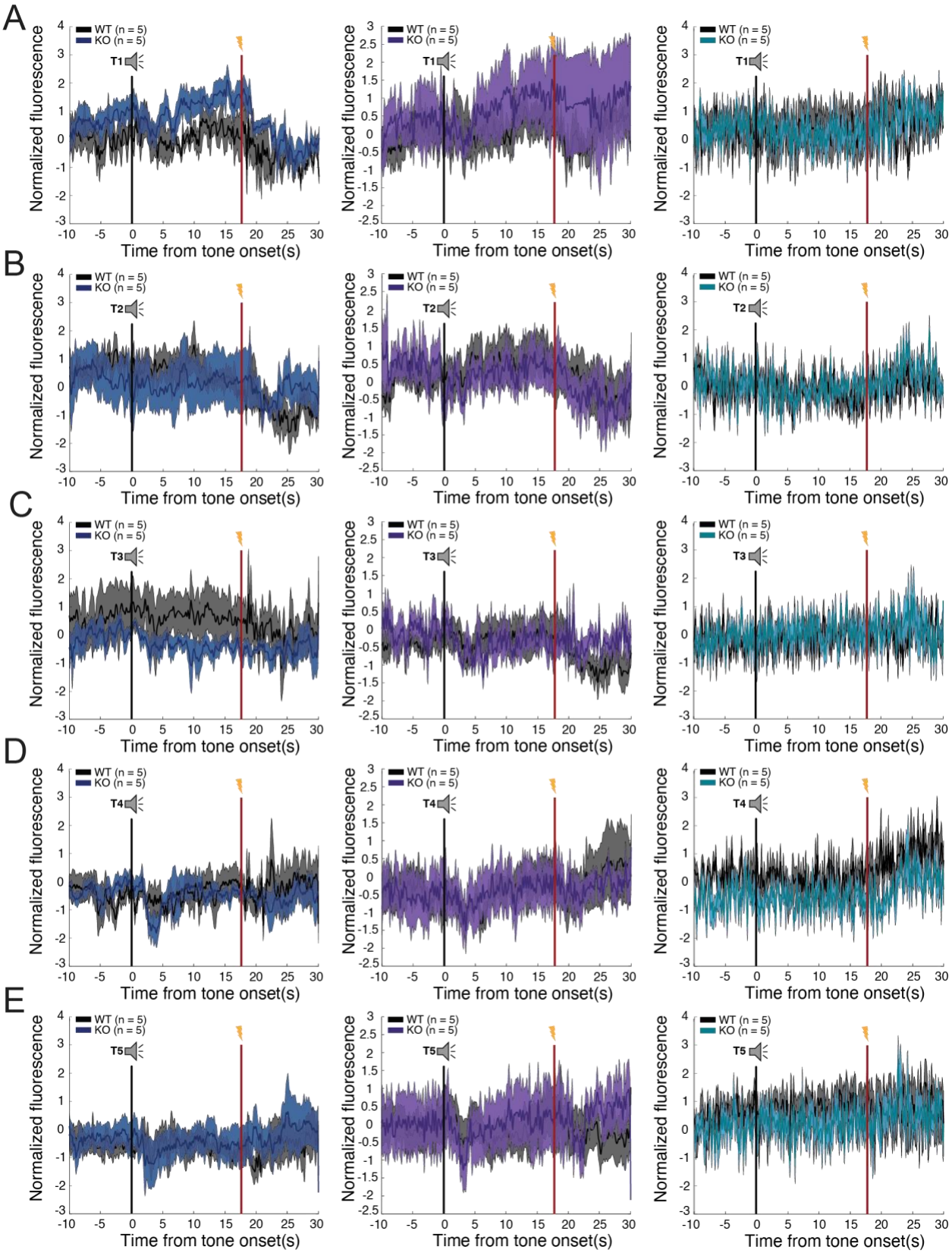
A
B
C
D
E
WT (n = 5)
KO (n = 5)
T1
T2
T3
T4
T5
Normalized fluorescence
Time from tone onset(s)

Appendix Figure 4. Between-genotype fluorescent fiber photometry control traces do not mirror calcium imaging conditioning patterns

A-E) WT and KO control traces for trials 1-5 (top to bottom) for PL soma (left, dark blue), PL-BLA terminals (middle, purple), and BLA soma (right, light blue). **A)** Left: main effect of time [F(4.582,36.65)=4.239, p=0.0047]. **B)** Left: main effect of time [F(3.359, 25.51)=3.036, p=0.0426]; time x genotype interaction [F(52,395)=1.636, p=0.0052].

Appendix Table 1. Freezing and velocity correlations with calcium signal

	Freezing probability x normalized fluoresence		Velocity (cm/s) x normalized fluoresence	
	WT	**KO**	**WT**	**KO**
Tone 1	r=-0.1749 p=0.383	**r=-0.4916** ***p=0.0092**	r=0.1224 p=0.5513	**r=0.7669** ***p<0.0001**
Tone 2	**r=-0.5158** ***p=0.0059**	**r=-0.5743** ***p=0.0017**	**r=0.4719** ***p=0.0149**	**r=0.4653** ***p=0.0166**
Tone 3	**r=-0.5728** ***p=0.0018**	**r=-0.4758** ***p=0.0163**	r=-0.09618 p=0.6402	**r=0.6781** ***p=0.0001**
Tone 4	**r=-0.5553** ***p=0.0026**	**r=-0.4929** ***p=0.009**	r=0.2565 p=0.206	r=-0.02988 p=0.8848
Tone 5	**r=-0.3972** ***p=0.0402**	**r=-0.551** ***p=0.0029**	r=-0.2848 p=0.1585	**r=0.4792** ***p=0.0132**
Baseline	r=-0.3075 p=0.1046	**r=-0.4761** ***p=0.009**	r=-0.08127 p=0.6751	r=-0.1574 p=0.4149

Correlations between normalized fluorescence and freezing probability (left) and velocity in cm/s (right) for WT and KO mice. R- and p-values are displayed for tones 1-5 and baseline period. Significant correlations are bolded and marked with asterisks.

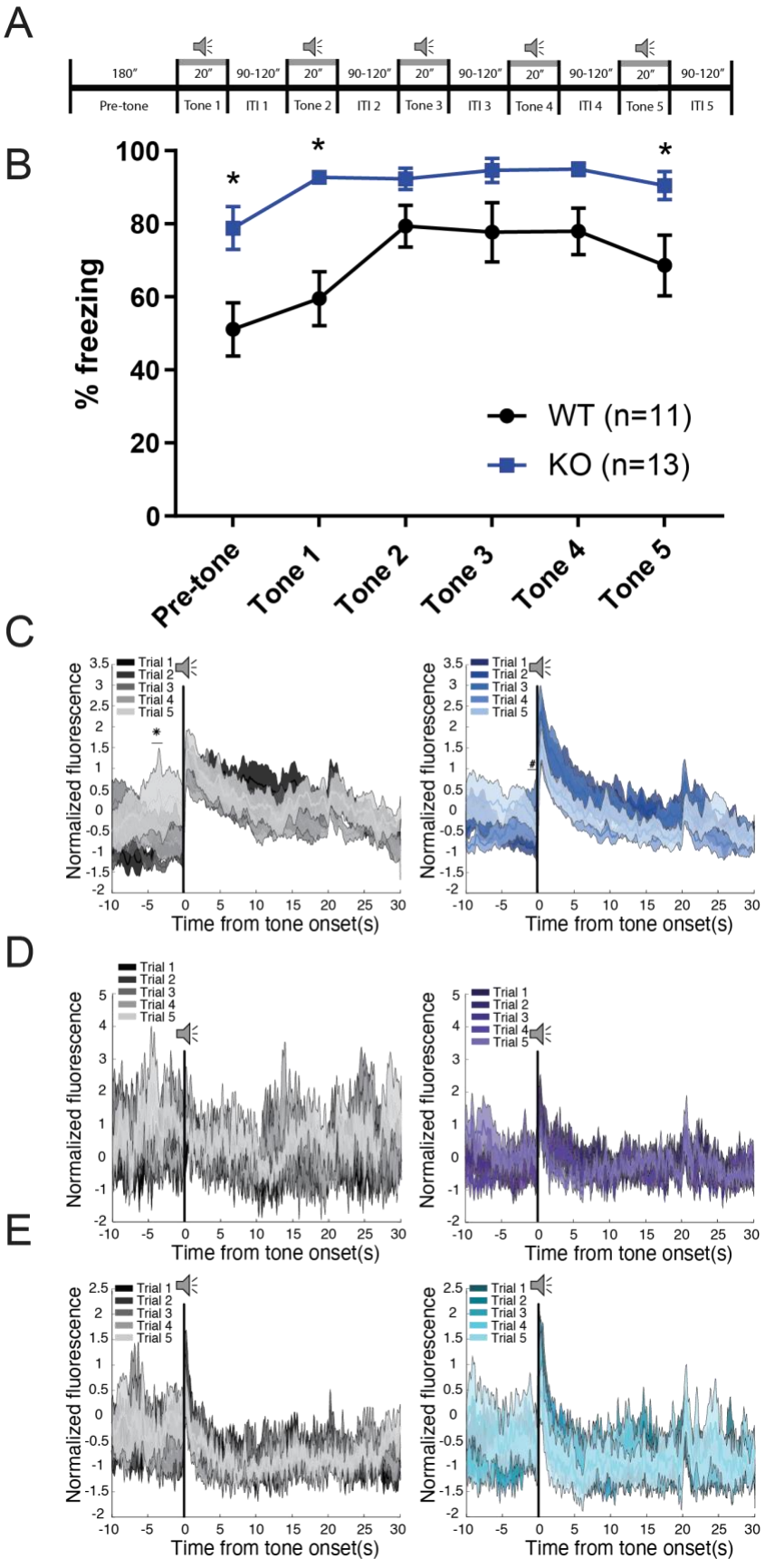
A
180″
20″
90-120″
Pre-tone
Tone 1
ITI 1
Tone 2
ITI 2
Tone 3
ITI 3
Tone 4
ITI 4
Tone 5
ITI 5
B
% freezing
WT (n=11)
KO (n=13)
Pre-tone
Tone 1
Tone 2
Tone 3
Tone 4
Tone 5
C
D
E
Trial 1
Trial 2
Trial 3
Trial 4
Trial 5
Normalized fluorescence
Time from tone onset(s)

Appendix Figure 5. Recall tone- and shock-associated calcium activity does not differ within genotype

A) Timeline of recall protocol. **B)** % freezing during the pre-tone period and tones 1-5 for WT and KO mice. Main effect of time [$F(3.674,80.83)=7.589$, $p<0.0001$] and genotype [$F(1,22)=16.77$, $p=0.0005$]. Post-hoc: WT vs. KO mice, tones 1 ($p=0.0026$), 2 ($p=0.0002$), and 5 ($p=0.0303$). **C-E)** Trial 1-5 calcium activity for WT (left) and KO (right) mice. **C)** Left: main effect of time [$F(4.756,166.4)=13.09$, $p<0.0001$]; time x trial interaction [$F(208,1820)=13.09$, $p=0.0005$]. Post-hoc: trial 2 vs. 5, -4.75 to -2.5s ($p<0.05$). Right: main effect of time [$F(6.369,382.1)=19.28$, $p<0.0001$]; time x trial interaction [$F(208,3120)=1.233$, $p=0.0153$]. Post-hoc tests: trend trial 1 vs. 3, -0.25 to 0.5s ($p=0.0524$). **D)** Right: main effect of time [$F(6.669,233.4)=4.292$, $p=0.0002$]; trend time x trial interaction [$F(208,1820)=1.15$, $p=0.08$]. **E)** Left: main effect of time [$F(7.932,317.3)=6.191$, $p<0.0001$]. Right: main effect of time [$F(8.838,441.9)=8.177$, $p<0.0001$].

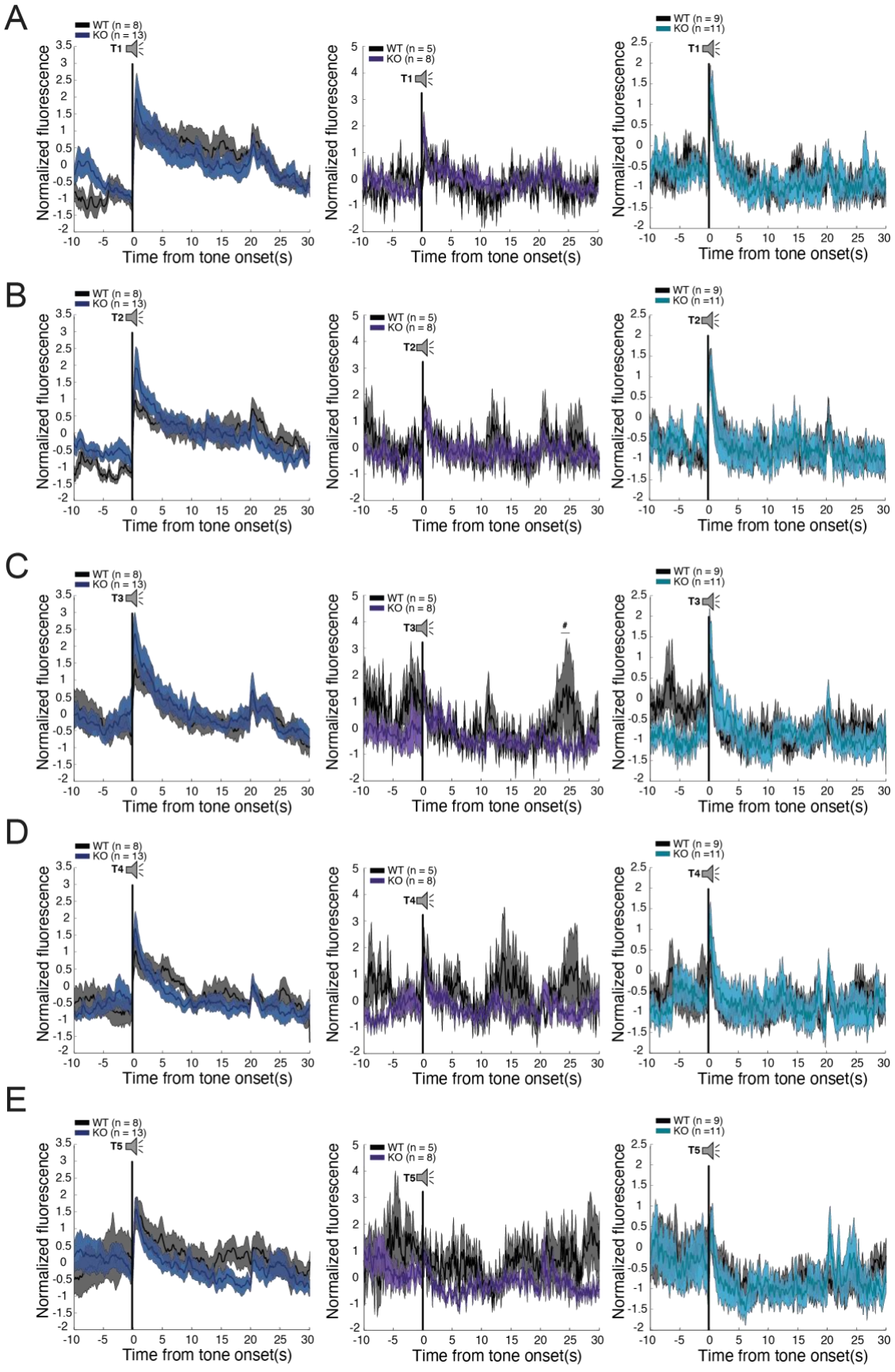
A
B
C
D
E
WT (n = 8)
KO (n = 13)
WT (n = 5)
KO (n = 8)
WT (n = 9)
KO (n =11)
T1
T2
T3
T4
T5
#
Normalized fluorescence
Time from tone onset(s)

Appendix Figure 6. Recall tone- and shock-associated calcium activity does not differ between genotypes across trials

A-E) WT and KO calcium activity in PL soma (left), PL-BLA terminals (middle), and BLA soma (right). **A)** Left: main effect of time [$F(3.811,72.42)=10.19$, $p<0.0001$]; time x genotype interaction [$F(52,988)=1.395$, $p=0.0359$]. Middle: main effect of time [$F(6.669,73.36)=2.644$, $p=0.0186$]. Right: main effect of time [$F(7.263,130.7)=5.082$, $p<0.0001$]. **B)** Left: main effect of time [$F(5.919,112.5)=10.70$, $p<0.0001$]; time x genotype interaction [$F(52,988)=1.668$, $p=0.0025$]. Right: main effect of time [$F(5.744,103.4)=3.607$, $p=0.0032$]. **C)** Left: main effect of time [$F(4.417,83.92)=7.265$, $p<0.0001$]. Middle: trend effect of time [$F(3.106,34.16)=2.584$, $p=0.0674$]; time x genotype interaction [$F(52,572)=1.49$, $p=0.0173$]. Post-hoc tests: trend 23.25-24.5s ($p=0.0672$). Right: main effect of time [$F(6.103,109.9)=4.102$, $p=0.0009$]; time x genotype interaction [$F(52,936)=2.57$, $p<0.0001$]. **D)** Left: main effect of time [$F(5.583,106.1)=6.31$, $p<0.0001$]. Right: trend effect of time [$F(5.716,102.9)=2.163$, $p=0.0555$]. **E)** Left: trend effect of time [$F(3.67,69.74)=2.565$, $p=0.0503$]. Middle: trend effect of genotype [$F(1,11)=4.61$, $p=0.0549$]. Right: main effect of time [$F(4.289,77.2)=3.11$, $p=0.0176$].

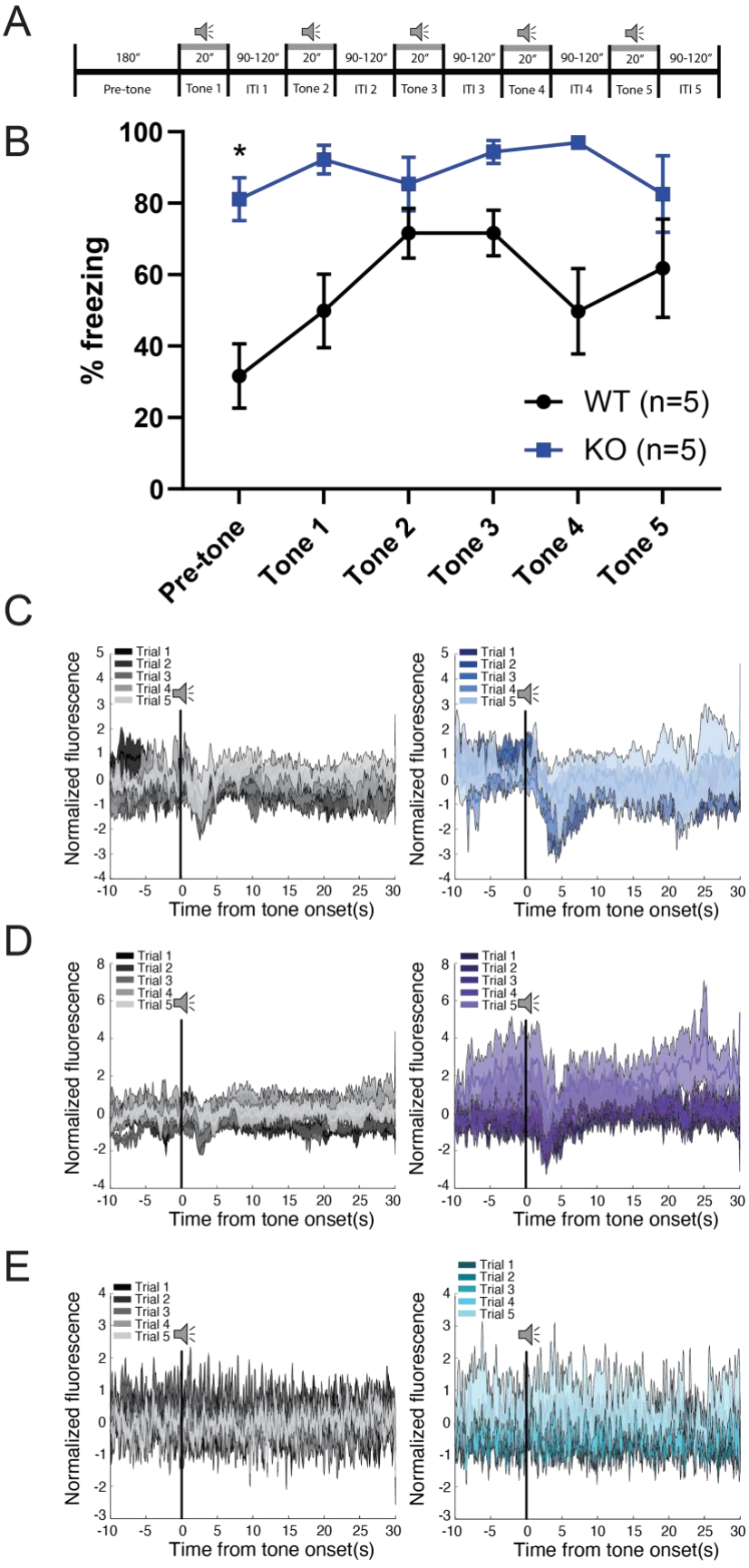
A
180″
20″
90-120″
Pre-tone
Tone 1
ITI 1
Tone 2
ITI 2
Tone 3
ITI 3
Tone 4
ITI 4
Tone 5
ITI 5
B
% freezing
WT (n=5)
KO (n=5)
Pre-tone
Tone 1
Tone 2
Tone 3
Tone 4
Tone 5
C
D
E
Normalized fluorescence
Time from tone onset(s)
Trial 1
Trial 2
Trial 3
Trial 4
Trial 5

Appendix Figure 7. Within-genotype fluorescent fiber photometry control traces do not mirror calcium imaging recall patterns

A) Timeline of fluorescent fiber photometry control experiment. **B)** % freezing during the pre-tone period and tones 1-5 for WT and KO mice. Main effect of genotype [$F(1,8)=46.78$, $p=0.0001$]. Post-hoc: WT vs. KO, tone 1 ($p=0.0157$). **C-E)** Trial 1-5 control traces for WT (left) and KO (right) mice for PL soma (C), PL-BLA terminals (D), and BLA soma (E). **C)** Left: main effect of time [$F(5.446,108.9)=2.689$, $p=0.0214$]. Right: main effect of time [$F(2.893,57.86)=7.435$, $p=0.0003$]. **D)** Right: main effect of time [$F(2.833,56.67)=3.264$, $p=0.0301$].

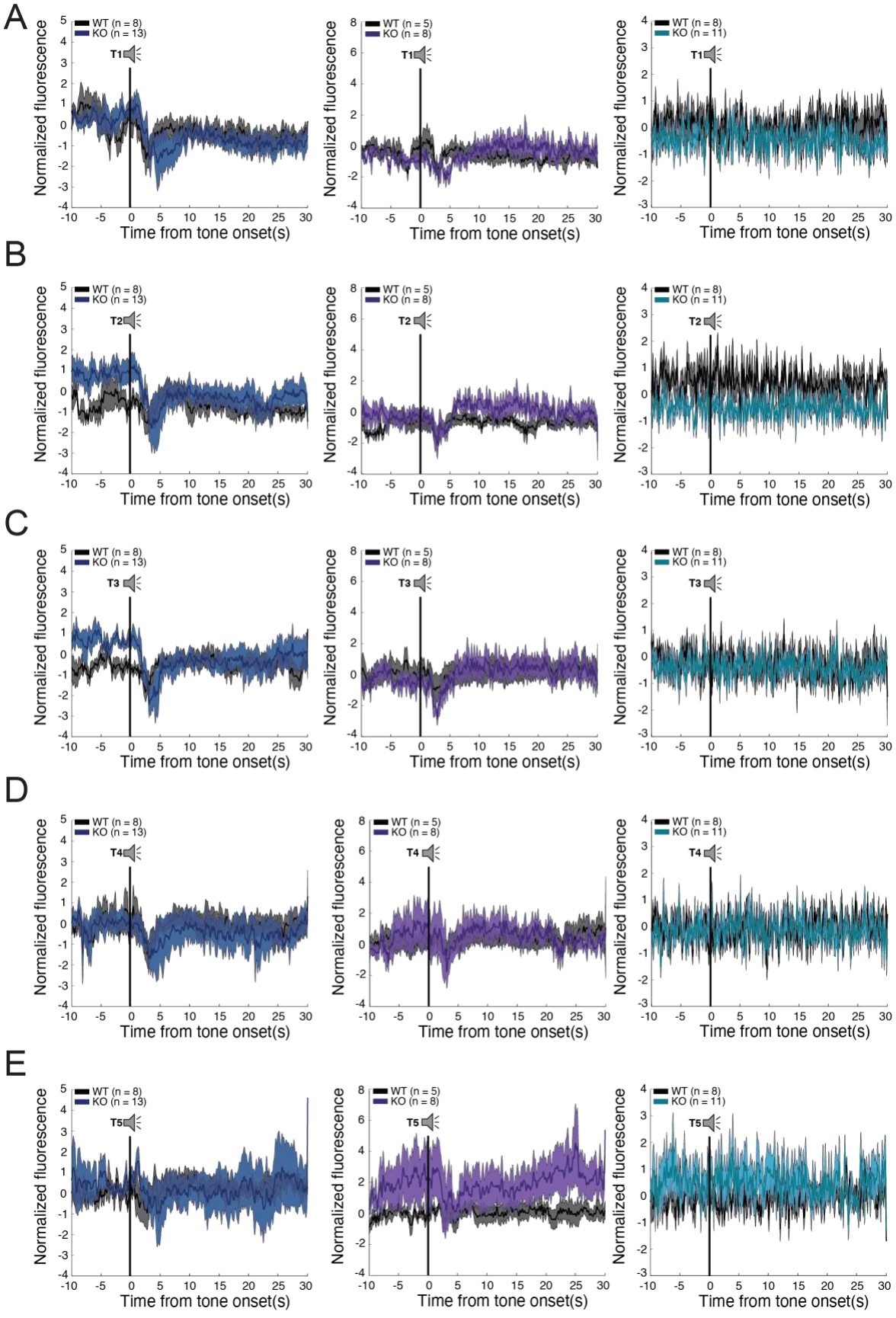
A
B
C
D
E
WT (n = 8)
KO (n = 13)
WT (n = 5)
KO (n = 8)
WT (n = 8)
KO (n = 11)
T1
T2
T3
T4
T5
Normalized fluorescence
Time from tone onset(s)

Appendix Figure 8. Between-genotype fluorescent fiber photometry control traces do not mirror calcium imaging recall patterns

A-E) WT and KO control traces for trials 1-5 (top to bottom) for PL soma (left), PL-BLA terminals (middle), and BLA soma (right). **A)** Left: main effect of time [$F(2.823,22.58)=3.173$, $p=0.0463$]. Middle: time x genotype interaction [$F(51,408)=1.491$, $p=0.02$]. **B)** Left: main effect of time [$F(3.649,28.77)=3.246$, $p=0.0289$]; time x genotype interaction [$F(52,410)=1.857$, $p=0.0005$]. Right: main effect of genotype [$F(1,8)=6.353$, $p=0.0358$]. **C)** Left: time x genotype interaction [$F(52,409)=2.138$, $p<0.0001$].

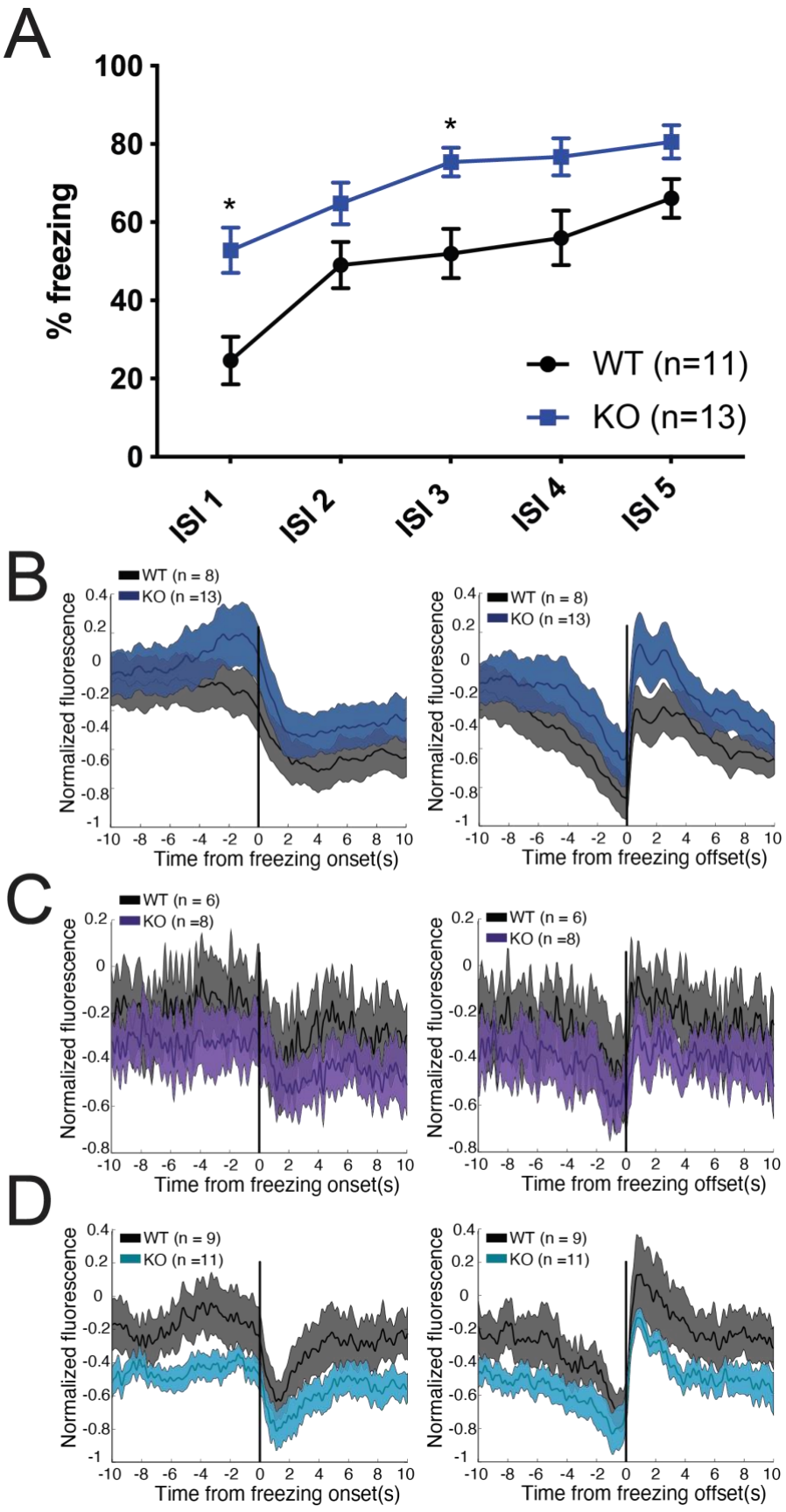
A
100
80
60
40
20
0
% freezing
*
*
WT (n=11)
KO (n=13)
ISI 1
ISI 2
ISI 3
ISI 4
ISI 5
B
WT (n = 8)
KO (n =13)
Normalized fluorescence
Time from freezing onset(s)
Time from freezing offset(s)
C
WT (n = 6)
KO (n =8)
Normalized fluorescence
Time from freezing onset(s)
Time from freezing offset(s)
D
WT (n = 9)
KO (n =11)
Normalized fluorescence
Time from freezing onset(s)
Time from freezing offset(s)

Appendix Figure 9. Conditioning freezing-associated PL activity during ITIs is elevated in KO mice

A) % freezing during conditioning ITIs for WT (n=11) and KO (n=13) mice. Main effects of time [$F(2.872,63.19)=26.73$, $p<0.0001$] and genotype [$F(1,22)=11.18$, $p=0.0029$]. Post-hoc tests: WT vs. KO ISI 1 ($p=0.0145$) and 3 ($p=0.0256$); WT ISI 1 vs ISIs 2 ($p=0.0001$), 3, 4, and 5 (all $p<0.0001$), ISI 2 vs. 5 ($p=0.0153$), and trend ISI 3 vs. 5 ($p=0.0683$); KO ISI 1 vs. ISIs 3 ($p=0.0001$), 4, and 5 (both $p<0.0001$), and ISI 2 vs. 5 ($p=0.0146$). **B-E)** Calcium activity during freezing onset (left) and freezing offset (right) for PL soma (B), PL-BLA terminals (C), and BLA soma (D). **B)** Left: main effect of time [$F(3.631,69)=49.88$, $p<0.0001$]; time x genotype interaction [$F(25,475)=1.973$, $p=0.0037$]. Right: main effect of time [$F(3.907,74.23)=22.58$, $p<0.0001$]; trend time x genotype interaction [$F(25,475)=1.51$, $p=0.0554$]. **C)** Left: main effect of time [$F(3.384,40.6)=6.341$, $p=0.0008$]. Right: main effect of time [$F(4.941,59.29)=4.113$, $p=0.0029$]. **D)** Left: main effect of time [$F(3.59,64.63)=12.55$, $p<0.0001$]. Right: main effect of time [$F(2.813,50.63)=16.01$, $p<0.0001$].

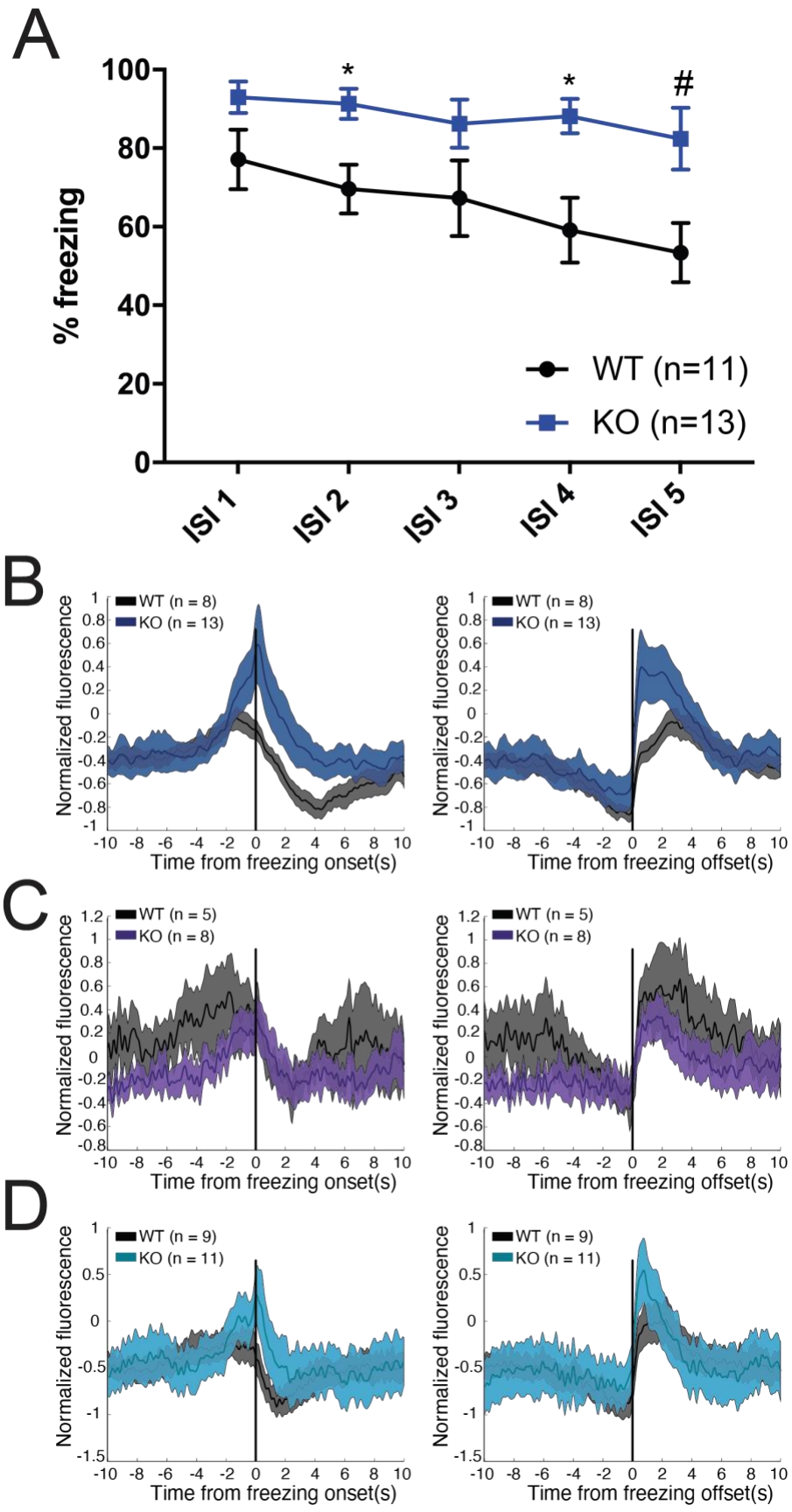
A
100
80
60
40
20
0
% freezing
*
*
#
WT (n=11)
KO (n=13)
ISI 1
ISI 2
ISI 3
ISI 4
ISI 5
B
WT (n = 8)
KO (n = 13)
Normalized fluorescence
Time from freezing onset(s)
Time from freezing offset(s)
C
WT (n = 5)
KO (n = 8)
D
WT (n = 9)
KO (n = 11)

Appendix Figure 10. Recall freezing-associated PL and BLA activity during ITIs is elevated in KO mice

A) % freezing during recall ITIs for WT (n=11) and KO (n=13) mice. Main effects of time [F(2.623,57.71)=4.907, p=0.0059] and genotype [F(1,22)=8.719, p=0.0074)]. Post-hoc tests: WT vs. KO ISIs 2 (p=0.0421) and 4 (p=0.0342), and trend for ISI 5 (p=0.0687); WT trend difference ISI 1 vs. 4 (p=0.0726) and 5 (p=0.0581). **B-E)** Calcium activity during freezing onset (left) and freezing offset (right) for PL soma (B), PL-BLA terminals (C), and BLA soma (D). **B)** Left: main effect of time [F(3.214,57.84)=12.53, p<0.0001]; time x genotype interaction [F(25,450)=3.187, p<0.0001]. Right: main effect of time [F(3.473,62.51)=16.73, p<0.0001]; time x genotype interaction [F(25,450)=2.685, p<0.0001]. **C)** Left: main effect of time [F(2.544,27.99)=3.732, p=0.0278]. Right: main effect of time [F(3.059,33.65)=7.216, p=0.0007]. **E)** Left: main effect of time [F(2.726,49.06)=5.982, p=0.002]; time x genotype interaction [F(25,450)=2.538, p<0.0001]. Right: main effect of time [F(2.915,52.46)=18.02, p<0.0001]; time x genotype interaction [F(25,450)=2.274, p=0.0005].

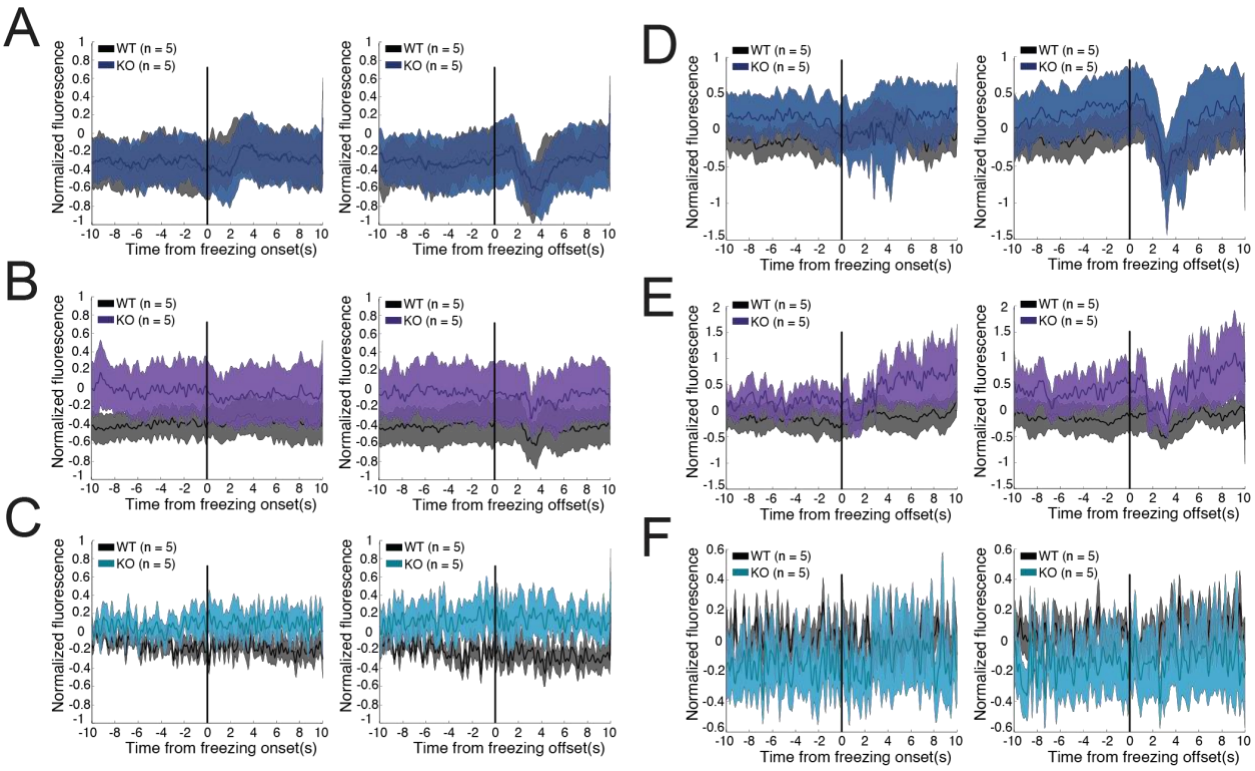

Appendix Figure 11. Fiber photometry control traces do not mirror calcium imaging ITI freezing patterns during conditioning and recall

A-C) WT and KO control traces for freezing onset (left) and offset (right) during conditioning ITIs for PL soma (A), PL-BLA terminals (C), and BLA soma (C). **A)** Right: main effect of time [F(3.434,27.47)=4.221, p=0.0113]. Middle: time x genotype interaction [F(51,408)=1.491, p=0.02]. **C)** Left: time x genotype interaction [F(25,200)=1.62, p=0.0373]. **D-F)** WT and KO control traces for freezing onset (left) and offset (right) during recall ITIs for PL soma (D), PL-BLA terminals (E), and BLA soma (F). **D)** Right: main effect of time [F(2.408,19.26)=5.66, p=0.0087].

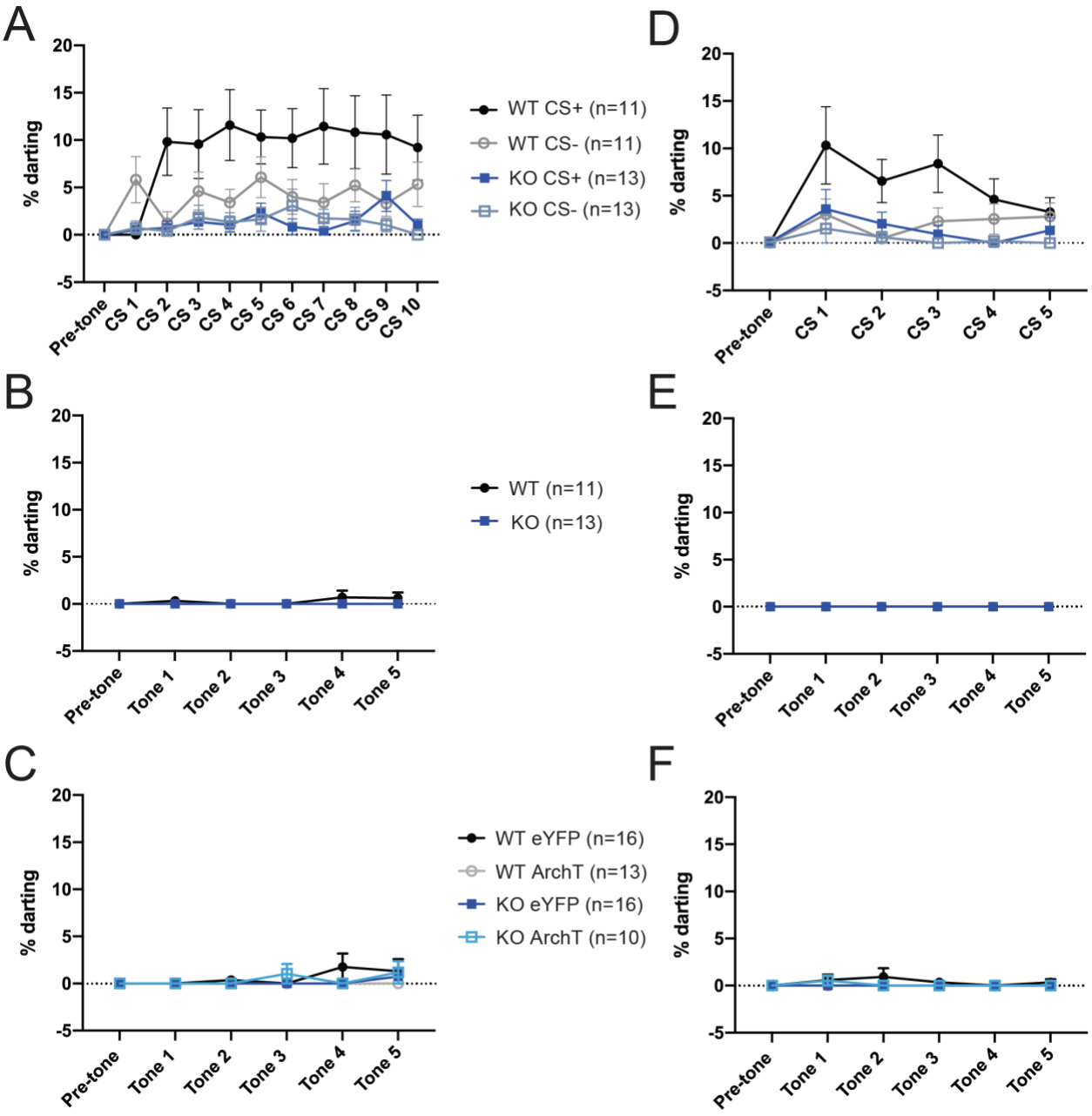

Appendix Figure 12. Darting is not significant during fiber photometry and optogenetic experiments

A-C) Darting during the conditioning session for discriminative fear conditioning (A), fiber photometry (B), and optogenetic experiments (C). **A)** Conditioning % darting for WT and KO mice during CS+ and CS- presentations. Main effect of time: $F(10,220)=4.783$, $p<0.0001$; main effect of genotype: $F(1,22)=39.07$, $p<0.0001$; time x genotype interaction: $F(10,220)=2.154$, $p=0.0217$; time x CS type interaction: $F(10,220)=2.15$, $p=0.0219$; time x genotype x CS type interaction: $F(10,220)=2.103$, $p=0.0253$. **B)** Conditioning % darting for WT and KO mice during fear conditioning with fiber photometry. No main effects or interactions. **C)** Conditioning % darting for WT eYFP, WT

ArchT, KO eYFP, and KO ArchT mice during fear conditioning with optogenetic inhibition. No main effects or interactions. **D-F)** Darting during the recall session for discriminative fear conditioning (D), fiber photometry (E), and optogenetic experiments (F). **D)** Recall % darting for WT and KO mice during CS+ and CS- presentations. Main effect of time: $F(5,110)=6.365$, $p<0.0001$; main effect of genotype: $F(1,22)=8.552$, $p=0.0079$; main effect of CS type: $F(1,22)=4.545$, $p=0.0444$; time x CS type interaction: $F(5,110)=2.603$, $p=0.0289$; trend time x genotype interaction: $F(5,110)=2.171$, $p=0.0625$. **E)** Recall % darting for WT and KO mice during fear conditioning with fiber photometry. No main effects or interactions. **F)** Recall % darting for WT eYFP, WT ArchT, KO eYFP, and KO ArchT mice during fear conditioning with optogenetic inhibition. No main effects or interactions.

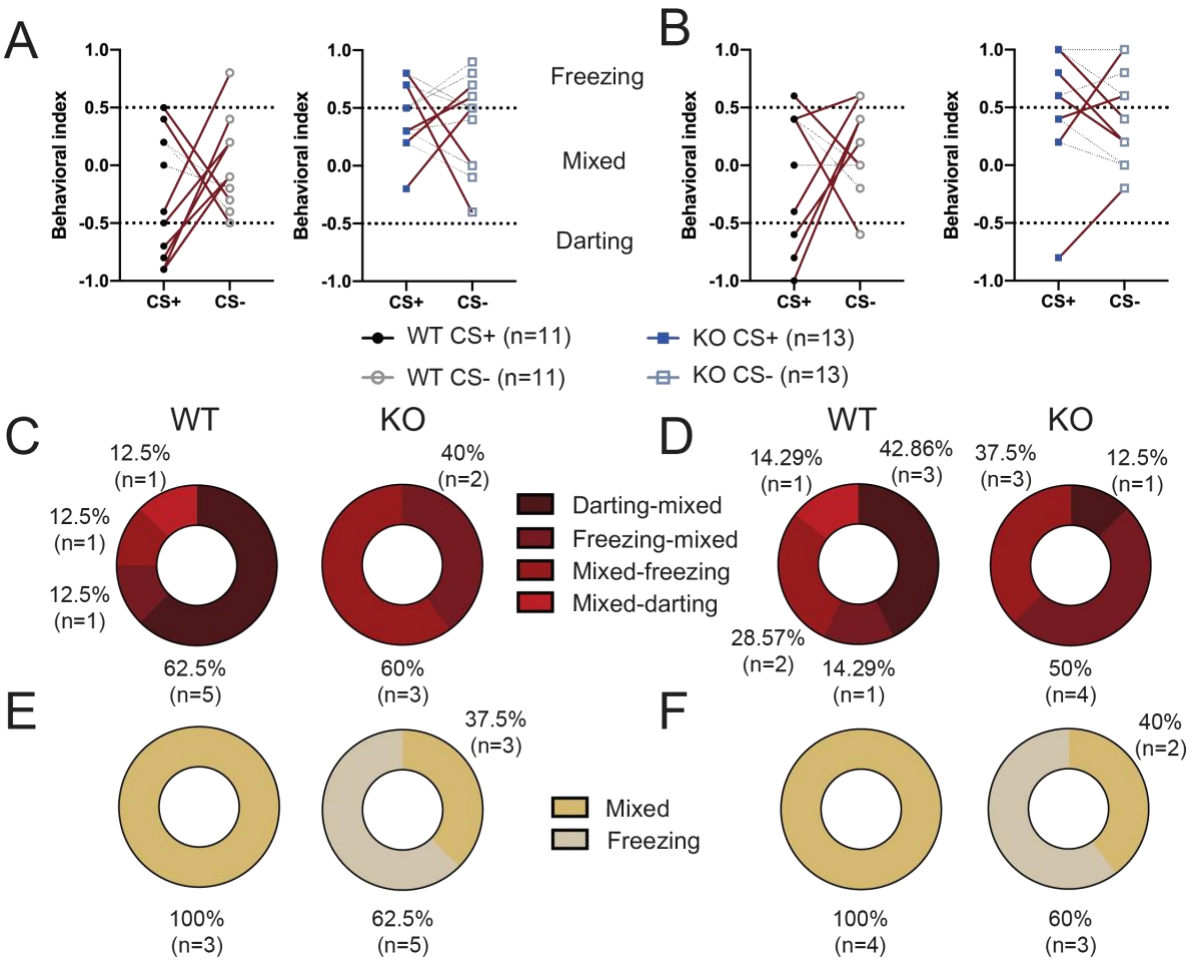

Appendix Figure 13. WT and KO mice display different defensive behavioral approaches during discriminative fear conditioning

A) Conditioning behavioral index for WT (left) and KO (right) mice. Filled points indicate CS+ strategy, open points indicate CS- strategy. Values from -1 to -0.5 were considered darting, -0.5 to 0.5 mixed, and 0.5 to 1 freezing. Discriminators are marked with red lines, generalizers are marked with black dotted lines. **B)** Recall behavioral index for WT (left) and KO (right) mice. **C)** Conditioning discriminator breakdown for WT (left) and KO (right) mice. **D)** Recall discriminator breakdown for WT (left) and KO (right) mice. **E)** Conditioning generalizer breakdown for WT (left) and KO (right) mice. **F)** Recall generalizer breakdown for WT (left) and KO (right) mice.

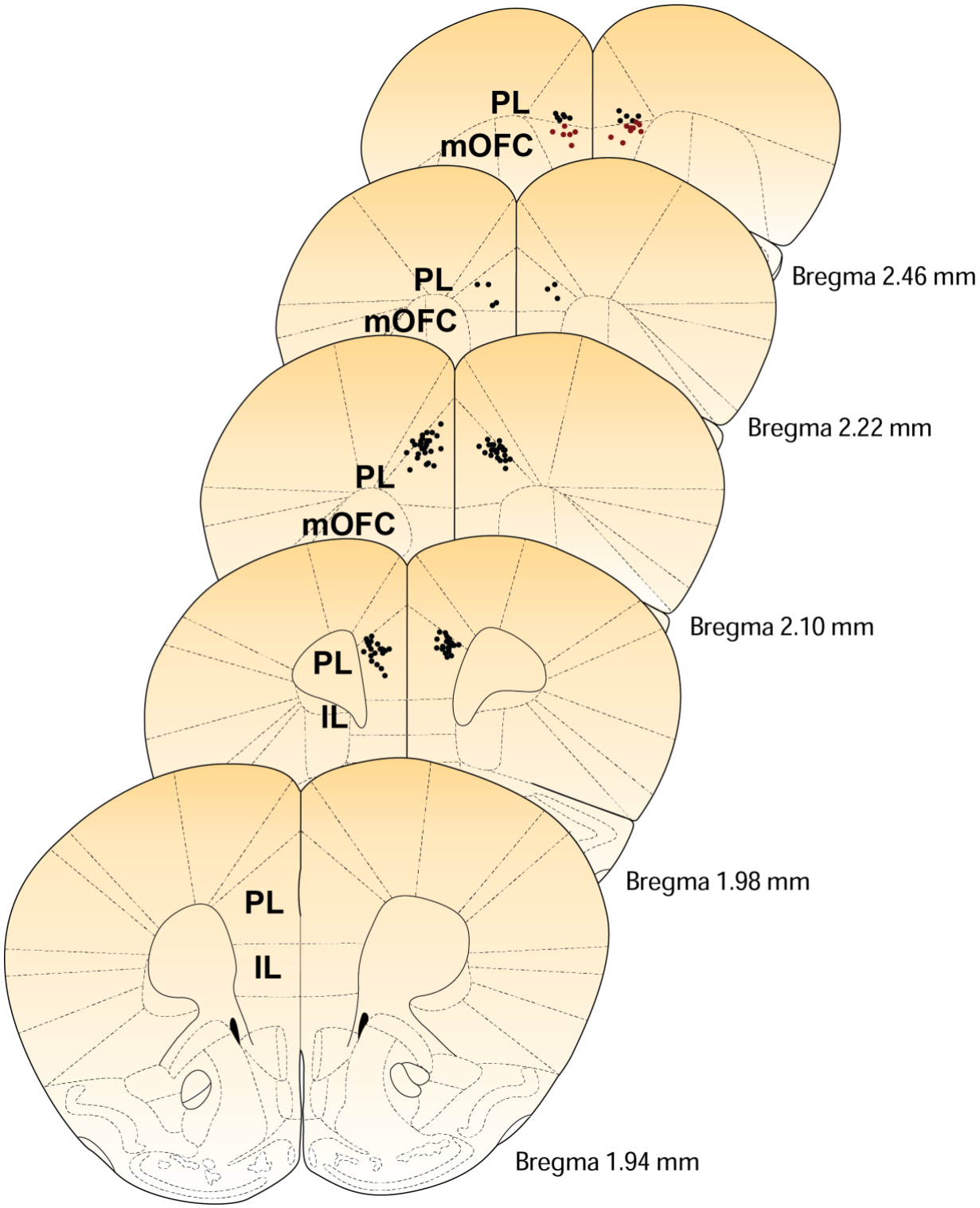

Appendix Figure 14. PL targeting of fiberoptic implants for optogenetics

Location of bilateral fiberoptic implants in the PL for optogenetic inhibition experiments. Dots represent the lowest point of the fiber tract. Black dots are hits, red dots are misses.

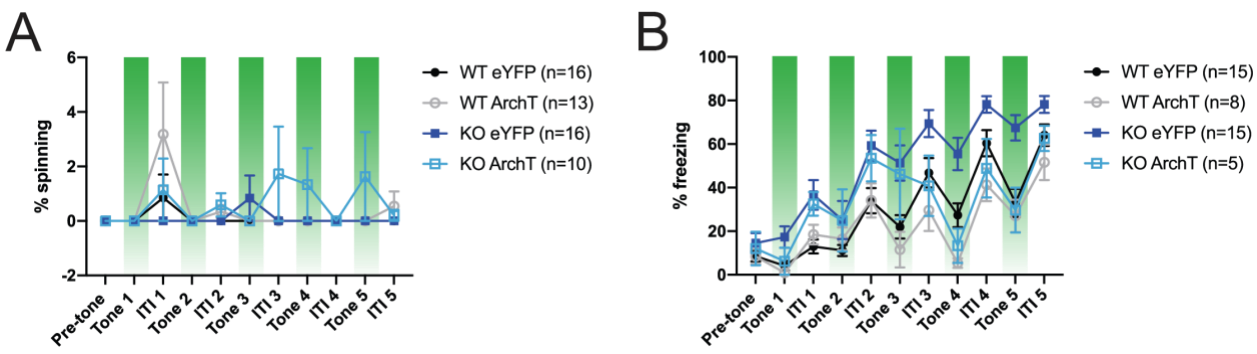

Appendix Figure 15. Spinning occurs in mice expressing ArchT, but does not affect freezing data

A) % spinning during the conditioning pre-tone period, tones 1-5, and ITIs 1-5 for WT eYFP, WT ArchT, KO eYFP, and KO ArchT mice. Green columns represent periods of illumination. Main effect of virus [$F(1,51)=7.177$, $p=0.0099$]; trend effect of time [$F(2.936,149.7)=2.379$, $p=0.0734$]; trend time x genotype interaction [$F(10,510)=1.705$, $p=0.0766$]. **B)** % freezing with spinners excluded during the conditioning pre-tone period, tones 1-5, and ITIs 1-5 for WT eYFP (n=15), WT ArchT (n=8), KO eYFP (n=15), and KO ArchT (n=5) mice. Green columns represent periods of illumination. Main effects of time [$F(5.555,216.6)=36.98$, $p<0.0001$], genotype [$F(1,39)=12.45$, $p=0.0011$], and virus [$F(1,39)=6.786$, $p=0.0129$]; time x virus interaction [$F(10,390)=3.776$, $p<0.0001$]; n.s. time x genotype interaction [$F(10,390)=1.455$, $p=0.1542$].

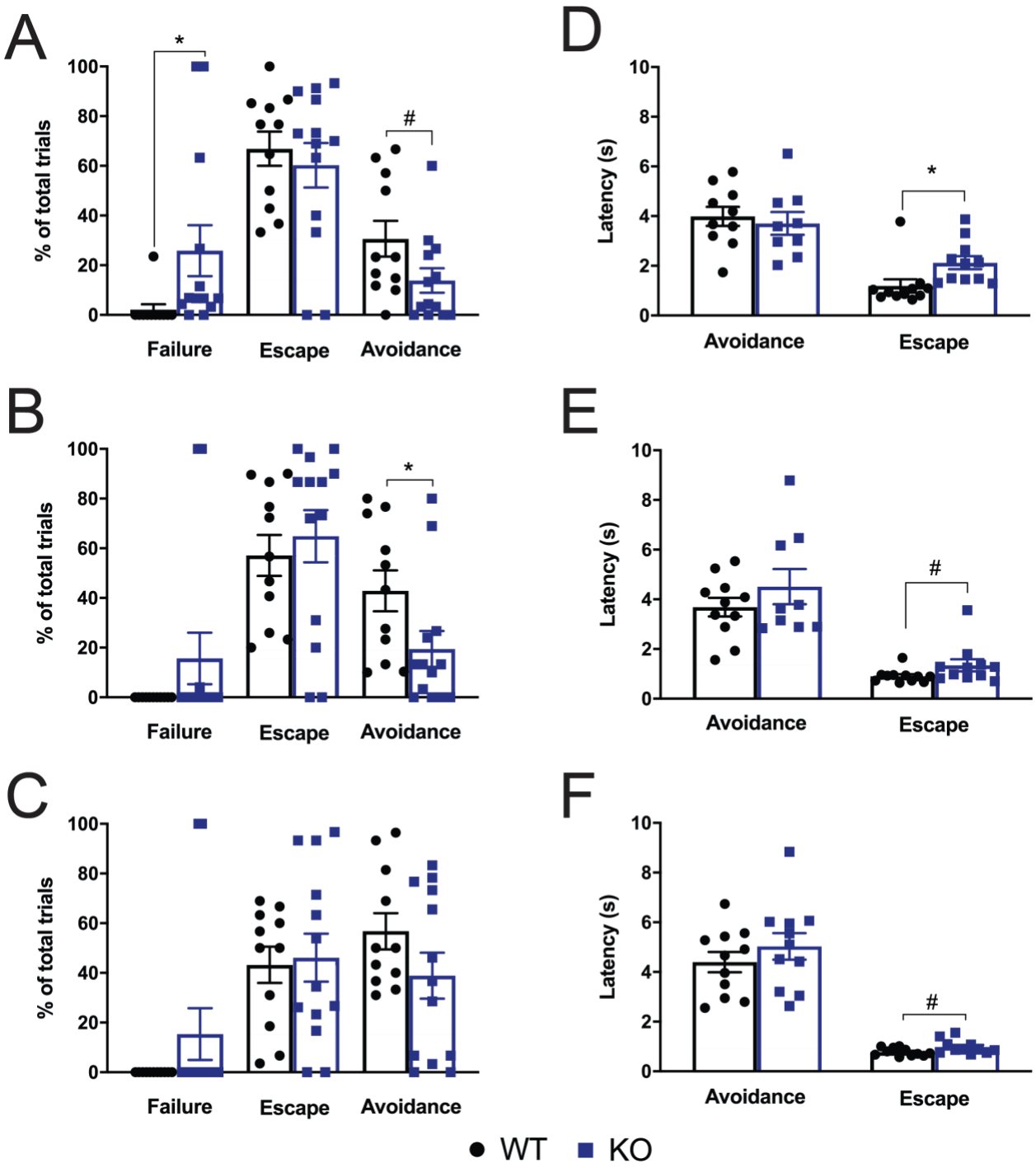

Appendix Figure 16. SAPAP3 KO mice perform worse than WTs in two-way shuttle avoidance

Active avoidance trial breakdown (A-C) and response latency (D-F) during three sequential training days for SAPAP3 WT (n=11) and KO (n=13) mice. **A)** Day 1 percentage of trials that result in failure, escapee, and avoidance. A greater percentage of trials for KO mice result in failure (t=1.09, df=22, p=0.0484). There is a trend lower percentage of avoidance responses in KO vs. WT mice (t-1.972, df=22, p=0.0613). **B)** Day 2 percentage of trials that result in

failure, escape, and avoidance. A smaller percentage of trials result in avoidance for KO vs. WT mice (t=2.139, df=22, p=0.0438). **C)** Day 3 percentage of trials that result in failure, escape, and avoidance. There are not genotype differences. **D)** Day 1 latency to avoid and escape. KO mice exhibit a longer escape latency compared to WTs (t=2.525, df=20, p=0.0201). **E)** Day 2 latency to avoid and escape. KO mice exhibit a trend longer escape latency compared to WTs (t=1.736, df=20, p=0.098). **F)** Day 3 latency to avoid and escape. KO mice exhibit a trend longer escape latency compared to WTs (t=2.054, df=20, p=0.0533).

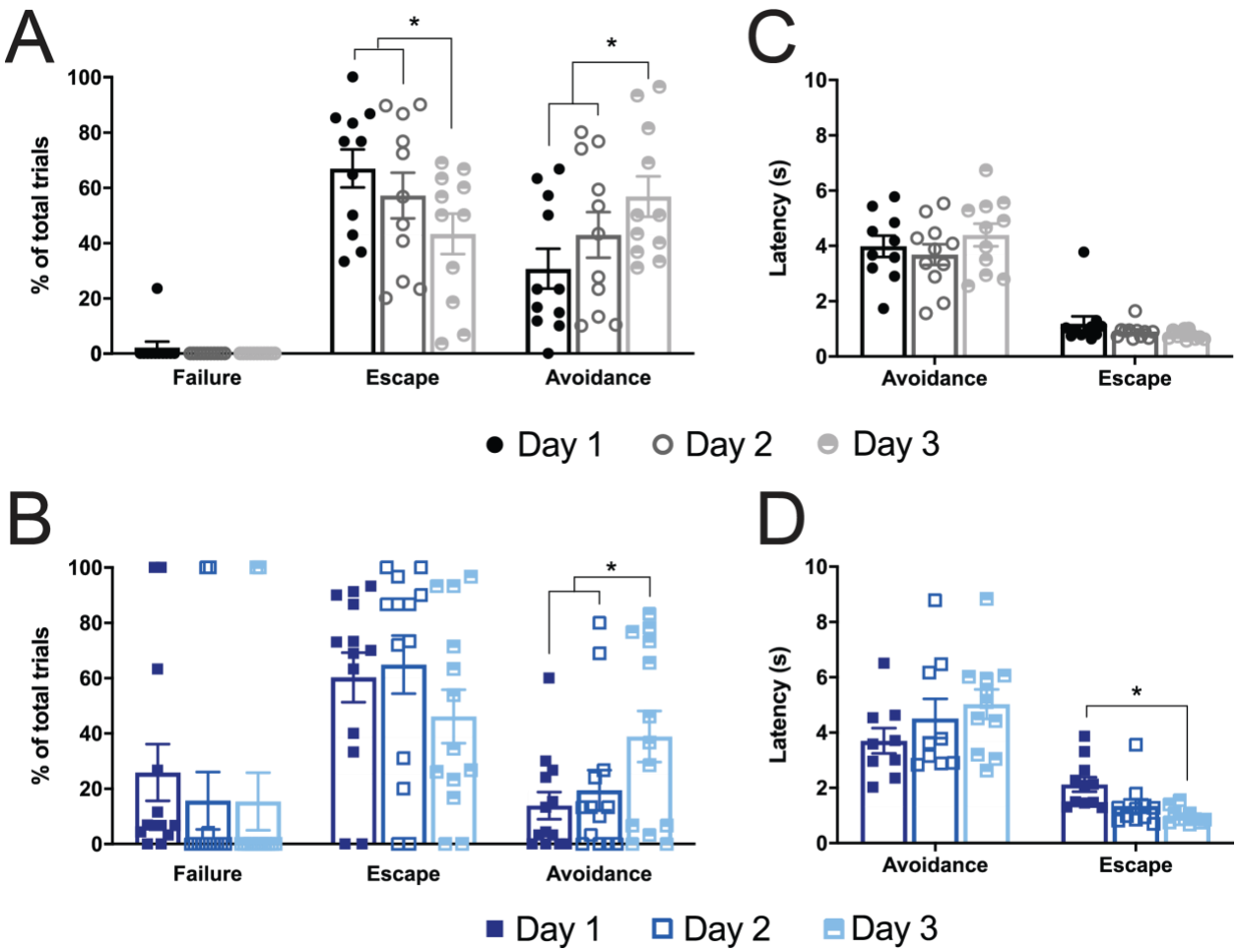

Appendix Figure 17. Learning of two-way shuttle avoidance is delayed in SAPAP3 KO mice

A,B) Percentage of total trials that result in failure, escape, and avoidance across all three days for WT (A) and KO (B) mice. **A)** Escape responses in WT mice decrease across days [main effect of day: $F(1.661,16.61)=7.852$, $p=0.0056$. Post-hoc tests: days 3 vs. 1 ($p=0.0075$) and 2 ($p=0.0332$)] while avoidance responses increase [main effect of day: $F(1.485,14.85)=7.084$, $p=0.0108$. Post-hoc tests: days 3 vs. 1 ($p=0.0123$) and 2 ($p=0.0332$)]. **B)** There is a trend main effect of day for both failure [$F(1,12)=4.418$, $p=0.0574$)] and escape responses [$F(1.744,20.93)=3.442$, $p=0.0566$] in KO mice. Avoidance responses increase across days [main effect of day: $F(1.688,20.25)=8.36$, $p=0.0033$. Post-hoc tests: days 3 vs. 1 ($p=0.0117$) and 2 ($p=0.0402$)]. **C,D)** Avoidance and escape latency across all three days for WT (C) and KO (D) mice. **C)** Avoidance and escape latencies do not differ across days for WT mice. **D)** Escape latency decreases across days in KO mice [main effect of day: $F(1.823,18.23)=10.19$, $p=0.0013$. Post-hoc tests: day 1 vs. 3 ($p=0.004$); trend day 1 vs. 2 ($p=0.0539$)]. There are no differences in avoidance latencies.

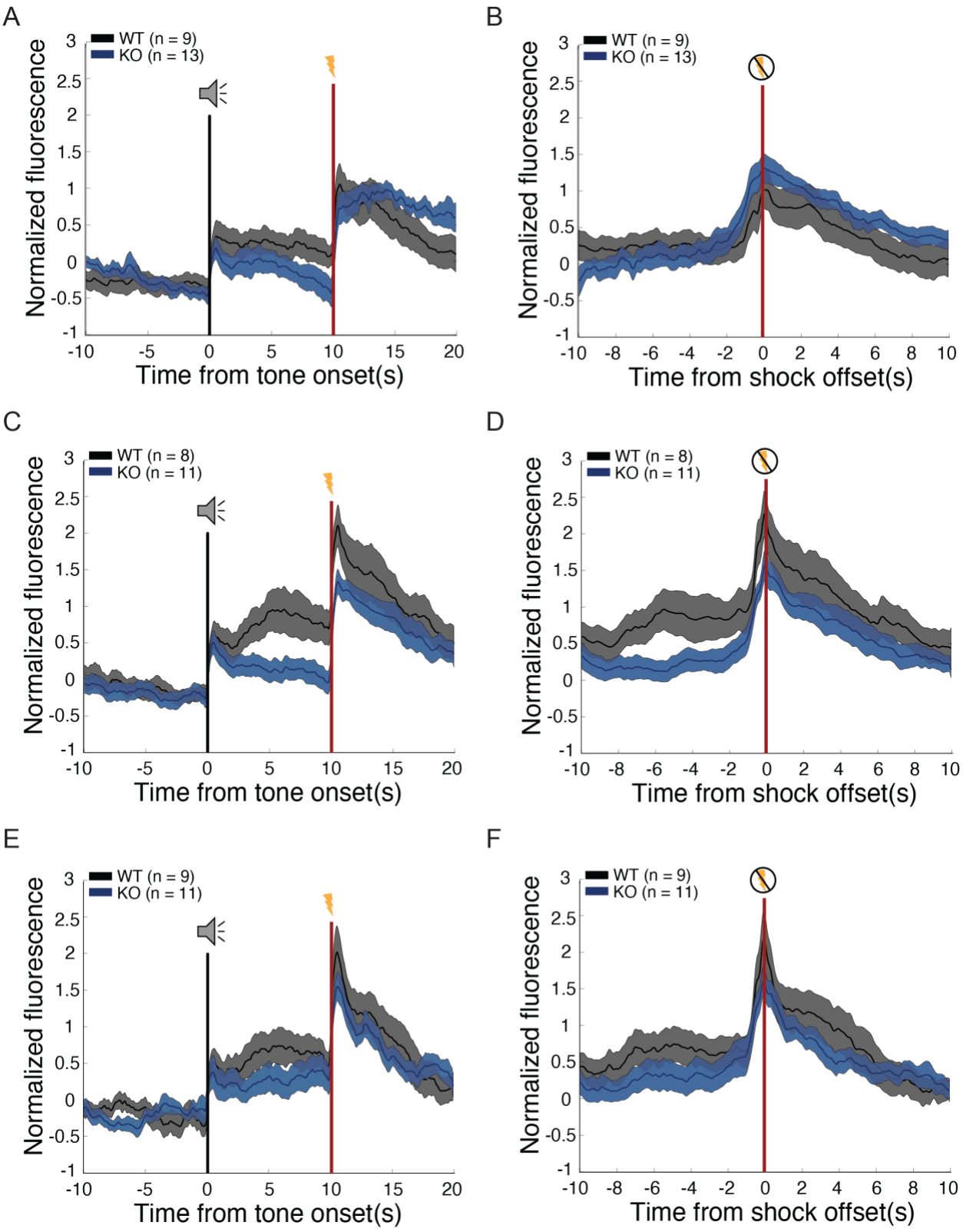

Appendix Figure 18. KO mice display diminshed PL activity compared to WTs during escape trials in 2-way shuttle avoidance

PL tone- and shock-associated calcium activity for SAPAP3 WT and KO mice during escape trials on days 1 (A, B), 2 (C, D), and 3 (E, F) of 2-way shuttle avoidance. **A)** Normalized fluorescence to day 1 tone and shock onset. Main effect of time [$F(2.857,57.14)=6.383$, $p=0.001$]. Time x genotype interaction [$F(25,500)=2.04$, $p=0.0023$]. **B)** Normalized fluorescence to day 1 shock offset. Main effect of time [$F(3.25,64.99)=24.45$, $p<0.0001$]. Time x genotype interaction [$F(25,500)=3.707$, $p<0.0001$]. **C)** Normalized fluorescence to day 2 tone and shock onset. Main effect of time [$F(3.046,51.78)=30.51$, $p<0.0001$]. Time x genotype interaction [$F(38,646)=2.177$, $p<0.0001$]. WT tone AUC is greater than KO tone AUC ($t=2.202$, $df=17$, $p=0.0418$; data not shown). **D)** Normalized fluorescence to day 2 shock offset. Main effect of time [$F(2.873,48.85)=16.87$, $p<0.0001$]. Trend effect of genotype [$F(1,17)=3.077$, $p=0.0974$]. **E)** Normalized fluorescence to day 3 tone and shock onset. Main effect of time [$F(3.852,69.33)=28.36$, $p<0.0001$]. Time x genotype interaction [$F(38,684)=1.446$, $p=0.0427$]. **F)** Normalized fluorescence to day 1 shock offset. Main effect of time [$F(3.065,55.17)=20.41$, $p<0.0001$].

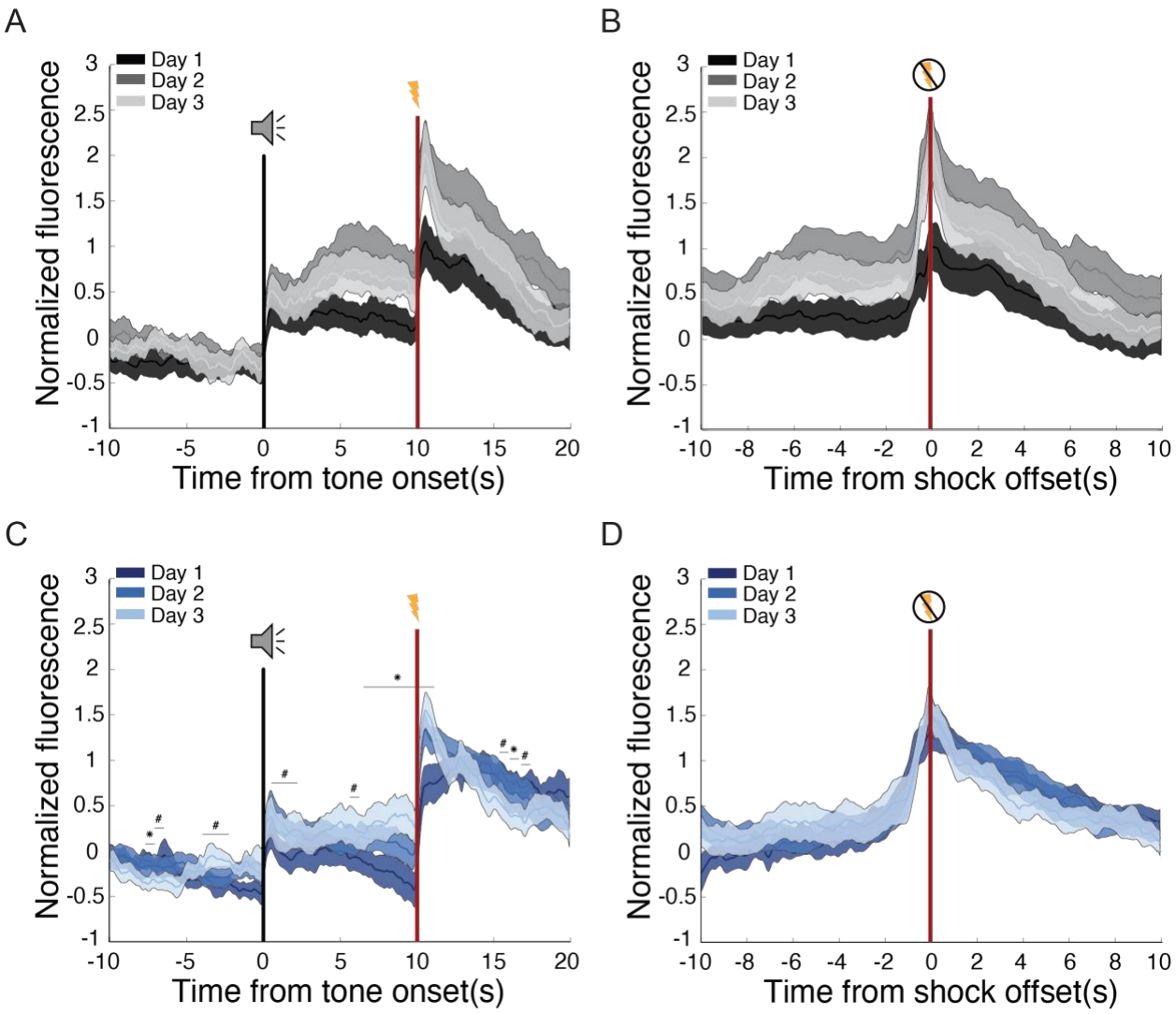

Appendix Figure 19. SAPAP3 WT and KO mice display different PL activity patterns during escape trials across multiple days of 2-way shuttle avoidance training

PL tone- and shock-associated calcium activity for SAPAP3 WT (A, B) and KO (C, D) mice during escape trials across three days of 2-way shuttle avoidance training. While the overall trends of the signals in WTs and KOs are quite similar, the shape of the calcium traces – particularly during tone onset and shock offset – appear to differ between genotypes. **A)** Normalized fluorescence to tone and shock onset for days 1-3 in WT mice. Main effect of time [$F(2.688,21.51)=32.61$, $p<0.0001$]. **B)** Normalized fluorescence to shock offset for days 1-3 in WT mice. Main effect of time [$F(2.969,23.751)=17.95$, $p<0.0001$]. **C)** Normalized fluorescence to tone and shock onset for days 1-3 in KO mice. Main effect of time [$F(3.048,36.58)=16.2$, $p<0.0001$]. Time x day interaction [$F(4.928,49.02)=3.321$, $p=0.0119$]. Post-hoc tests: day 1 vs. days 2 (6.5 to 11 seconds) and 3 (-7.75 to -7, 6.5 to 11, and 16.25 to 17 seconds)

and, all p-values <0.05. Trend day 1 vs. days 2 (-1.75 to -1, 0.5 to 2, and 5.75 to 6.5 seconds) and 3 (-7 to -6.25, -3.25 to -1, 15.5 to 16.25, and 17 to 17.75 seconds), all p-values < 0.1. Trend effect of day for tone AUC [F(1.343,13.43)=4.179, p=0.0517].

Bibliography

Ade KK, Wan Y, Hamann HC, O'Hare JK, Guo W, Quian A, Kumar S, Bhagat S, Rodriguiz RM, Wetsel WC, Conn PJ, Dzirasa K, Huber KM, Calakos N (2016) Increased Metabotropic Glutamate Receptor 5 Signaling Underlies Obsessive-Compulsive Disorder-like Behavioral and Striatal Circuit Abnormalities in Mice. Biol Psychiatry 80:522–533 Available at: http://dx.doi.org/10.1016/j.biopsych.2016.04.023.

Adhikari A, Topiwala MA, Gordon JA (2010) Synchronized Activity between the Ventral Hippocampus and the Medial Prefrontal Cortex during Anxiety. Neuron 65:257–269.

Adhikari A, Topiwala MA, Gordon JA (2011) Single units in the medial prefrontal cortex with anxiety-related firing patterns are preferentially influenced by ventral hippocampal activity. Neuron 71:898–910 Available at: http://www.ncbi.nlm.nih.gov/pubmed/21903082 [Accessed February 21, 2020].

Adler CM, McDonough-Ryan P, Sax KW, Holland SK, Arndt S, Strakowski SM (2000) fMRI of neuronal activation with symptom provocation in unmedicated patients with obsessive compulsive disorder. J Psychiatr Res 34:317–324 Available at: www.elsevier.com/locate/jpsychires [Accessed April 22, 2020].

Admon R, Bleich-Cohen M, Weizmant R, Poyurovsky M, Faragian S, Hendler T (2012) Functional and structural neural indices of risk aversion in obsessive-compulsive disorder (OCD). Psychiatry Res - Neuroimaging 203:207–213.

Ahmari SE, Risbrough VB, Geyer MA, Simpson HB (2012) Impaired sensorimotor gating in unmedicated adults with obsessive-compulsive disorder. Neuropsychopharmacology 37:1216–1223.

Aizenberg M, Mwilambwe-Tshilobo L, Briguglio JJ, Natan RG, Geffen MN (2015) Bidirectional Regulation of Innate and Learned Behaviors That Rely on Frequency Discrimination by Cortical Inhibitory Neurons. PLoS Biol 13:e1002308 Available at: http://www.ncbi.nlm.nih.gov/pubmed/26629746 [Accessed February 21, 2020].

Akirav I, Raizel H, Maroun M (2006) Enhancement of conditioned fear extinction by infusion of the GABA A agonist muscimol into the rat prefrontal cortex and amygdala. Eur J Neurosci 23:758–764.

Alves-Pinto A, Rus OG, Reess TJ, Wohlschläger A, Wagner G, Berberich G, Koch K (2019) Altered reward-related effective connectivity in obsessive-compulsive disorder: An fMRI study. J Psychiatry Neurosci 44:395–406 Available at: www.fil.ion.ucl.ac.uk/spm; [Accessed May 21, 2020].

Amano T, Duvarci S, Popa D, Paré D (2011) The fear circuit revisited: Contributions of the basal

amygdala nuclei to conditioned fear. J Neurosci 31:15481–15489.

Amorapanth P, Nader K, Ledoux JE (1999) Lesions of periaqueductal gray dissociate-conditioned freezing from conditioned suppression behavior in rats. Learn Mem 6:491–499.

Anglada-Figueroa D, Quirk GJ (2005) Lesions of the basal amygdala block expression of conditioned fear but not extinction. J Neurosci 25:9680–9685 Available at: http://www.ncbi.nlm.nih.gov/pubmed/16237172 [Accessed February 26, 2020].

Apergis-Schoute AM, Dębiec J, Doyère V, LeDoux JE, Schafe GE (2005) Auditory fear conditioning and long-term potentiation in the lateral amygdala require ERK/MAP kinase signaling in the auditory thalamus: A role for presynaptic plasticity in the fear system. J Neurosci 25:5730–5739.

Apergis-Schoute AM, Gillan CM, Fineberg NA, Fernandez-Egea E, Sahakian BJ, Robbins TW (2017) Neural basis of impaired safety signaling in Obsessive Compulsive Disorder. Proc Natl Acad Sci U S A 114:3216–3221.

Armony JL, Quirk GJ, Ledoux JE (1998) Differential effects of amygdala lesions on early and late plastic components of auditory cortex spike trains during fear conditioning. J Neurosci 18:2592–2601.

Arruda-Carvalho M, Clem RL (2014) Pathway-selective adjustment of prefrontal-amygdala transmission during fear encoding. J Neurosci 34:15601–15609.

Asok A, Kandel ER, Rayman JB (2019) The neurobiology of fear generalization. Front Behav Neurosci 12:329.

Attwells S, Setiawan E, Wilson AA, Rusjan PM, Mizrahi R, Miler L, Xu C, Richter MA, Kahn A, Kish SJ, Houle S, Ravindran L, Meyer JH (2017) Inflammation in the neurocircuitry of obsessive-compulsive disorder. JAMA Psychiatry 74:833–840 Available at: http://www.ncbi.nlm.nih.gov/pubmed/28636705 [Accessed February 21, 2020].

Baeg EH (2001) Fast Spiking and Regular Spiking Neural Correlates of Fear Conditioning in the Medial Prefrontal Cortex of the Rat. Cereb Cortex 11:441–451.

Banks GP, Mikell CB, Youngerman BE, Henriques B, Kelly KM, Chan AK, Herrera D, Dougherty DD, Eskandar EN, Sheth SA (2015) Neuroanatomical characteristics associated with response to dorsal anterior cingulotomy for obsessive-compulsive disorder. JAMA Psychiatry 72:127–135.

Barad M (2005) Fear extinction in rodents: Basic insight to clinical promise. Curr Opin Neurobiol 15:710–715.

Becker MPI, Nitsch AM, Schlösser R, Koch K, Schachtzabel C, Wagner G, Miltner WHR, Straube T (2014) Altered emotional and BOLD responses to negative, positive and ambiguous performance feedback in OCD. Soc Cogn Affect Neurosci 9:1127–1133.

Behbehani MM (1995) Functional characteristics of the midbrain periaqueductal gray. Prog Neurobiol 46:575–605.

Bienvenu OJ et al. (2009) Sapap3 and pathological grooming in humans: Results from the OCD collaborative genetics study. Am J Med Genet Part B Neuropsychiatr Genet 150:710–720.

Blanchard DC, Blanchard RJ (2008) Defensive behaviors, fear, and anxiety. In: Handbook of Anxiety and Fear, pp 63–79.

Blanchard RJ, Blanchard DC (1989) Antipredator defensive behaviors in a visible burrow system. J Comp Psychol 103:70–82.

Bloodgood DW, Sugam JA, Holmes A, Kash TL (2018) Fear extinction requires infralimbic cortex projections to the basolateral amygdala. Transl Psychiatry 8.

Bobes J, González MP, Bascarán MT, Arango C, Sáiz PA, Bousoño M (2001) Quality of life and disability in patients with obsessive compulsive disorder. Eur Psychiatry 16:239–245.

Bonin RP, Bories C, De Koninck Y (2014) A simplified up-down method (SUDO) for measuring mechanical nociception in rodents using von Frey filaments. Mol Pain 10:26 Available at: http://www.ncbi.nlm.nih.gov/pubmed/24739328 [Accessed February 11, 2020].

Bordi F, LeDoux JE (1994) Response properties of single units in areas of rat auditory thalamus that project to the amygdala - II. Cells receiving convergent auditory and somatosensory inputs and cells antidromically activated by amygdala stimulation. Exp Brain Res 98:275–286.

Botta P, Demmou L, Kasugai Y, Markovic M, Xu C, Fadok JP, Lu T, Poe MM, Xu L, Cook JM, Rudolph U, Sah P, Ferraguti F, Lüthi A (2015) Regulating anxiety with extrasynaptic inhibition. Nat Neurosci 18:1493–1500.

Bravo-Rivera C, Roman-Ortiz C, Brignoni-Perez E, Sotres-Bayon F, Quirk GJ (2014) Neural structures mediating expression and extinction of platform-mediated avoidance. J Neurosci 34:9736–9742 Available at: http://www.ncbi.nlm.nih.gov/pubmed/25031411 [Accessed February 21, 2020].

Bravo-Rivera C, Roman-Ortiz C, Montesinos-Cartagena M, Quirk GJ (2015) Persistent active avoidance correlates with activity in prelimbic cortex and ventral striatum. Front Behav Neurosci 9:184 Available at: http://www.ncbi.nlm.nih.gov/pubmed/26236209 [Accessed February 21, 2020].

Breiter HC, Rauch SL, Kwong KK, Baker JR, Weisskoff RM, Kennedy DN, Kendrick AD, Davis TL, Jiang A, Cohen MS, Stern CE, Belliveau JW, Baer L, Sullivan RLO, Savage CR, Jenike MA, Rosen BR (1996) Functioncal Magnetic Resonance Imaging of Symptom Provocation in Obsessive-compulsive Disorder. Arch Gen Psychiatry 53:595–606.

Brown LT, Mikell CB, Youngerman BE, Zhang Y, McKhann GM, Sheth SA (2016) Dorsal anterior cingulotomy and anterior capsulotomy for severe, refractory obsessive-compulsive

disorder: A systematic review of observational studies. J Neurosurg 124:77–89 Available at: http://www.ncbi.nlm.nih.gov/pubmed/26252455 [Accessed February 21, 2020].

Büchel C, Morris J, Dolan RJ, Friston KJ (1998) Brain systems mediating aversive conditioning: An event-related fMRI study. Neuron 20:947–957.

Burghardt NS, Sullivan GM, McEwen BS, Gorman JM, Ledoux JE (2004) The selective serotonin reuptake inhibitor citalopram increases fear after acute treatment but reduces fear with chronic treatment: A comparison with tianeptine. Biol Psychiatry 55:1171–1178.

Burgos-Robles A, Vidal-Gonzalez I, Quirk GJ (2009) Sustained conditioned responses in prelimbic prefrontal neurons are correlated with fear expression and extinction failure. J Neurosci 29:8474–8482.

Burgos-Robles A, Vidal-Gonzalez I, Santini E, Quirk GJ (2007) Consolidation of Fear Extinction Requires NMDA Receptor-Dependent Bursting in the Ventromedial Prefrontal Cortex. Neuron 53:871–880.

Burguière E, Monteiro P, Feng G, Graybiel AM (2013) Optogenetic stimulation of lateral orbitofronto-striatal pathway suppresses compulsive behaviors. Science (80-) 340:1243–1246 Available at: http://science.sciencemag.org/ [Accessed April 24, 2020].

Cambiaghi M, Grosso A, Likhtik E, Mazziotti R, Concina G, Renna A, Sacco T, Gordon JA, Sacchetti B (2016a) Higher-order sensory cortex drives basolateral amygdala activity during the recall of remote, but not recently learned fearful memories. J Neurosci 36:1647–1659.

Cambiaghi M, Grosso A, Renna A, Sacchetti B (2016b) Differential recruitment of auditory cortices in the consolidation of recent auditory fearful memories. J Neurosci 36:8586–8597.

Cambiaghi M, Renna A, Milano L, Sacchetti B (2017) Reversible inactivation of the higher order auditory cortex during fear memory consolidation prevents memory-related activity in the basolateral amygdala during remote memory retrieval. Front Behav Neurosci 11.

Campeau S, Davis M (1995a) Involvement of the central nucleus and basolateral complex of the amygdala in fear conditioning measured with fear-potentiated startle in rats trained concurrently with auditory and visual conditioned stimuli. J Neurosci 15:2301–2311 Available at: http://www.ncbi.nlm.nih.gov/pubmed/7891168 [Accessed February 26, 2020].

Campeau S, Davis M (1995b) Involvement of subcortical and cortical afferents to the lateral nucleus of the amygdala in fear conditioning measured with fear-potentiated startle in rats trained concurrently with auditory and visual conditioned stimuli. J Neurosci 15:2312–2327.

Capogna M (2014) GABAergic cell type diversity in the basolateral amygdala. Curr Opin Neurobiol 26:110–116.

Capuzzo G (University of BC, Floresco SB (University of BC (2020) Prelimbic and Infralimbic Prefrontal Regulation of Active and Inhibitory Avoidance and Reward-Seeking. J Neurosci Available at: https://doi.org/10.1523/JNEUROSCI.0414-20.2020 [Accessed May 18, 2020].

Cardoner N, Harrison BJ, Pujol J, Soriano-Mas C, Hernńdez-Ribas R, López-Solá M, Real E, Deus J, Ortiz H, Alonso P, Menchãn JM (2011) Enhanced brain responsiveness during active emotional face processing in obsessive compulsive disorder. World J Biol Psychiatry 12:349–363.

Carrive P, Leung P, Harris J, Paxinos G (1997) Conditioned fear to context is associated with increased Fos expression in the caudal ventrolateral region of the midbrain periaqueductal gray. Neuroscience 78:165–177.

Cavanagh JF, Gründler TOJ, Frank MJ, Allen JJB (2010) Altered cingulate sub-region activation accounts for task-related dissociation in ERN amplitude as a function of obsessive-compulsive symptoms. Neuropsychologia 48:2098–2109 Available at: http://www.ncbi.nlm.nih.gov/pubmed/20381506 [Accessed February 21, 2020].

Chen M, Wan Y, Ade K, Ting J, Feng G, Calakos N (2011) Sapap3 deletion anomalously activates short-term endocannabinoid-mediated synaptic plasticity. J Neurosci 31:9563–9573.

Chen XL, Xie JX, Han H Bin, Cui YH, Zhang BQ (2004) MR perfusion-weighted imaging and quantitative analysis of cerebral hemodynamics with symptom provocation in unmedicated patients with obsessive-compulsive disorder. Neurosci Lett 370:206–211.

Chen Y, Meng Z, Zhang Z, Zhu Y, Gao R, Cao X, Tan L, Wang Z, Zhang H, Li Y, Fan Q (2019) The right thalamic glutamate level correlates with functional connectivity with right dorsal anterior cingulate cortex/middle occipital gyrus in unmedicated obsessive–compulsive disorder: A combined fMRI and 1 H-MRS study. Aust N Z J Psychiatry 53:207–218.

Chen YH, Lan YJ, Zhang SR, Li WP, Luo ZY, Lin S, Zhuang JP, Li XW, Li SJ, Yang JM, Gao TM (2017) ErbB4 signaling in the prelimbic cortex regulates fear expression. Transl Psychiatry 7.

Cheng DT, Knight DC, Smith CN, Stein EA, Helmstetter FJ (2003) Functional MRI of human amygdala activity during Pavlovian fear conditioning: Stimulus processing versus response expression. Behav Neurosci 117:3–10.

Cheriyan J, Kaushik MK, Ferreira AN, Sheets PL (2016) Specific targeting of the basolateral amygdala to projectionally defined pyramidal neurons in prelimbic and infralimbic cortex. eNeuro 3:489–494 Available at: http://dx.doi.org/10.1523/ENEURO.0002-16.2016 [Accessed May 21, 2020].

Cho JH, Deisseroth K, Bolshakov VY (2013) Synaptic encoding of fear extinction in mPFC-amygdala circuits. Neuron 80:1491–1507 Available at: http://dx.doi.org/10.1016/j.neuron.2013.09.025.

Choi DC, Maguschak KA, Ye K, Jang SW, Myers KM, Ressler KJ (2010a) Prelimbic cortical BDNF is required for memory of learned fear but not extinction or innate fear. Proc Natl Acad Sci U S A 107:2675–2680.

Choi JS, Cain CK, Ledoux JE (2010b) The role of amygdala nuclei in the expression of auditory

signaled two-way active avoidance in rats. Learn Mem 17:139–147.

Ciocchi S, Herry C, Grenier F, Wolff SBE, Letzkus JJ, Vlachos I, Ehrlich I, Sprengel R, Deisseroth K, Stadler MB, Müller C, Lüthi A (2010) Encoding of conditioned fear in central amygdala inhibitory circuits. Nature 468:277–282 Available at: http://www.ncbi.nlm.nih.gov/pubmed/21068837 [Accessed February 21, 2020].

Colom-Lapetina J, Li AJ, Pelegrina-Perez TC, Shansky RM (2019) Behavioral diversity across classic rodent models is sex-dependent. Front Behav Neurosci 13:45 Available at: http://www.ncbi.nlm.nih.gov/pubmed/30894806 [Accessed March 4, 2020].

Concina G, Cambiaghi M, Renna A, Sacchetti B (2018) Coherent activity between the prelimbic and auditory cortex in the slow-gamma band underlies fear discrimination. J Neurosci 38:8313–8328.

Corbit VL, Manning EE, Gittis AH, Ahmari SE (2019) Strengthened inputs from secondary motor cortex to striatum in a mouse model of compulsive behavior. J Neurosci 39:2965–2975.

Corches A, Hiroto A, Bailey TW, Speigel JH, Pastore J, Mayford M, Korzus E (2019) Differential fear conditioning generates prefrontal neural ensembles of safety signals. Behav Brain Res 360:169–184 Available at: http://www.ncbi.nlm.nih.gov/pubmed/30502356 [Accessed February 21, 2020].

Corcoran KA, Quirk GJ (2007) Activity in prelimbic cortex is necessary for the expression of learned, but not innate, fears. J Neurosci 27:840–844.

Courtin J, Chaudun F, Rozeske RR, Karalis N, Gonzalez-Campo C, Wurtz H, Abdi A, Baufreton J, Bienvenu TCM, Herry C (2014) Prefrontal parvalbumin interneurons shape neuronal activity to drive fear expression. Nature 505:92–96.

Cruikshank SJ, Edeline J-M, Weinberger NM (1992) Stimulation at a site of auditory-somatosensory convergence in the medial geniculate nucleus is an effective unconditioned stimulus for fear conditioning. Behav Neurosci 106:471–483.

Cummings KA, Clem RL (2020) Prefrontal somatostatin interneurons encode fear memory. Nat Neurosci 23:61–74.

da Costa NM, Martin KAC, Sägesser FD (2017) A weighted graph of the projections to mouse auditory cortex. bioRxiv Available at: https://doi.org/10.1101/228726 [Accessed May 26, 2020].

Dana H, Mohar B, Sun Y, Narayan S, Gordus A, Hasseman JP, Tsegaye G, Holt GT, Hu A, Walpita D, Patel R, Macklin JJ, Bargmann CI, Ahrens MB, Schreiter ER, Jayaraman V, Looger LL, Svoboda K, Kim DS (2016) Sensitive red protein calcium indicators for imaging neural activity. Elife 5.

Davis M (1992) The Role Of The Amygdala In Fear And Anxiety. Annu Rev Neurosci 15:353–375 Available at: www.annualreviews.org [Accessed June 24, 2020].

De Bundel D, Zussy C, Espallergues J, Gerfen CR, Girault JA, Valjent E (2016) Dopamine D2 receptors gate generalization of conditioned threat responses through mTORC1 signaling in the extended amygdala. Mol Psychiatry 21:1545–1553.

De Leeuw AS, Oranje B, Van Megen HJGM, Kemner C, Westenberg HGM (2010) Sensory gating and sensorimotor gating in medication-free obsessive-compulsive disorder patients. Int Clin Psychopharmacol 25:232–240.

De Oca BM, DeCola JP, Maren S, Fanselow MS (1998) Distinct regions of the periaqueductal gray are involved in the acquisition and expression of defensive responses. J Neurosci 18:3426–3432.

De Ridder D, Leong SL, Manning P, Vanneste S, Glue P (2017) Anterior Cingulate Implant for Obsessive-Compulsive Disorder. World Neurosurg 97:754.e7-754.e16 Available at: http://www.ncbi.nlm.nih.gov/pubmed/27756670 [Accessed February 21, 2020].

Dejean C, Courtin J, Karalis N, Chaudun F, Wurtz H, Bienvenu TCM, Herry C (2016) Prefrontal neuronal assemblies temporally control fear behaviour. Nature 535:420–424 Available at: http://dx.doi.org/10.1038/nature18630.

Del Casale A, Kotzalidis GD, Rapinesi C, Serata D, Ambrosi E, Simonetti A, Pompili M, Ferracuti S, Tatarelli R, Girardi P (2011) Functional neuroimaging in obsessive-compulsive disorder. Neuropsychobiology 64:61–85.

Den Braber A, Zilhão NR, Fedko IO, Hottenga JJ, Pool R, Smit DJA, Cath DC, Boomsma DI (2016) Obsessive–compulsive symptoms in a large population-based twin-family sample are predicted by clinically based polygenic scores and by genome-wide SNPs. Transl Psychiatry 6:e731.

Di Scala G, Mana MJ, Jacobs WJ, Phillips AG (1987) Evidence of Pavlovian conditioned fear following electrical stimulation of the periaqueductal grey in the rat. Physiol Behav 40:55–63.

Diehl MM, Bravo-Rivera C, Rodriguez-Romaguera J, Pagan-Rivera PA, Burgos-Robles A, Roman-Ortiz C, Quirk GJ (2018) Active avoidance requires inhibitory signaling in the rodent prelimbic prefrontal cortex. Elife 7:1–19.

Diehl MM, Iravedra-García JM, Morán-Sierra J, Rojas-Bowe G, Gonzalez-Díaz F, Valentín-Valentín V, Quirk GJ (2020) Divergent projections of the prelimbic cortex bidirectionally regulate active avoidance. bioRxiv Available at: https://www.biorxiv.org/content/10.1101/2020.05.28.120659v1 [Accessed June 26, 2020].

Diniz JB, Miguel EC, de Oliveira AR, Reimer AE, Brandão ML, de Mathis MA, Batistuzzo MC, Costa DLC, Hoexter MQ (2012) Outlining new frontiers for the comprehension of obsessive-compulsive disorder: A review of its relationship with fear and anxiety. Rev Bras Psiquiatr 34:S81-91 Available at: http://www.ncbi.nlm.nih.gov/pubmed/22729451 [Accessed February 11, 2020].

Disterhoff JF, Stuart DK (1976) Trial sequence of changed unit activity in auditory system of alert rat during conditioned response acquisition and extinction. J Neurophysiol 39:266–281.

Diwadkar VA, Burgess A, Hong E, Rix C, Arnold PD, Hanna GL, Rosenberg DR (2015) Dysfunctional activation and brain network profiles in youth with obsessive-compulsive disorder: A focus on the dorsal anterior cingulate during working memory. Front Hum Neurosci 9:149 Available at: http://www.ncbi.nlm.nih.gov/pubmed/25852529 [Accessed February 21, 2020].

Do-Monte FH, Manzano-Nieves G, Quiñones-Laracuente K, Ramos-Medina L, Quirk GJ (2015a) Revisiting the role of infralimbic cortex in fear extinction with optogenetics. J Neurosci 35:3607–3615.

Do-Monte FH, Quinõnes-Laracuente K, Quirk GJ (2015b) A temporal shift in the circuits mediating retrieval of fear memory. Nature 519:460–463.

Dong HW, Swanson LW (2006) Projections from bed nuclei of the stria terminalis, anteromedial area: Cerebral hemisphere integration of neuroendocrine, autonomic, and behavioral aspects of energy balance. J Comp Neurol 494:142–178.

Duvarci S, Pare D (2014) Amygdala microcircuits controlling learned fear. Neuron 82:966–980 Available at: http://dx.doi.org/10.1016/j.neuron.2014.04.042.

Eaton WW, Martins SS, Nestadt G, Bienvenu OJ, Clarke D, Alexandre P (2008) The burden of mental disorders. Epidemiol Rev 30:1–14.

Edeline JM, Pham P, Weinberger NM (1993) Rapid Development of Learning-Induced Receptive Field Plasticity in the Auditory Cortex. Behav Neurosci 107:539–551.

Edeline JM, Weinberger NM (1992) Associative Retuning in the Thalamic Source of Input to the Amygdala and Auditory Cortex: Receptive Field Plasticity in the Medial Division of the Medial Geniculate Body. Behav Neurosci 106:81–105.

Fadok JP, Krabbe S, Markovic M, Courtin J, Xu C, Massi L, Botta P, Bylund K, Müller C, Kovacevic A, Tovote P, Lüthi A (2017) A competitive inhibitory circuit for selection of active and passive fear responses. Nature 542:96–99.

Falls WA, Miserendino MJD, Davis M (1992) Extinction of fear-potentiated startle: Blockade by infusion of an NMDA antagonist into the amygdala. J Neurosci 12:854–863.

Fanselow MS, Lester LS (1988) A functional behavioristic approach to aversively motivated behavior: Predatory imminence as a determinant of the topography of defensive behavior. In: Evolution and Learning, pp 185–212 Available at: https://psycnet.apa.org/record/1987-98812-010 [Accessed April 28, 2020].

Fanselow MS, Poulos AM (2005) The Neuroscience of Mammalian Associative Learning. Annu Rev Psychol 56:207–234.

Farris SG, McLean CP, Van Meter PE, Simpson HB, Foa EB (2013) Treatment response, symptom remission, and wellness in obsessive-compulsive disorder. J Clin Psychiatry 74:685–690.

Fendt M, Fanselow MS (1999) The neuroanatomical and neurochemical basis of conditioned fear. Neurosci Biobehav Rev 23:743–760 Available at: www.elsevier.com/locate/neubiorev [Accessed June 24, 2020].

Feng P, Feng T, Chen Z, Lei X (2014) Memory consolidation of fear conditioning: Bi-stable amygdala connectivity with dorsal anterior cingulate and medial prefrontal cortex. Soc Cogn Affect Neurosci 9:1730–1737.

Ferreira-Netto C, Borelli KG, Brandão ML (2007) Distinct Fos expression in the brain following freezing behavior elicited by stimulation with NMDA of the ventral or dorsal inferior colliculus. Exp Neurol 204:693–704 Available at: http://www.ncbi.nlm.nih.gov/pubmed/17289027 [Accessed February 17, 2020].

Ferreira GM, Albertella L, Moreira-de-Oliveira ME, Piquet-Pessôa M, Yücel M, Lee RSC, Batista KB, de Menezes GB, Fontenelle LF (2020) Fear driven compulsive behaviour is associated with worse long-term outcome in obsessive–compulsive disorder. Hum Psychopharmacol 35.

Fiddick L (2011) There is more than the amygdala: Potential threat assessment in the cingulate cortex. Neurosci Biobehav Rev 35:1007–1018 Available at: http://dx.doi.org/10.1016/j.neubiorev.2010.09.014.

Fitzgerald KD, Stern ER, Angstadt M, Nicholson-Muth KC, Maynor MR, Welsh RC, Hanna GL, Taylor SF (2010) Altered function and connectivity of the medial frontal cortex in pediatric obsessive-compulsive disorder. Biol Psychiatry 68:1039–1047 Available at: http://www.ncbi.nlm.nih.gov/pubmed/20947065 [Accessed February 21, 2020].

Fitzgerald PJ, Whittle N, Flynn SM, Graybeal C, Pinard CR, Gunduz-Cinar O, Kravitz A V, Singewald N, Holmes A (2014) Prefrontal single-unit firing associated with deficient extinction in mice. Neurobiol Learn Mem 113:69–81 Available at: http://www.ncbi.nlm.nih.gov/pubmed/24231425 [Accessed February 26, 2020].

Floyd NS, Price JL, Ferry AT, Keay KA, Bandler R (2000) Orbitomedial prefrontal cortical projections to distinct longitudinal columns of the periaqueductal gray in the rat. J Comp Neurol 422:556–578.

Fridgeirsson EA, Figee M, Luigjes J, Van Den Munckhof P, Schuurman PR, Van Wingen G, Denys D (2020) Deep brain stimulation modulates directional limbic connectivity in obsessive-compulsive disorder. Brain Available at: https://academic.oup.com/brain/advance-article-abstract/doi/10.1093/brain/awaa100/5826158 [Accessed May 3, 2020].

Friedman AL, Burgess A, Ramaseshan K, Easter P, Khatib D, Chowdury A, Arnold PD, Hanna GL, Rosenberg DR, Diwadkar VA (2017) Brain network dysfunction in youth with obsessive-compulsive disorder induced by simple uni-manual behavior: The role of the dorsal anterior cingulate cortex. Psychiatry Res - Neuroimaging 260:6–15 Available at: http://www.ncbi.nlm.nih.gov/pubmed/27992792 [Accessed February 21, 2020].

Fullana MA, Cardoner N, Alonso P, Subirà M, López-Solà C, Pujol J, Segalàs C, Real E, Bossa M, Zacur E, Martínez-Zalacaín I, Bulbena A, Menchón JM, Olmos S, Soriano-Mas C (2014) Brain regions related to fear extinction in obsessive-compulsive disorder and its relation to exposure therapy outcome: A morphometric study. Psychol Med 44:845–856.

Fullana MA, Zhu X, Alonso P, Cardoner N, Real E, López-Solà C, Segalàs C, Subirà M, Galfalvy H, Menchón JM, Simpson HB, Marsh R, Soriano-Mas C (2017) Basolateral amygdala-ventromedial prefrontal cortex connectivity predicts cognitive behavioural therapy outcome in adults with obsessive-compulsive disorder. J Psychiatry Neurosci 42:378–385.

Gafford GM, Ressler KJ (2016) Mouse models of fear-related disorders: Cell-type-specific manipulations in amygdala. Neuroscience 321:108–120 Available at: http://dx.doi.org/10.1016/j.neuroscience.2015.06.019.

Gehring WJ, Himle J, Nisenson LG (2000) Action-Monitoring Dysfunction in Obsessive-Compulsive Disorder.

Geller DA, McGuire JF, Orr SP, Pine DS, Britton JC, Small BJ, Murphy TK, Wilhelm S, Storch EA (2017) Fear conditioning and extinction in pediatric obsessive-compulsive disorder. Ann Clin Psychiatry 29:17–26.

Geller DA, McGuire JF, Orr SP, Small BJ, Murphy TK, Trainor K, Porth R, Wilhelm S, Storch EA (2019) Fear extinction learning as a predictor of response to cognitive behavioral therapy for pediatric obsessive compulsive disorder. J Anxiety Disord 64:1–8 Available at: http://www.ncbi.nlm.nih.gov/pubmed/30852257 [Accessed February 21, 2020].

Ghosh S, Chattarji S (2015) Neuronal encoding of the switch from specific to generalized fear. Nat Neurosci 18:112–120.

Gilbert KE, Barclay ME, Tillman R, Barch DM, Luby JL (2018) Associations of observed performance monitoring during preschool with obsessive-compulsive disorder and anterior cingulate cortex volume over 12 years. JAMA Psychiatry 75:940–948 Available at: http://www.ncbi.nlm.nih.gov/pubmed/30027206 [Accessed February 21, 2020].

Gilmartin MR, Helmstetter FJ (2010) Trace and contextual fear conditioning require neural activity and NMDA receptor-dependent transmission in the medial prefrontal cortex. Learn Mem 17:289–296.

Gilmartin MR, Kwapis JL, Helmstetter FJ (2013a) NR2A- and NR2B-containing NMDA receptors in the prelimbic medial prefrontal cortex differentially mediate trace, delay, and contextual fear conditioning. Learn Mem 20:290–294.

Gilmartin MR, McEchron MD (2005) Single neurons in the medial prefrontal cortex of the rat exhibit tonic and phasic coding during trace fear conditioning. Behav Neurosci 119:1496–1510.

Gilmartin MR, Miyawaki H, Helmstetter FJ, Diba K (2013b) Prefrontal activity links nonoverlapping events in memory. J Neurosci 33:10910–10914.

Giménez M, Cano M, Martínez-Zalacaín I, Real E, Alonso P, Segalàs C, Munuera J, Kegeles LS, Weinstein JJ, Xu X, Menchón JM, Cardoner N, Soriano-Mas C, Fullana MA (2019) Is glutamate associated with fear extinction and cognitive behavior therapy outcome in OCD? A pilot study. Eur Arch Psychiatry Clin Neurosci Available at: http://www.ncbi.nlm.nih.gov/pubmed/31432262 [Accessed February 21, 2020].

Giustino TF, Fitzgerald PJ, Maren S (2016) Fear expression suppresses medial prefrontal cortical firing in rats. PLoS One 11:1–13.

Giustino TF, Maren S (2015) The role of the medial prefrontal cortex in the conditioning and extinction of fear. Front Behav Neurosci 9:1–20.

Glorie D, Verhaeghe J, Miranda A, Kertesz I, Wyffels L, Stroobants S, Staelens S (2020) Progression of obsessive compulsive disorder-like grooming in Sapap3 knockout mice: A longitudinal [11C]ABP688 PET study. Neuropharmacology:108160.

Goosens KA, Hobin JA, Maren S (2003) Auditory-Evoked Spike Firing in the Lateral Amygdala and Pavlovian Fear Conditioning: Mnemonic Code or Fear Bias? Neuron 40:1013–1022.

Goosens KA, Maren S (2001) Contextual and auditory fear conditioning are mediated by the lateral, basal, and central amygdaloid nuclei in rats. Learn Mem 8:148–155 Available at: http://www.ncbi.nlm.nih.gov/pubmed/11390634 [Accessed February 26, 2020].

Goosens KA, Maren S (2003) Pretraining NMDA receptor blockade in the basolateral complex, but not the central nucleus, of the amygdala prevents savings of conditional fear. Behav Neurosci 117:738–750.

Greiner EM, Müller I, Norris MR, Ng KH, Sangha S (2019) Sex differences in fear regulation and reward-seeking behaviors in a fear-safety-reward discrimination task. Behav Brain Res 368:111903 Available at: http://www.ncbi.nlm.nih.gov/pubmed/30981735 [Accessed March 12, 2020].

Grosso A, Cambiaghi M, Milano L, Renna A, Sacco T, Sacchetti B (2017) Region- and Layer-Specific Activation of the Higher Order Auditory Cortex Te2 after Remote Retrieval of Fear or Appetitive Memories. Cereb Cortex 27:3140–3151 Available at: https://academic.oup.com/cercor/article-abstract/27/6/3140/3056420 [Accessed May 26, 2020].

Gruene TM, Flick K, Stefano A, Shea SD, Shansky RM (2015) Sexually divergent expression of active and passive conditioned fear responses in rats. Elife 4.

Gürsel DA, Avram M, Sorg C, Brandl F, Koch K (2018) Frontoparietal areas link impairments of large-scale intrinsic brain networks with aberrant fronto-striatal interactions in OCD: a meta-analysis of resting-state functional connectivity. Neurosci Biobehav Rev 87:151–160.

Hadjas LC, Schartner MM, Cand J, Meaghan C, Pascoli V, Lüscher C, Simmler LD (2020) Projection-specific deficits in synaptic transmission in adult Sapap3-knockout mice. Neuropsychopharmacology Available at:

https://www.nature.com/authors/policies/license.html#AAMtermsV1 [Accessed June 26, 2020].

Halladay LR, Blair HT (2015) Distinct ensembles of medial prefrontal cortex neurons are activated by threatening stimuli that elicit excitation vs. inhibition of movement. J Neurophysiol 114:793–807 Available at: http://www.ncbi.nlm.nih.gov/pubmed/25972588 [Accessed February 12, 2020].

Halpern ME, Güntürkün O, Hopkins WD, Rogers LJ (2005) Lateralization of the vertebrate brain: Taking the side of model systems. In: Journal of Neuroscience, pp 10351–10357. Society for Neuroscience. Available at: https://www.jneurosci.org/content/25/45/10351 [Accessed June 24, 2020].

Han JH, Yiu AP, Cole CJ, Hsiang HL, Neve RL, Josselyn SA (2008) Increasing CREB in the auditory thalamus enhances memory and generalization of auditory conditioned fear. Learn Mem 15:443–453.

Hartley CA, Fischl B, Phelps EA (2011) Brain structure correlates of individual differences in the acquisition and inhibition of conditioned fear. Cereb Cortex 21:1954–1962.

Hashimoto T, Shimizu E, Koike K, Orita Y, Suzuki T, Kanahara N, Matsuzawa D, Fukami G, Miyatake R, Shinoda N, Fujisaki M, Shirayama Y, Hashimoto K, Iyo M (2008) Deficits in auditory P50 inhibition in obsessive-compulsive disorder. Prog Neuro-Psychopharmacology Biol Psychiatry 32:288–296 Available at: www.elsevier.com/locate/pnpbp [Accessed May 14, 2020].

Haufler D, Nagy FZ, Pare D (2013) Neuronal correlates of fear conditioning in the bed nucleus of the stria terminalis. Learn Mem 20:633–641.

Hazen EP, Reichert EL, Piacentini JC, Miguel EC, Do Rosario MC, Pauls D, Geller DA (2008) Case series: Sensory intolerance as a primary symptom of pediatric OCD. Ann Clin Psychiatry 20:199–203.

Hefner K, Whittle N, Juhasz J, Norcross M, Karlsson RM, Saksida LM, Bussey TJ, Singewald N, Holmes A (2008) Impaired fear extinction learning and cortico-amygdala circuit abnormalities in a common genetic mouse strain. J Neurosci 28:8074–8085.

Herry C, Ciocchi S, Senn V, Demmou L, Müller C, Lüthi A (2008) Switching on and off fear by distinct neuronal circuits. Nature 454:600–606.

Herry C, Johansen JP (2014) Encoding of fear learning and memory in distributed neuronal circuits. Nat Neurosci 17:1644–1654 Available at: http://www.ncbi.nlm.nih.gov/pubmed/25413091 [Accessed February 11, 2020].

Herry C, Mons N (2004) Resistance to extinction is associated with impaired immediate early gene induction in medial prefrontal cortex and amygdala. Eur J Neurosci 20:781–790.

Herry C, Trifilieff P, Micheau J, Lüthi A, Mons N (2006) Extinction of auditory fear conditioning

requires MAPK/ERK activation in the basolateral amygdala. Eur J Neurosci 24:261–269.

Hezel DM, Simpson HB (2019) Exposure and response prevention for obsessive-compulsive disorder: A review and new directions. Indian J Psychiatry 61:S85–S92.

Hitchcock J, Davis M (1986) Lesions of the Amygdala, but Not of the Cerebellum or Red Nucleus, Block Conditioned Fear as Measured With the Potentiated Startle Paradigm. Behav Neurosci 100:11–22.

Hitchcock JM, Sananes CB, Davis M (1989) Sensitization of the Startle Reflex by Footshock: Blockade by Lesions of the Central Nucleus of the Amygdala or Its Efferent Pathway to the Brainstem. Behav Neurosci 103:509–518.

Hoenig K, Hochrein A, Quednow BB, Maier W, Wagner M (2005) Impaired prepulse inhibition of acoustic startle in obsessive-compulsive disorder. Biol Psychiatry 57:1153–1158 Available at: www.elsevier.com/locate/biopsych [Accessed May 14, 2020].

Hübner C, Bosch D, Gall A, Lüthi A, Ehrlich I (2014) Ex vivo dissection of optogenetically activated mPFC and hippocampal inputs to neurons in the basolateral amygdala: Implications for fear and emotional memory. Front Behav Neurosci 8.

Huey ED, Zahn R, Krueger F, Moll J, Kapogiannis D, Wassermann EM, Grafman J (2008) A psychological and neuroanatomical model of obsessive-compulsive disorder. J Neuropsychiatry Clin Neurosci 20:390–408 Available at: http://psychiatryonline.org/doi/abs/10.1176/jnp.2008.20.4.390 [Accessed May 24, 2020].

Ide Y, Takahashi M, Lauwereyns J, Sandner G, Tsukada M, Aihara T (2013) Fear conditioning induces guinea pig auditory cortex activation by foot shock alone. Cogn Neurodyn 7:67–77.

IOCDF-GC, OCGAS (2018) Revealing the complex genetic architecture of obsessive-compulsive disorder using meta-analysis. Mol Psychiatry 23:1181–1188.

Izquierdo I, Furini CRG, Myskiw JC (2016) Fear memory. Physiol Rev 96:695–750 Available at: http://www.ncbi.nlm.nih.gov/pubmed/26983799 [Accessed February 11, 2020].

Jacques A, Chaaya N, Hettiarachchi C, Carmody ML, Beecher K, Belmer A, Chehrehasa F, Bartlett S, Battle AR, Johnson LR (2019) Microtopography of fear memory consolidation and extinction retrieval within prefrontal cortex and amygdala. Psychopharmacology (Berl) 236:383–397.

Jiao Y, Sun Z, Lee T, Fusco FR, Kimble TD, Meade CA, Cuthbertson S, Reiner A (1999) A simple and sensitive antigen retrieval method for free-floating and slide-mounted tissue sections. J Neurosci Methods 93:149–162.

Jo YS, Heymann G, Zweifel LS (2018) Dopamine Neurons Reflect the Uncertainty in Fear Generalization. Neuron 100:916-925.e3 Available at: http://www.ncbi.nlm.nih.gov/pubmed/30318411 [Accessed February 21, 2020].

Johansen JP, Tarpley JW, Ledoux JE, Blair HT (2010) Neural substrates for expectation-modulated fear learning in the amygdala and periaqueductal gray. Nat Neurosci 13:979–986.

Jones CE, Monfils MH (2016) Fight, Flight, or Freeze? The Answer May Depend on Your Sex. Trends Neurosci 39:51–53 Available at: http://www.ncbi.nlm.nih.gov/pubmed/26776563 [Accessed March 4, 2020].

Jones GL, Soden ME, Knakal CR, Lee H, Chung AS, Merriam EB, Zweifel LS (2015) A genetic link between discriminative fear coding by the lateral amygdala, dopamine, and fear generalization. Elife 4.

Kaczkurkin AN, Lissek S (2013) Generalization of Conditioned Fear and Obsessive-Compulsive Traits. J Psychol Psychother 7:3 Available at: http://www.ncbi.nlm.nih.gov/pubmed/24567864 [Accessed April 22, 2020].

Kalisch R, Korenfeld E, Stephan KE, Weiskopf N, Seymour B, Dolan RJ (2006) Context-dependent human extinction memory is mediated by a ventromedial prefrontal and hippocampal network. J Neurosci 26:9503–9511.

Kessler RC, Berglund P, Demler O, Jin R, Merikangas KR, Walters EE (2005) Lifetime prevalence and age-of-onset distributions of DSM-IV disorders in the national comorbidity survey replication. Arch Gen Psychiatry 62:593–602.

Kessler RC, Petukhova M, Sampson NA, Zaslavsky AM, Wittchen HU (2012) Twelve-month and lifetime prevalence and lifetime morbid risk of anxiety and mood disorders in the United States. Int J Methods Psychiatr Res 21:169–184 Available at: http://doi.wiley.com/10.1002/mpr.1359 [Accessed May 18, 2020].

Kim EJ, Horovitz O, Pellman BA, Tan LM, Li Q, Richter-Levin G, Kim JJ (2013) Dorsal periaqueductal gray-amygdala pathway conveys both innate and learned fear responses in rats. Proc Natl Acad Sci U S A 110:14795–14800.

Kim HS, Cho HY, Augustine GJ, Han JH (2016) Selective Control of Fear Expression by Optogenetic Manipulation of Infralimbic Cortex after Extinction. Neuropsychopharmacology 41:1261–1273.

Kim J, Lee S, Park H, Song B, Hong I, Geum D, Shin K, Choi S (2007) Blockade of amygdala metabotropic glutamate receptor subtype 1 impairs fear extinction. Biochem Biophys Res Commun 355:188–193.

Kim JJ, Rison RA, Fanselow MS (1993) Effects of amygdala, hippocampus, and periaqueductal gray lesions on short- and long-term contextual fear. Behav Neurosci 107:1093–1098.

Kim M, Davis M (1993) Lack of a temporal gradient of retrograde amnesia in rats with amygdala lesions assessed with the fear-potentiated startle paradigm. Behav Neurosci 107:1088–1092.

Kim SC, Jo YS, Kim IH, Kim H, Choi JS (2010) Lack of medial prefrontal cortex activation underlies the immediate extinction deficit. J Neurosci 30:832–837.

Kincheski GC, Mota-Ortiz SR, Pavesi E, Canteras NS, Carobrez AP (2012) The Dorsolateral Periaqueductal Gray and Its Role in Mediating Fear Learning to Life Threatening Events. PLoS One 7.

Kindler S, Rehbein M, Classen B, Richter D, Böckers TM (2004) Distinct spatiotemporal expression of SAPAP transcripts in the developing rat brain: A novel dendritically localized mRNA. Mol Brain Res 126:14–21 Available at: www.elsevier.com/locate/molbrainres [Accessed April 24, 2020].

Kirry AJ, Durigan DJ, Twining RC, Gilmartin MR (2019) Estrous cycle stage gates sex differences in prefrontal muscarinic control of fear memory formation. Neurobiol Learn Mem 161:26–36 Available at: https://doi.org/10.1016/j.nlm.2019.03.001.

Knapska E, Macias M, Mikosz M, Nowak A, Owczarek D, Wawrzyniak M, Pieprzyk M, Cymerman IA, Werka T, Sheng M, Maren S, Jaworski J, Kaczmarek L (2012) Functional anatomy of neural circuits regulating fear and extinction. Proc Natl Acad Sci U S A 109:17093–17098 Available at: http://www.ncbi.nlm.nih.gov/pubmed/23027931 [Accessed February 11, 2020].

Knapska E, Maren S (2009) Reciprocal patterns of c-Fos expression in the medial prefrontal cortex and amygdala after extinction and renewal of conditioned fear. Learn Mem 16:486–493 Available at: http://www.ncbi.nlm.nih.gov/pubmed/19633138 [Accessed February 11, 2020].

Knight DC, Cheng DT, Smith CN, Stein EA, Helmstetter FJ (2004) Neural Substrates Mediating Human Delay and Trace Fear Conditioning. J Neurosci 24:218–228.

Knight DC, Nguyen HT, Bandettini PA (2005) The role of the human amygdala in the production of conditioned fear responses. Neuroimage 26:1193–1200.

Koch K, Reeß TJ, Rus OG, Gürsel DA, Wagner G, Berberich G, Zimmer C (2018) Increased default mode network connectivity in obsessive-compulsive disorder during reward processing. Front Psychiatry 9.

Koch K, Wagner G, Schachtzabel C, Peikert G, Schultz CC, Sauer H, Schlösser RG (2012) Aberrant anterior cingulate activation in obsessive-compulsive disorder is related to task complexity. Neuropsychologia 50:958–964.

Kühn S, Kaufmann C, Simon D, Endrass T, Gallinat J, Kathmann N (2013) Reduced thickness of anterior cingulate cortex in obsessive-compulsive disorder. Cortex 49:2178–2185 Available at: http://www.ncbi.nlm.nih.gov/pubmed/23067727 [Accessed February 21, 2020].

Kwon JT, Jhang J, Kim HS, Lee S, Han JH (2012) Brain region-specific activity patterns after recent or remote memory retrieval of auditory conditioned fear. Learn Mem 19:487–494.

Kwon JT, Nakajima R, Kim HS, Jeong Y, Augustine GJ, Han JH (2014) Optogenetic activation of presynaptic inputs in lateral amygdala forms associative fear memory. Learn Mem 21:627–633.

LaBar KS, Gatenby JC, Gore JC, LeDoux JE, Phelps EA (1998) Human amygdala activation during conditioned fear acquisition and extinction: A mixed-trial fMRI study. Neuron 20:937–945.

LaBar KS, LeDoux JE, Spencer DD, Phelps EA (1995) Impaired fear conditioning following unilateral temporal lobectomy in humans. J Neurosci 15:6846–6855.

Lai CSW, Adler A, Gan WB (2018) Fear extinction reverses dendritic spine formation induced by fear conditioning in the mouse auditory cortex. Proc Natl Acad Sci U S A 115:9306–9311.

Lange MD, Jüngling K, Paulukat L, Vieler M, Gaburro S, Sosulina L, Blaesse P, Sreepathi HK, Ferraguti F, Pape HC (2014) Glutamic acid decarboxylase 65: A link between GABAergic synaptic plasticity in the lateral amygdala and conditioned fear generalization. Neuropsychopharmacology 39:2211–2220 Available at: http://www.ncbi.nlm.nih.gov/pubmed/24663011 [Accessed February 21, 2020].

Laviolette SR, Lipski WJ, Grace AA (2005) A subpopulation of neurons in the medial prefrontal cortex encodes emotional learning with burst and frequency codes through a dopamine D 4 receptor-dependent basolateral amygdala input. J Neurosci 25:6066–6075 Available at: http://www.ncbi.nlm.nih.gov/pubmed/15987936 [Accessed February 13, 2020].

Law C, Boisseau CL (2019) Exposure and response prevention in the treatment of obsessive-compulsive disorder: Current perspectives. Psychol Res Behav Manag 12:1167–1174 Available at: http://doi.org/10.2147/PRBM.S211117 [Accessed May 18, 2020].

Lázaro-Muñoz G, LeDoux JE, Cain CK (2010) Sidman Instrumental Avoidance Initially Depends on Lateral and Basal Amygdala and Is Constrained by Central Amygdala-Mediated Pavlovian Processes. Biol Psychiatry 67:1120–1127 Available at: www.sobp.org/journal [Accessed April 29, 2020].

Lebow MA, Chen A (2016) Overshadowed by the amygdala: The bed nucleus of the stria terminalis emerges as key to psychiatric disorders. Mol Psychiatry 21:450–463 Available at: http://dx.doi.org/10.1038/mp.2016.1.

LeDoux JE, Cicchetti P, Xagoraris A, Romanski LM (1990) The lateral amygdaloid nucleus: Sensory interface of the amygdala in fear conditioning. J Neurosci 10:1062–1069.

LeDoux JE, Farb CR, Romanski LM (1991) Overlapping projections to the amygdala and striatum from auditory processing areas of the thalamus and cortex. Neurosci Lett 134:139–144.

LeDoux JE, Iwata J, Cicchetti P, Reis DJ (1988) Different projections of the central amygdaloid nucleus mediate autonomic and behavioral correlates of conditioned fear. J Neurosci 8:2517–2529.

LeDoux JE, Ruggiero DA, Reis DJ (1985) Projections to the subcortical forebrain from anatomically defined regions of the medial geniculate body in the rat. J Comp Neurol 242:182–213.

Lee YK, Choi J-S (2012) Inactivation of the Medial Prefrontal Cortex Interferes with the Expression But Not the Acquisition of Diff erential Fear Conditioning in Rats. Exp Neurobiol 21:23–29.

Leon MI, Miasnikov AA, Wright EJ, Weinberger NM (2017) CS-specific modifications of auditory evoked potentials in the behaviorally conditioned rat. Brain Res 1670:235–247.

Letzkus JJ, Wolff SBE, Meyer EMM, Tovote P, Courtin J, Herry C, Lüthi A (2011) A disinhibitory microcircuit for associative fear learning in the auditory cortex. Nature 480:331–335.

Li X, Marshall PR, Leighton LJ, Zajaczkowski EL, Wang Z, Madugalle SU, Yin J, Bredy TW, Wei W (2019) The DNA repair-associated protein gadd45γ regulates the temporal coding of immediate early gene expression within the prelimbic prefrontal cortex and is required for the consolidation of associative fear memory. J Neurosci 39:970–983.

Likhtik E, Paz R (2015) Amygdala-prefrontal interactions in (mal)adaptive learning. Trends Neurosci 38:158–166 Available at: http://www.ncbi.nlm.nih.gov/pubmed/25583269 [Accessed February 17, 2020].

Likhtik E, Stujenske JM, Topiwala MA, Harris AZ, Gordon JA (2014) Prefrontal entrainment of amygdala activity signals safety in learned fear and innate anxiety. Nat Neurosci 17:106–113.

Lin CH, Yeh SH, Lu HY, Gean PW (2003) The similarities and diversities of signal pathways leading to consolidation of conditioning and consolidation of extinction of fear memory. J Neurosci 23:8310–8317.

Linnman C, Zeidan MA, Pitman RK, Milad MR (2012) Resting cerebral metabolism correlates with skin conductance and functional brain activation during fear conditioning. Biol Psychol 89:450–459.

Lovelace JW, Vieira PA, Corches A, Mackie K, Korzus E (2014) Impaired fear memory specificity associated with deficient endocannabinoid-dependent long-term plasticity. Neuropsychopharmacology 39:1685–1693.

Lowery-Gionta EG, DiBerto J, Mazzone CM, Kash TL (2018) GABA neurons of the ventral periaqueductal gray area modulate behaviors associated with anxiety and conditioned fear. Brain Struct Funct 223:3787–3799 Available at: http://www.ncbi.nlm.nih.gov/pubmed/30076467 [Accessed February 21, 2020].

Lu KT, Walker DL, Davis M (2001) Mitogen-activated protein kinase cascade in the basolateral nucleus of amygdala is involved in extinction of fear-potentiated startle. J Neurosci 21 Available at: www.jneurosci.org.http://www.jneurosci.org/cgi/content/full/5555 [Accessed May 21, 2020].

Lucas EK, Jegarl AM, Morishita H, Clem RL (2016) Multimodal and Site-Specific Plasticity of Amygdala Parvalbumin Interneurons after Fear Learning. Neuron 91:629–643 Available at: http://www.ncbi.nlm.nih.gov/pubmed/27427462 [Accessed February 11, 2020].

Maho C, Hars B, Edeline JM, Hennevin E (1995) Conditioned changes in the basal forebrain: Relations with learning-induced cortical plasticity. Psychobiology 23:10–25.

Manning EE, Dombrovski AY, Torregrossa MM, Ahmari SE (2019a) Impaired instrumental reversal learning is associated with increased medial prefrontal cortex activity in Sapap3 knockout mouse model of compulsive behavior. Neuropsychopharmacology 44:1494–1504 Available at: http://www.ncbi.nlm.nih.gov/pubmed/30587851 [Accessed February 21, 2020].

Manning EE, Wang AY, Saikali LM, Winner A, Ahmari SE (2019b) Disruption of prepulse inhibition is associated with severity of compulsive behavior and nucleus accumbens dopamine system changes in Sapap3 knockout mice. bioRxiv:694935 Available at: https://www.biorxiv.org/content/10.1101/694935v1 [Accessed June 24, 2020].

Marcus DJ, Bedse G, Gaulden A, Ryan JD, Clauss J, Delpire E, Lee FS, Blackford J, Patel S (2019) Endocannabinoid Signaling Collapse Mediates Stress-Induced Amygdalo-Cortical Strengthening. SSRN Electron J 105:1–15 Available at: http://www.ncbi.nlm.nih.gov/pubmed/31948734 [Accessed February 11, 2020].

Marek R, Strobel C, Bredy TW, Sah P (2013) The amygdala and medial prefrontal cortex: Partners in the fear circuit. J Physiol 591:2381–2391 Available at: http://www.ncbi.nlm.nih.gov/pubmed/23420655 [Accessed February 11, 2020].

Marek R, Xu L, Sullivan RKP, Sah P (2018) Excitatory connections between the prelimbic and infralimbic medial prefrontal cortex show a role for the prelimbic cortex in fear extinction. Nat Neurosci 21:654–658.

Maren S (1999) Neurotoxic basolateral amygdala lesions impair learning and memory but not the performance of conditional fear in rats. J Neurosci 19:8696–8703 Available at: http://www.ncbi.nlm.nih.gov/pubmed/10493770 [Accessed February 26, 2020].

Maren S (2000) Auditory fear conditioning increases CS-elicited spike firing in lateral amygdala neurons even after extensive overtraining. Eur J Neurosci 12:4047–4054.

Maren S (2001) Neurobiology of Pavlovian Fear Conditioning. Annu Rev Neurosci 24:897–931.

Martínez-Rivera FJ, Bravo-Rivera C, Velázquez-Díaz CD, Montesinos-Cartagena M, Quirk GJ (2019) Prefrontal circuits signaling active avoidance retrieval and extinction. Psychopharmacology (Berl) 236:399–406 Available at: http://www.ncbi.nlm.nih.gov/pubmed/30259076 [Accessed February 21, 2020].

Martinez RCR, Gupta N, Lazaro-Munoz G, Sears RM, Kim S, Moscarello JM, LeDoux JE, Cain CK (2013) Active vs. reactive threat responding is associated with differential c-Fos expression in specific regions of amygdala and prefrontal cortex. Learn Mem 20:446–452 Available at: http://www.ncbi.nlm.nih.gov/pubmed/23869027 [Accessed February 21, 2020].

Mataix-Cols D, Wooderson S, Lawrence N, Brammer MJ, Speckens A, Phillips ML (2004) Distinct neural correlates of washing, checking, and hoarding symptom dimensions in obsessive-compulsive disorder. Arch Gen Psychiatry 61:564–576.

Matsumoto R, Ito H, Takahashi H, Ando T, Fujimura Y, Nakayama K, Okubo Y, Obata T, Fukui K, Suhara T (2010) Reduced gray matter volume of dorsal cingulate cortex in patients with obsessive-compulsive disorder: A voxel-based morphometric study. Psychiatry Clin Neurosci 64:541–547.

Mattheisen M et al. (2015) Genome-wide association study in obsessive-compulsive disorder: Results from the OCGAS. Mol Psychiatry 20:337–344.

McDonald AJ, Shammah-Lagnado SJ, Shi C, Davis M (1999) Cortical afferents to the extended amygdala. In: Annals of the New York Academy of Sciences, pp 309–338.

McEchron MD, Green EJ, Winters RW, Nolen TG, Schneiderman N, McCabe PM (1996) Changes of synaptic efficacy in the medial geniculate nucleus as a result of auditory classical conditioning. J Neurosci 16:1273–1283.

McEchron MD, McCabe PM, Green EJ, Llabre MM, Schneiderman N (1995) Simultaneous single unit recording in the medial nucleus of the medial geniculate nucleus and amygdaloid central nucleus throughout habituation, acquisition, and extinction of the rabbit's classically conditioned heart rate. Brain Res 682:157–166.

McGovern RA, Sheth SA (2017) Role of the dorsal anterior cingulate cortex in obsessive-compulsive disorder: Converging evidence from cognitive neuroscience and psychiatric neurosurgery. J Neurosurg 126:132–147 Available at: http://www.ncbi.nlm.nih.gov/pubmed/27035167 [Accessed February 21, 2020].

McGuire JF, Orr SP, Wu MS, Lewin AB, Small BJ, Phares V, Murphy TK, Wilhelm S, Pine DS, Geller D, Storch EA (2016) FEAR CONDITIONING and EXTINCTION in YOUTH with OBSESSIVE-COMPULSIVE DISORDER. Depress Anxiety 33:229–237.

McKernan MG, Shinnick-Gallagher P (1997) Fear conditioning induces a lasting potentiation of synaptic currents in vitro. Nature 390:607–611.

McLaughlin NCR, Strong D, Abrantes A, Garnaat S, Cerny A, O'Connell C, Fadok R, Spofford C, Rasmussen SA, Milad MR, Greenberg BD (2015) Extinction retention and fear renewal in a lifetime obsessive-compulsive disorder sample. Behav Brain Res 280:72–77 Available at: http://dx.doi.org/10.1016/j.bbr.2014.11.011.

Milad MR, Furtak SC, Greenberg JL, Keshaviah A, Im JJ, Falkenstein MJ, Jenike M, Rauch SL, Wilhelm S (2013) Deficits in conditioned fear extinction in obsessive-compulsive disorder and neurobiological changes in the fear circuit. JAMA Psychiatry 70:608–618.

Milad MR, Quinn BT, Pitman RK, Orr SP, Fischl B, Rauch SL (2005) Thickness of ventromedial prefrontal cortex in humans is correlated with extinction memory. Proc Natl Acad Sci U S A 102:10706–10711.

Milad MR, Quirk GJ (2002) Neurons in medial prefrontal cortex signal memory for fear extinction. Nature 420:70–74.

Milad MR, Quirk GJ (2012) Fear Extinction as a Model for Translational Neuroscience: Ten Years of Progress. Annu Rev Psychol 63:129–151.

Milad MR, Quirk GJ, Pitman RK, Orr SP, Fischl B, Rauch SL (2007a) A Role for the Human Dorsal Anterior Cingulate Cortex in Fear Expression. Biol Psychiatry 62:1191–1194 Available at: www.sobp.org/journal [Accessed April 22, 2020].

Milad MR, Wright CI, Orr SP, Pitman RK, Quirk GJ, Rauch SL (2007b) Recall of Fear Extinction in Humans Activates the Ventromedial Prefrontal Cortex and Hippocampus in Concert. Biol Psychiatry 62:446–454 Available at: http://www.nmr.mgh. [Accessed May 20, 2020].

Mobbs D, Headley DB, Ding W, Dayan P (2020) Space, Time, and Fear: Survival Computations along Defensive Circuits. Trends Cogn Sci Available at: http://www.ncbi.nlm.nih.gov/pubmed/32029360 [Accessed February 11, 2020].

Moczulska KE, Tinter-Thiede J, Peter M, Ushakova L, Wernle T, Bathellier B, Rumpel S (2013) Dynamics of dendritic spines in the mouse auditory cortex during memory formation and memory recall. Proc Natl Acad Sci U S A 110:18315–18320.

Morgan MA, LeDoux JE (1995) Differential contribution of dorsal and ventral medial prefrontal cortex to the acquisition and extinction of conditioned fear in rats. Behav Neurosci 109:681–688.

Morgan MA, Romanski LM, LeDoux JE (1993) Extinction of emotional learning: Contribution of medial prefrontal cortex. Neurosci Lett 163:109–113.

Morrow BA, Elsworth JD, Inglis FM, Roth RH (1999) An antisense oligonucleotide reverses the footshock-induced expression of Fos in the rat medial prefrontal cortex and the subsequent expression of conditioned fear-induced immobility. J Neurosci 19:5666–5673 Available at: http://rsb.info.nih.gov/nih-image [Accessed February 19, 2020].

Muller J, Corodimas KP, Fridel Z, LeDoux JE (1997) Functional inactivation of the lateral and basal nuclei of the amygdala by muscimol infusion prevents fear conditioning to an explicit conditioned stimulus and to contextual stimuli. Behav Neurosci 111:683–682.

Murray C, Lopez A (1996) The global burden of disease.

Naaijen J, Lythgoe DJ, Amiri H, Buitelaar JK, Glennon JC (2015) Fronto-striatal glutamatergic compounds in compulsive and impulsive syndromes: A review of magnetic resonance spectroscopy studies. Neurosci Biobehav Rev 52:74–88 Available at: http://dx.doi.org/10.1016/j.neubiorev.2015.02.009.

Nader K, Majidishad P, Amorapanth P, LeDoux JE (2001) Damage to the lateral and central, but not other, amygdaloid nuclei prevents the acquisition of auditory fear conditioning. Learn Mem 8:156–163.

Nakao T, Nakagawa A, Yoshiura T, Nakatani E, Nabeyama M, Yoshizato C, Kudoh A, Tada K, Yoshioka K, Kawamoto M, Togao O, Kanba S (2005) Brain activation of patients with

obsessive-compulsive disorder during neuropsychological and symptom provocation tasks before and after symptom improvement: A functional magnetic resonance imaging study. Biol Psychiatry 57:901–910 Available at: www.elsevier.com/locate/biopsych [Accessed April 22, 2020].

Nanbu M, Kurayama T, Nakazawa K, Matsuzawa D, Komiya Z, Haraguchi T, Ogura H, Hashimoto T, Yoshida S, Iyo M, Shimizu E (2010) Impaired P50 suppression in fear extinction in obsessive-compulsive disorder. Prog Neuro-Psychopharmacology Biol Psychiatry 34:317–322 Available at: http://dx.doi.org/10.1016/j.pnpbp.2009.12.005.

Norman LJ, Taylor SF, Liu Y, Radua J, Chye Y, De Wit SJ, Huyser C, Karahanoglu FI, Luks T, Manoach D, Mathews C, Rubia K, Suo C, van den Heuvel OA, Yücel M, Fitzgerald K (2019) Error Processing and Inhibitory Control in Obsessive-Compulsive Disorder: A Meta-analysis Using Statistical Parametric Maps. Biol Psychiatry 85:713–725.

Odynocki N, Poulos AM (2019) Delving into darting. Lab Anim (NY) 48:204–205 Available at: http://www.ncbi.nlm.nih.gov/pubmed/31217566 [Accessed March 12, 2020].

Ortiz S, Latsko MS, Fouty JL, Dutta S, Adkins JM, Jasnow AM (2019) Anterior Cingulate Cortex and Ventral Hippocampal Inputs to the Basolateral Amygdala Selectively Control Generalized Fear. J Neurosci 39:6526–6539 Available at: http://www.ncbi.nlm.nih.gov/pubmed/31209172 [Accessed February 21, 2020].

Padilla-Coreano N, Bolkan SS, Pierce GM, Blackman DR, Hardin WD, Garcia-Garcia AL, Spellman TJ, Gordon JA (2016) Direct Ventral Hippocampal-Prefrontal Input Is Required for Anxiety-Related Neural Activity and Behavior. Neuron 89:857–866 Available at: http://www.ncbi.nlm.nih.gov/pubmed/26853301 [Accessed February 21, 2020].

Parsons RG, Riedner BA, Gafford GM, Helmstetter FJ (2006) The formation of auditory fear memory requires the synthesis of protein and mRNA in the auditory thalamus. Neuroscience 141:1163–1170.

Paul S, Beucke JC, Kaufmann C, Mersov A, Heinzel S, Kathmann N, Simon D (2020) Amygdala – prefrontal connectivity during appraisal of symptom-related stimuli in obsessive – compulsive disorder. Psychol Med 29:278–286.

Pauls DL, Abramovitch A, Rauch SL, Geller DA (2014) Obsessive-compulsive disorder: An integrative genetic and neurobiological perspective. Nat Rev Neurosci 15:410–424 Available at: https://www.nature.com/articles/nrn3746 [Accessed June 23, 2020].

Pelrine E, Pasik SD, Bayat L, Goldschmiedt D, Bauer EP (2016) 5-HT2C receptors in the BNST are necessary for the enhancement of fear learning by selective serotonin reuptake inhibitors. Neurobiol Learn Mem 136:189–195.

Pendyam S, Bravo-Rivera C, Burgos-Robles A, Sotres-Bayon F, Quirk GJ, Nair SS (2013) Fear signaling in the prelimbic-amygdala circuit: A computational modeling and recording study. J Neurophysiol 110:844–861.

Penzo MA, Robert V, Li B (2014) Fear conditioning potentiates synaptic transmission onto long-range projection neurons in the lateral subdivision of central amygdala. J Neurosci 34:2432–2437.

Phelps EA, Delgado MR, Nearing KI, Ledoux JE (2004) Extinction learning in humans: Role of the amygdala and vmPFC. Neuron 43:897–905.

Piantadosi SC, Chamberlain BL, Glausier JR, Lewis DA, Ahmari SE (2019) Lower excitatory synaptic gene expression in orbitofrontal cortex and striatum in an initial study of subjects with obsessive compulsive disorder. Mol Psychiatry:1–13 Available at: https://www.nature.com/articles/s41380-019-0431-3 [Accessed June 24, 2020].

Pinto A, Eisen JL, Mancebo MC, Greenberg BD, Stout RL, Rasmussen SA (2007) Taboo thoughts and doubt/checking: A refinement of the factor structure for obsessive-compulsive disorder symptoms. Psychiatry Res 151:255–258 Available at: /pmc/articles/PMC2039929/?report=abstract [Accessed June 23, 2020].

Piras F, Piras F, Chiapponi C, Girardi P, Caltagirone C, Spalletta G (2015) Widespread structural brain changes in OCD: A systematic review of voxel-based morphometry studies. Cortex 62:89–108.

Pittenger C, Bloch MH (2014) Pharmacological treatment of obsessive-compulsive disorder. Psychiatr Clin North Am 37:375–391.

Pittenger C, Bloch MH, Williams K (2011) Glutamate abnormalities in obsessive compulsive disorder: Neurobiology, pathophysiology, and treatment. Pharmacol Ther 132:314–332.

Pittig A, Treanor M, LeBeau RT, Craske MG (2018) The role of associative fear and avoidance learning in anxiety disorders: Gaps and directions for future research. Neurosci Biobehav Rev 88:117–140.

Pollack GA, Bezek JL, Lee SH, Scarlata MJ, Weingast LT, Bergstrom HC (2018) Cued fear memory generalization increases over time. Learn Mem 25:298–308 Available at: http://www.ncbi.nlm.nih.gov/pubmed/29907637 [Accessed February 11, 2020].

Quirk GJ, Armony JL, LeDoux JE (1997) Fear conditioning enhances different temporal components of tone-evoked spike trains in auditory cortex and lateral amygdala. Neuron 19:613–624.

Quirk GJ, Mueller D (2008) Neural mechanisms of extinction learning and retrieval. Neuropsychopharmacology 33:56–72.

Quirk GJ, Repa JC, LeDoux JE (1995) Fear conditioning enhances short-latency auditory responses of lateral amygdala neurons: Parallel recordings in the freely behaving rat. Neuron 15:1029–1039.

Quirk GJ, Russo GK, Barron JL, Lebron K (2000) The role of ventromedial prefrontal cortex in the recovery of extinguished fear. J Neurosci 20:6225–6231.

Raij T, Nummenmaa A, Marin MF, Porter D, Furtak S, Setsompop K, Milad MR (2018) Prefrontal Cortex Stimulation Enhances Fear Extinction Memory in Humans. Biol Psychiatry 84:129–137.

Raines AM, Allan NP, Oglesby ME, Short NA, Schmidt NB (2015) Examination of the relations between obsessive-compulsive symptom dimensions and fear and distress disorder symptoms. J Affect Disord 183:253–257 Available at: http://www.ncbi.nlm.nih.gov/pubmed/26042633 [Accessed February 21, 2020].

Rajbhandari AK, Zhu R, Adling C, Fanselow MS, Waschek JA (2016) Graded fear generalization enhances the level of cfos-positive neurons specifically in the basolateral amygdala. J Neurosci Res 94:1393–1399 Available at: http://www.ncbi.nlm.nih.gov/pubmed/27661774 [Accessed February 21, 2020].

Rauch SL, Jenike MA, Alpert NM, Baer L, Breiter HCR, Savage CR, Fischman AJ (1994) Regional Cerebral Blood Flow Measured during Symptom Provocation in Obsessive-Compulsive Disorder using Oxygen 15—Labeled Carbon Dioxide and Positron Emission Tomography. Arch Gen Psychiatry 51:62–70.

Ravinder S, Burghardt NS, Brodsky R, Bauer EP, Chattarji S (2013) A role for the extended amygdala in the fear-enhancing effects of acute selective serotonin reuptake inhibitor treatment. Transl Psychiatry 3:e209–e209.

Reess TJ, Rus OG, Schmidt R, De Reus MA, Zaudig M, Wagner G, Zimmer C, Van Den Heuvel MP, Koch K (2016) Connectomics-based structural network alterations in obsessive-compulsive disorder. Transl Psychiatry 6:e882-8 Available at: http://dx.doi.org/10.1038/tp.2016.163.

Rizvi TA, Ennis M, Behbehani MM, Shipley MT (1991) Connections between the central nucleus of the amygdala and the midbrain periaqueductal gray: Topography and reciprocity. J Comp Neurol 303:121–131.

Rodgers LJ, Andrew RJ (2002) Comparative vertebrate lateralization. Available at: https://books.google.com/books?hl=en&lr=&id=lbS86Sx9tLMC&oi=fnd&pg=PP1&ots=cjop6GSWM7&sig=1aLFAJ3O021yLr3DpFFmnVqtUM0 [Accessed June 24, 2020].

Romanski LM, Ledoux JE (1993) Information cascade from primary auditory cortex to the amygdala: Corticocortical and corticoamygdaloid projections of temporal cortex in the rat. Cereb Cortex 3:515–532.

Romanski LM, LeDoux JE (1992) Equipotentiality of thalamo-amygdala and thalamo-cortico-amygdala circuits in auditory fear conditioning. J Neurosci 12:4501–4509.

Rosen JB, Donley MP (2006) Animal studies of amygdala function in fear and uncertainty: Relevance to human research. Biol Psychol 73:49–60.

Rosenberg DR, Keshavan MS (1998) Toward a neurodevelopmental model of obsessive-compulsive disorder. Biol Psychiatry 43:623–640.

Rossi S, Bartalini S, Ulivelli M, Mantovani A, Di Muro A, Goracci A, Castrogiovanni P, Battistini N, Passero S (2005) Hypofunctioning of sensory gating mechanisms in patients with obsessive-compulsive disorder. Biol Psychiatry 57:16–20 Available at: www.elsevier.com/locate/biopsych [Accessed May 14, 2020].

Rozenman M, Peris T, Bergman RL, Chang S, O'Neill J, McCracken JT, Piacentini J (2017) Distinguishing Fear Versus Distress Symptomatology in Pediatric OCD. Child Psychiatry Hum Dev 48:63–72 Available at: http://www.ncbi.nlm.nih.gov/pubmed/27225633 [Accessed February 21, 2020].

Rozeske RR, Jercog D, Karalis N, Chaudun F, Khoder S, Girard D, Winke N, Herry C (2018) Prefrontal-Periaqueductal Gray-Projecting Neurons Mediate Context Fear Discrimination. Neuron 97:898-910.e6.

Runyan JD, Moore AN, Dash PK (2004) A Role for Prefrontal Cortex in Memory Storage for Trace Fear Conditioning. J Neurosci 24:1288–1295 Available at: http://www.ncbi.nlm.nih.gov/pubmed/14960599 [Accessed February 26, 2020].

Rus OG, Reess TJ, Wagner G, Zimmer C, Zaudig M, Koch K (2017) Functional and structural connectivity of the amygdala in obsessive-compulsive disorder. NeuroImage Clin 13:246–255 Available at: http://dx.doi.org/10.1016/j.nicl.2016.12.007.

Russo M, Naro A, Mastroeni C, Morgante F, Terranova C, Muscatello MR, Zoccali R, Calabrò RS, Quartarone A (2014) Obsessive-compulsive disorder: A "sensory-motor" problem? Int J Psychophysiol 92:74–78 Available at: http://dx.doi.org/10.1016/j.ijpsycho.2014.02.007 [Accessed May 14, 2020].

Sananes CB, Davis M (1992) N-Methyl-D-Aspartate Lesions of the Lateral and Basolateral Nuclei of the Amygdala Block Fear-Potentiated Startle and Shock Sensitization of Startle. Behav Neurosci 106:72–80.

Santini E, Porter JT (2010) M-type potassium channels modulate the intrinsic excitability of infralimbic neurons and regulate fear expression and extinction. J Neurosci 30:12379–12386.

Santini E, Quirk GJ, Porter JT (2008) Fear conditioning and extinction differentially modify the intrinsic excitability of infralimbic neurons. J Neurosci 28:4028–4036.

Savander V, Go CG, LeDoux JE, Pitkanen A (1996) Intrinsic connections of the rat amygdaloid complex: Projections originating in the accessory basal nucleus. J Comp Neurol 374:291–313.

Saxena S, Brody AL, Schwartz JM, Baxter LR (1998) Neuroimaging and frontal-subcortical circuitry in obsessive-compulsive disorder.

Schlösser RGM, Wagner G, Schachtzabel C, Peikert G, Koch K, Reichenbach JR, Sauer H (2010) Fronto-cingulate effective connectivity in obsessive compulsive disorder: A study with fMRI and dynamic causal modeling. Hum Brain Mapp 31:1834–1850.

Senn V, Wolff SBE, Herry C, Grenier F, Ehrlich I, Gründemann J, Fadok JP, Müller C, Letzkus JJ, Lüthi A (2014) Long-range connectivity defines behavioral specificity of amygdala neurons. Neuron 81:428–437.

Shaban H, Humeau Y, Herry C, Cassasus G, Shigemoto R, Ciocchi S, Barbieri S, Van Der Putten H, Kaupmann K, Bettler B, Lüthi A (2006) Generalization of amygdala LTP and conditioned fear in the absence of presynaptic inhibition. Nat Neurosci 9:1028–1035 Available at: http://www.ncbi.nlm.nih.gov/pubmed/16819521 [Accessed February 21, 2020].

Sierra-Mercado D, Padilla-Coreano N, Quirk GJ (2011) Dissociable roles of prelimbic and infralimbic cortices, ventral hippocampus, and basolateral amygdala in the expression and extinction of conditioned fear. Neuropsychopharmacology 36:529–538 Available at: http://dx.doi.org/10.1038/npp.2010.184.

Simon D, Adler N, Kaufmann C, Kathmann N (2014) Amygdala hyperactivation during symptom provocation in obsessive-compulsive disorder and its modulation by distraction. NeuroImage Clin 4:549–557.

Simon D, Kaufmann C, Müsch K, Kischkel E, Kathmann N (2010) Fronto-striato-limbic hyperactivation in obsessive-compulsive disorder during individually tailored symptom provocation. Psychophysiology 47:728–738.

Soomro GM, Altman D, Rajagopal S, Oakley-Browne M (2008) Selective serotonin re-uptake inhibitors (SSRIs) versus placebo for obsessive compulsive disorder (OCD). Cochrane Database Syst Rev.

Sotres-Bayon F, Bush DEA, LeDoux JE (2007) Acquisition of fear extinction requires activation of NR2B-containing NMDA receptors in the lateral amygdala. Neuropsychopharmacology 32:1929–1940.

Sotres-Bayon F, Sierra-Mercado D, Pardilla-Delgado E, Quirk GJ (2012) Gating of Fear in Prelimbic Cortex by Hippocampal and Amygdala Inputs. Neuron 76:804–812 Available at: http://www.ncbi.nlm.nih.gov/pubmed/23177964 [Accessed February 12, 2020].

Stern ER, Welsh RC, Fitzgerald KD, Gehring WJ, Lister JJ, Himle JA, Abelson JL, Taylor SF (2011) Hyperactive error responses and altered connectivity in ventromedial and frontoinsular cortices in obsessive-compulsive disorder. Biol Psychiatry 69:583–591.

Stewart SE et al. (2013) Genome-wide association study of obsessive-compulsive disorder. Mol Psychiatry 18:788–798.

Stujenske JM, Likhtik E, Topiwala MA, Gordon JA (2014) Fear and Safety Engage Competing Patterns of Theta-Gamma Coupling in the Basolateral Amygdala. Neuron 83:919–933.

Sun Y, Blanco-Centurion C, Zou B, Bendell E, Shiromani PJ, Liu M (2019) Amygdala GABA Neurons Project To vlPAG And mPFC. IBRO Reports 6:132–136.

Sun Y, Gooch H, Sah P (2020) Fear conditioning and the basolateral amygdala. F1000Research 9.

Supple WF, Kapp BS (1989) Response Characteristics of Neurons in the Medial Component of the Medial Geniculate Nucleus During Pavlovian Differential Fear Conditioning in Rabbits. Behav Neurosci 103:1276–1286.

Szeszko PR, MacMillan S, McMeniman M, Lorch E, Madden R, Ivey J, Banerjee SP, Moore GJ, Rosenberg DR (2004) Amygdala volume reductions in pediatric patients with obsessive-compulsive disorder treated with paroxetine: Preliminary findings. Neuropsychopharmacology 29:826–832.

Takemoto M, Song WJ (2019) Cue-dependent safety and fear learning in a discriminative auditory fear conditioning paradigm in the mouse. Learn Mem 26:284–290.

Ting JT, Feng G (2011) Neurobiology of obsessive-compulsive disorder: Insights into neural circuitry dysfunction through mouse genetics. Curr Opin Neurobiol 21:842–848.

Todd TP, Jiang MY, De Angeli NE, Bucci DJ (2018) A functional circuit for the retrieval of remote cued fear memory. Behav Neurosci 132:403–408.

Tracy JA, Ghose SS, Stecher T, McFall RM, Steinmetz JE (1999) Classical conditioning in a nonclinical obsessive-compulsive population. Psychol Sci 10:9–13.

Tsukano H, Hou X, Horie M, Kitaura H, Nishio N, Hishida R, Takahashi K, Kakita A, Takebayashi H, Sugiyama S, Shibuki K (2019) Reciprocal connectivity between secondary auditory cortical field and amygdala in mice. Sci Rep 9:1–12.

Tsvetkov E, Carlezon WA, Benes FM, Kandel ER, Bolshakov VY (2002) Fear conditioning occludes LTP-induced presynaptic enhancement of synaptic transmission in the cortical pathway to the lateral amygdala. Neuron 34:289–300.

Ursu S, Stenger VA, Katherine Shear M, Jones MR, Carter CS (2003) Overactive Action Monitoring in Obsessive-Compulsive Disorder: Evidence from Functional Magnetic Resonance Imaging. Psychol Sci 14:347–353.

van den Heuvel OA, Veltman DJ, Groenewegen HJ, Dolan RJ, Cath DC, Boellaard R, Mesina CT, Van Balkom AJLM, Van Oppen P, Witter MP, Lammertsma AA, Van Dyck R (2004) Amygdala activity in obsessive-compulsive disorder with contamination fear: A study with oxygen-15 water positron emission tomography. Psychiatry Res - Neuroimaging 132:225–237 Available at: www.elsevier.com/locate/psychresns [Accessed April 22, 2020].

VanElzakker MB, Kathryn Dahlgren M, Caroline Davis F, Dubois S, Shin LM (2014) From Pavlov to PTSD: The extinction of conditioned fear in rodents, humans, and anxiety disorders. Neurobiol Learn Mem 113:3–18 Available at: http://dx.doi.org/10.1016/j.nlm.2013.11.014.

Venkataraman A, Brody N, Reddi P, Guo J, Rainnie DG, Dias BG (2019) Modulation of fear generalization by the zona incerta. Proc Natl Acad Sci U S A 116:9072–9077 Available at: http://www.ncbi.nlm.nih.gov/pubmed/30967506 [Accessed February 21, 2020].

Via E, Cardoner N, Pujol J, Alonso P, López-Solà M, Real E, Contreras-Rodríguez O, Deus J, Segalàs C, Menchón JM, Soriano-Mas C, Harrison BJ (2014) Amygdala activation and symptom dimensions in obsessive-compulsive disorder. Br J Psychiatry 204:61–68.

Vianna DML, Borelli KG, Ferreira-Netto C, Macedo CE, Brandão ML (2003) Fos-like immunoreactive neurons following electrical stimulation of the dorsal periaqueductal gray at freezing and escape thresholds. Brain Res Bull 62:179–189 Available at: http://www.ncbi.nlm.nih.gov/pubmed/14698351 [Accessed February 18, 2020].

Vianna DML, Graeff FG, Brandão ML, Landeira-Fernandez J (2001a) Defensive freezing evoked by electrical stimulation of the periaqueductal gray: Comparison between dorsolateral and ventrolateral regions. Neuroreport 12:4109–4112.

Vianna DML, Graeff FG, Landeira-Fernandez J, Brandão ML (2001b) Lesion of the ventral periaqueductal gray reduces conditioned fear but does not change freezing induced by stimulation of the dorsal periaqueductal gray. Learn Mem 8:164–169.

Vidal-Gonzalez I, Vidal-Gonzalez B, Rauch SL, Quirk GJ (2006) Microstimulation reveals opposing influences of prelimbic and infralimbic cortex on the expression of conditioned fear. Learn Mem 13:728–733.

Vieira PA, Corches A, Lovelace JW, Westbrook KB, Mendoza M, Korzus E (2015) Prefrontal NMDA receptors expressed in excitatory neurons control fear discrimination and fear extinction. Neurobiol Learn Mem 119:52–62 Available at: http://www.ncbi.nlm.nih.gov/pubmed/25615540 [Accessed February 21, 2020].

Vieira PA, Lovelace JW, Corches A, Rashid AJ, Josselyn SA, Korzus E (2014) Prefrontal consolidation supports the attainment of fear memory accuracy. Learn Mem 21:394–405.

Vouimba RM, Maroun M (2011) Learning-induced changes in mpfc-bla connections after fear conditioning, extinction, and reinstatement of fear. Neuropsychopharmacology 36:2276–2285 Available at: http://www.ncbi.nlm.nih.gov/pubmed/21750582 [Accessed February 11, 2020].

Wan Y, Ade KK, Caffall Z, Ilcim Ozlu M, Eroglu C, Feng G, Calakos N (2014) Circuit-selective striatal synaptic dysfunction in the sapap3 knockout mouse model of obsessive-compulsive disorder. Biol Psychiatry 75:623–630 Available at: http://dx.doi.org/10.1016/j.biopsych.2013.01.008.

Wan Y, Feng G, Calakos N (2011) Sapap3 deletion causes mGluR5-dependent silencing of AMPAR synapses. J Neurosci 31:16685–16691.

Wang R, Fan Q, Zhang Z, Chen Y, Tong S, Li Y (2017) White matter integrity correlates with choline level in dorsal anterior cingulate cortex of obsessive compulsive disorder patients: A combined DTI-MRS study. In: Proceedings of the Annual International Conference of the IEEE Engineering in Medicine and Biology Society, EMBS, pp 3521–3524. Institute of Electrical and Electronics Engineers Inc. Available at: http://www.ncbi.nlm.nih.gov/pubmed/29060657 [Accessed February 21, 2020].

Weinberger NM (1998) Physiological memory in primary auditory cortex: Characteristics and mechanisms. Neurobiol Learn Mem 70:226–251.

Weinberger NM (2011) The medial geniculate, not the amygdala, as the root of auditory fear conditioning. Hear Res 274:61–74.

Weinberger NM, Javid R, Lepan B (1993) Long-term retention of learning-induced receptive-field plasticity in the auditory cortex. Proc Natl Acad Sci U S A 90:2394–2398.

Welch JM, Lu J, Rodriguiz RM, Trotta NC, Peca J, Ding JD, Feliciano C, Chen M, Adams JP, Luo J, Dudek SM, Weinberg RJ, Calakos N, Wetsel WC, Feng G (2007) Cortico-striatal synaptic defects and OCD-like behaviours in Sapap3-mutant mice. Nature 448:894–900.

Welch JM, Wang D, Feng G (2004) Differential mRNA Expression and Protein Localization of the SAP90/PSD-95-Associated Proteins (SAPAPs) in the Nervous System of the Mouse. J Comp Neurol 472:24–39.

Wilensky AE, Schafe GE, Kristensen MP, LeDoux JE (2006) Rethinking the fear circuit: The central nucleus of the amygdala is required for the acquisition, consolidation, and expression of pavlovian fear conditioning. J Neurosci 26:12387–12396.

Wilensky AE, Schafe GE, LeDoux JE (1999) Functional inactivation of the amygdala before but not after auditory fear conditioning prevents memory formation. J Neurosci 19.

Wolff SBE, Gründemann J, Tovote P, Krabbe S, Jacobson GA, Müller C, Herry C, Ehrlich I, Friedrich RW, Letzkus JJ, Lüthi A (2014) Amygdala interneuron subtypes control fear learning through disinhibition. Nature 509:453–458.

Wood J, Ahmari SE (2015) A framework for understanding the emerging role of corticolimbic-ventral striatal networks in OCD-associated repetitive behaviors. Front Syst Neurosci 9:1–22.

Wood J, LaPalombara Z, Ahmari SE (2018) Monoamine abnormalities in the SAPAP3 knockout model of obsessive-compulsive disorder-related behaviour. Philos Trans R Soc B Biol Sci 373 Available at: http://www.ncbi.nlm.nih.gov/pubmed/29352023 [Accessed February 21, 2020].

Wu K, Hanna GL, Easter P, Kennedy JL, Rosenberg DR, Arnold PD (2013) Glutamate system genes and brain volume alterations in pediatric obsessive-compulsive disorder: A preliminary study. Psychiatry Res - Neuroimaging 211:214–220.

Wu K, Hanna GL, Rosenberg DR, Arnold PD (2012) The role of glutamate signaling in the pathogenesis and treatment of obsessive-compulsive disorder. Pharmacol Biochem Behav 100:726–735.

Xu W, Morishita W, Buckmaster PS, Pang ZP, Malenka RC, Südhof TC (2012) Distinct Neuronal Coding Schemes in Memory Revealed by Selective Erasure of Fast Synchronous Synaptic Transmission. Neuron 73:990–1001.

Xu W, Südhof TC (2013) A neural circuit for memory specificity and generalization. Science (80-) 339:1290–1295 Available at: http://www.ncbi.nlm.nih.gov/pubmed/23493706 [Accessed February 21, 2020].

Xue YX, Zhu ZZ, Han H Bin, Liu JF, Meng SQ, Chen C, Yang JL, Wu P, Lu L (2015) Overexpression of Protein Kinase Mζ in the Prelimbic Cortex Enhances the Formation of Long-Term Fear Memory. Neuropsychopharmacology 40:2146–2156 Available at: http://dx.doi.org/10.1038/npp.2015.56.

Yang Y, Liu DQ, Huang W, Deng J, Sun Y, Zuo Y, Poo MM (2016) Selective synaptic remodeling of amygdalocortical connections associated with fear memory. Nat Neurosci 19:1348–1355.

Yin D, Zhang CC, Lv Q, Chen X, Zeljic K, Gong H, Zhan S, Jin H, Wang Z, Sun B (2018) Dissociable Frontostriatal Connectivity: Mechanism and Predictor of the Clinical Efficacy of Capsulotomy in Obsessive-Compulsive Disorder. Biol Psychiatry 84:926–936 Available at: http://www.ncbi.nlm.nih.gov/pubmed/29778276 [Accessed February 21, 2020].

Yizhar O, Fenno LE, Prigge M, Schneider F, Davidson TJ, Ogshea DJ, Sohal VS, Goshen I, Finkelstein J, Paz JT, Stehfest K, Fudim R, Ramakrishnan C, Huguenard JR, Hegemann P, Deisseroth K (2011) Neocortical excitation/inhibition balance in information processing and social dysfunction. Nature 477:171–178.

Yu K, Ahrens S, Zhang X, Schiff H, Ramakrishnan C, Fenno L, Deisseroth K, Zhao F, Luo MH, Gong L, He M, Zhou P, Paninski L, Li B (2017) The central amygdala controls learning in the lateral amygdala. Nat Neurosci 20:1680–1685 Available at: http://www.ncbi.nlm.nih.gov/pubmed/29184202 [Accessed February 13, 2020].

Yücel M, Wood SJ, Wellard RM, Harrison BJ, Fornito A, Pujol J, Velakoulis D, Pantelis C (2008) Anterior cingulate glutamate-glutamine levels predict symptom severity in women with obsessive-compulsive disorder. Aust N Z J Psychiatry 42:467–477 Available at: http://www.ncbi.nlm.nih.gov/pubmed/18465373 [Accessed February 21, 2020].

Zhang W-H, Zhou J, Pan H-Q, Wang X-Y, Liu W-Z, Zhang J-Y, Yin X-P, Pan B-X (2017a) δ Subunit-containing GABAA receptor prevents overgeneralization of fear in adult mice. Learn Mem 24:381–384 Available at: http://www.ncbi.nlm.nih.gov/pubmed/28716958 [Accessed February 21, 2020].

Zhang Z, Fan Q, Zhu Y, Tan L, Chen Y, Gao R, Zhang H, Li Y, Xiao Z (2017b) Intrinsic functional connectivity alteration of dorsal and rostral anterior cingulate cortex in obsessive-compulsive disorder: A resting fMRI study. Neurosci Lett 654:86–92 Available at: http://www.ncbi.nlm.nih.gov/pubmed/28636929 [Accessed February 21, 2020].

Zhu L, Zhu L, Huang Y, Shi W, Yu B (2018) Memory reconsolidation and extinction of fear conditioning induced different Arc/Arg3.1 expression. Neuroreport 29:1036–1045.

Zimmerman JM, Maren S (2010) NMDA receptor antagonism in the basolateral but not central amygdala blocks the extinction of Pavlovian fear conditioning in rats. Eur J Neurosci 31:1664–1670.

Zimmerman JM, Rabinak CA, McLachlan IG, Maren S (2007) The central nucleus of the amygdala is essential for acquiring and expressing conditional fear after overtraining. Learn Mem 14:634–644.

Züchner S, Wendland JR, Ashley-Koch AE, Collins AL, Tran-Viet KN, Quinn K, Timpano KC, Cuccaro ML, Pericak-Vance MA, Steffens DC, Krishnan KR, Feng G, Murphy DL (2009) Multiple rare SAPAP3 missense variants in trichotillomania and OCD. Mol Psychiatry 14:6–9.